DYNAMIC STABILITY OF BEAMS UNDER PARAMETRIC EXCITATION

THESIS SUBMITTED TO THE NATIONAL INSTITUTE OF TECHNOLOGY, ROURKELA FOR THE AWARD OF THE DEGREE OF

DOCTOR OF PHILOSOPHY

IN

MECHANICAL ENGINEERING

BY

Sukesh Chandra Mohanty

DEPARTMENT OF MECHANICAL ENGINEERING
NATIONAL INSTITUTE OF TECHNOLOGY
ROURKELA-769008, INDIA
SEPTEMBER, 2005

To my parents

Certificate

This is to certify that the thesis entitled "**Dynamic stability of beams under parametric excitation**", being submitted to the National Institute of Technology, Rourkela (India) by Mr. Sukesh Chandra Mohanty for the award of the degree of **Doctor of Philosophy (Mechanical Engineering)** is a record of bonafide research work carried out by him under my supervision and guidance. Mr. Mohanty has worked for more than three years on the above problem and it has reached the standard fulfilling the requirements of the regulations of the degree. The results embodied in this thesis have not been submitted in part or full to any other university or institute for the award of any degree or diploma.

Rourkela
Date:

(Dr.Niranjan Kavi)
Professor
Department of Mechanical Engineering
National Institute of Technology
Rourkela-769008
Orissa, India.

Acknowledgement

I express my deep sense of gratitude and reverence to my thesis supervisor Dr.N.Kavi, Professor, Department of Mechanical Engineering, National Institute of Technology, Rourkela, for his invaluable encouragement, helpful suggestions and supervision through out the course of this work.

I express my sincere thanks to the Director, N.I.T, Rourkela for providing me the necessary facilities for this study.

I would like to thank Prof. A.K.Behera and Prof. N.S.Dash ex-heads of the Mechanical Engineering Department and Prof. B.K.Nanda present head of the department for their help and cooperation during the progress of this work.

My thanks are due to Prof. R.K.Sahoo and Dr.P.K.Roy of Mechanical Engineering Department and Dr. M.R.Barik and Dr. S.K.Sahoo of Civil Engineering Department for their valuable suggestions and help at various stages of the work.

I acknowledge with thanks the help rendered to me by my colleagues, Dr. S.S.Mohaptra, Mr.R.K.Behera, Mr. Alok Satpathy and Dr. A.K.Satpathy.

The help extended by the staff of the Mechanical Engineering Department and Central Workshop in fabrication of the experimental set up is acknowledged with thanks.

I am extremely grateful to my wife Madhumita and daughters Simun and Gungun for their loving support and sacrifice.

(Sukesh Chandra Mohanty)

ABSTRACT

The present investigation is an attempt to contribute towards the improved understanding of the dynamic stability of beams under parametric excitation. The dynamic stability of ordinary and sandwich beams subjected to longitudinal parametric excitation has been investigated theoretically and experiments have been carried out to validate some of the theoretical findings. The equations of motion have been derived using finite element method. For ordinary beams the instability regions have been established using Floquet's theory and for sandwich beams modified Hsu's method proposed by Saito and Otomi has been applied to determine the boundary frequencies of the instability regions.

The dynamic stability of a Timoshenko beam with localised damage and having fixed-free, pinned-pinned, fixed-fixed and fixed-pinned boundary conditions has been investigated to study the effects of parameters such as extent of damage, position of damage, static load factor and boundary conditions on its dynamic stability behaviour.

The parametric instability of a twisted cantilever beam with localised damage has been investigated to study the effect of angle of pretwist, location of damage, extent of damage and static load factor on its dynamic stability characteristics.

The governing equations of motion for a general multilayered symmetric cantilever sandwich beam subjected to parametric excitation have been derived. Numerical results have been presented for three, five and seven layered beams to study the effects of various system parameters, such as core thickness parameter, core loss factor and number of layers on the stability behaviour of the sandwich beams. The dynamic stability behaviour of multilayered beams of various configurations based on some important criteria such as constant size, constant weight, constant flexural rigidity, constant size and flexural rigidity and constant weight and flexural rigidity has also been discussed.

Effects of static load factor and thermal gradient factor on the dynamic stability of a simply supported tapered beam with thermal gradient along its length have been studied.

Experimental work has been carried out to verify some of the theoretical results for beams with localised damage and multi layered symmetric cantilever sandwich beam.

Keywords: Parametric excitation, Dynamic stability, Localised damage, Boundary condition, Pretwist, Thermal gradient, Sandwich beam, Simple resonance and combination resonance.

Contents

LIST OF FIGURES

LIST OF TABLES

NOMENCLATURE

Although all the principal symbols used in this thesis are defined in the text as they occur, a list of them is presented below for easy reference. On some occasions, a single symbol is used for different meanings depending on the context and thus uniqueness is lost. The contextual explanation of the symbol at its appropriate place of use is hoped to eliminate the confusion.

English symbols

A	Cross-sectional area of the uniform beam.
$A(x)$	Area of cross-section of the tapered beam at any section x.
$A_{(2k-1)}$	Cross-sectional area of the (2k-1)th constraining elastic layer.
$A_{v(2j)}$	Cross-sectional area of the 2jth viscoelastic elastic layer.
$a_1 - a_8$	Set of generalised coordinates.
b	Width of the beam.
b_1	Width of the tapered beam at the root.
c	X-coordinate of the end of the damaged region.
d	X-coordinate of the end of the damaged region.
E	Young’s modulus of the beam material.
$E(x)$	Modulus of elasticity for the beam material at any section x.
E_1	Young’s modulus for the tapered beam material at the reference temperature $T_{o,}$ at the reference point, x = L.
EK_b	Effective bending stiffness for the damaged region.
$E_{(2k-1)}$	Young's modulus of the (2k-1)th constraining elastic layer.

f	X-coordinate of the center of the damage portion.
G	Shear modulus.
GK_s	Effective shear stiffness for the damaged region.
$G_{v(2j)}$	Complex shear modulus of 2jth viscoelastic material layer.
$G^*_{v(2j)}$	The in-phase shear modulus of the 2jth viscoelastic material layer.
g	Shear parameter.
h	Height of the beam.
h_1	Tapered beam height at the root,x = 0.
I	The second moment of inertia.
I_1	Area moment of inertia of the tapered beam section at x = 0.
$I_{(2k-1)}$	Area moment of inertia of the (2k-1)th constraining elastic layer.
$I(x)$	Area moment of inertia at any section x.
I_{yy}	Cross-sectional area moment of inertia of the beam about the Y-axis.
I_{zz}	Cross-sectional area moment of inertia of the beam about the Z-axis.
I_{yz}	Product of inertia of the beam cross-section with respect to the Y and Z-axes.
$I_{y'y'}$	Moment of inertia of the beam cross section about principal inertia axis Y′Y′.
$I_{z'z'}$	Moment of inertia of the beam cross section about principal inertia axis Z′Z′.
$[K]$	Global elastic stiffness matrix.
k'	Shear coefficient.

K_b	Constant representing the capacity of the damaged region to store bending strain energy.
K_s	Constant representing the capacity of the damaged region to store shear strain energy.
$\left[K^{(e)}\right]$	Element elastic stiffness matrix.
$\left[K_b^{(e)}\right]$	Element bending stiffness matrix.
$\left[K_g\right]$	Global geometric stiffness matrix.
$\left[K_g^{(e)}\right]$	Element geometric stiffness matrix.
$\left[K_s^{(e)}\right]$	Element shear stiffness matrix.
l	Length of an element.
L	Length of the beam.
$\left[M\right]$	Global mass matrix.
$\left[M^{(e)}\right]$	Element mass matrix.
$\left[M_r^{(e)}\right]$	Element rotary inertia mass matrix.
$\left[M_t^{(e)}\right]$	Element translational mass matrix.
$\left[N_S\right]$	Shape function matrix for twisted beam.
$[N_v]$	Shape function matrix for lateral displacement, v.
$[N_\theta]$	Shape function matrix for rotation, θ.
$P(t)$	Axial periodic load.
P_s	Static component of the periodic load.

P_t	Time dependent component of the periodic load.
R	Flexural strain or curvature.
T	Kinetic energy of the beam.
t	Time coordinate.
$T^{(e)}$	Elemental kinetic energy.
T_o	Temperature at the reference point, x = L.
$t_{(2k-1)}$	Thickness of the (2k-1)th constraining elastic layer.
$t_{v(2j)}$	Thickness of the 2jth viscoelastic layer.
$U_d^{(e)}$	Total strain energy of an element within the damaged region.
U	Total strain energy of the beam.
$U^{(e)}$	Elemental potential energy.
$u_{(2k-1)}$	Axial displacement of the (2k-1)th elastic layer.
$u_{v(2j)}$	Axial displacement of the 2jth viscoelastic layer.
v	Transverse displacement of the beam.
w	Transverse displacement of the beam.
x	Axial coordinate.

Greek symbols

α	Static load factor.
$\alpha_1 - \alpha_8$	Set of generalised coordinates.
β	Dynamic load factor.
β_t	Slope of variation of Young's modulus E with temperature T.

γ	Shear strain.
$\gamma_{v(2j)}$	Shear strain of the 2jth viscoelastic layer.
$\{\Delta\}$	Global displacement vector.
$\{\Delta^{(e)}\}$	Elemental nodal displacement vector.
δ	Thermal gradient factor, $\delta = \beta_t\, T_o$.
ζ	= x/l
$(\eta_c)_{(2j)}$	Core loss factor of 2jth viscoelastic layer.
Θ	Non-dimensional excitation frequency, $= \left(\frac{\Omega}{\omega_1}\right)^2$.
θ	Cross-sectional rotation.
θ_1	Angle of pretwist at the free end with respect to the fixed end.
θ_t	Angle of twist θ_t at cross section x.
ξ_b	Extent of damage in bending sense, = EK_b/EI.
ξ_s	Extent of damage in shear sense, =$GK_s/k'GA$.
$\rho_{(2k-1)}$	Mass density of the (2k-1)th constraining elastic layer.
$\rho_{v(2j)}$	Mass density of the 2jth viscoelastic layer.
$\{\Gamma\}$	Set of generalised coordinates.
τ	Size parameter of the damaged region = (d-c)/L.
$[\Phi]$	Normalized modal matrix corresponding to $[M]^{-1}[\overline{K}]$.
φ	Cross-sectional rotation.
ψ = f/L	Non-dimensional position of damage.

Ω Excitation frequency of the dynamic load component.

Superscripts

(e) Element

Operators

‘.‘	$\frac{\partial}{\partial t}$
‘ ′ ‘	$\frac{\partial}{\partial x}$
‘ ″ ‘	$\frac{\partial^2}{\partial x^2}$

Chapter 1

INTRODUCTION

1.1 Introduction

The environmental interaction with the deformable continuum is usually represented by means of body forces and surface tractions. When the body deforms, dead loads acting on the deformable bodies retain their magnitude as well as their initial direction. In general the forces acting on the body may not always be dead loads. The environmental mechanical action on a body may be due to forces, which are motion and/or time dependent. Such forces are instationary in nature. When these instationary external excitations are parametric with respect to certain form of deformation of the body, they appear as one of the coefficients in the homogeneous governing differential equation of motion of the system. Such systems are said to be parametrically excited and the associated instability of the system is called parametric resonance. Whereas in case of forced vibration of the systems, the equation of motion of the system is inhomogeneous and the disturbing forces appear as inhomogeneity. In parametric instability the rate of increase in amplitude is generally exponential and thus potentially dangerous, while in typical resonance due to external excitation the rate of increase in response is linear. More over damping reduces the severity of typical resonance, but may only reduce the rate of increase during parametric resonance. Parametric instability occurs over a region of parameter space and not at discrete points. It may occur due to excitation at frequencies remote from the natural frequencies.

In practice parametric excitation can occur in structural systems subjected to vertical ground motion, aircraft structures subjected to turbulent flow, and in machine components and mechanisms. Other examples are longitudinal excitation of rocket tanks and their liquid propellant by the combustion chambers during powered flight, helicopter blades in forward flight in a free-stream that varies periodically, and spinning satellites in elliptic orbits passing through a periodically varying gravitational field. In industrial machines and mechanisms, their components and instruments are frequently subjected to periodic or random excitation transmitted through elastic coupling elements. A few examples include those associated with electromagnetic and aeronautical instruments, vibratory conveyers, saw blades, belt drives and robot manipulators etc.

The system can experience parametric instability, when the excitation frequency or any integer multiple of it is twice the natural frequency that is to say

$$m\Omega = 2\omega_n, m = 1,2,3,4 - - - - n$$

The case $\Omega = 2\omega_n$ is known to be the most important in application and is called main or principal parametric resonance.

One of the main objectives of the analysis of parametrically excited systems is to establish the regions in the parameter space in which the system becomes unstable. These regions are known as regions of dynamic instability. The boundary separating a stable region from an unstable one is called a stability boundary. Plot of these boundaries on the parameter space is called a stability diagram.

Many machines and structural members can be modeled, as beams with different geometries, like beams of uniform cross-section, tapered beams and twisted beams. These elements may have different boundary conditions depending on their applications. Advances in material science have contributed many alloys and composite materials having high strength to weight ratio. However during manufacturing of these materials, inclusion of flaws affects their structural strength. These flaws can be modeled as localised damage [90]. The modulus of elasticity of the material is greatly affected by the temperature. In high-speed atmospheric flights, nuclear engineering applications, drilling operations and steam and gas turbines, the mechanical and structural parts are subjected to very high temperature. Most of the engineering materials are found to have a linear relationship between the Young’s modulus and temperature [44,114]. Geometry of the beam, boundary conditions, localised damage and thermal conditions have greater effect on the dynamic behaviour of the beams and hence need to be studied in depth.

Vibration control of machines and structures incorporating viscoelastic materials in suitable arrangement is an important aspect of investigation [87]. The use of viscoelastic layers constrained between elastic layers is known to be effective for damping of flexural vibrations of structures over a wide range of frequencies. The energy dissipated in these arrangements is due to shear deformation in the viscoelastic layers, which occurs due to flexural vibration of the structures. Multilayered cantilever sandwich beam like structures can be used in aircrafts and other applications such as robot arms for effective vibration control. These members may experience parametric instability when subjected to time dependant forces.

1.2 Outline of the present work

The present work mainly deals with the parametric instability of ordinary and sandwich beams. The main objectives are to study the effects of various parameters on the dynamic stability of the beams. Theoretical investigations have been carried out and experimental verification of the theoretical findings has been done for some cases.

The equations of motion for the systems have been derived using finite element method. The stability boundary for ordinary beams have been established by using the Floquet's theory [17] and for sandwich beams the stability diagrams have been obtained by using the modified Hsu's method proposed by Saito and Otomi [104]. For numerical computations computer programs have been developed using MATLAB [135]. For experimental work, an experimental set up capable of producing variable loading conditions has been designed and fabricated.

This thesis contains eight chapters including this chapter.

A detailed survey of relevant literature is reported in chapter 2.

In chapter 3 dynamic stability of a Timoshenko beam with a localised damage and with common boundary conditions, such as fixed-free, pinned-pinned, fixed-fixed and fixed-pinned has been analysed. Effects of parameters such as extent of damage, static load factor, position of damage and boundary conditions on the dynamic stability of the beam have been investigated.

Chapter 4 deals with the dynamic stability of a pretwisted cantilever beam with localised damage under periodic axial force. Effects of parameters namely angle of pretwist, position of damage, extent of damage and static load factor on the dynamic stability of the beam have been studied.

In chapter 5 dynamic stability of a multilayered symmetric cantilever sandwich beam subjected to parametric excitation has been reported. The effects of various system parameters, such as core thickness parameter, core loss factor and number of layers, as well as various beam configurations based on some important criteria on the stability behaviour of multilayered beams have been investigated.

Chapter 6 addresses to the problem of dynamic stability of a simply supported tapered beam with thermal gradient. Effects of thermal gradient and static load component on the stability behaviour of the beam have been studied.

In chapter 7 details of experimental set up and testing procedure have been outlined. Experimentally obtained stability diagrams for a few typical cases related to problems described in chapters (3-5) have been reported. The theoretical and experimental stability diagrams have been compared to make a qualitative assessment of the theoretical results.

Finally in chapter 8 important conclusions drawn from the present investigations reported in chapters 3-7 along with suggestions for further work have been presented.

Chapter 2

REVIEW OF LITERATURE

2.1 Introduction

Discovery of parametric resonance dates back to 1831. Faraday [40] was first to observe the phenomenon of parametric excitation, when he noticed that when a fluid filled container vibrates vertically, fluid surface oscillates at half the frequency of the container. Melde [79] reported parametric resonance in the case of lateral vibration of a string. Beliaev [13] was first to provide a theoretical analysis of parameter resonance while dealing with the stability of prismatic rods. These are a few early works.

Several review articles on parameter resonance have also been published. Evan-Iwanoski [39], Ibrahim and coworkers [54-60], Ariaratnam [5] and Simitses [113] gave exhaustive account of literature on vibration and stability of parametrically excited systems. Review article of Habip [49] gives an account of developments in the analysis of sandwich structures. Articles of Nakra [84-86] have extensively treated the aspect of vibration control with viscoelastic materials. Books by Bolotin [17], Schmidt [109] and

Neyfeh and Mook [88] deals extensively on the basic theory of dynamic stability of systems under parameter excitations .In this chapter further developments in subsequent years in the field of parametric excitation of system with specific reference to ordinary and sandwich beams is reported. Reference cited in the above mentioned review works are not repeated except at a few places for the sake of continuity. The reported literature mainly deal with the methods of stability analysis, types of resonance, study of different system parameters on the parameter instability of the system and experimental verification of the theoretical findings.

2.2 Methods of stability analysis of parametrically excited system

The governing equations for parametrically excited systems are second order differential equations with periodic coefficients, which have no exact solutions. The researchers for a long time have been interested to explore different solution methods to this class of problem. The two main objectives of this class of researchers are to establish the existence of periodic solutions and their stability. When the governing equation of motion for the system is of Matheiu-Hill type, a few well known solution methods those are commonly used are, method proposed by Bolotin based on Floquet's theory, perturbation and iteration techniques, the Galerkin's method, the Lyapunov second method and the asymptotic technique by Krylov, Bogoliubov and Mitroploskii.

Bolotin's [17] method based on Floquet's theory can be used to get satisfactory results for simple resonance only. Steven [115] later modified the Bolotin's method for system with complex differentials equation of motion. Hsu [52-53] proposed an approximate method of stability analysis of systems having small parameter excitations

Hsu's method can be used to obtain instability zones of main, combination and difference types. Later Saito and Otomi [104] modified Hsu's method to suit systems with complex differential equation of motion. Takahashi [122] proposed a method free from the limitations of small parameter assumption. This method establishes both the simple and combination type instability zones. Zajaczkowski and Lipinski [131] and Zajaczkowski [132] based on Bolotin's method derived formulae to establish the regions of instability and to calculate the steady state response of systems described by a set of linear differential equations with time dependent parameters represented by a trigonometric series. Lau et al. [73] proposed a variable parameter incrementation method, which is free from limitations of small excitation parameters. It has the advantage of treating non-linear systems.

Many investigators to study the dynamic stability of elastic systems have also applied finite element method. Brown et al. [18] studied the dynamic stability of uniform bars by applying this method. Abbas [2] studied the effect of rotational speed and root flexibility on the stability of a rotating Timoshenko beam by finite element method. Abbas and Thomas [1] and Yokoyama [130] used finite element method to study the effect of support condition on the dynamic stability of Timoshenko beams. Shastry and Rao by finite element method obtained critical frequencies [110] and the stability boundaries [111-112] for a cantilever column under an intermediate periodic concentrated load for various load positions. Bauchau and Hong [11] studied the non-linear response and stability of beams using finite element in time. Briseghella et al. [16] studied the dynamic stability problems of beams amd frames by using finite element method. Svensson [121] by this method studied the stability properties of a periodically loaded non-linear dynamic system, giving special attention to damping effects.

2.3 Types of parametric resonance

Multi degree freedom systems may exhibit simple resonance, resonance of sum type or resonance of difference type depending upon the type of loading, support conditions and system parameter.

Mettler [80] furnished a classification for various kinds of resonances exhibited by linear periodic system. Iwatsubo and his co-workers [63-64] from their investigation on stability of columns found that uniform columns with simple supported ends do not exhibit combination type resonances. Saito and Otomi [104] on the basis of their investigation of stability of viscoelastic beams with viscoelastic support concluded that combination resonances of different type do not occur for axial loading, but it exits for tangential type of loading. Celep [21] found that for a simply supported pretwisted column, combination resonances of the sum type may exit or disappear depending on the pretwist angle and rigidity ratio of the cross-section. Ishida et al. [62] showed that an elastic shaft with a disk exhibits only difference type combination resonance. Chen and Ku [23] from their investigations found that for a cantilever shaft disk system, the gyroscopic moment can enlarge the principal regions of dynamic instability.

2.4 Effects of system parameters

2.4.1 Effect of localised damage

Parekh and Carlson [90] developed a model to study the dynamic stability of a bar with a localised damage. They introduced the concept of effective stiffness for the damaged region, which reflects the energy storing capacity of the damaged region. Later Datta and Nagraj [31] used the concept of Parekh and Carlson and analysed the effect of foundation stiffness, extent of damage and position of damage on the dynamic stability of a tapered bar with flaws supported on elastic foundation. Datta and Lal [30] investigated the static stability of tapered beams with localized damage and subjected to intermediate concentrated load. Datta and Lal [34] work was extended by Mohanty and Kavi [81] by adding shear deformation to their analysis. Das and Dey [28] investigated the random vibration of beams with localised zones of damage under stochastic excitation.

2.4.2 Effect of pretwist angle

Dokumaci [37] investigated the effects of pretwist, ratio of bending rigidities and loading angle on the unstable zones of pretwisted blades under lateral parametric excitation. Celep [21] studied the stability of a pretwisted simply supported column subjected to static and periodic axial loads. He found that combination resonance of sum type exists for small pretwist and vanishes for large pretwist angle. Gürgöze [47] studied the dynamic stability of pretwisted beams with hinged-hinged, clamped-clamped and clamped-hinged boundary conditions and found that increasing the pretwist angle broadens the instability zones. Chen and Liao [24] carried out a dynamic analysis of a pretwisted spinning beam under constant axial compressive loads with elastic constraints using assumed mode method. Yang and Tsao [129] studied the vibration and stability of a pretwisted blade under non-constant rotating speed and they found that instability can be minimised by increasing the pretwist angle. Tan et al. [123] investigated the parametric instability of spinning pretwisted beams using Euler beam theory and the method of multiple scales. They found that increasing the pretwist angle the first instability region width decreases, while the second instability region becomes wider and both the regions move towards each other.

2.5 Experimental investigations

Experimental studies in the field of parametric instability are relatively few. Bolotin [17] experimentally verified his own theoretical findings. Stevens and Evan-Iwanowski [116] experimentally studied the effect of viscoelastic material of the parametric instability of the columns. Iwatsubo et al [63] carried out experiments to check their result obtained by finite difference method for the stability of clamped-clamped and clamped-simply supported columns. Saito and Koizumi [105] from experiment obtained the amplitude frequency curves of a simply supported horizontal beam subjected to non-linear parametric excitation. Sunakawa and Higuchi [120] through experiment studied the non-linear response of thin columns under parametric excitations. The theoretical results obtained for a slender cantilever beam carrying a lumped mass was experimentally verified by Zovodney [133] and Zavodney and Nayfeh [134]. Dufour and Berlioz [38] carried out experiments to study the dynamic stability of a beam under axial periodic force and torque and compared their theoretical results with the experimental one. Sugiyama et al [118] conducted experiments to verify the stabilizing effect of non-conservative follower force on the vibration and stability of cantilevered columns initially subjected to a conservative force due the rocket motor’s weight. Svensson [121] carried out experiments to study the effect of material damping as well as the damping effects at the hinges on the dynamic stability of a beam.

2.6 Sandwich Beams

The main objectives of the researchers dealing with sandwich beams may be grouped in the following categories.

i) Prediction of resonant frequencies and loss factor

ii) Static and dynamic analysis of sandwich beams

iii) Stability study of sandwich beams and columns

iv) Experimental investigations

2.6.1 Resonant frequencies and loss factor prediction

Kerwin [71] was the first to carry out a quantitative analysis of the damping effectiveness of a constrained viscoelastic layer and he obtained an expression to estimate the loss factor. Ungar [127] derived general expressions for the loss factors of uniform linear composites in terms of the properties of the constituting materials. Di Taranto [35] developed a theory to estimate natural frequencies, loss factors for a for a finite length sandwich beam. Jones et al. [67] theoretically and experimentally evaluated the damping capacity of a sandwich beam with viscoelastic core. Asnani and Nakra [6] analysed multilayer simply supported sandwich beams and estimated loss factors and displacement response effectiveness for beams of different number of layers. Chatterjee and Baungarten [22] obtained for a simply supported sandwich beam, the damped natural frequencies and logarithmic decrement for the fundamental mode of vibration. They also conducted experiments to verify their theoretical results, which showed good agreement. Nakra and Grootenhuis [83] studied theoretically as well as experimentally, the vibration characteristics of asymmetric dual core sandwich beams. They did not include the rotary and longitudinal inertia terms in their analysis. Later Rao [98] included both these effects in his analysis. Asnani and Nakra [8] studied the effect of number of layers and thickness ratio on the system loss factors for a simply supported multilayer beam. Rao [92] investigated the influence of pretwist on resonant frequency and loss factor for a symmetric pretwisted simply supported sandwich beam and found that pretwisting reduces the loss factor and very soft thick cored beams is especially sensitive to even small changes of pretwist. Rao and Stühler [93] analysed the damping effectiveness of tapered sandwich beam with simply supported and clamped free end conditions. Rao [98] investigated the free vibration of a short sandwich beam considering the higher order effects such as inertia, extension and shear of all the layers. He found that if these parameters are neglected for short sandwich beam there is an error as high as 45% in estimation of the loss factor and frequencies. Rubayi and Charoenee [103] carried theoretical and experimental investigations to obtain the natural frequencies of cantilever sandwich beams subjected to gravity force only. Rao [96] in another work gave graphs and equations to estimate frequencies and loss factors for sandwich beam under various boundary conditions. Johnson and his coworkers [65-66] used the finite element method to solve frequencies and loss factors for beams and plates with constrained viscoelastic layer. Vaswani et al. [128] derived equations of motion for a multilayer curved sandwich beam subjected to harmonic excitation. Lall et al. [72] analysed the partially covered sandwich beams using three different methods and found that method by Marcus [77] estimates modal loss factor only, where as Rayleigh-Ritz and classical search method give both loss factor and resonant frequencies. Dewa et al. [33] studied the damping effectiveness of partially covered sandwich beams. They found that partially covered beams have better damping capacity than fully covered beams. Also through experiments he validated his theoretical findings. Imaino and Harrison [61] adopted modal strain energy method and finite element technique to investigate damping of the first and second bending resonance of a sandwich beam with constrained damping layer. He and Rao [50] developed an analytical model to carry out a parameter study of the coupled flexural and longitudinal vibration of a curved sandwich beam. Effects of parameters such as curvature, core thickness and adhesive shear modulus on the system loss factors and resonant frequencies were investigated. Same authors [51] in another work studied the vibration of multispan beams with arbitrary boundary condition. Effects of parameter like location of intermediate supports and adhesive thickness on the resonant frequencies and loss factors were investigated. Bhimaraddi [15] solved both the resonant frequencies and loss factors for a simply supported beam with constrained layer damping using a model, which accounted for the continuity of displacements and the transverse shear stresses across the interfaces of the layers. Sakiyama et al. [106] developed an analytical method for free vibration analysis of a three layer continuous sandwich beam and investigated the effect of shear parameter and core thickness on the resonant frequencies and loss factors. Fasana and Marchesiello [41] calculated the mode shapes, frequencies and loss factors for sandwich beams by Rayleigh-Ritz method. They choose polynomials, which satisfy the geometric boundary conditions as admissible function. Banerjee [10] studied the free vibration of a three layer sandwich beam using dynamic stiffness matrix method. He calculated the natural frequencies and mode shapes.

2.6.2 Static and dynamic analysis of sandwich beams

Mead and Markus [78] carried out the forced vibration analysis of a three-layered sandwich beam with viscoelastic core and with arbitrary boundary conditions. They followed the method used by Di Taranto [35] in their analysis. Asnani and Nakra [7] carried out forced vibration analysis of sandwich beams with viscoelastic core and with fixed-fixed and cantilever type end conditions. The forced vibration response obtained by applying Ritz method matched well with the experimental results. Rao [95] studied the forced vibration of a damped sandwich beam subjected to moving forces and found that increasing the shear stiffness of the core materials can reduce the dynamic magnification of the central deflection of the beam. Kapur [68] considered both rotary and longitudinal inertia in his analysis to study the dynamic response of two and three-layered viscoelastically damped beams subjected to half-sine shock excitation. Sharma and Rao [108] determined static deflections and stresses in sandwich beams for both concentrated and distributed loads under various conditions. Frosting and Baruch [43] from their analysis of stresses in a sandwich beam with flexible core under concentrated and distributed loading found that transverse normal stresses at the interface between the skin and core in some cases are significant in determining the sudden failure of the beam. Sun et al. [119] developed a finite element model to study the effect of add-on viscoelastic layer in damping and vibration control of unidirectional composite laminates. Their theoretical results compared well with the experimental findings. Qian and Demao [91] carried out modal analysis as well as response calculation in time domain using finite element technique. Salet and Hamelink [107] developed a numerical model based on finite difference method, for non-linear analysis of sandwich beams with simply supported boundary conditions. Ha [48] suggested an exact analysis procedure for bending and buckling analysis of sandwich beam systems.

2.6.3 Stability study of sandwich beams and columns

Bauld [12] investigated the stability of sandwich columns with simply supported end conditions and subjected to pulsating axial loads. The stability of two layer sandwich cantilever beams with imperfect bonding was studied was studied by Chonan [26]. They obtained critical loads for divergence and flutter type instabilities and found that these are functions of shear and normal stiffness of the bond. In another work Chonan [27] studied the divergence and flutter type instabilities in symmetric sandwich beams with elastic bonding and found that critical divergence and flutter loads depends on the interface bond stiffness. Kar and Hauger [69] investigated the dynamic stability of a sandwich beam subjected to a direction controlled non-conservative force and determined the critical divergence and flutter loads. Ray and Kar [99] have investigated the dynamic stability of sandwich beams under various boundary conditions. The same authors [100-102] also investigated the parameter stability of partially covered sandwich beams, dual cored sandwich beams and symmetric sandwich beams with higher order effects. Ray and Kar in these works derived the governing equation of motion by using Hamilton’s principle and converted the equations of motion to a set of coupled Hill’s equation in the time domain by Galerkin’s method. They assumed approximate series solutions, which satisfy majority of the boundary conditions. Lin and Chen [75] studied the effect of rotating speed, setting angle and hub radius on the dynamic stability of a rotating sandwich beam with a constrained damping layer.

2.6.4 Experimental investigations

The reported experimental works are mainly related to the experimental validation of theoretically predicted dynamic response, damping values, resonant frequencies and loss factors of sandwich beams. Chatterjee and Baumgarten [22] experimentally determined the logarithmic decrement to validate their theoretically obtained values for damped natural frequencies and damping values for a simply supported sandwich beam. Asnani and Nakra [7] compared their theoretically obtained resonant frequencies by applying Ritz method with experimental results for a three-layer sandwich beam. Trompette et al. [125] carried out experiments to obtain resonant frequency and damping values and compared with their theoretical results, which showed good agreement. Mace [76] compared the frequency response curve obtained from experiment with his theoretical results and drew the conclusion that his predicted theory is efficient in predicting the dynamic response of beams that are damped by means of a thin viscoelastic film. Gorrepati and Rao [45] measured from experiment, the natural frequencies and loss factor for a simply supported beam with adhesively bonded double strap joint to validate their results obtained by modal strain energy method. Chen and Chan [25] in order to establish their results obtained from integral finite element method experimentally obtained frequency response functions for elastic-viscoelastic composite structures. In a recent work Nayfeh [89] conducted experiment to obtain resonant frequencies and loss factors and compared with values predicted by his developed model for vibration parallel to the plane of lamination of a symmetric elastic-viscoelastic sandwich beam.

Chapter 3

DYNAMIC STABILITY OF A TIMOSHENKO BEAM WITH LOCALISED DAMAGE DUE TO PARAMETRIC EXCITATION AND TO BOUNDARY CONDITIONS

3.1 Introduction

Dynamic analysis of many machine and structural components can be done by modeling them as uniform beams with different boundary conditions. These components quite often are subjected to time varying parametric excitation, which may lead to their instability. Advances in material science have contributed many alloys and composite materials having high strength to weight ratio. However during the manufacturing of these materials, inclusion of flaws affects their structural strength. Hence the effect of localised damage on the dynamic stability of beams with various common boundary conditions forms an important aspect of investigation.

Earlier studies on effect of localised damages on the stability behaviour of structural elements were mainly on static and fatigue strength consideration

[14,74]. Parekh and Carlson [90] introduced the concept of effective stiffness for the damaged region and analysed the dynamic stability of a bar with localised damage. They developed analytically an approximate solution for establishing principal regions of instability. Datta and Nagaraj [31] studied the dynamic stability of tapered bars with flaws and with simply supported end conditions resting on an elastic foundation. They considered Euler beam theory in their analysis. Datta and Lal [30] analysed the static stability behaviour of a tapered beam with localised damage subjected to an intermediate concentrated load, but shear deformation was not included in their analysis. The same work [30] was extended by Mohanty and Kavi [81] considering shear deformation.

This work is an attempt to study the dynamic stability of a uniform Timoshenko beam with localised damage subjected to parametric excitation under various boundary conditions. Finite element method along with Floquet's theory has been used to carry out the analysis. Four parameters are used to characterise the damaged zone: location, size and effective bending and shear stiffness at the damaged region. Effective bending and shear stiffness at the damaged region is a measure of the extent of damage. Instability zones for different locations of the damage and for various boundary conditions of the beam have been established to study the effects of different parameters namely extent of damage, damage location, boundary conditions and static load factor.

3.2 Formulation of the problem

The beam is of uniform rectangular cross-section having a length L, width b and depth h. The effect of the damage is represented by the presence of a flaw in the region $c < x < d$. Beams with end conditions such as fixed-free, pinned-pinned, fixed- fixed and fixed-pinned as shown in fig.–3.1 are considered. The beam is subjected to a pulsating axial force $P(t) = P_s + P_t \cos\Omega t$, acting along its undeformed axis. Ω is the excitation frequency of the dynamic load component, P_s is the static and P_t is the amplitude of the time dependent component of the load.

A typical finite element is shown in fig.-3.2. The element consists of two nodes i and j with v_i ,θ_i, v_j and θ_j as the nodal displacements. v is the lateral displacement and θ represents the cross-sectional rotation. The translation v consists of two displacement components, one due to bending and other due to transverse shear deformation. The rotation θ is only due to bending deformation.

3.2.1 Element matrices

The total strain energy $\left(U^{(e)}\right)$ of an undamaged beam element of length l including the shear deformation is written in the form.

$$U^{(e)} = \frac{1}{2}\int_0^l E\,I\left(\frac{\partial\theta}{\partial x}\right)^2 dx + \frac{1}{2}\int_0^l k'G\,A\left(\frac{\partial v}{\partial x} - \theta\right)^2 dx - \frac{1}{2}\int_0^l P(t)\left(\frac{\partial v}{\partial x}\right)^2 dx \tag{3.1}$$

where E is the Young's modulus, I is the second moment of inertia, k' is the shear coefficient, G is the shear modulus and A is the cross-sectional area.

The kinetic energy $(T^{(e)})$ of the beam element considering rotary inertia is given by

$$T^{(e)} = \frac{1}{2}\int_0^l \rho\,A\left(\frac{\partial v}{\partial t}\right)^2 dx + \frac{1}{2}\int_0^l \rho\,I\left(\frac{\partial\theta}{\partial t}\right)^2 dx \tag{3.2}$$

A cubic displacement distribution for v is assumed over the element as

$$v = \alpha_1 + \alpha_2\,x + \alpha_3\,x^2 + \alpha_4 x^3 \tag{3.3}$$

where $\alpha_1, \alpha_2, \alpha_3, \alpha_4$ are called the generalised coordinates. The lateral displacement *v* and the cross sectional rotation θ within the element can be expressed in terms of the shape function matrix and nodal displacement vector $\{\Delta^{(e)}\}$ respectively as,

$$v = [\, N_{v1}\ N_{v2}\ N_{v3}\ N_{v4}\,] \begin{Bmatrix} v_i \\ \theta_i \\ v_j \\ \theta_j \end{Bmatrix}$$

$$= [N_v] \left\{\Delta^{(e)}\right\} \tag{3.4}$$

$$\theta = [N_{\theta 1}\ N_{\theta 2}\ N_{\theta 3}\ N_{\theta 4}] \begin{Bmatrix} v_i \\ \theta_i \\ v_j \\ \theta_j \end{Bmatrix}$$

$$= [N_\theta] \left\{\Delta^{(e)}\right\} \tag{3.5}$$

where

$N_{v1} = [1-3\zeta^2 + 2\zeta^3 + (1-\zeta)\Phi]/(1+\Phi)$

$N_{v2} = [\zeta - 2\zeta^2 + \zeta^3 + (\zeta-\zeta^2)\,\Phi/2]\, l/(1+\Phi)$

$N_{v3} = [3\zeta^2 - 2\zeta^3 + \zeta\Phi]/(1+\Phi)$

$N_{v4} = [-\zeta^2 + \zeta^3 - (\zeta-\zeta^2)\,\Phi/2]\, l/(1+\Phi)$

$N_{\theta 1} = 6\,[-\zeta+\zeta^2]/[l\,(1+\Phi)]$

$N_{\theta 2} = [1-4\zeta + 3\zeta^2 + (1-\zeta)\Phi]/(1+\Phi)$

$N_{\theta 3} = 6\,[\zeta-\zeta^2]/[l\,(1+\Phi)]$

$N_{\theta 4} = [-2\zeta + 3\zeta^2 + \zeta\Phi]/(1+\Phi)$

$\zeta = x/l$

$\Phi = 12\, E\, I / [k' G\, A\, l^2]$

The flexural strain or curvature R and the shear strain γ within the element can be written as

$$R = \frac{d\theta}{dx} = [B_b] \left\{\Delta^{(e)}\right\} \tag{3.6}$$

$$\gamma = \frac{dv}{dx} - \theta = [B_s] \left\{\Delta^{(e)}\right\} \tag{3.7}$$

where

$$[B_b] = \frac{d}{dx}[N_\theta] \tag{3.8}$$

$$[B_s] = \frac{d}{dx}[N_v] - [N_\theta]$$

$$= [B_v] - [N_\theta] \tag{3.9}$$

With the help of equations (3.4-3.9) the potential energy $\left(U^{(e)}\right)$ and the kinetic energy $\left(T^{(e)}\right)$ of the element can be written in terms of nodal displacement vector, $\left\{\Delta^{(e)}\right\}$ as,

$$U^{(e)} = \frac{1}{2}\left\{\Delta^{(e)}\right\}^T \left[K_b^{(e)}\right]\left\{\Delta^{(e)}\right\} + \frac{1}{2}\left\{\Delta^{(e)}\right\}^T \left[K_s^{(e)}\right]\left\{\Delta^{(e)}\right\} - \frac{1}{2}\left\{\Delta^{(e)}\right\}^T P(t)\left[K_g^{(e)}\right]\left\{\Delta^{(e)}\right\}$$

$$= \frac{1}{2}\left\{\Delta^{(e)}\right\}^T \left(\left[K_b^{(e)}\right] + \left[K_s^{(e)}\right]\right)\left\{\Delta^{(e)}\right\} - \frac{1}{2}\left\{\Delta^{(e)}\right\}^T P(t)\left[K_g^{(e)}\right]\left\{\Delta^{(e)}\right\}$$

$$= \frac{1}{2}\left\{\Delta^{(e)}\right\}^T \left[K^{(e)}\right]\left\{\Delta^{(e)}\right\} - \frac{1}{2}\left\{\Delta^{(e)}\right\}^T P(t)\left[K_g^{(e)}\right]\left\{\Delta^{(e)}\right\} \tag{3.10}$$

$$T^{(e)} = \frac{1}{2}\left\{\dot{\Delta}^{(e)}\right\}^T \left[M_t^{(e)}\right]\left\{\dot{\Delta}^{(e)}\right\} + \frac{1}{2}\left\{\dot{\Delta}^{(e)}\right\}^T \left[M_r^{(e)}\right]\left\{\dot{\Delta}^{(e)}\right\}$$

$$= \frac{1}{2}\left\{\dot{\Delta}^{(e)}\right\}^T \left(\left[M_t^{(e)}\right] + \left[M_r^{(e)}\right]\right)\left\{\dot{\Delta}^{(e)}\right\}$$

$$= \frac{1}{2}\left\{\dot{\Delta}^{(e)}\right\}^T \left[M^{(e)}\right]\left\{\dot{\Delta}^{(e)}\right\} \tag{3.11}$$

where

$$\left[K_b^{(e)}\right] = \int_0^l \left[B_b\right]^T E \ I \left[B_b\right] dx \tag{3.12}$$

$$\left[K_s^{(e)}\right] = \int_0^l \left[B_s\right]^T k' \ G \ A \left[B_s\right] dx \tag{3.13}$$

$$\left[K^{(e)}\right] = \left[K_b^{(e)}\right] + \left[K_s^{(e)}\right] \tag{3.14}$$

$$\left[K_g^{(e)}\right] = \int_0^l \left[B_v\right]^T \left[B_v\right] dx \tag{3.15}$$

$$\left[M_t^{(e)}\right] = \int_0^l \left[N_v\right]^T \rho \ A \left[N_v\right] dx \tag{3.16}$$

$$\left[M_r^{(e)}\right] = \int_0^l \left[N\theta\right]^T \rho \ I \ \left[N\theta\right] dx \tag{3.17}$$

$$\left[M^{(e)}\right] = \left[M_t^{(e)}\right] + \left[M_r^{(e)}\right] \tag{3.18}$$

$\left[K_b^{(e)}\right]$, $\left[K_s^{(e)}\right]$, $\left[K^{(e)}\right]$ and $\left[K_g^{(e)}\right]$ are element bending stiffness , element shear stiffness, element elastic stiffness and element geometric stiffness matrix respectively.

$\left[M_t^{(e)}\right]$, $\left[M_r^{(e)}\right]$ and $\left[M^{(e)}\right]$ are element translational mass matrix and element rotary inertia mass matrix and element mass matrix respectively.

The total strain energy $\left(U_d^{(e)}\right)$ of an element within the damaged region including the shear deformation is written in the form,

$$U_d^{(e)} = \frac{1}{2}\int_0^l E \, K_b \left(\frac{\partial \theta}{\partial x}\right)^2 dx + \frac{1}{2}\int_0^l GK_s \left(\frac{\partial v}{\partial x} - \theta\right)^2 dx - \frac{1}{2}\int_0^l P(t) \left(\frac{\partial v}{\partial x}\right)^2 dx \tag{3.19}$$

The constants K_b and K_s are the measure of the deterioration within the damaged portion and they represent the capacity of the region to store strain energy. The elastic stiffness matrix for an element in the damaged portion of the beam can be calculated from eqs.(3.12-3.14) by using the corresponding effective stiffness EK_b and GK_s for the damaged region.

Under the assumption that the deterioration produced does not involve a loss of material, the expressions for the mass matrices of an element in the damaged region is same as those given in eqs.(3.16-3.18).

3.2.2 Governing equations of motion

The total strain energy (U) of the beam with damaged portion can be written as

$$U = \frac{1}{2}\int_0^L EI\left(\frac{\partial\theta}{\partial x}\right)^2 dx + \frac{1}{2}\int_c^d (EK_b - EI)\left(\frac{\partial\theta}{\partial x}\right)^2 dx + \frac{1}{2}\int_0^L k'GA\left(\frac{\partial v}{\partial x} - \theta\right)^2 dx + \frac{1}{2}\int_c^d (GK_s - k'GA)\left(\frac{\partial v}{\partial x} - \theta\right)^2 dx - \frac{1}{2}\int_0^L P(t)\left(\frac{\partial v}{\partial x}\right)^2 dx \tag{3.20}$$

Under the assumption that the deterioration produced does not involve a loss of material, the expression for kinetic energy (T) of the damaged beam is given as

$$T = \frac{1}{2}\int_0^L \rho A\left(\frac{\partial v}{\partial t}\right)^2 dx + \frac{1}{2}\int_0^L \rho I\left(\frac{\partial\theta}{\partial t}\right)^2 dx \tag{3.21}$$

By dividing the beam in to several elements and assembling the element matrices, the potential energy (*U*) and the kinetic energy (*T)* for the damaged beam can be written in terms of global displacement vector $\{\Delta\}$ as,

$$U = \frac{1}{2}\{\Delta\}^T[K]\{\Delta\} - \frac{1}{2}\{\Delta\}^T P(t)\left[K_g\right]\{\Delta\} \tag{3.22}$$

$$T = \frac{1}{2}\{\dot{\Delta}\}^T[M]\{\dot{\Delta}\} \tag{3.23}$$

where $[K]$, $[M]$ and $[K_g]$ are the global elastic stiffness matrix, global mass matrix and global geometric stiffness matrix respectively.

The equation of motion for the beam is obtained by using the Lagrangian, $L=T-U$ in the Lagrange's equation.

$$\frac{d}{dt}\left(\frac{\partial L}{\partial \dot{\Delta}_k}\right)-\left(\frac{\partial L}{\partial \Delta_k}\right)=0 \text{, For k=1 to n, n is the total number of coordinates.} \tag{3.24}$$

The equation of motion in matrix form for the axially loaded discretised system is,

$$[M]\{\ddot{\Delta}\}+[K]\{\Delta\}-P(t)[K_g]\{\Delta\}=0 \tag{3.25}$$

P_s, the static and P_t, the amplitude of time dependent component of the load, can be represented as the fraction of the fundamental static buckling load P^* of the beam without localised damage and having the similar end conditions. Hence substituting, $P(t) = \alpha P^* + \beta P^* \cos\Omega t$, with α and β as called static and dynamic load factors respectively.

The eq. (3.25) becomes

$$[M]\{\ddot{\Delta}\}+\left([K]-\alpha P^*[K_g]_s-\beta P^*\cos\Omega t[K_g]_t\right)\{\Delta\}=0 \tag{3.26}$$

where the matrices $[K_g]_s$ and $[K_g]_t$ reflect the influence of P_s and P_t respectively. If the static and time dependent components of the load are applied in the same manner, then $[K_g]_s = [K_g]_t = [K_g]$.

3.2.3 Regions of instability

Equation (3.26) represents a system of second order differential equations with periodic coefficients of the Mathieu-Hill type. From the theory of Mathieu functions [17], it is evident that the nature of solution is dependent on the choice of load frequency and load amplitude. The frequency amplitude domain is divided in to regions, which give rise to stable solutions and to regions, which cause unstable solutions.

The eq.(3.26) does not change its form on addition of the period, $T = \frac{2\Pi}{\Omega}$ to t. This follows from the fact that $\cos\Omega(t+T) = \cos\Omega t$. Therefore if $\Delta(t)$ is a solution of the eq.(3.26), then $\Delta(t+T)$ is also its solution.

According to the Floquet solutions the kth solution of eq.(3.26) can be written as,

$$\Delta_k(t+T) = \rho_k \, \Delta_k(t) \tag{3.27}$$

where ρ_k is the characteristic constant.

These solutions which acquire a constant multiplier by the addition of the period T to t, can be represented in the form

$$\Delta_k(t) = \chi_k(t) e^{(t/T)\ln\rho_k} \tag{3.28}$$

where $\chi_k(t)$ is a periodic function of period T.

It follows from the eq.(3.28) that the behaviour of the solutions as $t \to \infty$, depends on the value of the characteristic roots, more precisely, on the value of its moduli.

Taking in to account that $\ln\rho_k = \ln|\rho_k| + i \arg\rho_k$,

$$\Delta_k(t) = \Phi_k(t) e^{(t/T)\ln|\rho_k|} \tag{3.29}$$

where $\Phi_k(t) = \chi_k(t) e^{(it/T)\arg\rho_k}$ (3.30)

If the characteristic number ρ_k is greater than unity, then the corresponding solution, eq.(3.29) will have an unbounded exponential multiplier, hence the solution is unlimited. If the same characteristic number is less than unity, then the corresponding solution is damped as t increases. Finally, if the characteristic number is equal to unity, then the solution is periodic, i.e. it will be bounded in time. These are the conclusions of the Floquet theory.

Thus the periodic solutions characterise the boundary conditions between the dynamic stability and instability zones. So the periodic solution can be expressed as Fourier series.

A solution with period $2T$ is represented by:

$$\Delta(t) = \sum_{K=1,3...}^{\infty} \left[\{a_k\} \sin \frac{K\Omega\ t}{2} + \{b_k\} \cos \frac{K\Omega\ t}{2} \right] \tag{3.31}$$

A solution with period T is represented by:

$$\Delta(t) = \{a_o\} + \sum_{K=2,4...}^{\infty} \left[\{a_k\} \sin \frac{K\Omega\ t}{2} + \{b_k\} \cos \frac{K\Omega\ t}{2} \right]$$

(3.32)

The boundaries of the principal instability regions with period $2T$ are of practical importance [17]. If the series expansions of eq.(3.31) are used in eq.(3.26), term wise comparison of the sine and cosine coefficients will give infinite systems of homogeneous algebraic equations for the vectors $\{a_k\}$ and $\{b_k\}$ for the solutions on the stability borders. Non-trivial solutions exist if the determinant of the coefficient matrices of these equation systems of infinite order vanishes. When looking for numerical solutions, systems of finite order are required and as it is shown in reference [17], a sufficiently close approximation of the infinite eigenvalue problem is obtained by taking k=1 in the expansion in eq.(3.31) and putting the determinant of the coefficient matrices of the first order equal to zero. This technique is adopted originally in reference [17].

Substituting the first order (k=1) Fourier series expansion of eq.(3.31) in eq.(3.26) and comparing the coefficients of $\sin\frac{\Omega t}{2}$ and $\cos\frac{\Omega t}{2}$ terms, the condition for existence of these boundary solutions with period 2T is given by

$$\left([K]-(\alpha \pm \beta/2)P^{*}[K_g]-\frac{\Omega^2}{4}[M]\right)\{\Delta\}=0 \tag{3.33}$$

Equation(3.33) represents an eigenvalue problem for known values of α, β *and* P^{*}. This equation gives two sets of eigenvalues (Ω) bounding the regions of instability due to the presence of plus and minus sign. The instability boundaries can be determined from the solution of the equation

$$\left|[K]-(\alpha \pm \beta/2)P^{*}[K_g]-\frac{\Omega^2}{4}[M]\right|=0 \tag{3.34}$$

Also the eq. (3.33) represents the solution to a number of related problems.

(i) For free vibration: $\alpha = 0, \beta = 0$ & $\omega = \frac{\Omega}{2}$

Equation (3.33) becomes

$$\left([K]-\omega^2[M]\right)\{\Delta\}=0 \tag{3.35}$$

(ii) For vibration with static axial load:

$$\beta = 0, \alpha \neq 0, \omega = \frac{\Omega}{2}$$

Equation (3.33) becomes

$$\left([K]-\alpha P^{*}[K_g]-\omega^2\ [M]\right)\{\Delta\}=0$$

(3.36)

(iii) For static stability: $\alpha = 1, \beta = 0, \Omega = 0$

Equation (3.33) becomes

$$\left([K] - P^*[K_g] \right)\{\Delta\} = 0 \tag{3.37}$$

(iv) For dynamic stability, when all terms are present

Let $\Omega = \left(\dfrac{\Omega}{\omega_1}\right) \omega_1$

where ω_1 is the fundamental natural frequency of the beam without damage and having similar boundary conditions. Equation (3.33) then becomes

$$\left([K] - \left(\alpha \pm \frac{\beta}{2}\right) P^*[K_g] - \Theta \frac{\omega_1^2}{4}[M] \right)\{\Delta\} = 0 \tag{3.38}$$

where $\Theta = \left(\dfrac{\Omega}{\omega_1}\right)^2$

The fundamental natural frequency ω_1 and critical static buckling load P^* can be solved using the eqs. (3.35) and (3.37) respectively. The regions of dynamic instability can be determined from eq.(3.38).

3.3 Computational procedure

In the initialisation phase, geometry and material parameters are specified. For example for a Timoshenko beam with localised damage, material parameters like Young's modulus, mass density and shear modulus of the beam material and geometric parameters like dimensions of the beam, also the specifications of the damage like size of the damage, location of the damage and extent of damage are supplied as input data to the computer program. The beam is divided in to n number of elements and n+1 number of nodes. The elements of the element mass, elastic stiffness and geometric stiffness matrices are computed by Gauss-Legendre numerical integration method. The program uses the built in Matlab function, ‘quadl’ to carry out the integration. Element matrices are assembled to obtain the global matrices. Boundary conditions are imposed by elimination method. For example for Timoshenko beam with fixed-free end conditions the first two rows and columns of the global matrices are eliminated to obtain the reduced matrices. The natural frequencies and buckling loads are calculated solving the eigenvalue problems in eq. (3.35) and eq.(3.37) respectively. The built in Matlab function ‘eig’ is used to calculate the eigenvalues and eigenvectors. The static load factor α is set to the required value. The dynamic load factor β is increased in steps from zero and for each set of values of α, β and P^* the excitation frequencies at the stability boundaries are obtained by solving for the eigenvalues of the eq.(3.34). The lower limit (boundary frequency ratios Θ_1) of the instability region is obtained; calculating the eigenvalues of $\left| \frac{4}{\omega_1^2}\left[[M]^{-1}[K]-\left(\alpha+\frac{\beta}{2}\right)P*[M]^{-1}\left[K_g\right]\right]-\Theta\,\mathrm{I} \right| = 0$ and upper limit (boundary frequency ratios Θ_2) of the instability regions are obtained; calculating the eigenvalues of $\left| \frac{4}{\omega_1^2}\left[[M]^{-1}[K]-\left(\alpha-\frac{\beta}{2}\right)P*[M]^{-1}\left[K_g\right]\right]-\Theta\,\mathrm{I} \right| = 0$. The plot of Θ_1 versus β gives the lower boundary of the instability region, whereas plot of Θ_2 versus β gives the upper boundary of the instability regions. The computational procedure to obtain the boundary frequencies of the instability regions is shown schematically in the flow chart given in Appendix-A. The entire computational process has been accomplished by computer codes developed in MATLAB [135].

3.4 Results and discussion

A beam of length 0.5m, width 20mm and thickness 6.0mm is considered for theoretical analysis. The Young's modulus of the beam material is taken to be 2.07×10^{11} N/m^2. The following non-dimensional parameters are used to study the effects of the damage; (i)ξ_b = EK_b/EI, the ratio of the effective stiffness of the damaged portion to that of the undamaged beam - this is a measure of the extent of damage in bending sense;(ii) ξ_s =$GK_s/k'GA$, ratio of the effective stiffness of the damaged portion to that of undamaged beam - this is a measure of the extent of damage in shear sense, (iii) ψ = f/L, the non-dimensional position of damage and (iv) τ = (d-c)/L, size parameter of the damaged region.

The extent of damage both in bending ξ_b and shear ξ_s has been taken equal and results are obtained for values of ξ_b and ξ_s equal to 0.5 and 1.0 (undamaged condition). Position parameters (ψ) of the damaged region are taken to be 0.1, 0.3, 0.5, 0.7 and 0.9 respectively. In the computations the shear coefficient K' is taken as 0.85. The size parameter (τ) of the damaged region is taken as 0.2. $\xi_b = \xi_s = \xi$ has been taken to mark the extent of damage on the graphs. Convergence for the natural frequencies and buckling loads for the first five modes was obtained with a ten-element discretisation. This discretisation also gives satisfactory convergence for the boundary frequencies of the instability regions.

The boundary frequencies of the first instability region for an undamaged Euler beam with pinned-pinned end condition have been compared with those of reference [16] and they are found to be in very good agreement. This is presented in Table 3.1.

Table-3.1 Comparison of boundary frequencies of the first instability region obtained from present analysis with reference [16], for an undamaged Euler beam with pinned-pinned end conditions. Static load factor α = 0.0.

Dynamic load factor(β)	Lower limit of boundary frequency ratio (Ω_1/ω_1)		Upper limit of boundary frequency ratio (Ω_2/ω_1)	
	Reference[16]	Present	Reference[16]	Present
0	2.0057	2.0006	2.0057	2.0006
0.2	1.8994	1.8979	2.0971	2.0983
0.4	1.7924	1.7893	2.1886	2.1917
0.6	1.6827	1.6736	2.28	2.2812
0.8	1.5547	1.5494	2.3565	2.3674
1.0	1.4114	1.4142	2.4476	2.4505

The boundary frequencies obtained from the present analysis for a cantilever column for different static load factors α=0.0 and α=0.75, have been compared with reference [111] and they are found to be in very good agreement. The comparison is presented in Table 3.2.

Table-3.2 Comparison of boundary frequencies of the first instability region obtained from the present analysis with reference [111], for an undamaged cantilever beam for static load factors α=0.0 and α=0.75.

Dynamic load factor(β)	α = 0.0				α = 0.75			
	Lower limit of boundary frequency ratio (Ω_1/ω_1)		Upper limit of boundary frequency ratio (Ω_2/ω_1)		Lower limit of boundary frequency ratio (Ω_1/ω_1)		Upper limit of boundary frequency ratio (Ω_2/ω_1)	
	Present	Ref.[111]	Present	Ref.[111]	Present	Ref.[111]	Present	Ref.[111]
0	2.000	2.000	2.000	2.000	1.029	1.030	1.029	1.030
0.2	1.905	1.904	2.090	2.090	0.979	0.979	1.079	1.079
0.4	1.801	1.802	2.174	2.175	0.925	0.924	1.127	1.126
0.6	1.694	1.692	2.257	2.257	0.865	0.865	1.172	1.171
0.8	1.573	1.573	2.334	2.334	0.802	0.802	1.213	1.214
1.0	1.442	1.442	2.409	2.408	0.733	0.733	1.256	1.256

Figure (3.3) shows the effect of damage position parameter on the fundamental natural frequency of the beam under four boundary conditions considered. As expected for the fixed-fixed case the frequency has the highest value and is minimum for the fixed-free end condition for any position of the damage. For fixed-free end condition the fundamental frequency has the minimum value when the damage is located near to the fixed end and it increases as the damage moves towards the free end. For pinned-pinned and fixed-fixed end conditions the minimum value occurs, when the damage is at the middle. For fixed-pinned case the beam has minimum fundamental frequency when the damage position is in between middle and pinned end.

Figures (3.4-3.5) show the second and third mode frequencies, which shows that values of both the frequencies depend on the damage position for different boundary conditions.

Figure (3.6) shows the effect of damage position on the critical buckling load. The buckling load varies with damage position in the same manner as that of fundamental frequency for the four boundary conditions.

In figs.(3.7–3.10) the instability regions for a damaged beam for various locations of damage are shown along with the instability region for an undamaged beam(ξ=1.0) for the four boundary conditions . It is seen that the instability regions for an undamaged beam occur at higher excitation frequency compared to a beam with damage at any location. This means that presence of localised damage or in other words extent of damage enhances the instability of the beam, since parametric instability occurs at lower frequency of excitation.

Figures 3.7(a)-3.7(c) show the first three instability regions respectively for fixed-free end condition for different damage positions. It is seen from fig. 3.7(a) that as the damage moves from the fixed end to the free end the first principal instability region moves away from the dynamic load factor axis and the width of the instability regions reduces. When the damage is near to the free end the instability region almost coincides with the instability region for the undamaged beam. This means that the damage near the fixed end is more severe on the dynamic instability behavior than that of the damage located at other positions, so far as first instability region is concerned. Figure 3.7(b) shows that the beam is most unstable so far as second instability region is concerned, when the damage is located at the middle. Figure 3.7(c) shows that the third principal instability region occurs at minimum frequency of excitation when the damage position is in between the middle and free end.

Figures 3.8(a)-3.8(c) show the first three instability regions respectively for pinned-pinned end conditions. The first instability region occurs at minimum frequency of excitation when the damage is located at the middle. When the damage moves towards any of the pinned end from middle the first instability zone moves away from the dynamic load factor axis. The second instability region occurs at minimum frequency of excitation when the damage is located in between middle and any one of the pinned ends and at highest frequency when the damage is located at the middle. The third instability zone occurs at minimum frequency of excitation when the damage is at the middle. Because of symmetry, instability zones for ψ =0.1 coincides with ψ =0.9 and ψ =0.3 coincides with ψ =0.7.

Figures 3.9(a)-3.9(c) show the first three instability regions respectively for the beam with fixed-fixed end conditions. The first instability region occurs at minimum frequency of excitation when the damage is at the middle and relocates itself at higher frequency when the damage is away from the middle position. The second instability region occurs at minimum frequency of excitation when the damage is in between middle and either of the fixed ends of the beam and at highest frequency of excitation for ψ =0.5.

Third instability region occurs at minimum frequency of excitation when the damage is at the middle. Because of symmetry instability zones for ψ =0.1 coincides with ψ =0.9 and ψ =0.3 coincides with ψ =0.7.

Figures 3.10(a)-3.10(c) show the first three instability regions respectively for fixed-pinned end condition. From fig. 3.10(a) it is seen that the first instability region occurs at minimum frequency of excitation when the damage position is in between the middle and the pinned end and it occurs at highest frequency of excitation when the damage is in between the middle and fixed end. The second principal instability region occurs at minimum frequency of excitation when the damage is located in between the fixed end and the middle, fig. 3.10(b). Whereas the third principal instability region occurs at minimum frequency of excitation when the damage is located nearer to the pinned end, fig. 3.10(c).

Figures 3.11(a)-3.11(c) show the first three instability regions respectively for fixed-free end condition for static load factor α=0.0 and α=0.5. It is seen that the static load component shifts the instability regions towards the lower frequency of excitation and there is also increase in areas of the instability regions. The effect is more predominant on the first instability region than on other two regions. This means that the static load component has a destabilising effect in terms of the shifting of the instability regions towards lower frequencies of excitation and increase in areas of the instability regions.

Figures 3.12(a)-3.12(c) show the first three instability regions respectively for pinned-pinned end condition for static load factor α=0.0 and α=0.5. Similar behaviour as those for fixed-free end condition is also observed in this case.

Figures 3.13(a)-3.13(c) show the effect of α on the instability regions for fixed-fixed end condition. Static load component has a destabilising effect in terms of shifting of the instability regions to lower frequencies of excitation and increase in areas.

Figures 3.14(a)-3.14(c) show the effect of α for fixed-pinned case. The effect is same as those for other three end conditions discussed earlier.

3.5 Closure

The effect of localised damage on the stability of a beam with various boundary conditions has been analysed. The critical position of the damage for minimum values of natural frequencies depends on the boundary conditions and mode number. Critical buckling load also depends on the damage location and boundary conditions. Presence of damage always increases the instability of the beam. The critical position of the damage for maximum destabilising effect on the beam is different depending on the boundary conditions and the principal regions of instability of interest. Increase in static load component has a destabilising effect for all boundary conditions considered. It is observed that the dynamic stability behaviour of the beam depends not only upon the boundary conditions but also on the location of the damage.

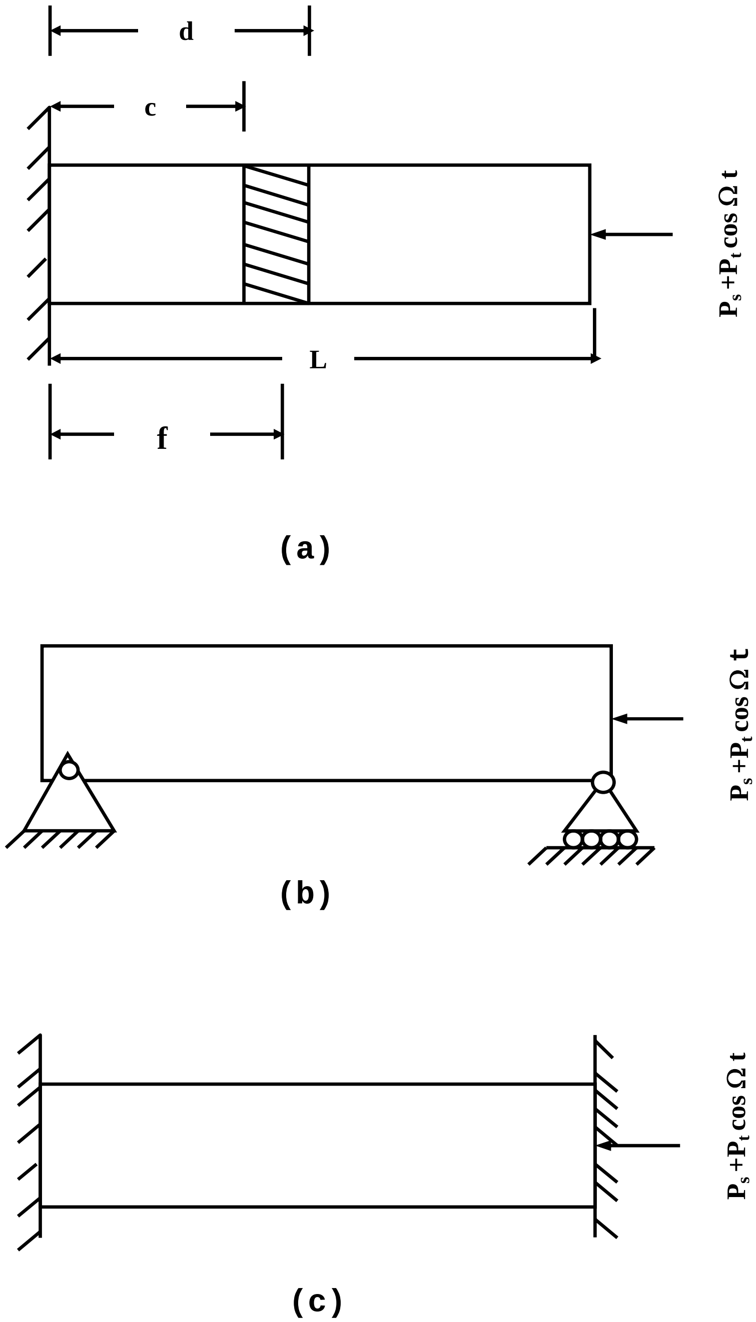

Fig 3.1

Fig.-3.1, Beam with boundary conditions;
(a) Fixed-free, (b) Pinned-pinned, (c) Fixed-fixed,
(d) Fixed-pinned.

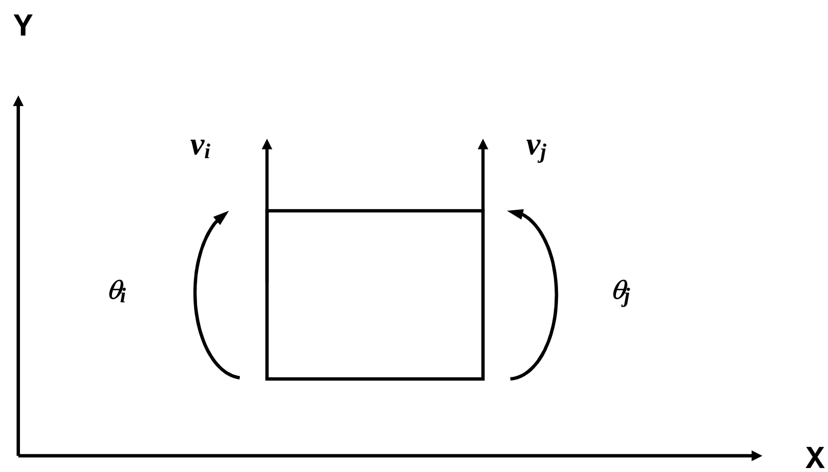

Fig.-3.2, Timoshenko beam element.

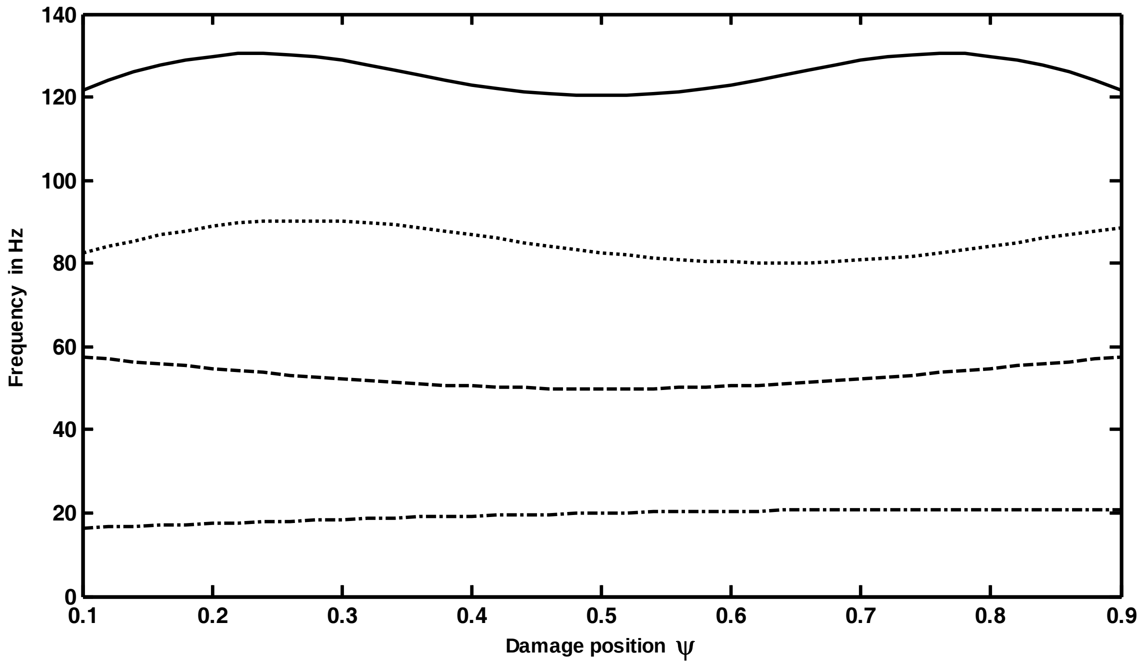

Fig.- 3.3,Effect of damage position on first mode frequency, ξ=0.5, fixed-fixed;- ,fixed-pinned;...,pinned-pinned; - -, fixed-free;-.- ,.

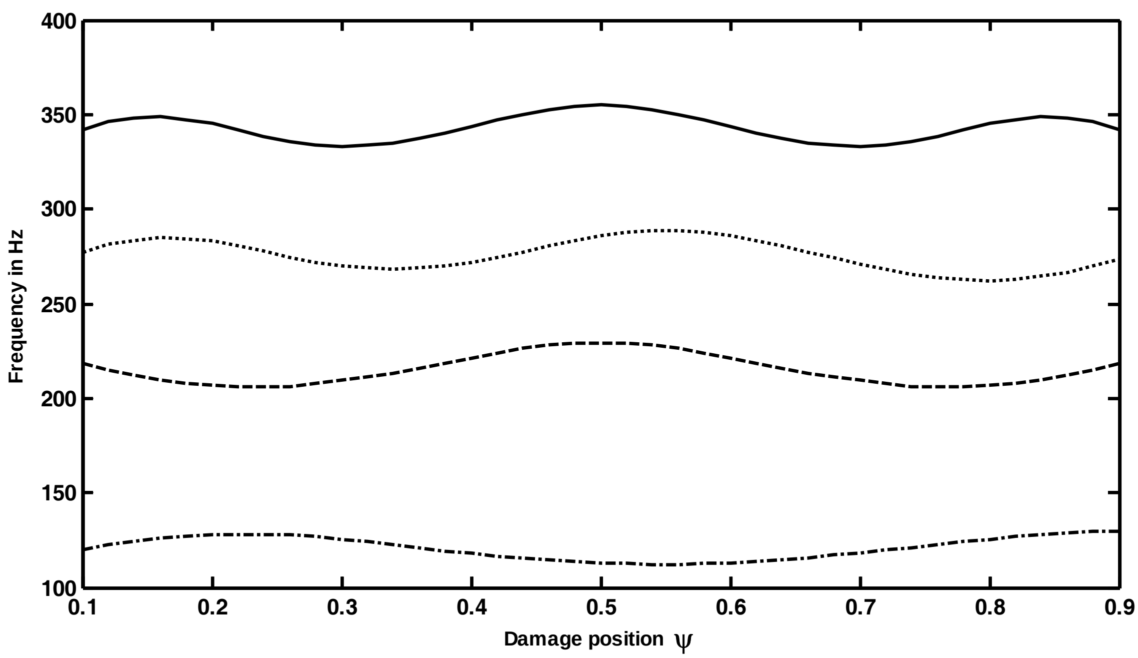

Fig.- 3.4,Effect of damage position on second mode frequency, ξ=0.5,key as fig.- 3.3.

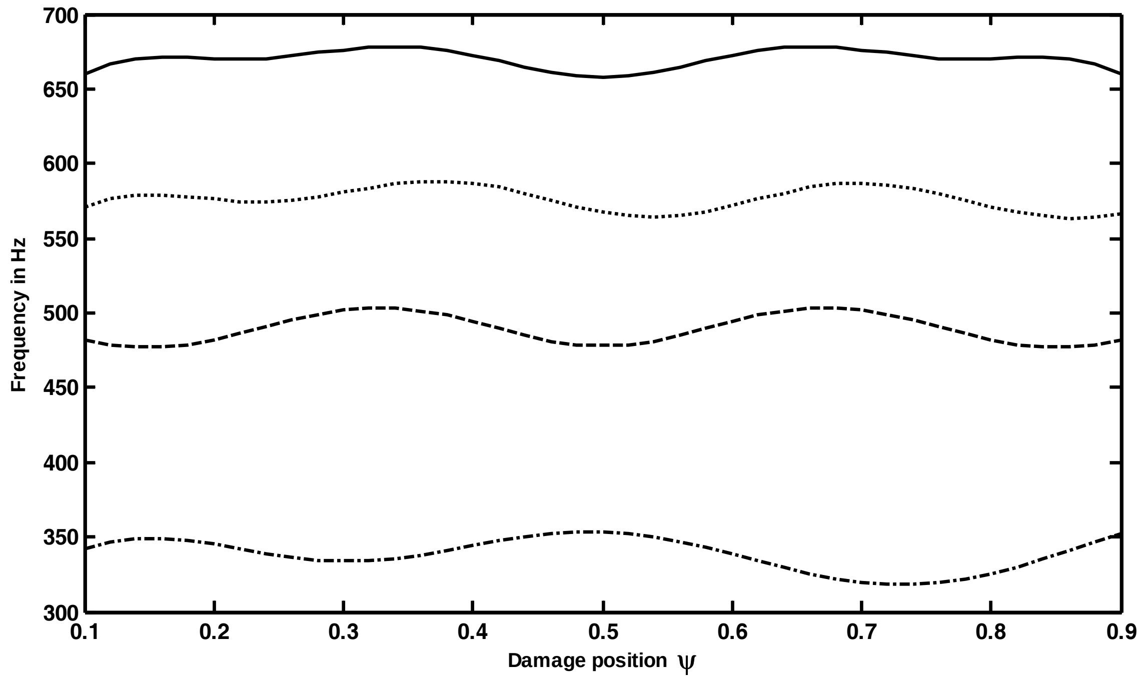

Fig.- 3.5,Effect of damage position on third mode frequency, ξ=0.5,key as fig.- 3.3.

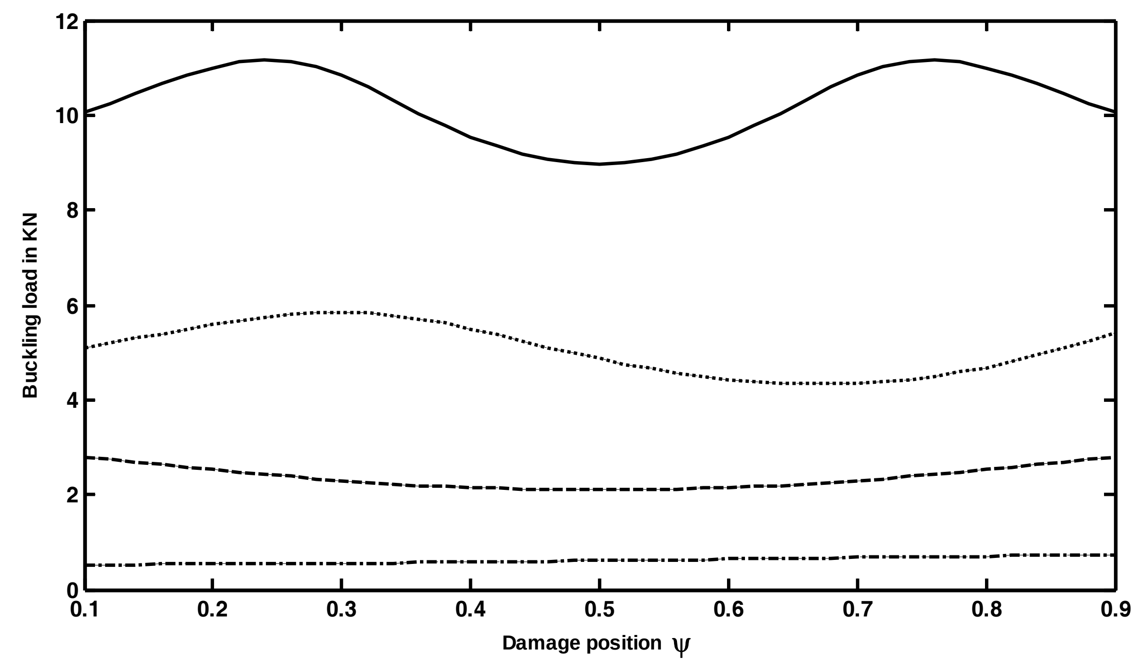

Fig.- 3.6,Effect of damage position on first mode buckling load, ξ=0.5,key as fig.- 3.3.

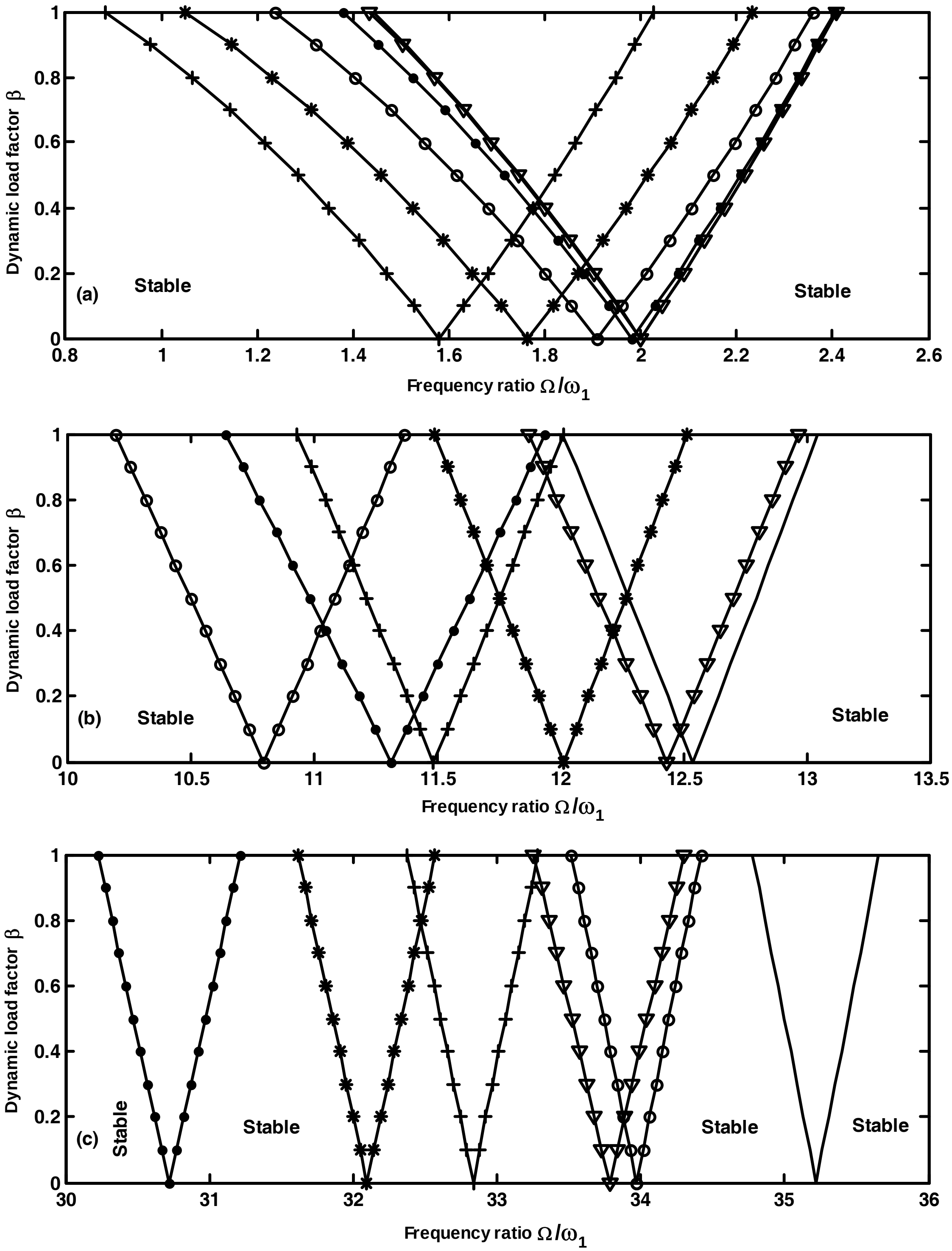

Fig.- 3.7,Effect of damage position on instability regions,fixed-free end condition, α=0.0,ξ=1.0;-,ξ=0.5;ψ = 0.1(+),ψ = 0.3 (*),ψ = 0.5(o),ψ =0.7(•),ψ =0.9($\vee$).

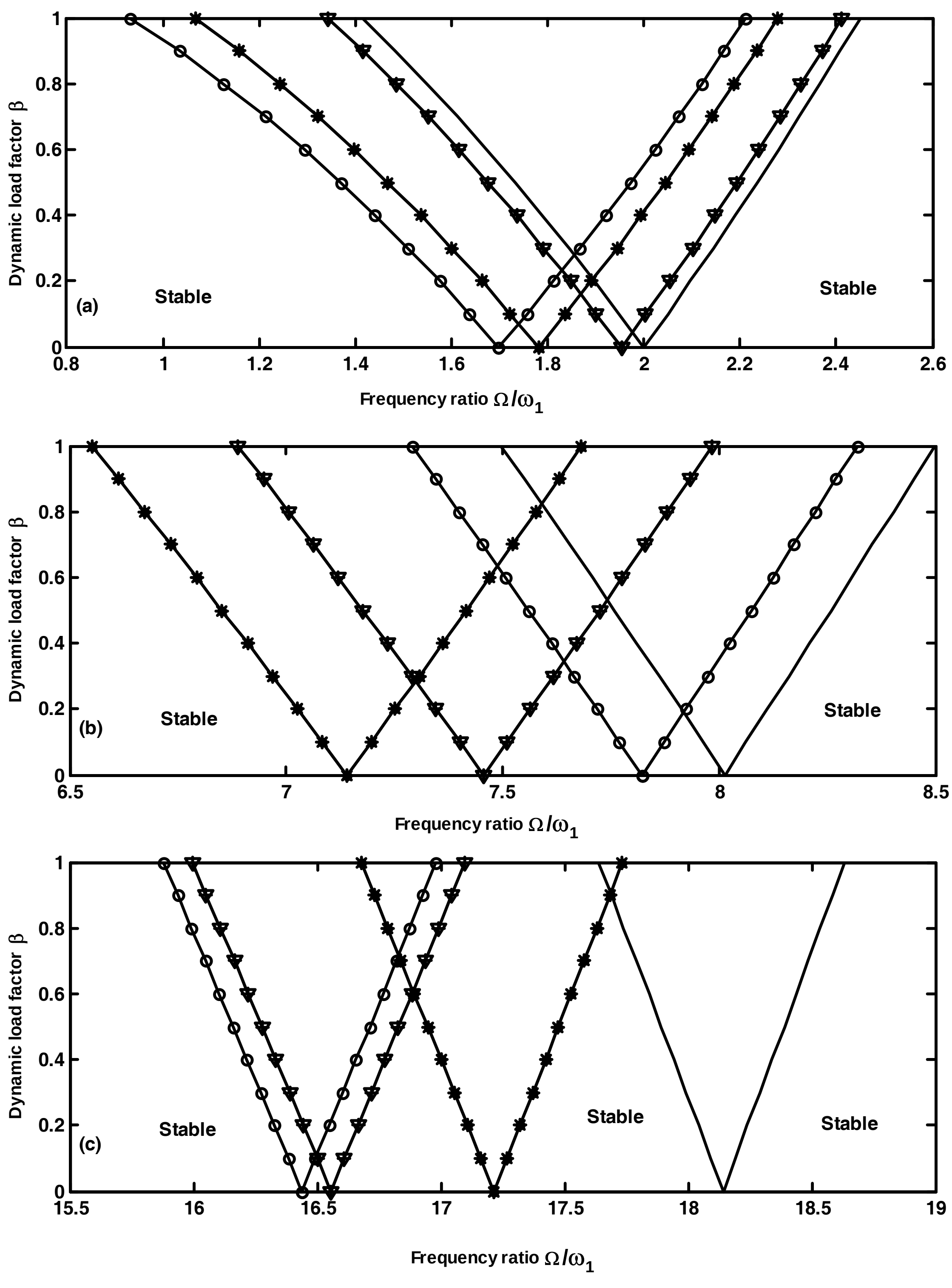

Fig.- 3.8,Effect of damage position on instability regions, pinned-pinned end condition,α =0.0,ξ=1.0;-,ξ=0.5;key as fig.- 3.7.

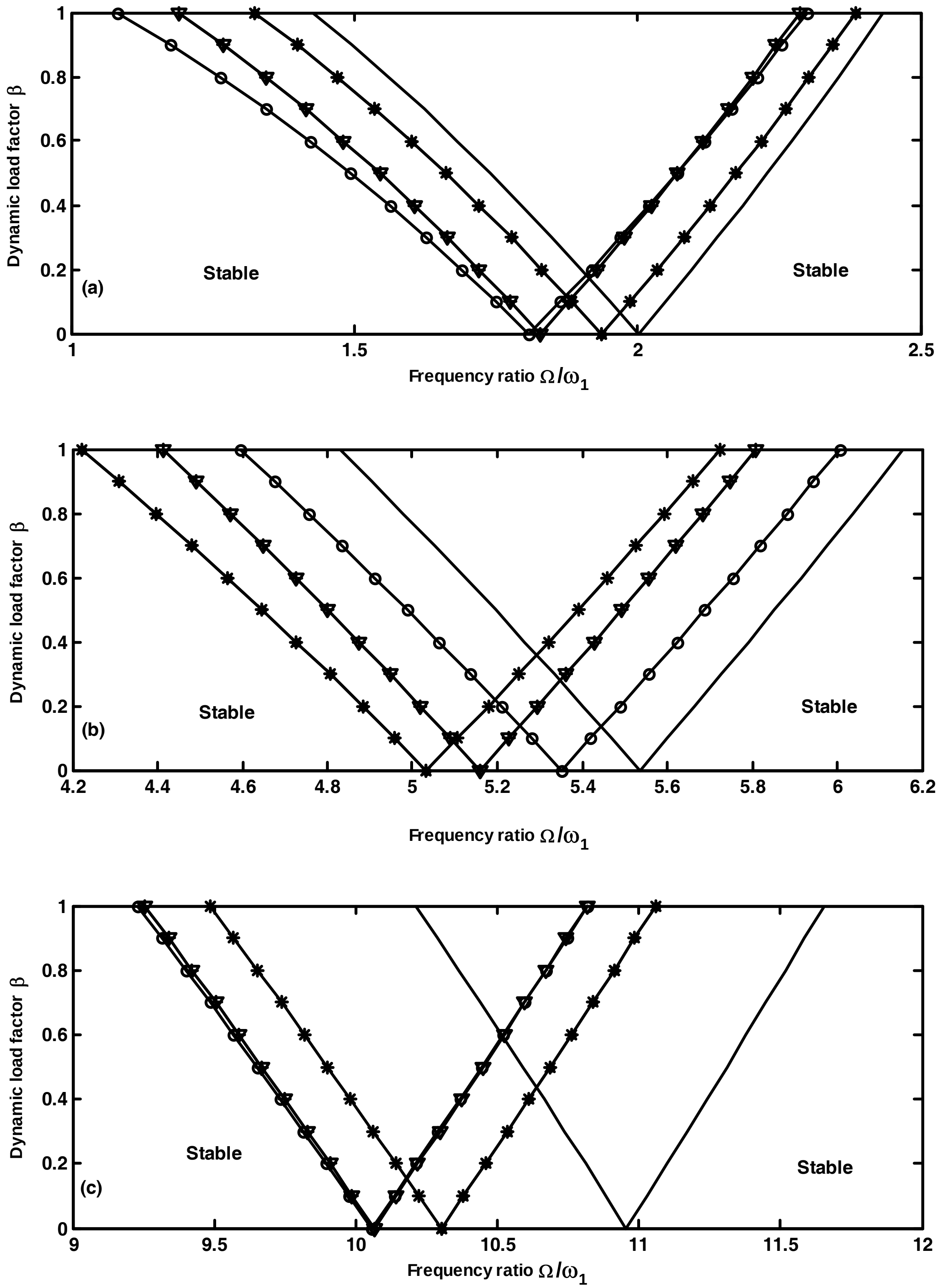

Fig.- 3.9,Effect of damage position on instability regions,fixed-fixed end condition, α =0.0,ξ=1.0;-,ξ=0.5;key as fig.- 3.7.

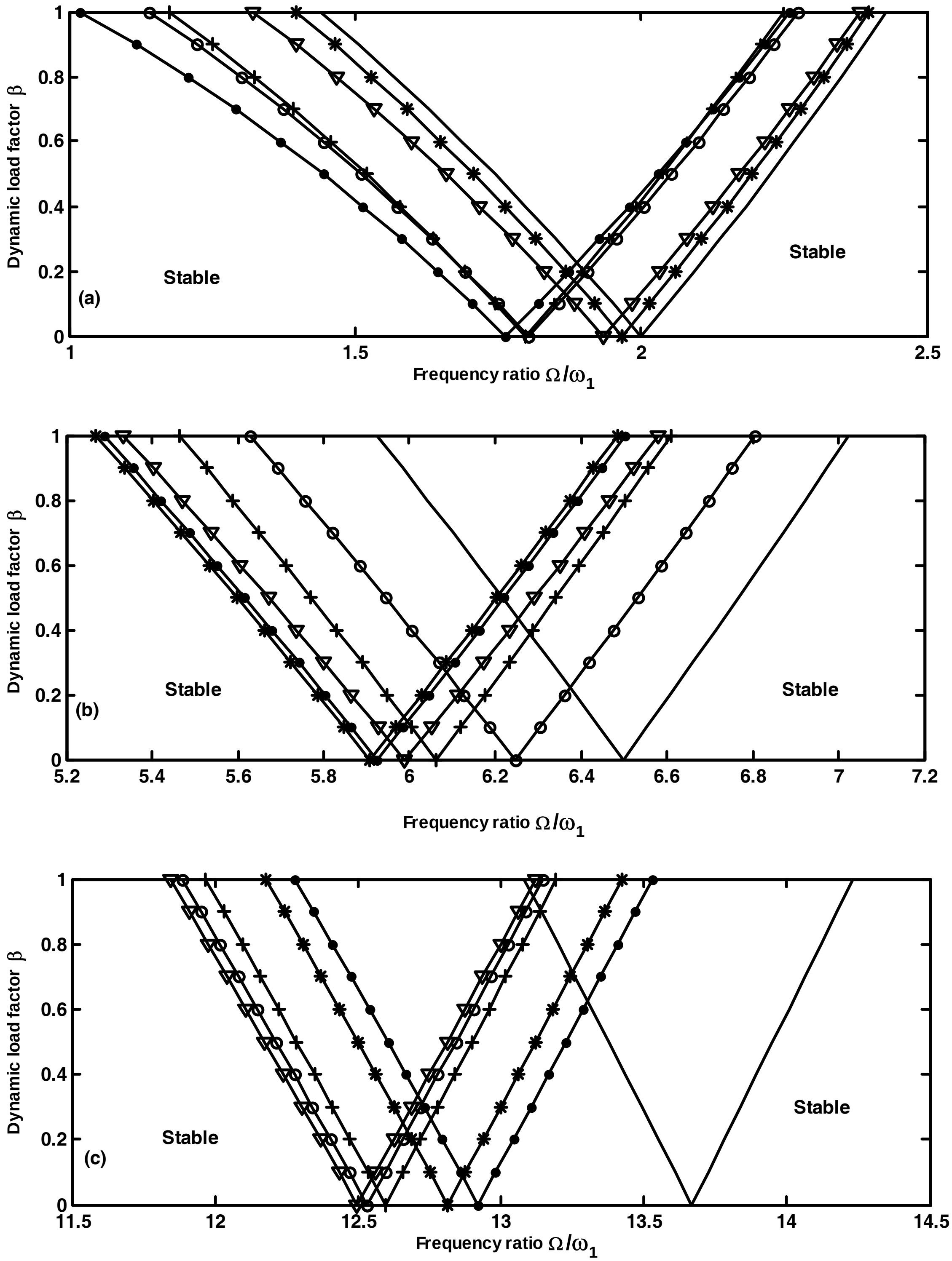

Fig.- 3.10,Effect of damage position on instability regions,

fixed-pinned end condition,α =0.0,ξ=1.0;-,ξ=0.5;key as fig.- 3.7.

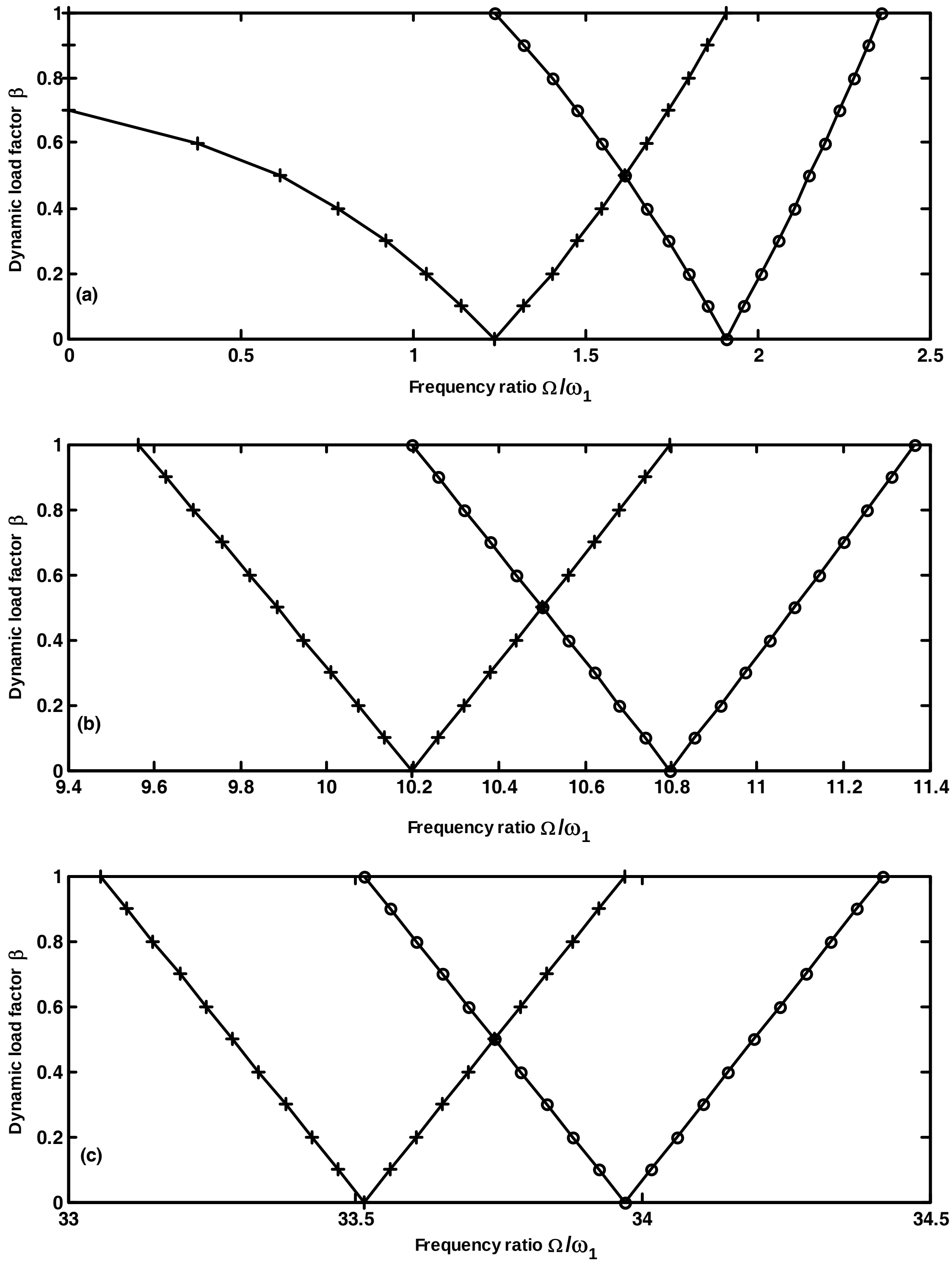

Fig.- 3.11,Effect of static load factor on instability regions,fixed-free end condition, ξ=0.5,ψ =0.5;α=0.0(o);α =0.5(+).

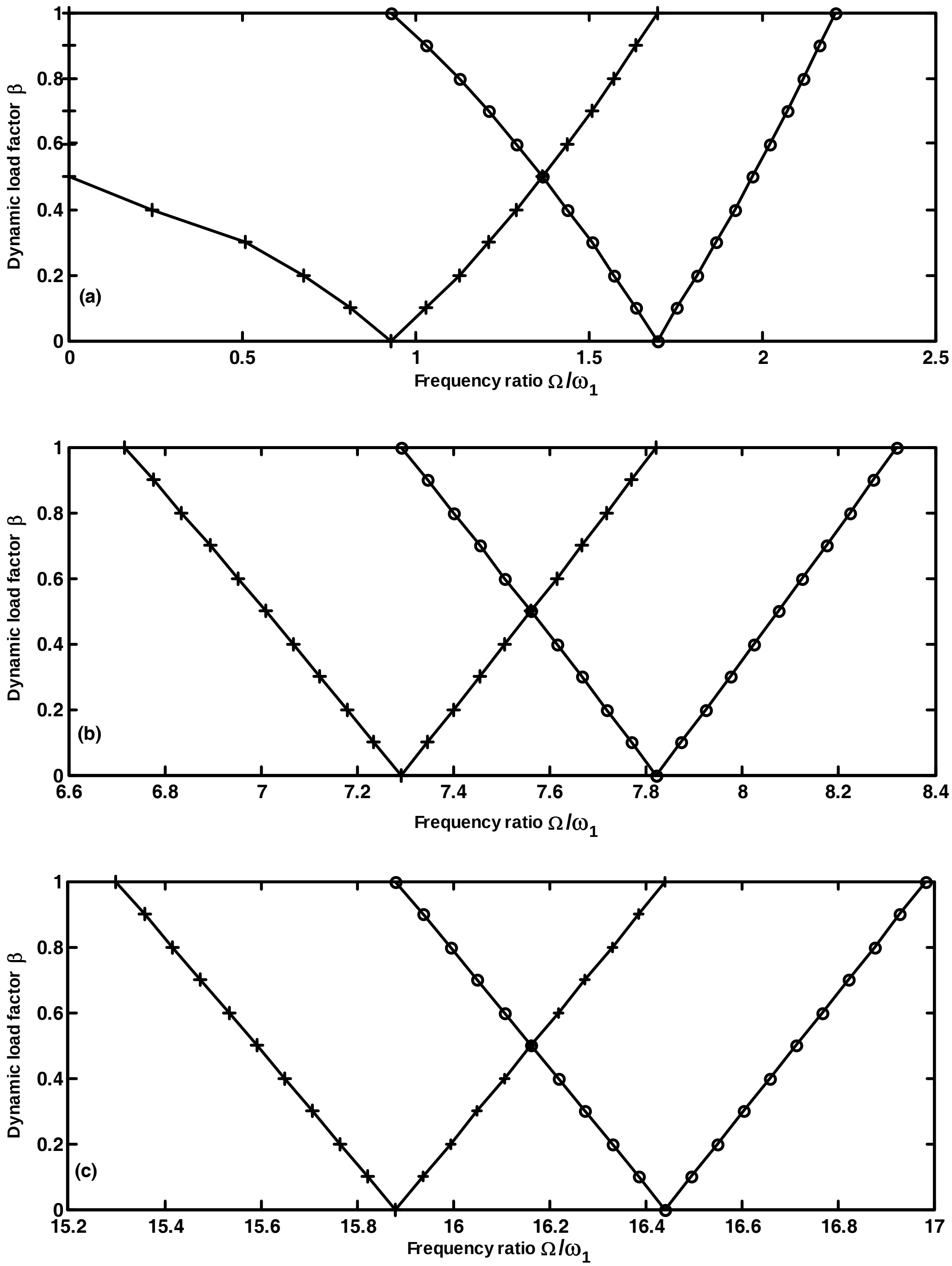

Fig.- 3.12, Effect of static load factor on instability regions, pinned-pinned end condition, ξ=0.5, ψ =0.5; key as fig.- 3.11.

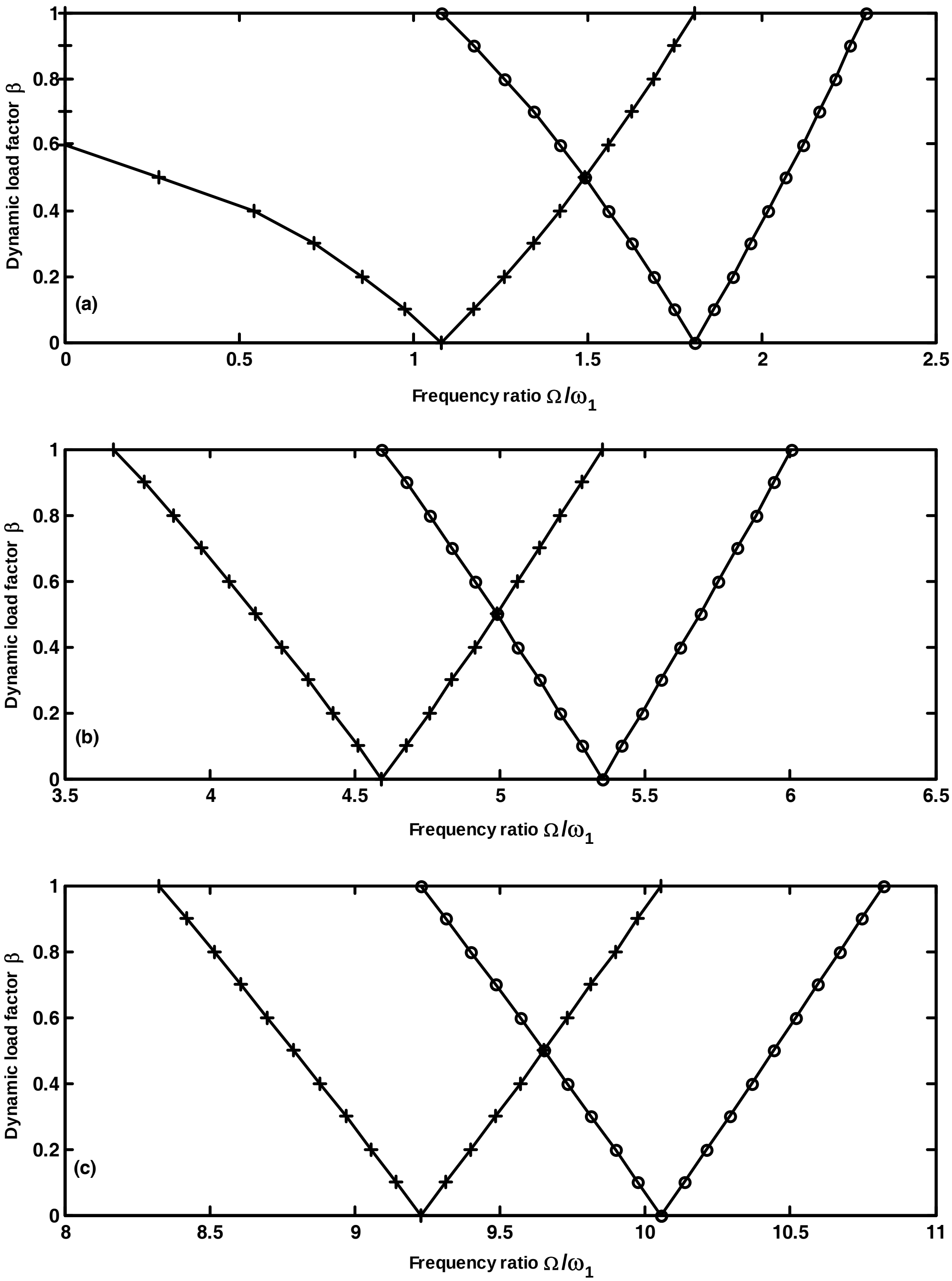

Fig.- 3.13,Effect of static load factor on instability regions,fixed-fixed end condition, ξ=0.5,ψ =0.5;key as fig.- 3.11.

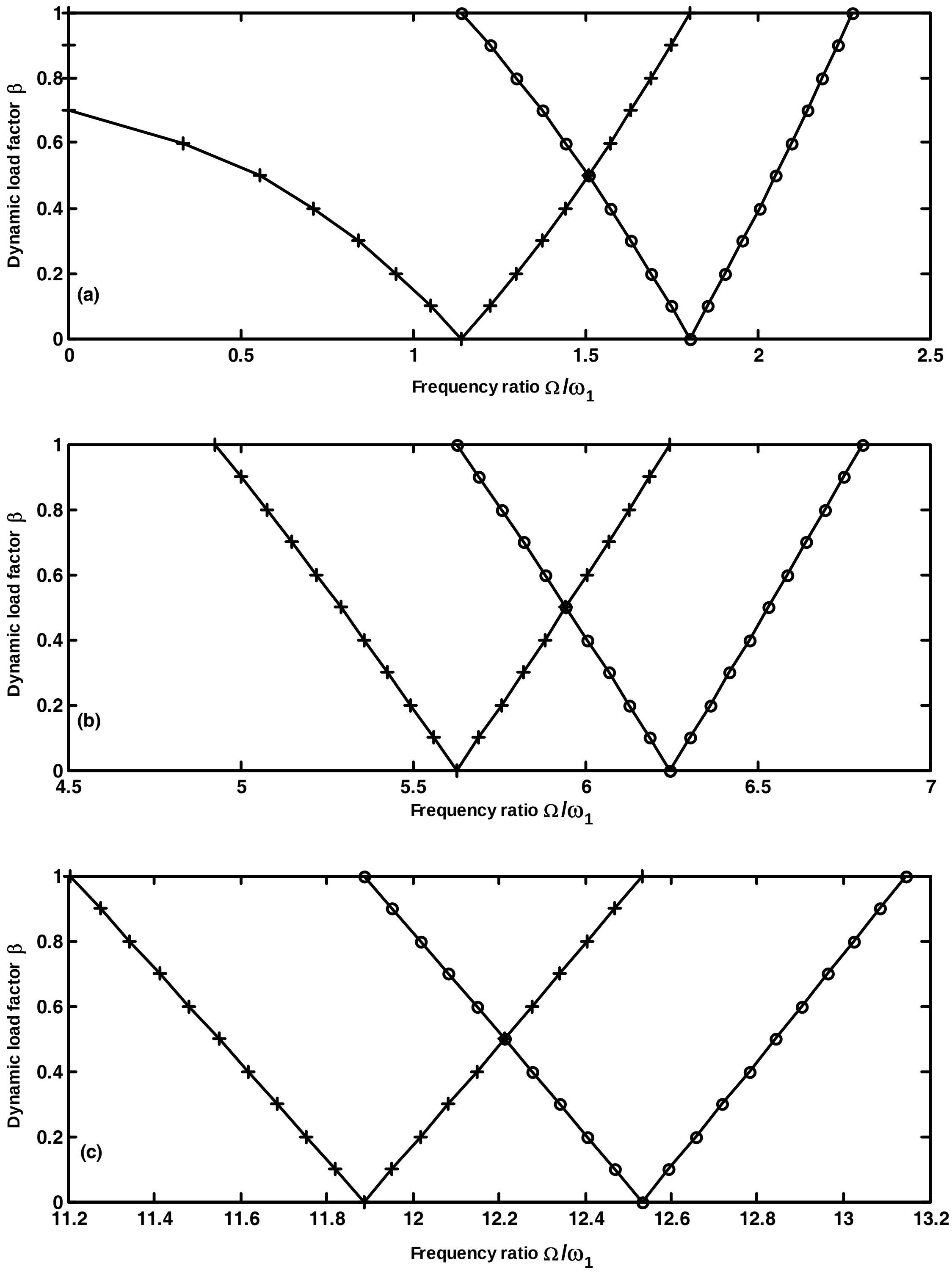

Fig.- 3.14,Effect of static load factor on instability regions, fixed-pinned end condition, ξ=0.5,ψ =0.5;key as fig.- 3.11.

Chapter 4

DYNAMIC STABILITY OF A PRETWISTED CANTILEVER BEAM WITH LOCALISED DAMAGE UNDER PERIODIC AXIAL FORCE

4.1 Introduction

Twisted beams have wide application in many industrial problems. Compressor blades, turbine blades, aircraft propeller blades, helicopter rotor blades, twist drill bits etc. can be modeled as twisted cantilever beams. The dynamic stability analysis of these elements is of considerable importance. Though there are many alloys and composite materials having high strength to weight ratio have been developed, during the manufacturing of these materials, inclusion of flaws affects their structural strength. Effect of localised damages on the stability behaviour of structural elements is of great importance.

There are relatively a few studies on the dynamic behaviour of pre-twisted beams. The earliest vibration analysis of pre-twisted beams was reported by Troesch et al. [126] and Anlinker and Troesch [4]. Gupta and Rao [46] reported the natural frequencies of tapered Timoshenko beam using finite element method. Carniege Thomas [20] analysed the coupled bending-bending vibration of pretwisted cantilever Euler beams. Subrahmanyam et al. [117] studied the vibration of pre-twisted cantilever beams using the Reissner method. Banerjee [9] studied the free vibration of twisted beams by dynamic stiffness method. The stability of pretwisted columns under compressive axial loads was reported by Frisch-Fay [42]. Celep [21] analysed the dynamic stability of a simply supported pretwisted column. Gürgöze [47] studied the dynamic stability of pretwisted beams with hinged-hinged, clamped-clamped and clamped-hinged boundary conditions.

Many investigators as mentioned earlier have studied the effect of localised damage on the dynamic stability of beams. Reported literature show that the effect of localised damage on the dynamic stability of a pretwisted cantilever beam has not been investigated.

In the present work the effects of a localised damage on the dynamic stability of a pretwisted cantilever beam subjected to a time-dependent conservative end axial force is studied. The effects of parameters like the pretwist angle, the extent of damage, position of the damage and static load factor are studied. Three parameters are used to characterise the damaged region: location, size, and effective stiffness of the damaged region. Euler beam theory is used in the analysis. The equation of motion has been derived using finite element method. The principal instability regions are established by Floquet's theory.

4.2 Formulation of the problem

The considered twisted beam configuration is shown in fig.4.1(a). The beam is of uniform rectangular cross-section and the angle of twist of the cross-section is assumed to be varying linearly along the length. The beam has a length L, width b and depth h. The angle of pretwist at the free end is θ_l with respect to the fixed end. The effect of the damage is represented by the presence of a flaw in the region c < x < d. The beam is subjected to a pulsating axial force $P(t) = P_s + P_t \cos \Omega t$ acting along its undeformed axis, where Ω is the excitation frequency of the dynamic load, P_s is the static and P_t is the amplitude of the time dependent component of the load.

The degrees of freedom of a typical finite beam element are shown in fig.4.2. The element consists of two nodes and each node has four degrees of freedom: two translations and two rotations. v and w are the two translations in Y and Z directions and θ and φ are the two rotations about Z and Y axes. The translations and rotations are due to bending only.

4.2.1 Element matrices

The total strain energy ($U^{(e)}$) of an undamaged beam element of length l is expressed in the form

$$U^{(e)} = \frac{1}{2}\int_0^l EI_{zz}\left(\frac{\partial^2 v}{\partial x^2}\right)^2 dx + \frac{1}{2}\int_0^l EI_{yy}\left(\frac{\partial^2 w}{\partial x^2}\right)^2 dx + \int_0^l EI_{yz}\left(\frac{\partial^2 v}{\partial x^2}\right)\left(\frac{\partial^2 w}{\partial x^2}\right) dx - \frac{1}{2}\int_0^l P(t)\left[\left(\frac{\partial v}{\partial x}\right)^2 + \left(\frac{\partial w}{\partial x}\right)^2\right] dx \qquad (4.1)$$

where E is the Young's modulus. I_{yy}, I_{zz} and I_{yz} are the cross-sectional area moments and product of inertia of the beam with respect to the Y and Z axes, respectively.

The kinetic energy ($T^{(e)}$) of an undamaged beam element of length l is given as

$$\begin{aligned} T^{(e)} = & \frac{1}{2}\int_0^l \rho A\left(\frac{\partial v}{\partial t}\right)^2 dx + \frac{1}{2}\int_0^l \rho A\left(\frac{\partial w}{\partial t}\right)^2 dx + \frac{1}{2}\int_0^l \rho I_{zz}\left(\frac{\partial^2 v}{\partial x \partial t}\right)^2 dx \\ & + \frac{1}{2}\int_0^l \rho I_{yy}\left(\frac{\partial^2 w}{\partial x \partial t}\right)^2 dx + \int_0^l \rho I_{yz}\left(\frac{\partial^2 v}{\partial x \partial t}\right)\left(\frac{\partial^2 w}{\partial x \partial t}\right) dx \end{aligned} \qquad (4.2)$$

As the element is twisted, the moment of inertia I_{yy}, I_{zz} and I_{yz} are function of x. I_{yy}, I_{zz} and I_{yz} at any cross section x, can be expressed in terms of moment of inertia $I_{y'y'}$

and $I_{z'z'}$ of the cross section about principal inertia axes Y′Y′ and Z′Z′ respectively and angle of twist θ_t at the cross section x, fig.4.1(b).

$$\left.\begin{array}{l} I_{zz}\,(\mathrm{x}) = I_{z'z'} \cos^2\theta_t \;+ I_{y'y'} \sin^2\theta_t \\ I_{yy}\,(\mathrm{x}) = I_{y'y'} \cos^2\theta_t \;+ I_{z'z'} \sin^2\theta_t \\ I_{yz}\,(\mathrm{x}) \;= \frac{1}{2}(I_{z'z'} - I_{y'y'}) \sin 2\theta_t \\ I_{z'z'} = bh^3/12 \\ I_{y'y'} = hb^3/12 \end{array}\right\}$$

(4.3)

A cubic displacement distribution for both *v and w* is assumed over the element as

$$v = a_1 + a_2\, x + a_3\, x^2 + a_4\, x^3$$

$$w = a_5 + a_6\, x + a_7\, x^2 + a_8\, x^3 \tag{4.4}$$

where $a_1 - a_8$ are the generalised coordinates. The lateral displacements *v, w* within the element can be expressed in terms of the nodal displacement vector $\{\Delta^{(e)}\}$ and the shape function matrix $[N_S]$.

$$\{\Delta^{(e)}\} = \{v_i\ \theta_i\ v_j\ \theta_j\ w_i\ \varphi_i\ \ w_j\ \varphi_j\}^T$$

$$= \left[\{\Delta_v^{(e)}\}\{\Delta_w^{(e)}\}\right]^T$$

(4.5)

where $\{\Delta_v^{(e)}\} = \{v_i\, \theta_i\, v_j\, \theta_j\}$ and $\{\Delta_w^{(e)}\} = \{w_i\, \varphi_i\, w_j\, \varphi_j\}$

$$\begin{Bmatrix} v \\ w \end{Bmatrix} = \begin{bmatrix} \mathrm{N}_1 & \mathrm{N}_2 & \mathrm{N}_3 & \mathrm{N}_4 & 0 & 0 & 0 & 0 \\ 0 & 0 & 0 & 0 & \mathrm{N}_1 & \mathrm{N}_2 & \mathrm{N}_3 & \mathrm{N}_4 \end{bmatrix} \{\Delta^{(e)}\}$$

$$= \begin{bmatrix} [N] & [0] \\ [0] & [N] \end{bmatrix} \begin{bmatrix} \{\Delta_v^{(e)}\} \\ \{\Delta_w^{(e)}\} \end{bmatrix}$$

$$= [N_S]\{\Delta^{(e)}\} \tag{4.6}$$

where $[N] = [N_1\ N_2\ N_3\ N_4]$, $[0] = [0\ 0\ 0\ 0]$

$N_1 = [1\text{-}3\zeta^2 + 2\zeta^3]$

$N_2 = [\zeta\text{-}2\zeta^2 + \zeta^3]\ 1$

$N_3 = [3\zeta^2 \text{-} 2\zeta^3]$

$N_4 = [\text{-}\zeta^2 + \zeta^3]\ 1$

$\zeta = x/l$

With the help of equation (4.6) the potential energy $\left(U^{(e)}\right)$ and kinetic energy $\left(T^{(e)}\right)$ of the element can be expressed in terms of nodal displacement vector $\{\Delta^{(e)}\}$ as,

$$U^{(e)} = \frac{1}{2}\{\Delta^{(e)}\}^T [K^{(e)}]\{\Delta^{(e)}\} - \frac{1}{2}\{\Delta^{(e)}\}^T P(t)[K_g^{(e)}]\{\Delta^{(e)}\} \tag{4.7}$$

$$T^{(e)} = \frac{1}{2}\{\dot{\Delta}^{(e)}\}^T [M^{(e)}]\{\dot{\Delta}^{(e)}\} \tag{4.8}$$

where $[K^{(e)}], [K_g^{(e)}]$ *and* $[M^{(e)}]$ are element elastic stiffness matrix, geometric stiffness matrix and mass matrix respectively.

$$[K^{(e)}] = \begin{bmatrix} [K^1] & [K^3] \\ [K^3] & [K^2] \end{bmatrix} \tag{4.9}$$

$$[K^1] = \int_0^l [N]''^T E\, I_{zz}\ [N]''\ dx \tag{4.10}$$

$$[K^2] = \int_0^l [N]''^T E\, I_{yy}\ [N]''\ dx \tag{4.11}$$

$$\left[K^{3}\right]=\int_{0}^{l}\left[N\right]''^{T} E\, I_{yz}\left[N\right]'' \, dx \tag{4.12}$$

$$\left[K_{g}^{(e)}\right]=\begin{bmatrix}\left[K_{g}^{4}\right] & [0] \\ [0] & \left[K_{g}^{4}\right]\end{bmatrix} \tag{4.13}$$

$$\left[K_{g}^{4}\right]=\int_{0}^{l}\left[N\right]'^{T}\left[N\right]' dx \tag{4.14}$$

$$\left[M^{(e)}\right]=\begin{bmatrix}\left[M^{1}\right]+\left[M^{2}\right] & \left[M^{4}\right] \\ \left[M^{4}\right] & \left[M^{1}\right]+\left[M^{3}\right]\end{bmatrix} \tag{4.15}$$

$$\left[M^{1}\right]=\int_{o}^{l}\left[N\right]^{T}\rho\, A\left[N\right] dx \tag{4.16}$$

$$\left[M^{2}\right]=\int_{o}^{l}\left[N\right]'^{T} I_{zz}\left[N\right]' dx \tag{4.17}$$

$$\left[M^{3}\right]=\int_{o}^{l}\left[N\right]'^{T} I_{yy}\left[N\right]' dx \tag{4.18}$$

$$\left[M^{4}\right]=\int_{o}^{l}\left[N\right]'^{T} I_{yz}\left[N\right]' dx \tag{4.19}$$

$$\left[N\right]''=\frac{\partial^{2}}{\partial x^{2}}\left[N\right],\ \left[N\right]'=\frac{\partial}{\partial x}\left[N\right]$$

The total strain energy $\left(U_{d}^{(e)}\right)$ of an element within the damaged region is expressed in the form.

$$U_{d}^{(e)}=\frac{1}{2}\int_{0}^{l}(\xi_{b} EI_{zz})\left(\frac{\partial^{2} v}{\partial x^{2}}\right)^{2} dx+\frac{1}{2}\int_{0}^{l}(\xi_{b} EI_{yy})\left(\frac{\partial^{2} w}{\partial x^{2}}\right)^{2} dx+\int_{0}^{l}(\xi_{b} EI_{yz})\left(\frac{\partial^{2} v}{\partial x^{2}}\right)\left(\frac{\partial^{2} w}{\partial x^{2}}\right) dx-\frac{1}{2}\int_{0}^{l} P(t)\left[\left(\frac{\partial v}{\partial x}\right)^{2}+\left(\frac{\partial w}{\partial x}\right)^{2}\right] dx \tag{4.20}$$

The constant ξ_b represents the extent of damage in sense of bending stiffness. The elastic stiffness matrix of an element in the damaged region of the beam can be calculated

from eqs. (4.9-4.12) by using the corresponding effective stiffness of the damaged region.

Under the assumption that the deterioration produced does not involve a loss of material, the expression for the mass matrix of an element in the damaged region is same as that given in eq.(4.15).

4.2.2 Governing equations of motion

The potential energy *(U)* of the beam with damaged portion can be written as,

$$U = \frac{1}{2}\int_0^L EI_{zz}\left(\frac{\partial^2 v}{\partial x^2}\right)^2 dx + \frac{1}{2}\int_0^L EI_{yy}\left(\frac{\partial^2 w}{\partial x^2}\right)^2 dx + \int_0^L EI_{yz}\left(\frac{\partial^2 v}{\partial x^2}\right)\left(\frac{\partial^2 w}{\partial x^2}\right) dx + \frac{1}{2}\int_c^d (E\,I_{zz}(\xi_b - 1)\left(\frac{\partial^2 v}{\partial x^2}\right)^2 dx$$
$$+\frac{1}{2}\int_c^d EI_{yy}(\xi_b - 1)\left(\frac{\partial^2 w}{\partial x^2}\right)^2 dx + \int_c^d EI_{yz}(\xi_b - 1)\left(\frac{\partial^2 v}{\partial x^2}\right)\left(\frac{\partial^2 w}{\partial x^2}\right) dx - \frac{1}{2}\int_0^L P(t)\left[\left(\frac{\partial v}{\partial x}\right)^2 + \left(\frac{\partial w}{\partial x}\right)^2\right] dx \qquad (4.21)$$

Under the assumption that the deterioration produced does not involve a loss of material, the expression for kinetic energy (T) of the damaged beam is given as

$$T = \frac{1}{2}\int_0^L \rho A\left(\frac{\partial v}{\partial t}\right)^2 dx + \frac{1}{2}\int_0^L \rho A\left(\frac{\partial w}{\partial t}\right)^2 dx + \frac{1}{2}\int_0^L \rho I_{zz}\left(\frac{\partial^2 v}{\partial x \partial t}\right)^2 dx + \frac{1}{2}\int_0^L \rho I_{yy}\left(\frac{\partial^2 w}{\partial x \partial t}\right)^2 dx + \int_0^L \rho I_{yz}\left(\frac{\partial^2 v}{\partial x \partial t}\right)\left(\frac{\partial^2 w}{\partial x \partial t}\right) dx \qquad (4.22)$$

By dividing the beam in to several elements, the potential energy (U) and the kinetic energy (T) for the damaged beam can be written in terms of global displacement vector, $\{\Delta\}$ as

$$U = \frac{1}{2}\{\Delta\}^T [K]\{\Delta\} - \frac{1}{2}\{\Delta\}^T P(t)[K_g]\{\Delta\} \qquad (4.23)$$

$$T = \frac{1}{2}\{\dot{\Delta}\}^T [M] \{\dot{\Delta}\} \tag{4.24}$$

where $[K]$, $[M]$ and $[K_g]$ are the global elastic stiffness, global mass and global geometric stiffness matrices respectively.

Substituting Lagrangian, $L=T-U$ in the Lagrange's equation, the final equation of motion for the damaged beam in matrix form is written as,

$$[M]\{\ddot{\Delta}\} + [K]\{\Delta\} - P(t)[K_g]\{\Delta\} = 0 \tag{4.25}$$

P_s the static and P_t the amplitude of time dependent component of the load, can be represented as the fraction of the fundamental static buckling load P^* of a geometrically similar undamaged straight cantilever beam. Hence substituting, $P(t) = \alpha P^* + \beta P^* \cos \Omega t$ with α and β as static and dynamic load factors respectively.

The eq. (4.25) becomes

$$[M]\{\ddot{\Delta}\} + \left([K] - \alpha P^* [K_g]_s - \beta P^* \cos \Omega t [K_g]_t\right)\{\Delta\} = 0 \tag{4.26}$$

If the static and time dependent component of loads are applied in the same manner, then $[K_g]_s = [K_g]_t = [K_g]$.

Equation (4.26) represents a system of second order differential equations with periodic coefficients of the Mathieu-Hill type. The regions of instability are established using Floquet's theory which reduces eq.(4.26) to an eigenvalue problem given below, eq.(4.27).

$$\left([K] - \left(\alpha \pm \frac{\beta}{2} \right) P^* [K_g] - \Theta \frac{\omega_1^2}{4} [M] \right) \{\Delta\} = 0 \tag{4.27}$$

ω_1 is the fundamental frequency of the geometrically similar undamaged straight cantilever beam. Following the same computational procedure as described in chapter 3 the boundaries of the instability regions can be established.

4.3 Results and discussion

To check the accuracy of the present computation, natural frequencies for the first four modes were compared with those of numerical results reported relating to pre-twisted blade treated experimentally and by theoretical means, by Dawson [32], Rao [97], Carnegie [19] and Banerjee [9].

Table 4.1(a), Comparison of natural frequencies [Hz] with those of [32], [97] and [19]

Mode No.	Present FEM analysis (7- Elements)	Dawson [32]	Rao [97]	Carnegie [19] Experimental
1	61.997	62.0	61.9	59.0
2	301.4	301.0	305.0	290.0
3	950.4	953.0	949.0	920.0
4	1194.5	1230.0	1220.0	1110.0

Table 4.1(b), Comparison of natural frequencies [rad/s] with those of [9]

Mode No.	1	2	3	4
Present FEM analysis (7- Elements)	3.4742	13.3604	25.1918	56.4764
Banerjee [9]	3.47173	13.3465	25.1707	56.3716

The above results show close matching of the present one with the available results.

The following properties of the beam are taken for numerical computations: Length of the beam = 0.152m; cross – sectional dimension = 25.4 x 4.6 mm; material mass density of the beam = 8000 kg /m^3. The size parameter τ is equal to 0.2 unless stated otherwise.

Figures (4.3-4.5) show the effect of pretwist angle (θ_l) on the first three natural frequencies for a beam with an extent of damage $\xi_b = \xi = 0.5$ and for different positions of the damage (ψ). On the same figures, variation of natural frequencies for an undamaged beam (ξ=1.0) with pretwist angle is also shown. It is seen that the first and third mode natural frequencies increase with increase in pretwist angle, whereas the second mode natural frequency decreases with increase in pretwist angle. This is due to the fact that with increase in pretwist angle, moment of inertia about the axis of first and third mode vibration increases, whereas it decreases about the axis of second mode vibration. All the three frequencies have minimum value when the damage is located nearest to the fixed end. The variation in first mode natural frequency with pretwist angle is very less compared to the change in second and third mode natural frequencies. When the damage is very near to the free end (ψ=0.9) the frequency curves for the damaged beam are very close to those for the undamaged beam.

Figures (4.6-4.8) show the variation of first three natural frequencies with damage location for angles of pretwist 30^0, 60^0 and 90^0 respectively. The first mode natural frequency increases as the damage position moves from the fixed end towards the free end for all values of θ_l. As the damage moves towards the free end, the rate of increase of frequency with respect to pretwist angle reduces. The second and third mode frequencies have minimum and maximum values when the damage is near the fixed end and free end respectively. For intermediate positions of the damage the values of these two frequencies fluctuate between these maximum and minimum limits.

Figure (4.9) shows the effect of pretwist angle on the first mode buckling load. It is observed that the first mode-buckling load increases with pretwist angle irrespective of damage position. The fundamental buckling load is minimum when damage is near the fixed end and as the damage moves towards the free end, the buckling load increases and approaches the value for an undamaged beam when it is nearest to the free end.

Figures (4.10-4.12) show the effect of pretwist angle on the first three instability zones for a beam with extent of damage $\xi = 0.5$ and damage position $\psi = 0.3$, 0.5 and 0.7 respectively. It is seen that with increase in pretwist angle the first and third instability zones shift to higher frequencies of excitation, whereas the second instability zone shifts to lower frequency of excitation. The effect is more pronounced on second and third zones as compared to first one. This is due to the fact that the first mode natural frequency is least affected by the change in pretwist angle. There is also change in areas of the instability zones. There is very small change in the area of the first instability zone, whereas there is a marked increase in area of the second zone and decrease in third zone area.

Figures 4.13(a)-4.13(c) show the effect of location of damage (ψ) on the first three instability regions respectively for ξ=0.5 and $\theta_l = 30^0$. It is seen that all the three instability regions occur at minimum frequency of excitation when the damage is nearest to the fixed end. When the damage is at the free end the instability regions occur at maximum frequency of excitation. As the damage moves from the fixed end to free end the first instability region moves away from the dynamic factor axis. There is reversal of positions of second and third instability zones as the damage moves from fixed end to the free end. This is due the reason that when damage moves from the fixed end to the free end, the second and third mode natural frequencies may increase or decrease depending on the damage position (Figs. 4.7 and 4.8). Figures (4.14 and 4.15) show the instability regions for $\theta_l = 60^0$ and 90^0 respectively. Similar trends as those for $\theta_l = 30^0$ are observed for these two cases also.

Figures (4.16-4.18) show the effect of extent of damage ξ on instability zones for angles of pretwist 30^0,60^0 and 90^0 respectively for damage position $\psi = 0.1$. The values of ξ considered are 0.5 and 0.75. It is noticed that with increase in extent of damage the instability zones shift to lower frequencies of excitation irrespective of pretwist angle. Also the areas of the instability zones increase with increase in extent of damage. That is as the extent of damage increases the instability increases.

Figures (4.19-4.21) show the effect of static load factor α on instability zones for angle of pretwist 30^0,60^0 and 90^0 respectively for damage position $\psi = 0.1$. The values of α considered are 0.0 and 0.5. It is noticed that with increase in static load component the instability regions are relocated at lower frequencies of excitation and their areas also increase. The effect is more pronounced on first instability region. This means that increase in static load component enhances the instability of the beam.

4.4 Closure

From the study of dynamic stability of a pretwisted cantilever beam with localised damage subjected to end parametric excitation it is revealed that angle of pretwist has significant effect on second and third instability zones. Increase in pretwist angle has a stabilising effect on the third instability zone and destabilising effect on the second instability zone. Variation in pretwist angle does not have significant effect on the first instability region. Extent of damage has always a destabilising effect for any pretwist angle. Localised damage has a greater destabilising effect when it is located near the fixed end than when it is towards the free end, irrespective of the pretwist angle. Increase in static load component has a destablising effect irrespective of the value of pretwist angle.

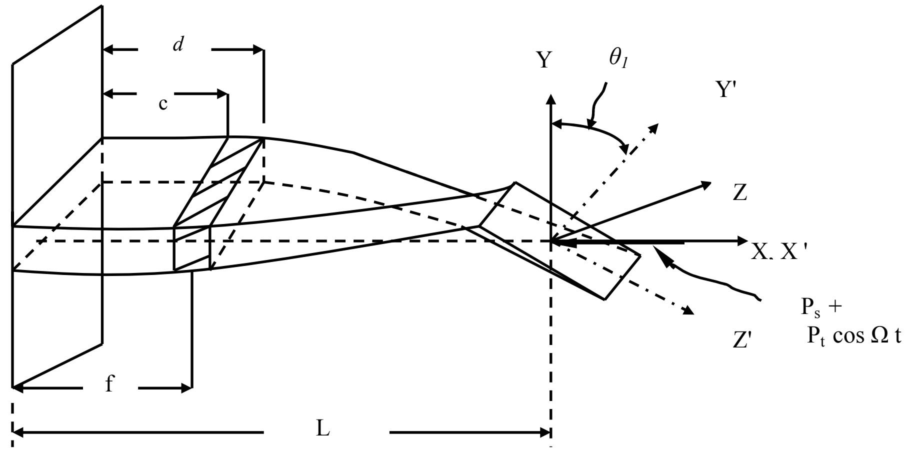

Fig.- 4.1(a), Pretwisted beam and coordinate axes

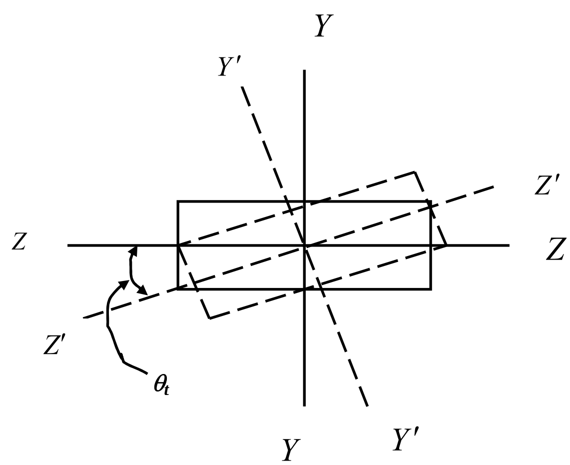

Fig.- 4.1(b), Angle of twist (θ_t)

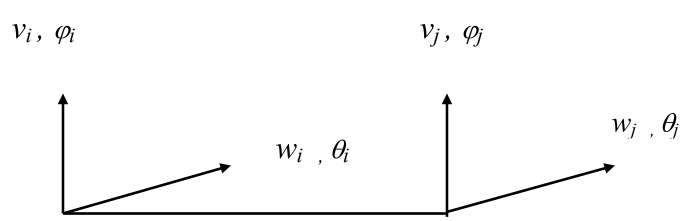

Fig.- 4.2, Degrees of freedom of a beam element

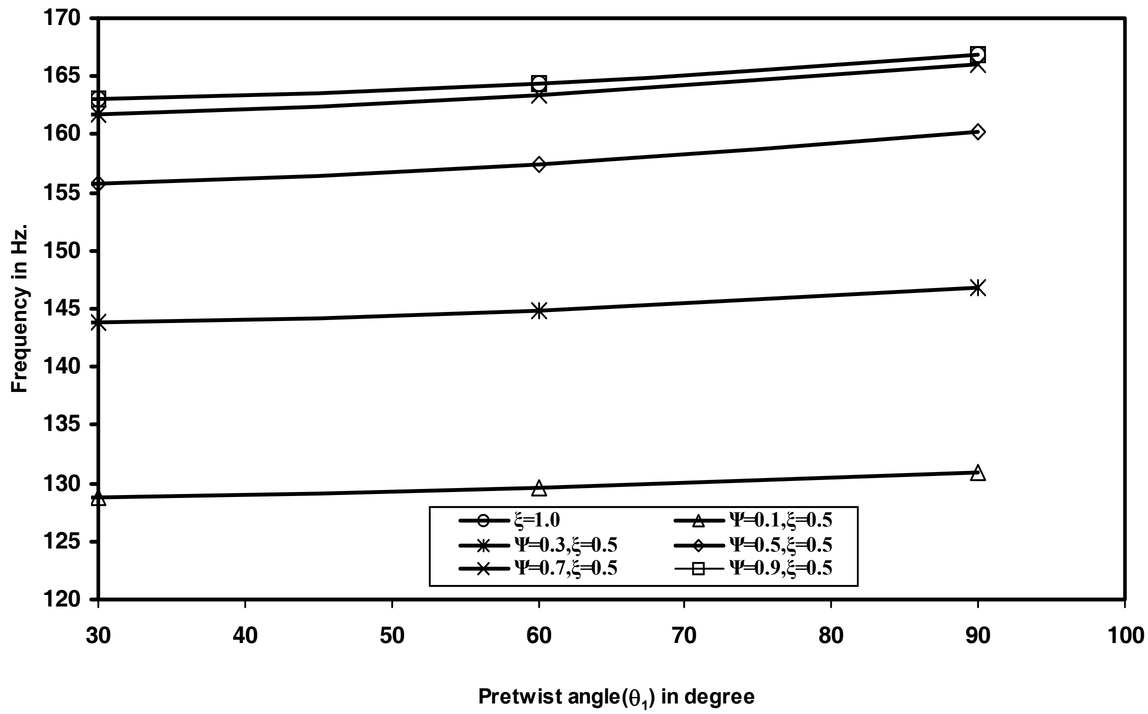

Fig.- 4.3, Effect of pretwist angle on first mode natural frequency

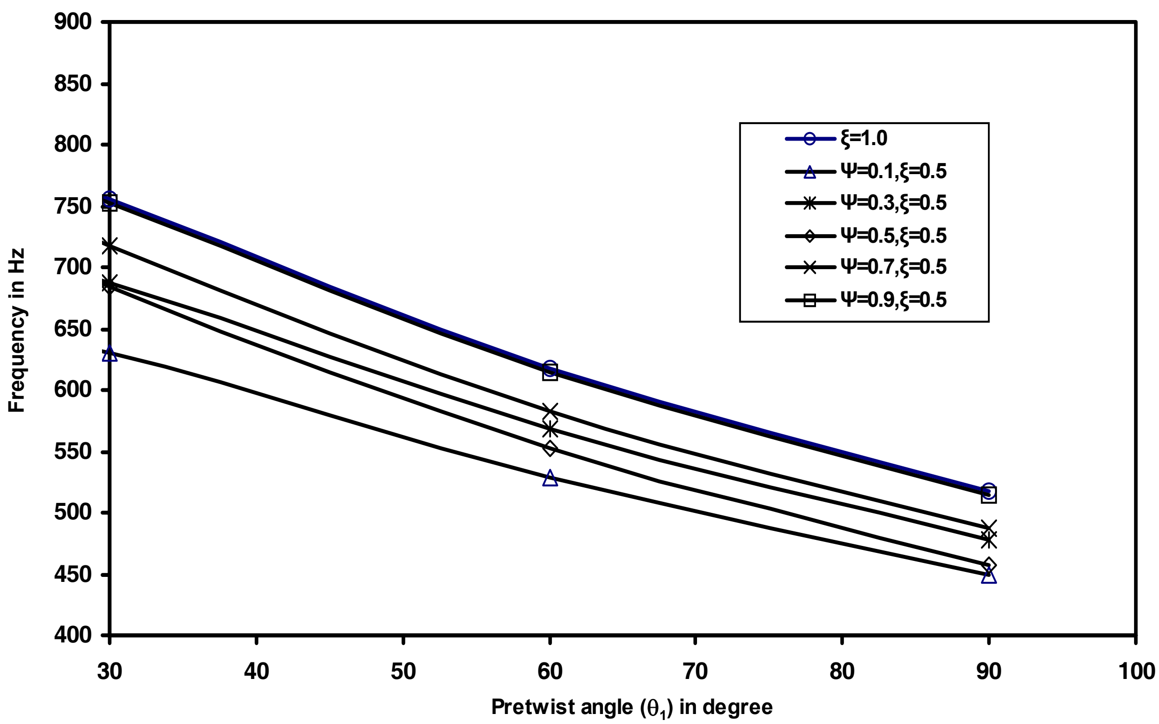

Fig.- 4.4,Effect of pretwist angle on second mode natural frequency

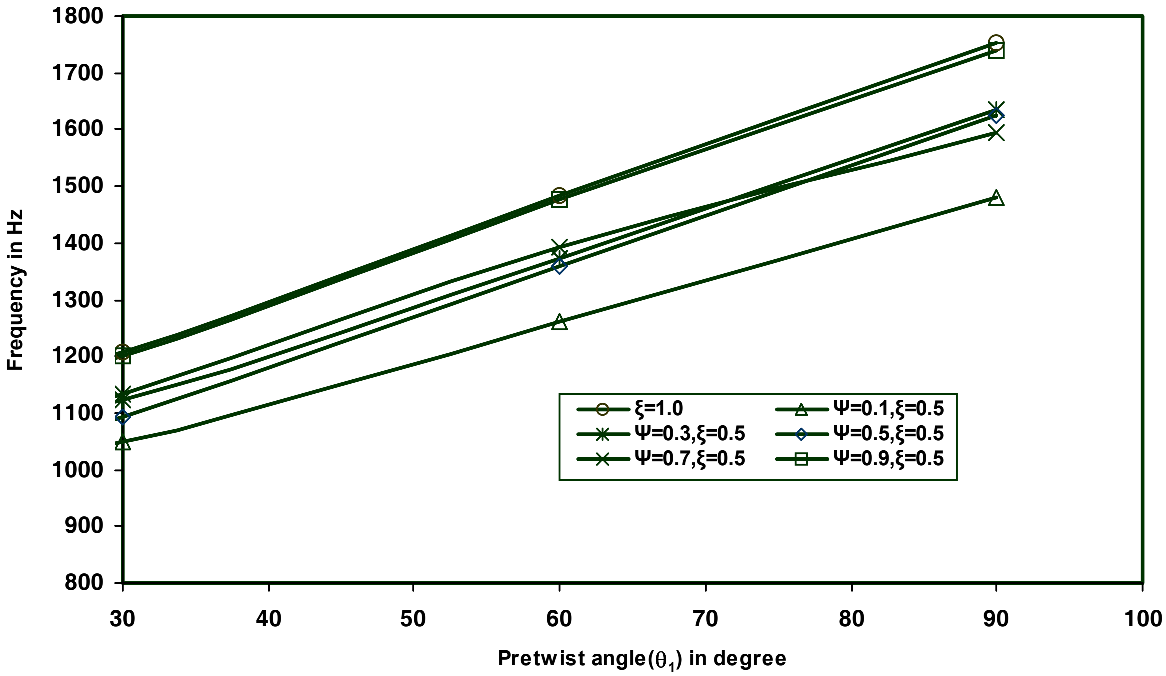

Fig.- 4.5, Effect of pretwist angle on third mode natural frequency

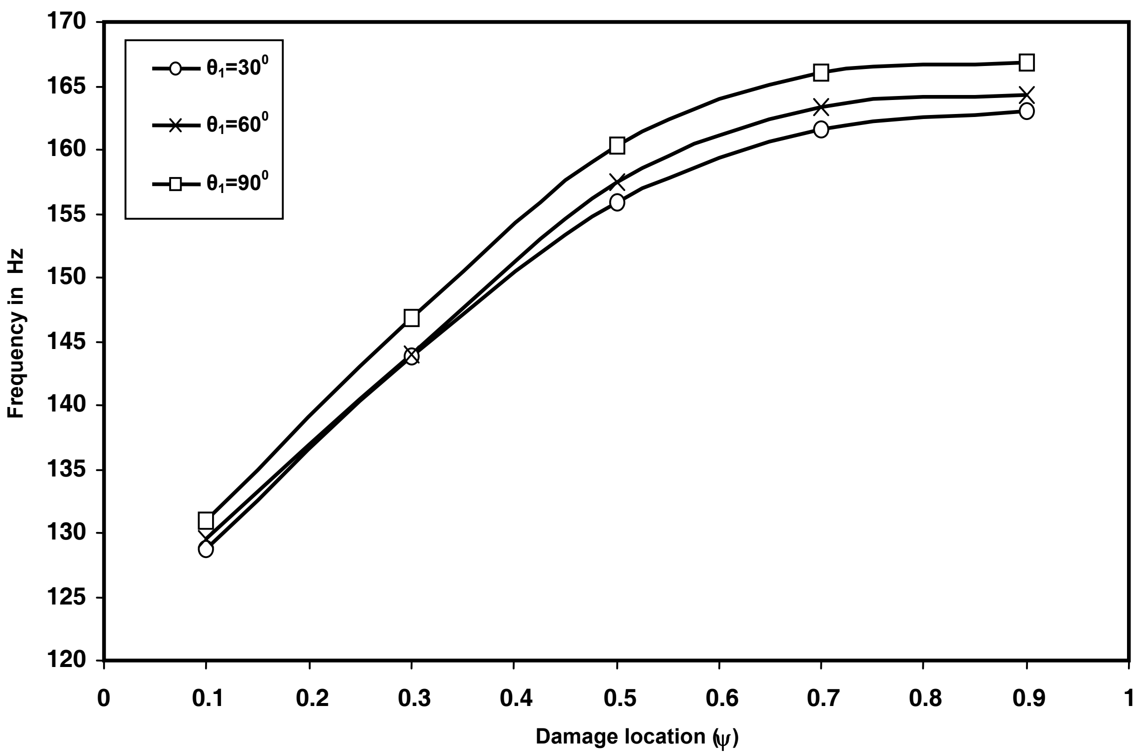

Fig.- 4.6, Effect of damage location on first mode natural frequency

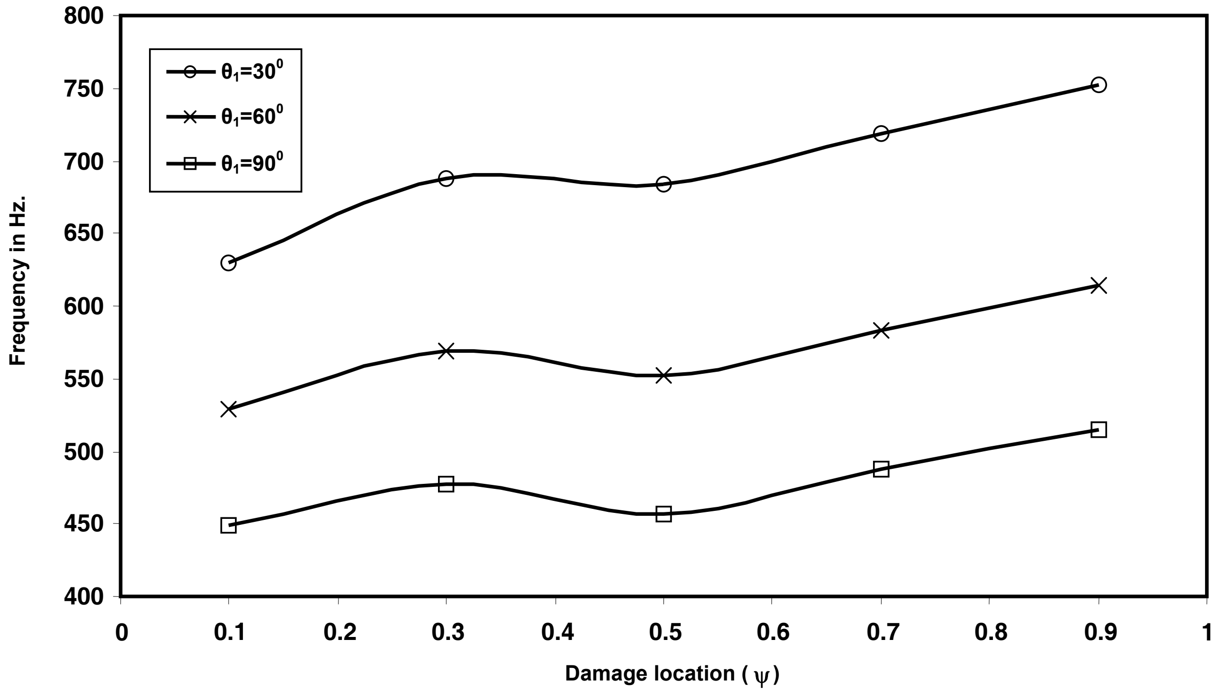

Fig.- 4.7,Effect of damage location on the second mode natural frequency

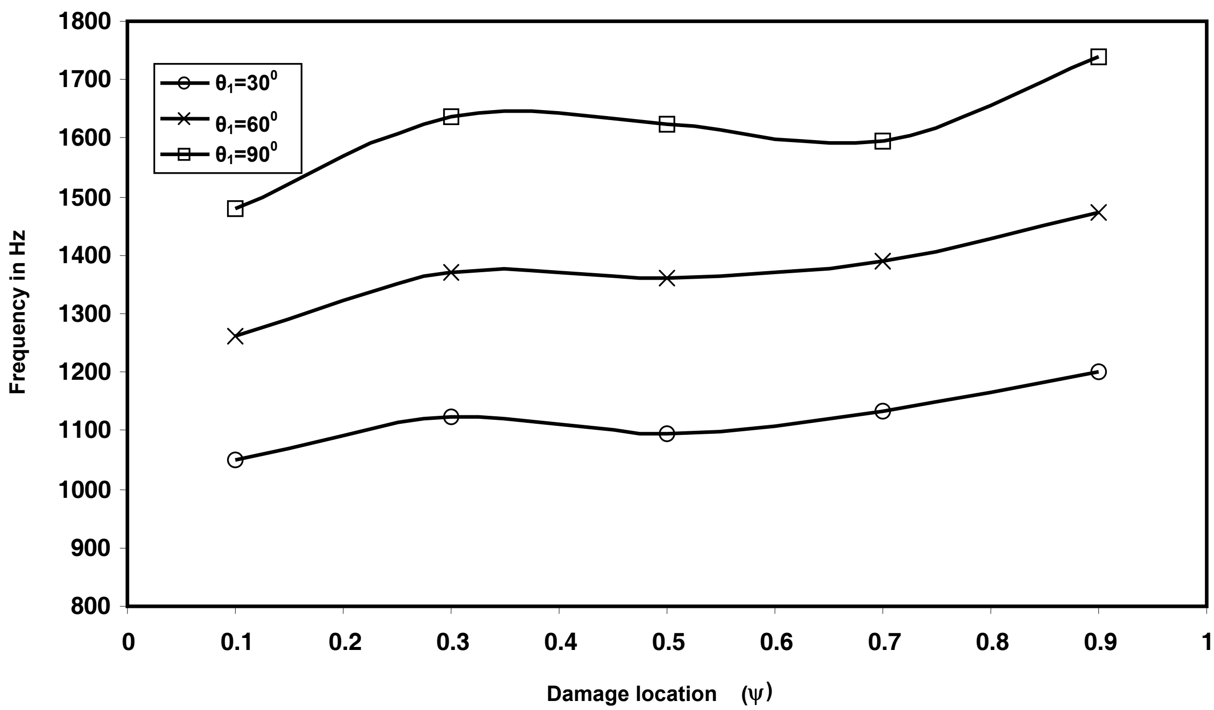

Fig.- 4.8, Effect of damage location on third mode natural frequency

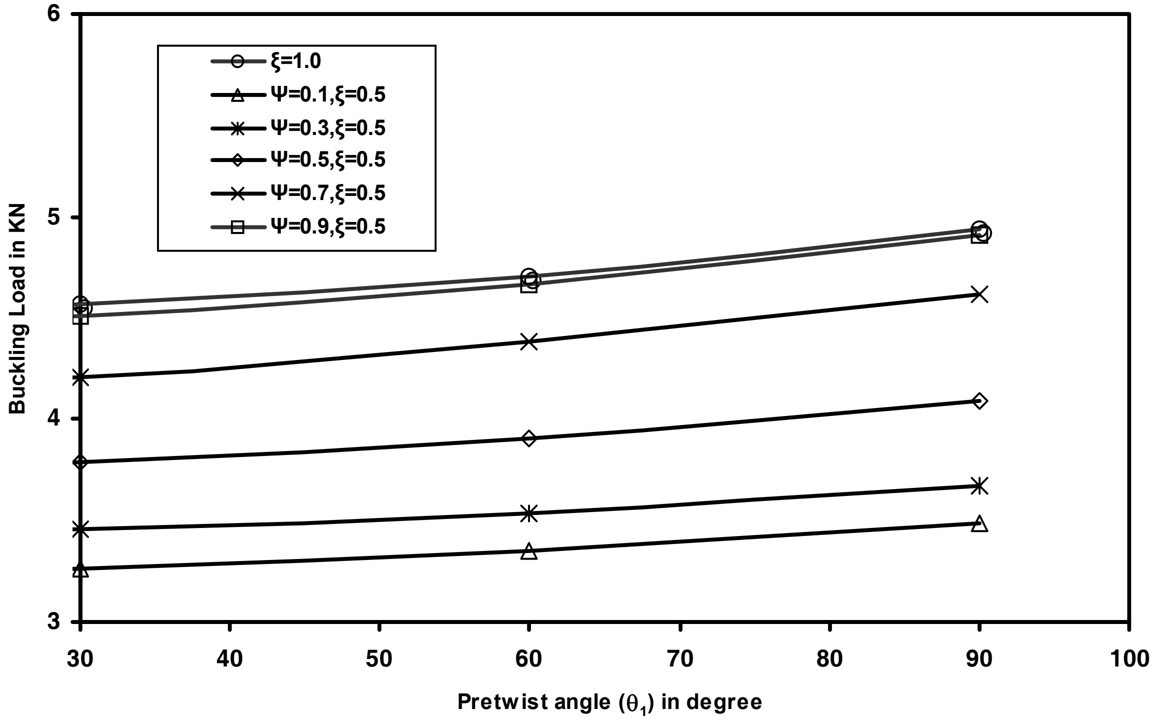

Fig.- 4.9,Effect of pretwist angle on critical buckling load

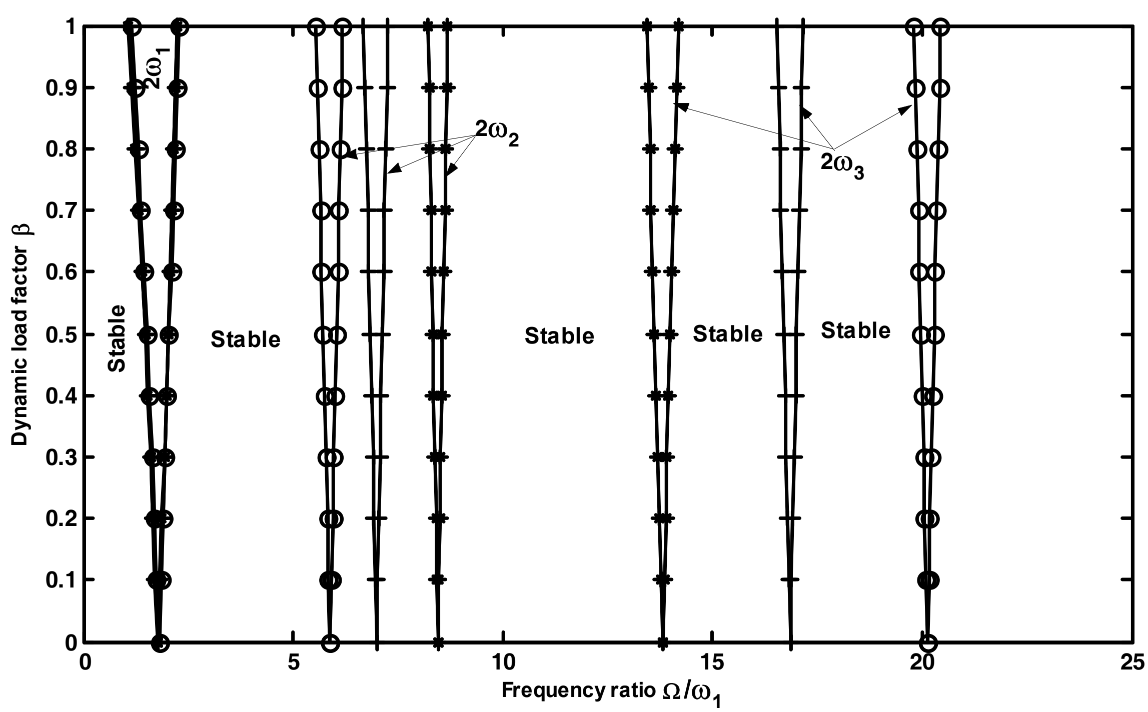

Fig.- 4.10,Effect of pretwist angle on instability regions,
ξ=0.5,ψ =0.3,θ_1= 30^0(*),θ_1= 60^0(+),θ_1= 90^0(o).

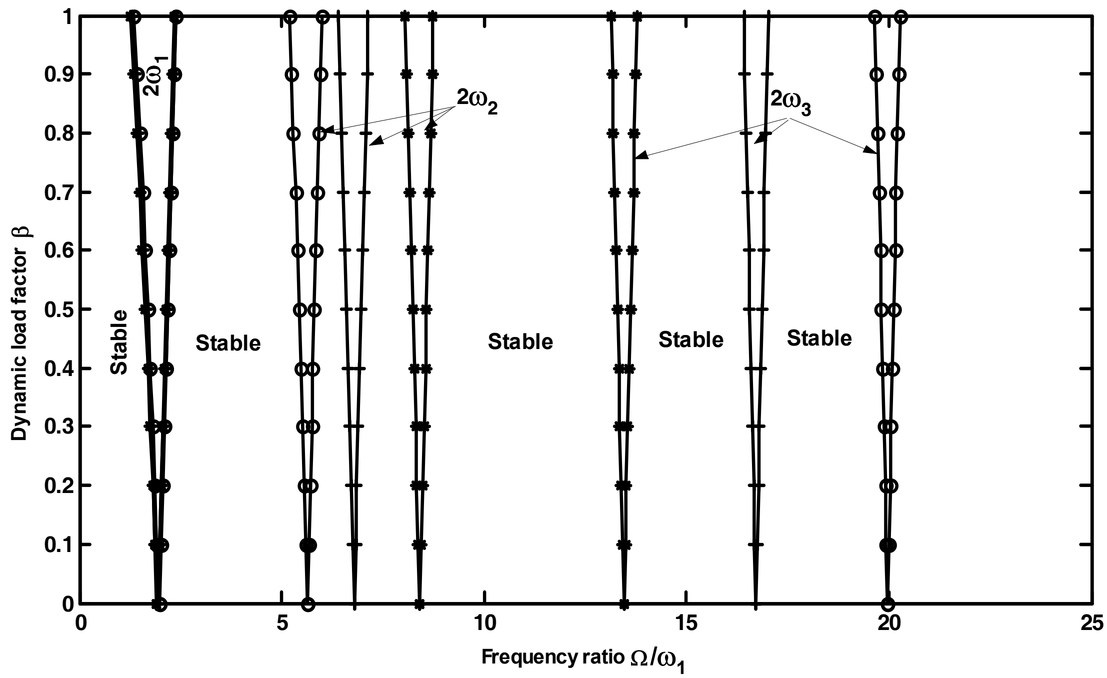

Fig.- 4.11,Effect of pretwist angle on instability regions, ξ =0.5,ψ =0.5,key as fig.- 4.10.

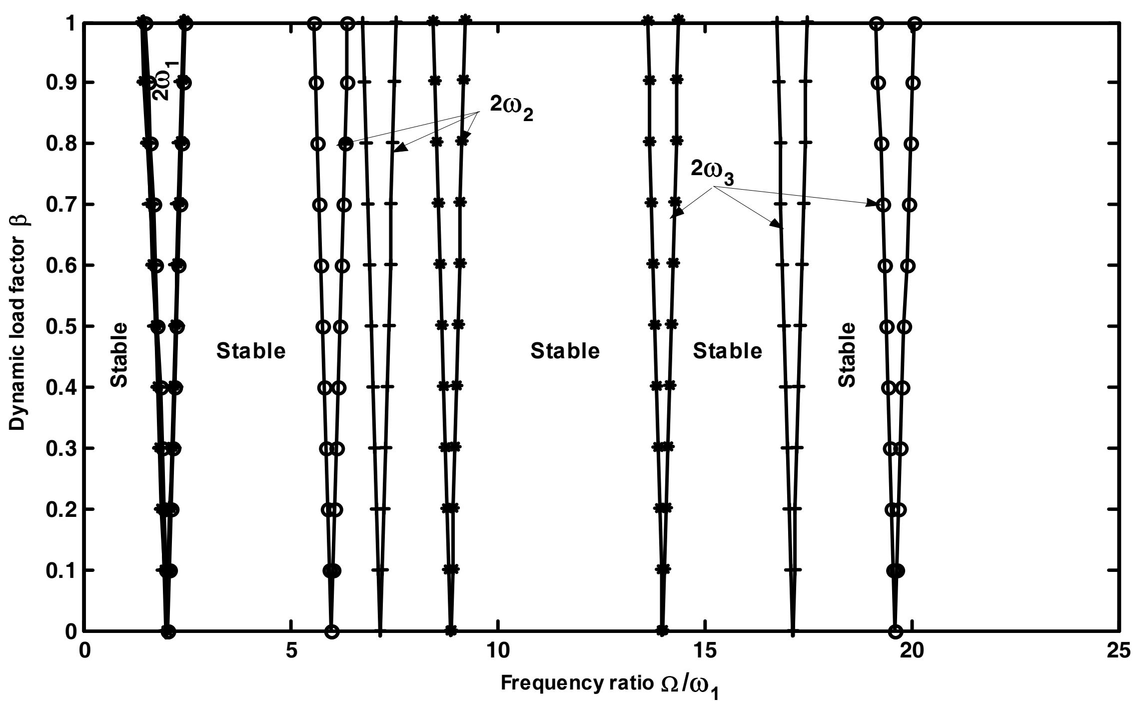

Fig.- 4.12,Effect of pretwist angle on instability regions, ξ=0.5,ψ =0.7,key as fig.- 4.10.

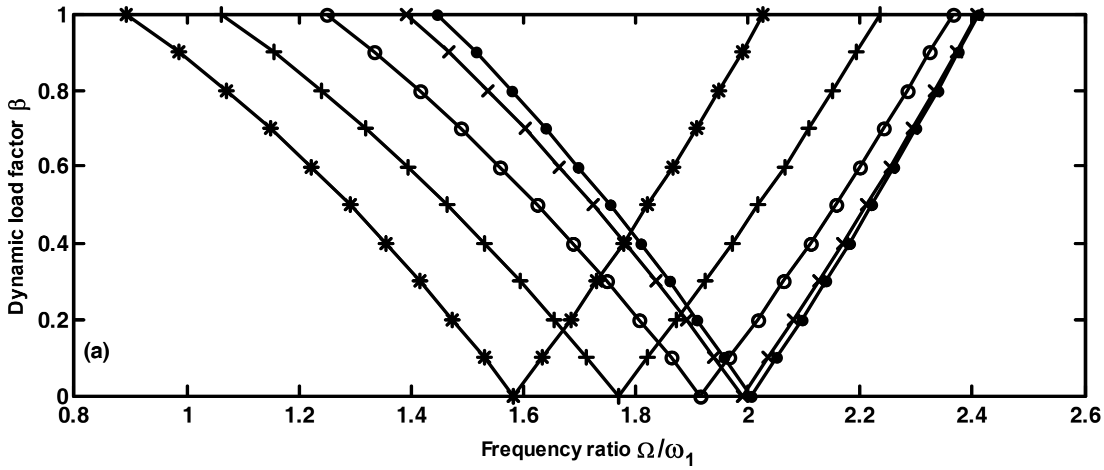

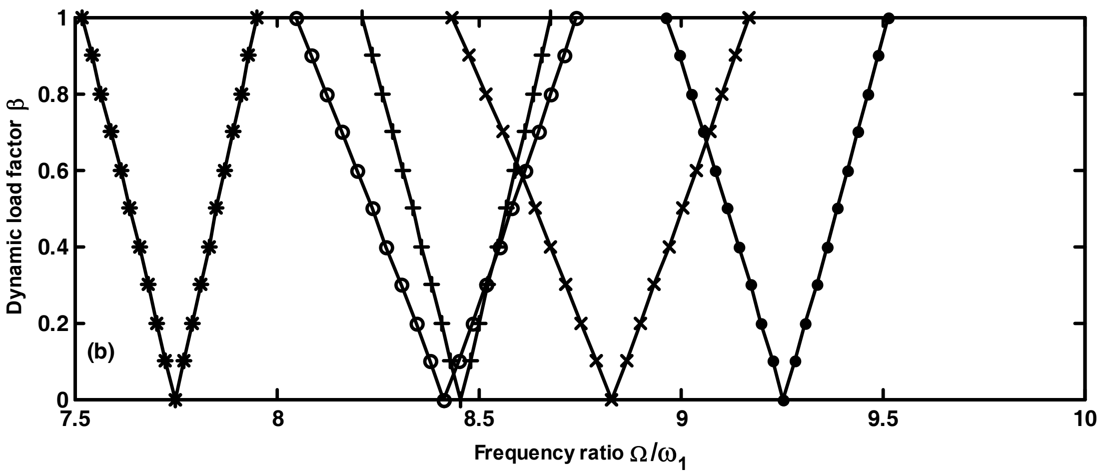

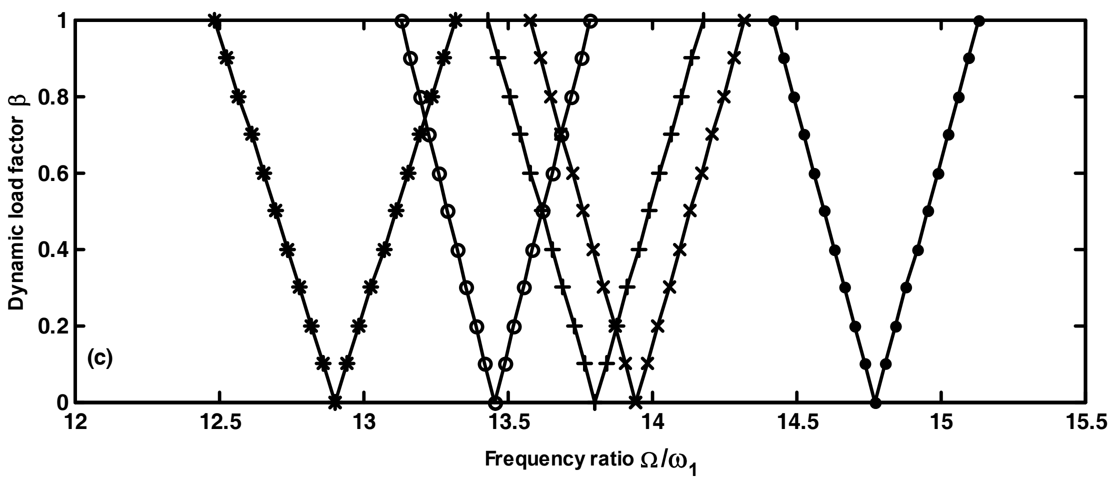

Fig.- 4.13,Effect of damage location on instability regions,

ξ=0.5,θ_1=30^0,ψ = 0.1(*),ψ = 0.3 (+),ψ = 0.5(o),ψ =0.7(x),ψ =0.9(•).

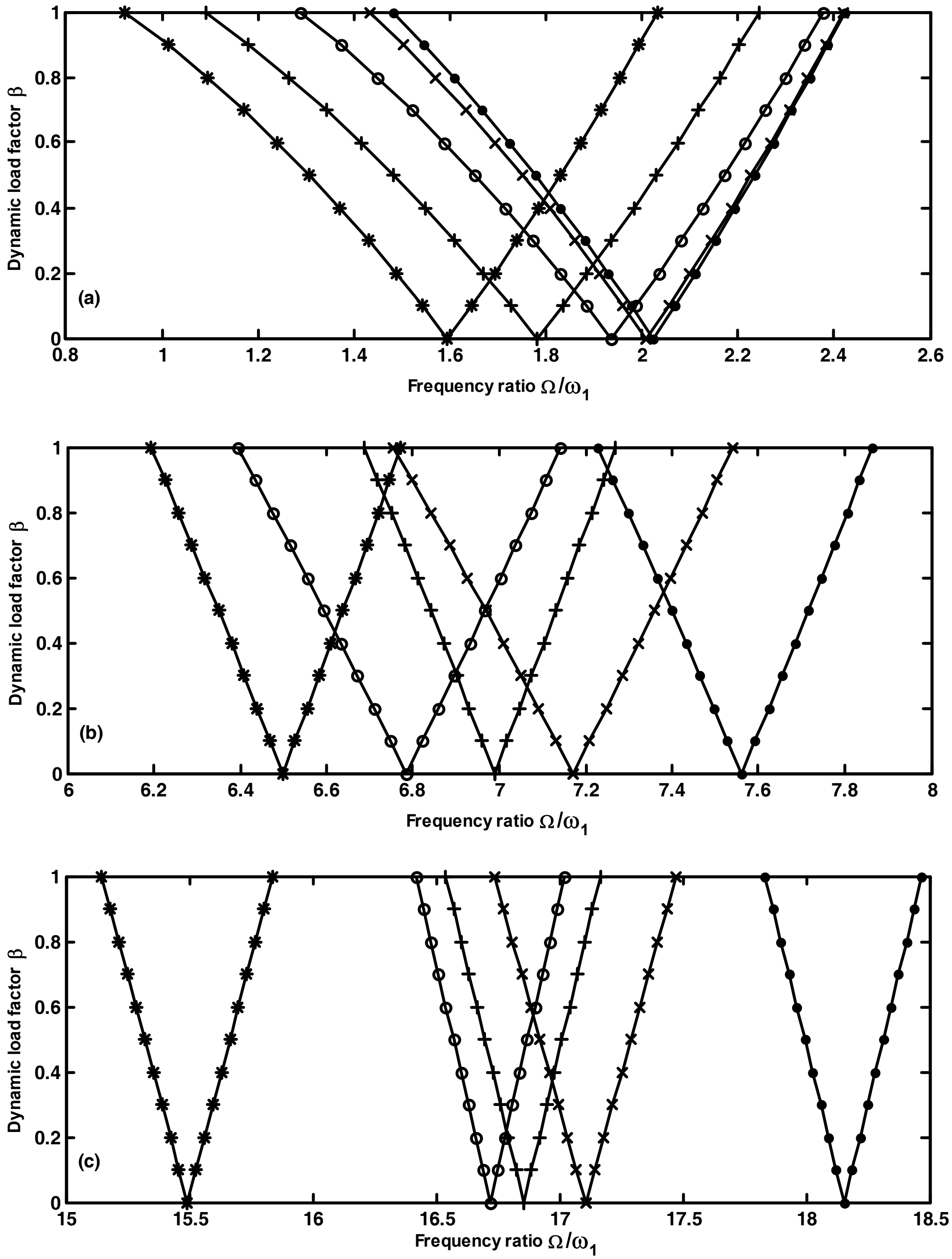

Fig.- 4.14,Effect of damage location on instability regions,ξ=0.5,θ_1=60^0, key as fig.- 4.13.

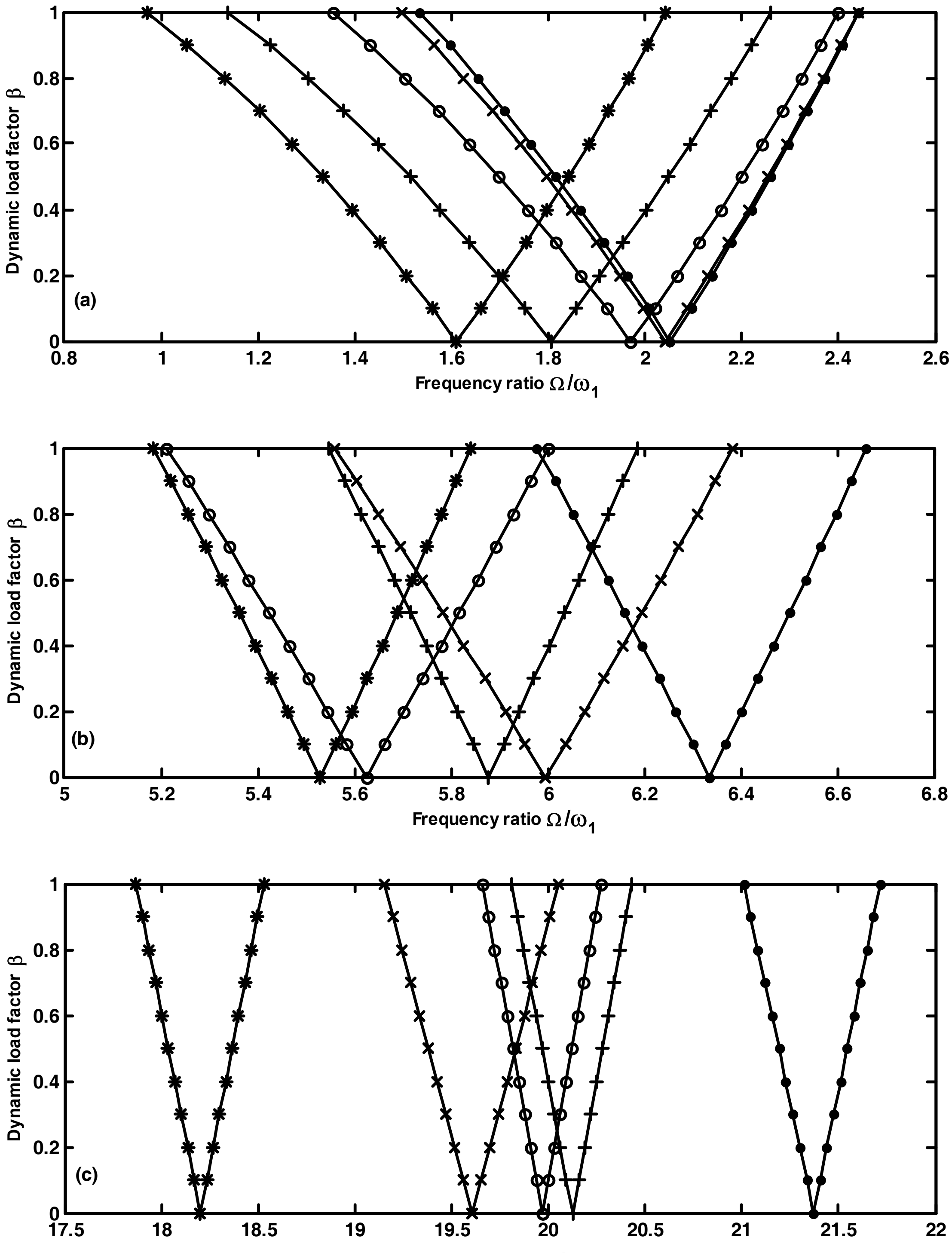

Fig.- 4.15,Effect of damage location on instability regions,ξ=0.5,θ_1=90^0, key as fig.- 4.13.

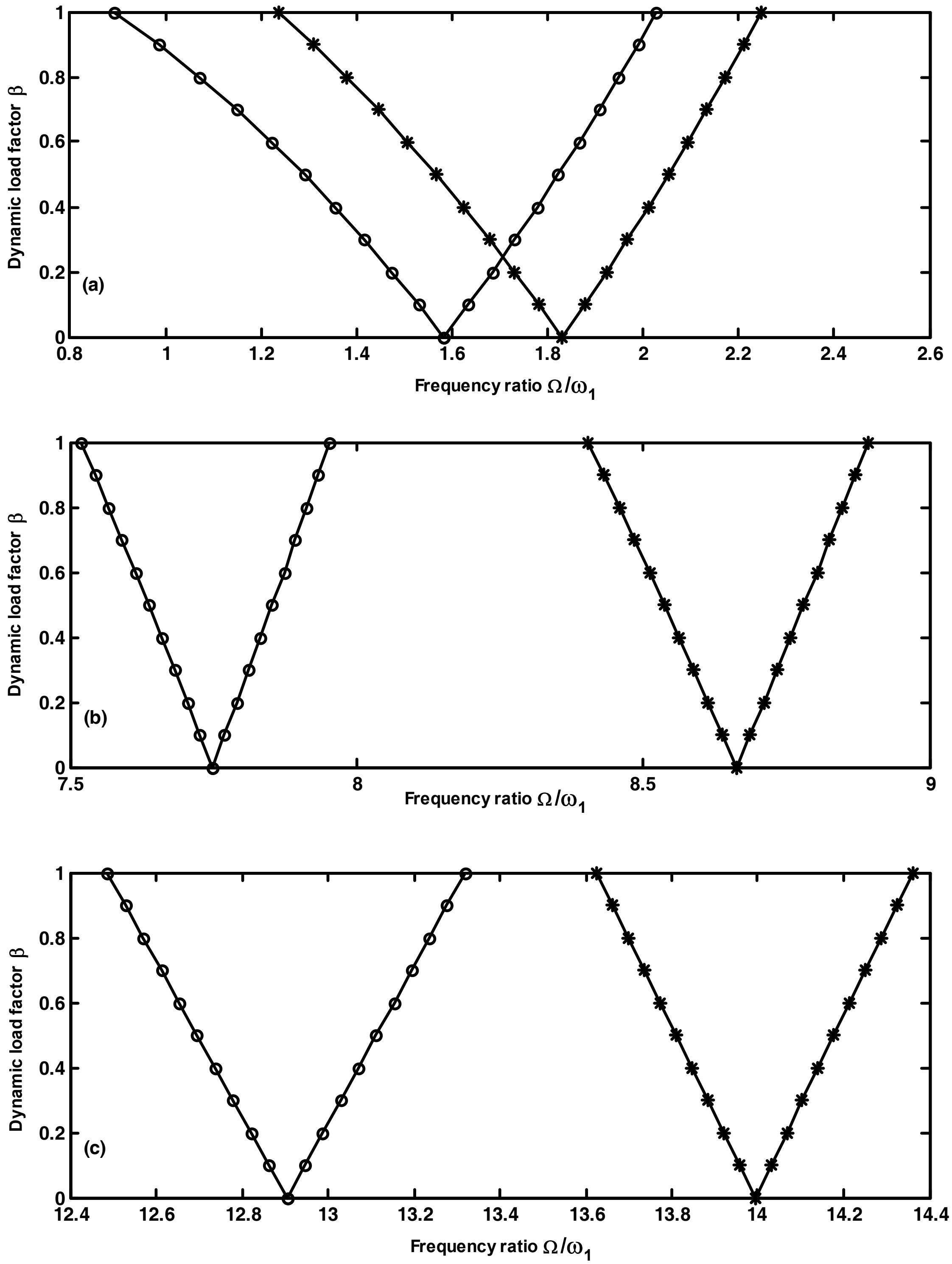

Fig. - 4.16,Effect of extent of damage on instability regions,

$\theta_1 = 30^0$, $\psi = 0.1$, $\xi = 0.75$,(*), $\xi = 0.5$,(o).

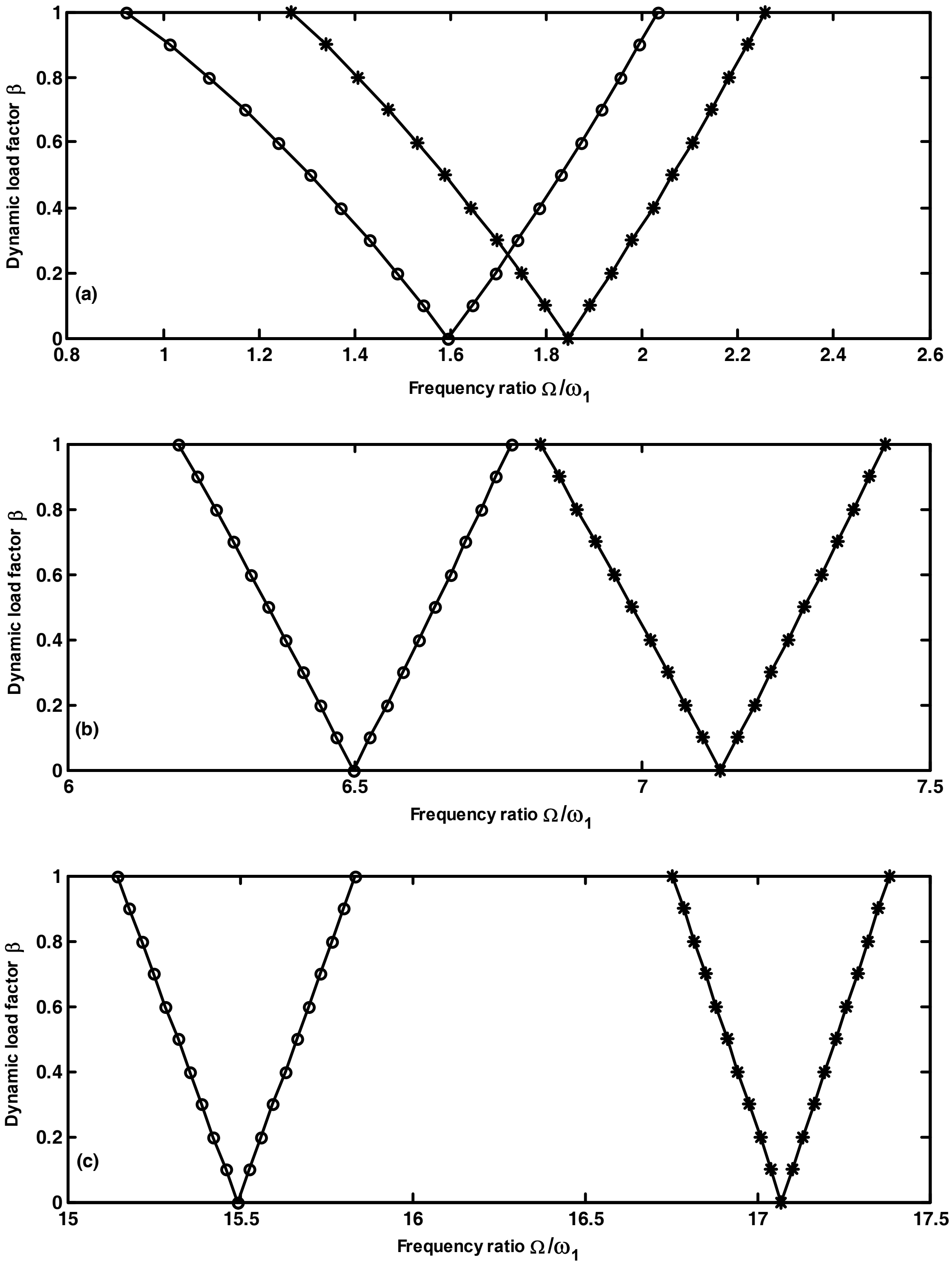

Fig.- 4.17,Effect of extent of damage on instability regions, $\theta_1 = 60^o$,ψ =0.1, key as fig.- 4.16.

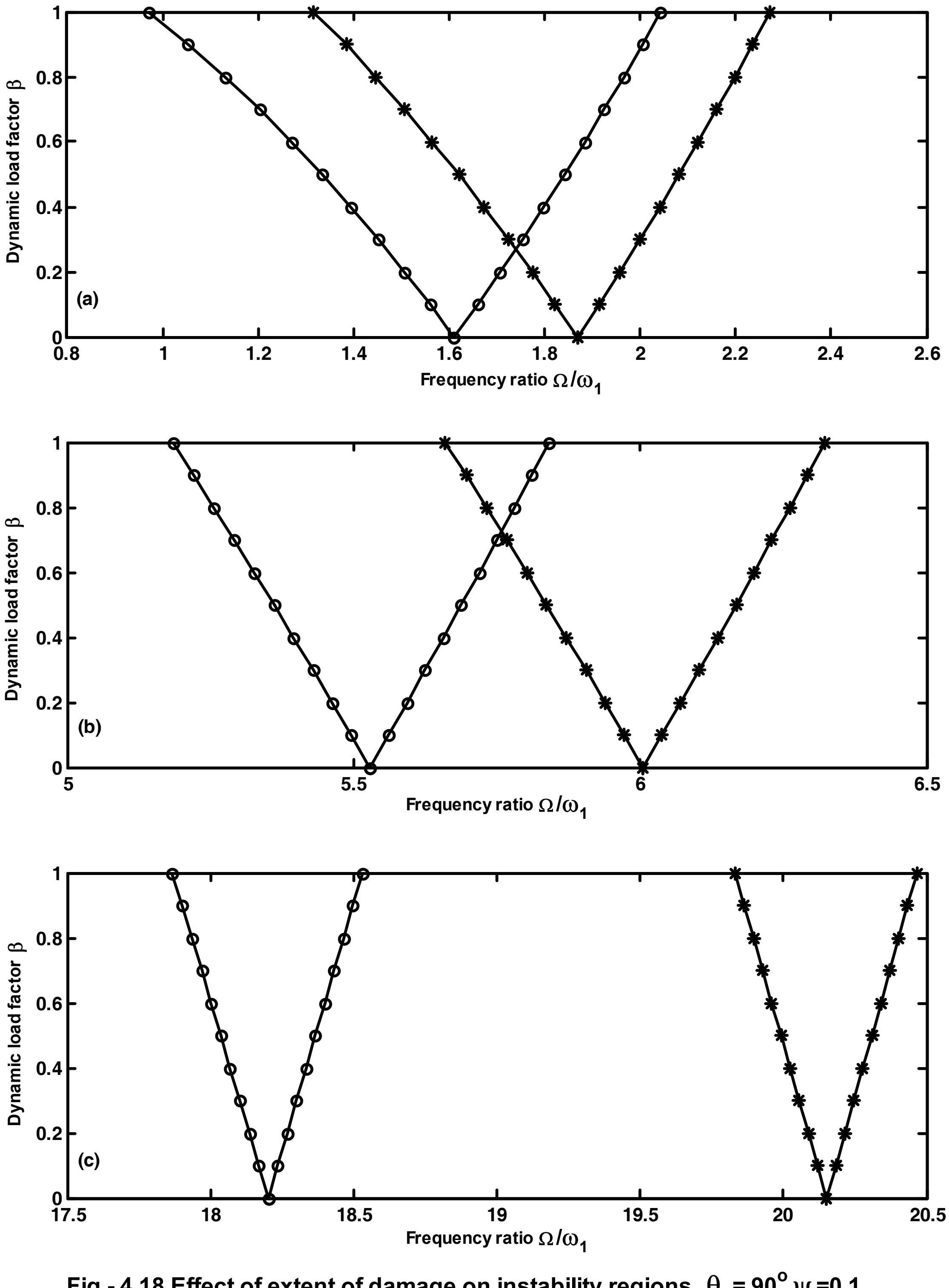

Fig.- 4.18,Effect of extent of damage on instability regions, θ_1= 90^o,ψ =0.1, key as fig.- 4.16.

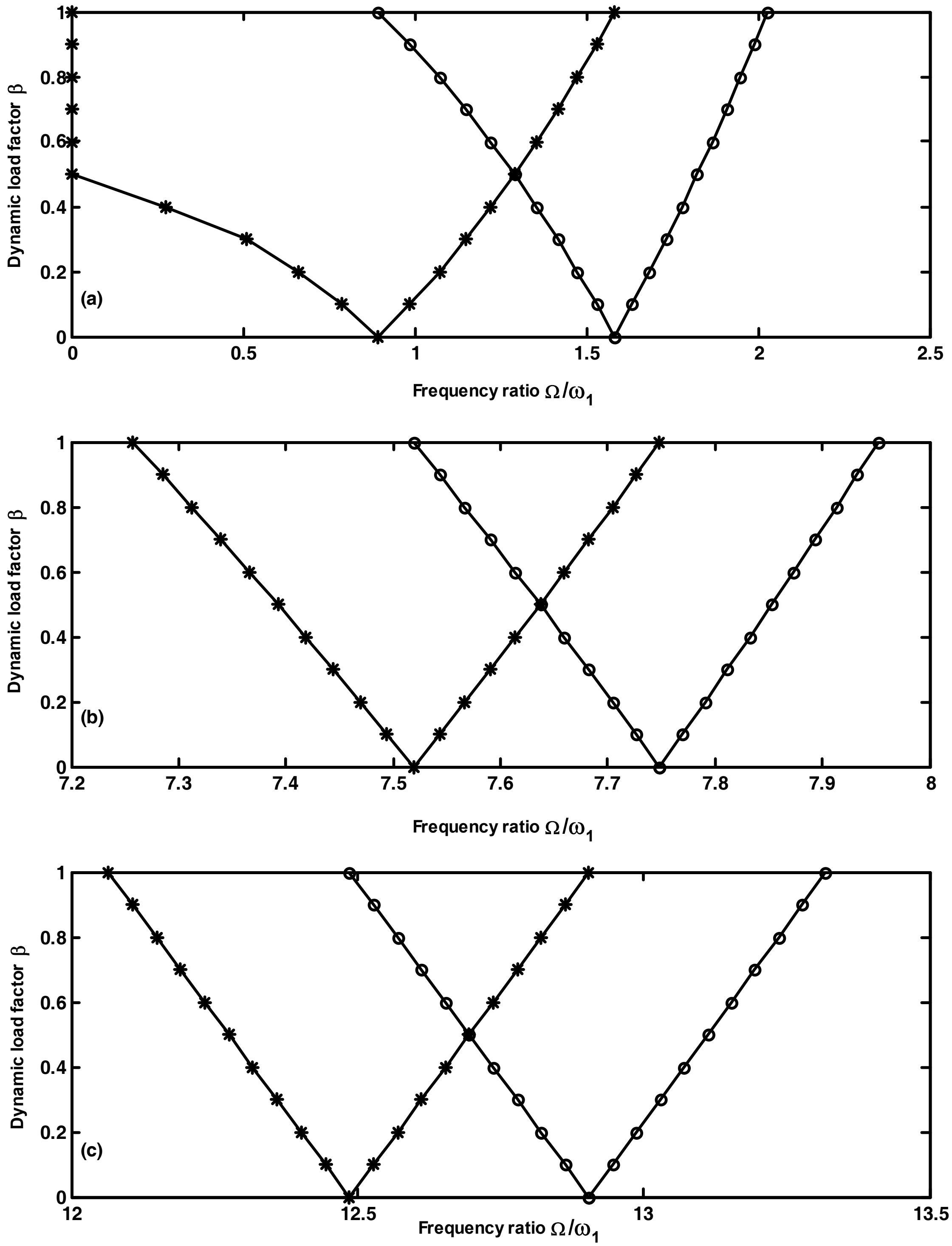

Fig.- 4.19,Effect of static load factor on instability regions,
$\theta_1 = 30^0, \psi = 0.1, \alpha = 0.5$,(*),$\alpha = 0.0$,(o).

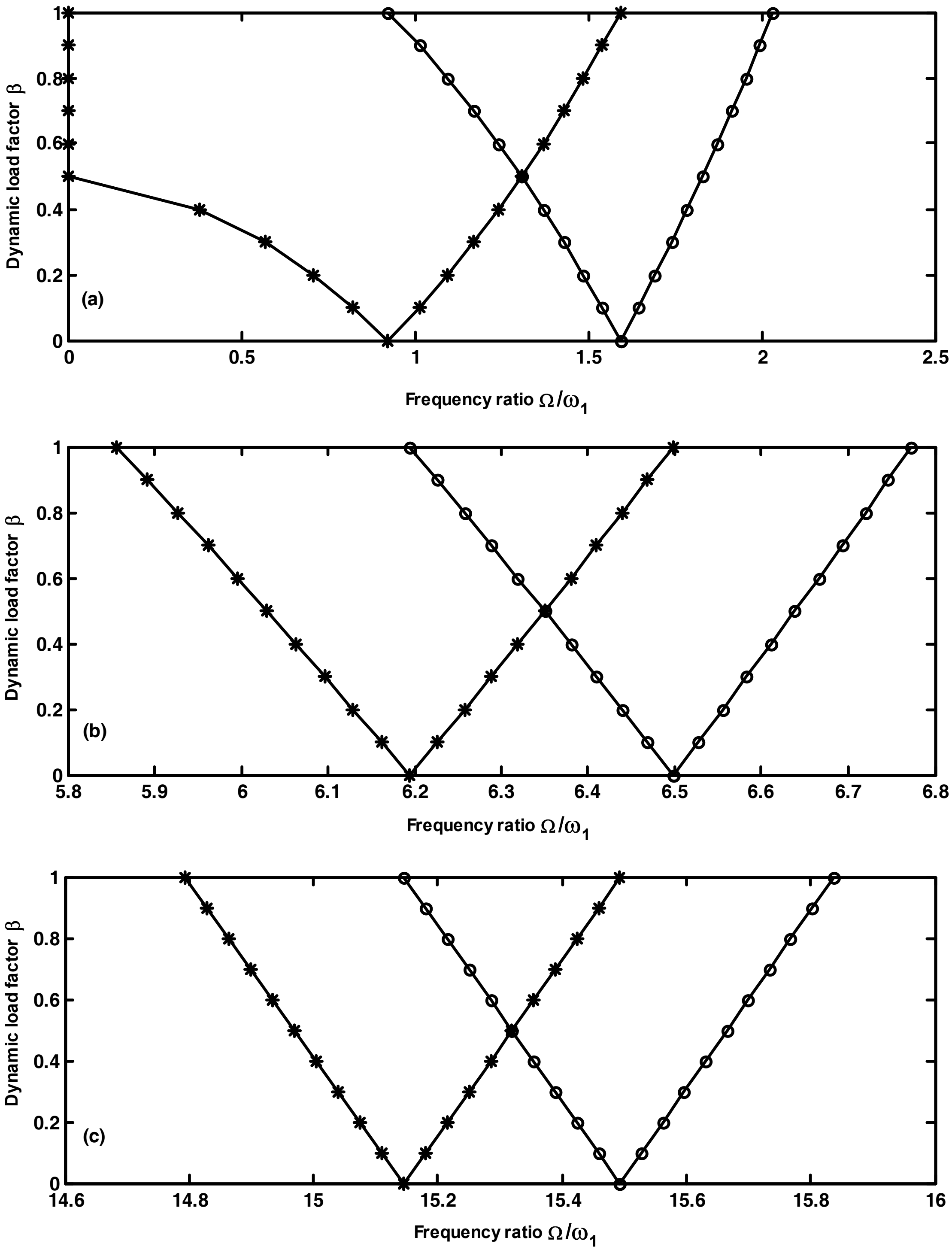

Fig.- 4.20,Effect of static load factor on instability regions,$\theta_1 = 60^0$,ψ =0.1, key as fig.4.19.

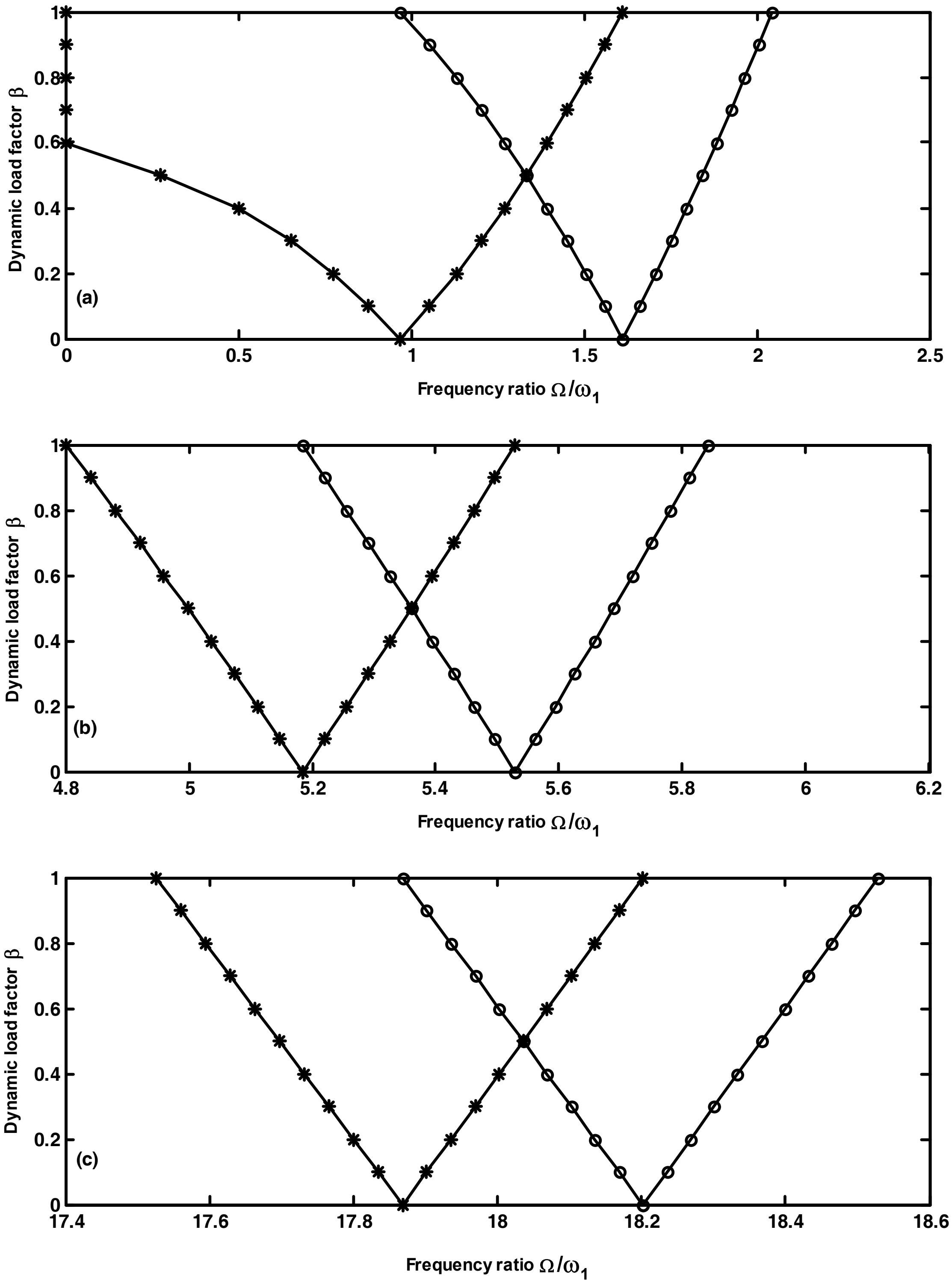

Fig.- 4.21,Effect of static load factor on instability regions,θ_1= 90^0,ψ =0.1, key as fig.4.19.

Chapter 5

DYNAMIC STABILITY OF A MULTILAYERED SYMMETRIC CANTILEVER SANDWICH BEAM SUBJECTED TO PARAMETRIC EXCITATION

5.1 Introduction

Vibration control of machines and structures incorporating viscoelastic materials in suitable arrangement is an important aspect of investigation [87]. The use of viscoelastic layers constrained between elastic layers is known to be effective for damping of flexural vibrations of structures, over a wide frequency range. The energy dissipated in these arrangements is due to shear deformation in the viscoelastic layers, which occurs due to flexural vibration of the structures. Multilayered cantilever sandwich beam like structures can be used in aircraft structures and other applications, such as robot arms for effective vibration control. Such members may experience parametric instability when subjected to time dependant forces.

DiTaranto and Balsingame [36] obtained composite loss factor for selected laminated beams. Mead and Markus [78] studied the forced vibration of a three layer damped sandwich beam with arbitrary boundary conditions. Rao [96] calculated the frequency parameters and loss factors of sandwich beams under various boundary conditions and presented them in the form of equations and graphs. Kavi and Asnani [70] studied the forced vibrations of stinger stiffened damped sandwich panel under point and line excitations. They determined the resonant frequencies, loss factors and frequency response by transfer matrix method. Banerjee [10] carried out free vibration analysis of three layered symmetric sandwich beams using dynamic stiffness method.

The theory of flexural vibration of symmetric multilayered beams was analysed by Agbasiere and Grootenhuis [3]. Asnani and Nakra [6] investigated the flexural vibration of multilayered unsymmetrical beams. Asnani and Nakra in their later work [8] explored the damping effectiveness during flexural vibration of multilayered beams with number of layers up to 15, with simply supported end conditions. Vaswani, et al. [128] obtained resonant frequency and system loss factor for general multilayered curved beams.

The purpose of the present work is to study the parametric instability of a multilayered cantilever sandwich beam subjected to end periodic axial load. Equation of motion for a general 2n+1 layered beam is derived using finite element method in conjunction with Hamilton’s principle. The regions of instability for simple and combination resonance are established using modified Hsu's method proposed by Saito and Otomi [104].

5.2 Formulation of the problem

A 2n+1 layer sandwich beam, incorporating viscoelastic damping material is shown in fig.(5.1). There are n number of viscoelastic layers and n+1 numbers of elastic layers. A layer of viscoelastic material separates two adjacent stiff elastic material layers. The beam is symmetric and has a length L and width b respectively. It is subjected to a pulsating axial force $P(t) = P_s + P_t \cos\Omega t$, where P_s is the static, P_t is the amplitude of the time dependent component of the load acting along its undeformed axis at the free end and Ω is the excitation frequency of the dynamic load component. The finite element model is developed based on the following assumptions:

(1) The transverse displacement w of the beam is small and is same for all points of a given cross section.

(2) The rotary inertia and shear deformation in the constraining layers are neglected. That is the elastic face layers obey the Euler- Bernoulli beam theory.

(3) Linear theories of elasticity and viscoelasticity are applicable to the layers.

(4) The layers are perfectly bonded so that displacements are continuous across the interfaces

(5) Damping in the viscoelastic layer is primarily due to shear. Bending and extensional effects in the core are neglected.

(6) Young's modulus of the viscoelastic material is negligible compared to the elastic material.

5.2.1 Element matrices

As shown in fig.(5.2) the beam element model presented here consists of two nodes and each node has n+3 degrees of freedom. Nodal displacements are given by

$$\left\{\Delta^{(e)}\right\} = \{w_p \ \ \varphi_p \ \ u_{1p} \ \ u_{3p} \ldots u_{(2n+1)p} \ \ w_q \ \ \varphi_q \ u_{1q} \ \ u_{3q} \ldots u_{(2n+1)q}\}^{T} \tag{5.1}$$

where p and q are elemental nodal numbers. The axial displacement, ($u_{(2k-1)}$) of the constraining layers, the transverse displacement,(w) and the rotational angle,(φ) can be expressed in terms of nodal displacements and finite element shape functions.

$$u_{(2k-1)} = [\ N_{(2k-1)}\ ]\ \left\{\Delta^{(e)}\right\}, \quad k=1,2 \ldots n+1,$$

$$w = [N_w]\ \left\{\Delta^{(e)}\right\},\ \varphi = [N_w]'\ \left\{\Delta^{(e)}\right\} \tag{5.2}$$

where the prime denotes differentiation with respect to axial coordinate x. The shape functions are given as below.

The shape function matrices, $[N_{(2k-1)}]$ are of $1\times(2n+6)$ size with the elements $[N_{(2k-1)}]_{(1,(k+2))} = 1-\zeta$ and $[N_{(2k-1)}]_{(1,(n+k+5))} = \zeta$ respectively and all other elements are zero.

The size of the shape function matrix $[N_w]$ is $1\times(2n+6)$ with the elements

$[N_w]_{(1,1)} = (1-3\zeta^2+2\zeta^3)$; $[N_w]_{(1,2)} = (\zeta-2\zeta^2+\zeta^3)\,l$; $[N_w]_{(1,(n+4))} = (3\zeta^2-2\zeta^3)$;

$[N_w]_{(1,(n+5))} = (-\zeta^2+\zeta^3)\,l$ and all other elements are zero.

where $\zeta = x / l$, l is the length of the element.

5.2.1.1 Element stiffness matrix

Elemental potential energy ($U^{(e)}$) is equal to the sum of the potential energy of the constraining layers and viscoelastic layers.

$$U^{(e)} = U_c^{(e)} + U_v^{(e)} \tag{5.3}$$

(i) Potential energy of the constraining layers

The potential energy of the constraining layers due to axial extension and bending is given as

$$U_c^{(e)} = \sum_{k=1}^{n+1} \frac{1}{2}\int_0^l E_{(2k-1)}\, I_{(2k-1)} \left(\frac{\partial^2 w}{\partial x^2}\right)^2 dx + \frac{1}{2}\int_0^l E_{(2k-1)}\, A_{(2k-1)} \left(\frac{\partial u_{(2k-1)}}{\partial x}\right)^2 dx \tag{5.4}$$

where $E_{(2k-1)}$, $A_{(2k-1)} = b\{t_{(2k-1)}\}$ and $I_{(2k-1)} = b\{t_{(2k-1)}\}^3/12$ are the Young's modulus, cross-sectional area and area moment of inertia of the (*2k-1*)th constraining layer respectively.

By substituting eq.(5.2) in to eq. (5.4) the element potential energy of the constraining layers can be written as

$$U_c^{(e)} = \sum_{k=1}^{n+1} \frac{1}{2} \{\Delta^{(e)}\}^T \left(\left[K_{(2k-1)w}^{(e)}\right] + \left[K_{(2k-1)u}^{(e)}\right]\right)\{\Delta^{(e)}\} \tag{5.5}$$

where

$$\left.\begin{aligned} \left[K_{(2k-1)u}^{(e)}\right] &= E_{(2k-1)}\, A_{(2k-1)} \int_0^l \left[N_{(2k-1)}\right]'^T \left[N_{(2k-1)}\right]' \, dx \\ \left[K_{(2k-1)w}^{(e)}\right] &= E_{(2k-1)}\, I_{(2k-1)} \int_0^l \left[N_w\right]''^T \left[N_w\right]'' \, dx \end{aligned}\right\} \tag{5.6}$$

(ii) Potential energy of the viscoelastic layers

The potential energy of the viscoelastic layers due to shear deformation is given as

$$U_v^{(e)} = \sum_{j=1}^{n} \frac{1}{2}\int_0^l G_{v(2j)}\, A_{v(2j)}\, \gamma_{v(2j)}^2 \, dx \tag{5.7}$$

where $A_{v(2j)}$ is the cross-sectional area and $G_{v(2j)}$ is the complex shear modulus of 2jth layer. $\mathrm{G}_{\mathrm{v(2j)}} = \mathrm{G}^*_{\mathrm{v(2j)}} \left[1 + i(\eta_{\mathrm{c}})_{(2j)} \right]$, where $G^*_{v(2j)}$ is the in-phase shear modulus of the 2jth viscoelastic material layer, $(\eta_{\mathrm{c}})_{(2j)}$ is the associated core loss factor and $i = \sqrt{-1}$.

The shear strain $\gamma_{v(2j)}$ of the 2jth viscoelastic layer from kinematic relationships between the constraining layers[78] is expressed as follows:

$$\gamma_{v(2j)} = \frac{u_{2j+1} - u_{2j-1}}{t_{v(2j)}} + \frac{(t_{2j+1} + 2t_{v(2j)} + t_{2j-1})}{2t_{v(2j)}} \frac{\partial w}{\partial x} \tag{5.8}$$

Substituting eq. (5.2) in to eq.(5.8) $\gamma_{v(2j)}$ can be expressed in terms of nodal displacements and element shape functions:

$$\gamma_{v(2\mathrm{j})} = \left[N_{\gamma(2\mathrm{j})}\right] \left\{\Delta^{(e)}\right\} \tag{5.9}$$

where $$\left[N_{\gamma(2j)}\right] = \frac{\left(\left[N_{2j+1}\right] - \left[N_{2j-1}\right]\right)}{t_{v(2j)}} + \frac{(t_{2j+1} + 2t_{v(2j)} + t_{2j-1})}{2t_{v(2j)}} \left[N_w\right]' \tag{5.10}$$

Substituting eq. (5.9) in to eq. (5.7), the potential energy of the viscoelastic material layers is given by

$$U_v^{(e)} = \sum_{j=1}^{n} \frac{1}{2} \left\{\Delta^{(e)}\right\}^T \left(\left[K^{(e)}_{v\gamma(2j)}\right]\right) \left\{\Delta^{(e)}\right\} \tag{5.11}$$

where $$\left[K^{(e)}_{v\gamma}\right] = \sum_{j=1}^{n} G_{v(2j)} A_{v(2j)} \int_0^l \left[N_{\gamma(2\mathrm{j})}\right]^T \left[N_{\gamma(2\mathrm{j})}\right] dx \tag{5.12}$$

From eq. (5.3) elemental potential energy

$$U^{(e)} = \sum_{k=1}^{n+1} \frac{1}{2} \left\{\Delta^{(e)}\right\}^T \left(\left[K^{(e)}_{(2k-1)u}\right] + \left[K^{(e)}_{(2k-1)w}\right]\right) \left\{\Delta^{(e)}\right\} + \sum_{j=1}^{n} \frac{1}{2} \left\{\Delta^{(e)}\right\}^T \left(\left[K^{(e)}_{v\gamma(2j)}\right]\right) \left\{\Delta^{(e)}\right\}$$

$$= \frac{1}{2}\left\{\Delta^{(e)}\right\}^{T}\left(\left[K^{(e)}\right]\right)\left\{\Delta^{(e)}\right\}$$

(5.13)

where $\left[K^{(e)}\right] = \sum_{k=1}^{n+1}\left(\left[K^{(e)}_{(2k-1)u}\right] + \left[K^{(e)}_{(2k-1)w}\right]\right) + \sum_{j=1}^{n}\left(\left[K^{(e)}_{v\gamma(2j)}\right]\right)$ (5.14)

$\left[K^{(e)}\right]$ is the element stiffness matrix

5.2.1.2 Element mass matrix

Elemental kinetic energy ($T^{(e)}$) is equal to the sum of the kinetic energy of the constraining layers and viscoelastic layers.

$$T^{(e)} = T_{c}^{(e)} + T_{v}^{(e)} \tag{5.15}$$

(i) Kinetic energy of the constraining layers is written as

$$T_{c}^{(e)} = \sum_{k=1}^{n+1}\frac{1}{2}\int_{0}^{l}\rho_{(2k-1)}\,A_{(2k-1)}\left(\frac{\partial w}{\partial t}\right)^{2}dx + \frac{1}{2}\int_{0}^{l}\rho_{(2k-1)}\,A_{(2k-1)}\left(\frac{\partial u_{(2k-1)}}{\partial t}\right)^{2}dx \tag{5.16}$$

where $\rho_{(2k-1)}$ is the mass density of the (*2k-1*)th constraining layer.

By substituting eq. (5.2) in to eq. (5.16), the element kinetic energy of the constraining layers can be written as

$$T_{c}^{(e)} = \sum_{k=1}^{n+1}\frac{1}{2}\left\{\dot{\Delta}^{(e)}\right\}^{T}\left(\left[M^{(e)}_{(2k-1)u}\right] + \left[M^{(e)}_{(2k-1)w}\right]\right)\left\{\dot{\Delta}^{(e)}\right\} \tag{5.17}$$

where

$$\left.\begin{aligned}\left[M^{(e)}_{(2k-1)u}\right] &= \rho_{(2k-1)}\,A_{(2k-1)}\int_{0}^{l}\left[N_{(2k-1)u}\right]^{T}\left[N_{(2k-1)u}\right]dx\\ \left[M^{(e)}_{(2k-1)w}\right] &= \rho_{(2k-1)}\,A_{(2k-1)}\int_{0}^{l}\left[N_{w}\right]^{T}\left[N_{w}\right]dx\end{aligned}\right\} \tag{5.18}$$

and the dot denotes differentiation with respect to time t.

(ii) Kinetic energy of the viscoelastic layers is written as

$$T_v^{(e)} = \sum_{j=1}^{n} \frac{1}{2} \int_0^l \rho_{v(2j)}\ A_{v(2j)} \left\{ \left(\frac{\partial w}{\partial t} \right)^2 + \left(\frac{\partial u_{v(2j)}}{\partial t} \right)^2 \right\} dx \tag{5.19}$$

where $A_{v(2j)}$ is the cross-sectional area and $\rho_{v(2j)}$ is the mass density of the 2jth viscoelastic layer

The axial displacement $u_{v(2j)}$ of the 2jth viscoelastic layer derived from kinematic relationships between the constraining layers[78] is expressed as follows:

$$u_{v(2j)} = \frac{u_{2j+1} + u_{2j-1}}{2} + \frac{(t_{2j+1} - t_{2j-1})}{4} \frac{\partial w}{\partial x} \tag{5.20}$$

Substituting eq. (5.2) in to eq. (5.20) u_v can be expressed in terms of nodal displacements and element shape functions:

$$u_{v(2j)} = \left[N_{v(2j)} \right] \left\{ \Delta^{(e)} \right\} \tag{5.21}$$

where $$\left[N_{v(2j)} \right] = \frac{1}{2} \left(\left[N_{2j+1} \right] + \left[N_{2j-1} \right] \right) \frac{(t_{2j+1} - t_{2j-1})}{4} \left[N_w \right]' \tag{5.22}$$

Substituting eq. (5.2) in to eqs. (5.21) and (5.19), the kinetic energy of viscoelastic material layers is given by

$$T_v^{(e)} = \sum_{j=1}^{n} \frac{1}{2} \left\{ \dot{\Delta}^{(e)} \right\} \left(\left[M_{v(2j)}^{(e)} \right] \right) \left\{ \dot{\Delta}^{(e)} \right\} \tag{5.23}$$

where $$\left[M_{v(2j)}^{(e)} \right] = \sum_{j=1}^{n} \rho_{v(2j)}\ A_{v(2j)} \int_0^l \left[N_{v(2j)} \right]^T \left[N_{v(2j)} \right] dx + \rho_{v(2j)}\ A_{v(2j)} \int_0^l \left[N_w \right]^T \left[N_w \right] dx \tag{5.24}$$

From eq.(5.15)

$$T^{(e)} = \sum_{k=1}^{n+1} \frac{1}{2} \left\{ \dot{\Delta}^{(e)} \right\}^T \left(\left[M_{(2k-1)u}^{(e)} \right] + \left[M_{(2k-1)w}^{(e)} \right] \right) \left\{ \dot{\Delta}^{(e)} \right\} + \sum_{j=1}^{n} \frac{1}{2} \left\{ \dot{\Delta}^{(e)} \right\}^T \left(\left[M_{v(2j)}^{(e)} \right] \right) \left\{ \dot{\Delta}^{(e)} \right\} \tag{5.25}$$

$$T^{(e)} = \frac{1}{2}\left\{\dot{\Delta}^{(e)}\right\}^T \left(\left[M^{(e)}\right]\right) \left\{\dot{\Delta}^{(e)}\right\} \tag{5.26}$$

where $$\left[M^{(e)}\right] = \sum_{k=1}^{n+1} \left(\left[M^{(e)}_{(2k-1)u}\right] + \left[M^{(e)}_{(2k-1)w}\right]\right) + \sum_{j=1}^{n} \left(\left[M^{(e)}_{v(2j)}\right]\right)$$

(5.27)

and $\left[M^{(e)}\right]$ is the elemental mass matrix.

5.2.1.3 Element geometric stiffness matrix

The elemental work done by axial periodic force $P(t)$ is written as

$$W_p^{(e)} = \frac{1}{2}\int_0^l P(t)\left(\frac{\partial w}{\partial x}\right)^2 dx$$

(5.28)

Substituting eq.(5.2) in to eq.(5.28), the work done by the axial periodic load can be rewritten as

$$W_p^{(e)} = \frac{1}{2}\left\{\Delta^{(e)}\right\}^T P(t)\, K_g^{(e)} \left\{\Delta^{(e)}\right\} \tag{5.29}$$

where $[K_g^{(e)}] = \int_0^l \left[N_w\right]'^T \left[N_w\right]' \, dx$, the elemental geometric stiffness matrix.

5.2.2 Governing equations of motions

The element equation of motion for a sandwich beam is obtained by using Hamilton's principle.

$$\delta\int_{t_1}^{t_2}\left(T^{(e)} - U^{(e)} + W_p^{(e)}\right)dt = 0 \tag{5.30}$$

Substituting eqs.(5.13), (5.26) and (5.29) in to eq. (5.30) the equation of motion for the sandwich beam element is obtained as follows:

$$\left[M^{(e)}\right]\left\{\ddot{\Delta}^{(e)}\right\}+\left[K^{(e)}\right]\left\{\Delta^{(e)}\right\}-P(t)\left[K_g^{(e)}\right]\left\{\Delta^{(e)}\right\}=0 \tag{5.31}$$

Assembling mass, elastic stiffness and geometric stiffness matrices of individual element, the equation of motion for the beam is written as

$$[M]\{\ddot{\Delta}\}+[K]\{\Delta\}-P(t)[K_g]\{\Delta\}=0 \tag{5.32}$$

where $\{\Delta\}$ is the global displacement matrix.

The static component P_s and dynamic component P_t of the load $P(t)$, can be represented in terms of P^* as $P_s = \alpha P^*$ and $P_t = \beta P^*$ and, where $P^*=D/L^2$ and $D=\sum_{k=1}^{n+1} E_{(2k-1)} I_{(2k-1)}$.

Hence substituting $P(t)=\alpha P^*+\beta P^* cos\,\Omega\, t$, where α and β are static and dynamic load factors respectively.

Substituting $P(t)$, eq.(5.32) becomes

$$[M]\{\ddot{\Delta}\}+[K]\{\Delta\}-(\mathrm{P_s}+\mathrm{P_t}\cos\Omega t)\,[K_g]\,\{\Delta\}=0 \tag{5.33}$$

$$[M]\{\ddot{\Delta}\}+\left([K]-\mathrm{P_s}\,[K_g]_S\right)\{\Delta\}-\mathrm{P_t}\,\cos\Omega t\,[K_g]_t\,\{\Delta\}=0 \tag{5.34}$$

where the matrices $[K_g]_s$ and $[K_g]_t$ reflect the influence of P_s and P_t respectively. If the static and time dependent component of loads are applied in the same manner, then $[K_g]_s=[K_g]_t=[K_g]$.

$$[M]\{\ddot{\Delta}\}+[\overline{K}]\{\Delta\}-\left(\beta\,\mathrm{P}^*\cos\Omega\,t\right)\,[K_g]\{\Delta\}=0 \tag{5.35}$$

where $[\overline{K}]=[K]-P_s\,[K_g]$ (5.36)

The global displacement matrix $\{\Delta\}$ can be assumed as

$$\{\Delta\} = [\Phi]\{\Gamma\} \tag{5.37}$$

where $[\Phi]$ is the normalized modal matrix corresponding to

$$[M]\{\ddot{\Delta}\} + [\overline{K}]\{\Delta\} = 0 \tag{5.38}$$

and $\{\Gamma\}$ is a new set of generalised coordinates .

Substituting eq.5.37 in eq.5.35, eq.5.35 is transformed to the following set of N_c coupled Mathieu equations.

$$\ddot{\Gamma}_m + \left(\omega_m^2\right)\Gamma_m + \beta P^* \cos\Omega t \sum_{n=1}^{N_c} b_{mn}\Gamma_n = 0 \qquad m = 1,2,........ N_c. \tag{5.39}$$

where $\left(\omega_m^2\right)$ are the distinct eigenvalues of $[M]^{-1}[\overline{K}]$ and b_{mn} are the elements of the complex matrix $[B] = -[\Phi]^{-1}[M]^{-1}[K_g]\,[\Phi]$ and

$\omega_m = \omega_{m.R} + i\,\omega_{m.I}, \qquad b_{mn} = b_{mn.R} + i\; b_{mn.I}$ and $\mathrm{i} = \sqrt{-1}$

5.2.3 Regions of instability

Hsu [52] developed a procedure for obtaining the regions of instability for simple and combination resonances by applying the series expansion of perturbation method and method of constant variation of parameters to a system having multiple degrees of freedom. Saito and Otomi [104] applied the Hsu's method to the Matheiu equation (5.39), which has complex coefficients and obtained the conditions for the existence of regions of instability for simple and combination resonances of sum and difference types. The conditions are as given below.

Case (A): Simple resonance

The boundaries of the instability regions are given by

$$\left|\frac{\Omega}{2\omega_0}-\overline{\omega}_{\mu,R}\right|\langle\frac{1}{4}\left[\frac{\beta^2(b^2{}_{\mu\mu,R}+b^2{}_{\mu\mu,I})}{\overline{\omega}^2{}_{\mu,R}}-16\,\overline{\omega}^2{}_{\mu,I}\right]^{1/2},\quad \mu=1,2.........N_c. \tag{5.40}$$

where $\omega_0=\sqrt{D/mL^4}$, $\overline{\omega}_{\mu,R}=\omega_{\mu,R}/\omega_0$, $\overline{\omega}_{\mu,I}=\omega_{\mu,I}/\omega_0$, m is mass per unit length of the multilayered sandwich beam.

When damping is neglected, the regions of instability are given by

$$\left|\frac{\Omega}{2\omega_0}-\overline{\omega}_{\mu,R}\right|\langle\frac{1}{4}\left[\frac{\left|\beta(b_{\mu\mu,R})\right|}{\overline{\omega}_{\mu,R}}\right],\qquad \mu=1,2,......N_c. \tag{5.41}$$

Case (B): Combination resonance of sum type

The boundaries of the regions of instability of sum type are given by

$$\left|\frac{\Omega}{2\omega_0}-\frac{1}{2}(\overline{\omega}_{\mu,R}+\overline{\omega}_{\nu,R})\right|\langle\frac{1}{8}\frac{(\overline{\omega}_{\mu,I}+\overline{\omega}_{\nu,I})}{(\overline{\omega}_{\mu,I}\,\overline{\omega}_{\nu,I})^{1/2}}\left[\frac{\beta^2(b_{\mu\nu,R}b_{\nu\mu,R}+b_{\mu\nu,I}b_{\nu\mu,I})}{\overline{\omega}_{\mu,R}\,\overline{\omega}_{\nu,R}}-16\overline{\omega}_{\mu,I}\overline{\omega}_{\nu,I}\right]^{1/2} \tag{5.42}$$

$\mu\neq\nu,\mu,\nu=1,2,...N_c.$

When damping is neglected, the regions of instability are given by

$$\left|\frac{\Omega}{2\omega_0}-\frac{1}{2}(\overline{\omega}_{\mu,R}+\overline{\omega}_{\nu,R})\right|\langle\frac{1}{4}\left[\frac{\beta^2(b_{\mu\nu,R}\,b_{\nu\mu,R})}{\overline{\omega}_{\mu,R}\,\overline{\omega}_{\nu,R}}\right]^{1/2},\ \mu\neq\nu,\ \mu,\nu=1,2,...N_c. \tag{5.43}$$

Case (C): Combination resonance of difference type

The boundaries of the regions of instability of difference type are given by

$$\left|\frac{\Omega}{2\omega_0}-\frac{1}{2}(\overline{\omega}_{\nu,R}-\overline{\omega}_{\mu,R})\right|\langle\frac{1}{8}\frac{(\overline{\omega}_{\mu,I}+\overline{\omega}_{\nu,I})}{(\overline{\omega}_{\mu.I}\,\overline{\omega}_{\nu.I})^{1/2}}\left[\frac{\beta^2(b_{\mu\nu,I}\,b_{\nu\mu,I}-b_{\mu\nu,R}b_{\nu\mu,R})}{\overline{\omega}_{\mu,R}\,\overline{\omega}_{\nu,R}}-16\overline{\omega}_{\mu,I}\overline{\omega}_{\nu,I}\right]^{1/2},$$

$$\nu\rangle\mu,\mu,\nu=1,2,...N_c. \tag{5.44}$$

When damping is neglected, the unstable regions are given by

$$\left|\frac{\Omega}{2\omega_0}-\frac{1}{2}(\bar{\omega}_{\nu,R}-\bar{\omega}_{\mu,R})\right|\langle\frac{1}{4}\left[-\frac{\beta^{2}(b_{\mu\nu,R}\,b_{\nu\mu,R})}{\bar{\omega}_{\mu,R}\,\bar{\omega}_{\nu,R}}\right]^{1/2},\quad \nu\rangle\mu,\ \mu,\nu=1,2,..N_c. \tag{5.45}$$

For a combination of excitation frequency ($\Omega/2\omega_o$), natural frequency/frequencies (ω_μ or/and ω_ν), and dynamic load factor (β), when one or more of the above conditions are satisfied, instability of the system is indicated. For example if for a particular pair of $\Omega/2\omega_o$ and β, the condition given by eq.(5.40) is satisfied for $\mu = 1(\omega_\mu=\omega_1)$, then this will lead to instability of simple resonance of type $2\omega_1$ of the system. Similarly if for a pair of $\Omega/2\omega_o$ and β, the condition given by eq.(5.40) is satisfied for $\mu = 2(\omega_\mu=\omega_2)$, this will lead to simple resonance of type $2\omega_2$. For a pair of $\Omega/2\omega_o$ and β, if eq.(5.42) is satisfied when $\mu = 1(\omega_\mu=\omega_1)$ and $\nu = 2$ $(\omega_\nu=\omega_2)$, then the system will have combination resonance of sum type ($\omega_1+\omega_2$). If eq.(5.44) is satisfied when $\mu=1$, ($\omega_\mu=\omega_1$) and $\nu = 2$, ($\omega_\nu=\omega_2$), then this will lead to combination resonance of difference type, (ω_2-ω_1). When pairs of $\Omega/2\omega_o$ and β, satisfying a particular instability condition is plotted in the parameter space of dynamic load component (β) and excitation frequency ($\Omega/2\omega_o$), the corresponding instability region is obtained.

5.3 Computational procedure

In the initialisation phase, geometry and material parameters are specified. The input data to the computer program are material parameters like Young's modulus of the elastic layers, in phase shear modulus and core loss factor of the viscoelastic layers, mass density of both the elastic and viscoelastic layers and geometric parameters like length and width of the beam and thickness of the elastic and viscoelastic layers. The beam is divided in to n_s number of elements and n_s+1 number of nodes. The elements of the element mass, elastic stiffness and geometric stiffness matrices $\left(\left[M^{(e)}\right],\left[K^{(e)}\right]\text{and}\left[K_g{}^{(e)}\right]\right)$ are computed by Gauss-Legendre numerical integration method. The program uses the built in Matlab function, 'quadl' to carry out the integration. Element matrices are assembled to obtain global matrices $\left([M],[K]\text{and}[K_g]\right)$. Boundary conditions are imposed by elimination method. For example for fixed-free end condition, the first n+3 rows and columns of the global matrices are eliminated to obtain the reduced matrices. The static load factor (α) is set to the required value. The normalised modal matrix $[\Phi]$ corresponding to eq.(5.38) is obtained by solving for the associated eigenvectors of $[M]^{-1}[\overline{K}]$ matrix. The built in Matlab function 'eig' is used to calculate the eigenvectors. Coefficient matrices of eq.(5.35) are premultiplied by $[M]^{-1}$ and $[\Phi]^{-1}$ and postmultiplied by $[\Phi]$ to obtain the eq.(5.39). The dynamic load factor β and the excitation frequency $\Omega/2\omega_0$ are increased in steps. For a particular pair of values of β and $\Omega/2\omega_0$ the eqs.(5.40, 5.42, 5.44) are checked and if at least one of the conditions is satisfied, the program stores the pair, β and $\Omega/2\omega_0$. When pairs of $\Omega/2\omega_0$ and β, satisfying a particular instability condition is plotted in the parameter space of dynamic load component (β) and excitation frequency ($\Omega/2\omega_0$), the corresponding instability region is obtained. The detailed computational procedure is shown schematically in the flow chart given in Appendix-B. The entire computational process has been implemented by computer programs developed in MATLAB [135].

5.4 Results and discussion

The multilayered beam considered being symmetric with identical viscoelastic and elastic layers, for the viscoelastic layers $t_{v(2j)} = t_2$, $G^*_{v(2j)} = G^*_v$, $(\eta_c)_{(2j)} = \eta_c$ and $\rho_{v(2j)} = \rho_2$ for all j and for the elastic layers $t_{(2k-1)} = t_1$, $E_{(2K-1)} = E_1$ and $\rho_{(2k-1)} = \rho_1$ for all k have been taken. For calculation purpose the young's modulus E_1 of the elastic layers and the in phase shear modulus of the viscoelastic material layers G^*_v are taken as 70×10^9 N/m^2 and 2.6×10^5 N/m^2 respectively. The ratio of mass density ρ_{21} of the viscoelastic material layer and elastic material layer is taken to be 0.4.With a ten element discretisation of the beam, the resonant frequencies and modal system loss factors obtained for a three-layer beam are compared with those of Rao [96] and results are found to be in good agreement. Resonant frequencies obtained from experiment for beams of three, five and seven numbers of layers, also compare well with the calculated values and these data are given in Table-7.6. The boundary frequencies of a three layer cantilever sandwich beam, obtained from the present analysis have been compared with those of [75] and these are found to be in good agreement. This is shown in Table 5.1.

Table 5.1: Comparison of the boundary frequencies for a three layer cantilever sandwich beam from the present analysis with those of reference [75].

To study the effect of various system parameters, such as core thickness parameter t_{21}, (defined as the ratio of the thickness of the viscoelastic core to the thickness of the elastic layer), number of layers and core loss factor, numerical results have been obtained for three, five and seven layered beams. As well as five special cases for which beams with different number of layers and all having (i) constant size or (ii) constant weight or (iii) constant flexural rigidity or (iv) constant size and flexural rigidity or (v)

Dynamic load factor (β)		Simple resonance instability region ($2\omega_1$)		Simple resonance instability region ($2\omega_2$)		Combination resonance of difference type instability region (ω_2 - ω_1)	
		Lower	Upper	Lower	Upper	Lower	Upper
0.05	Present	3.876	3.981				
	Ref [75]	3.869	4.000				
0.1	Present	3.668	4.256				
	Ref [75]	3.672	4.262				
0.2	Present	3.440	4.592	19.87	25.25	12.2	12.811
	Ref [75]	3.443	4.590	20	25.333	12.15	12.85
0.3	Present	3.123	4.79	19.44	26.928	11.702	12.912
	Ref [75]	3.118	4.787	19.6	26.933	11.8	13.1
0.4	Present	2.785	5.087	19.11	29.114	11.601	13.390
	Ref [75]	2.787	5.082	19.2	29.227	11.55	13.35
0.5	Present	2.622	5.415	19.00	31.392	11.300	13.621
	Ref [75]	2.623	5.41	19.013	31.493	11.32	13.69

constant weight and flexural rigidity have also been investigated. For first three cases core thickness parameter (t_{21}) is same for beams of any number of layers.

In the following discussion, N=2n+1 is the total number of layers of the beam and $(g)_N = \dfrac{G_v^*}{(t_{21})_N} \left(\dfrac{L}{t_1}\right)_N^2 \left(\dfrac{2}{E_1}\right)$ as defined in Rao [96], is the shear parameter for an N layered beam.

If n_e *and* n'_e are the number of viscoelastic layers in $(2n_e+1)$ and $(2n'_e+1)$ layered beams with t_1 *and* t'_1 being the thickness of elastic layers in corresponding beams the relation between t_1 *and* t'_1 for above mentioned cases are;

(i) Constant size

$$\frac{(t_1)_{(2n_e+1)}}{(t'_1)_{(2n'_e+1)}} = \frac{[(n'_e+1)+(t_{21})n'_e]}{[(n_e+1)+(t_{21})\; n_e]}$$

(ii) Constant weight

$$\frac{(t_1)_{(2n_e+1)}}{(t'_1)_{(2n'_e+1)}} = \frac{[(n'_e+1)+(\rho_{21})(t_{21})n'_e]}{[(n_e+1)+(\rho_{21})(t_{21})\; n_e]}$$

(iii)Constant flexural rigidity

$$\frac{(t_1)_{(2n_e+1)}}{(t'_1)_{(2n'_e+1)}} = \left(\frac{n'_e+1}{n_e+1}\right)^{\frac{1}{3}}$$

(iv)Constant size and flexural rigidity

$$(t_{21})_{(2n'_e+1)} = \frac{\left(\frac{n'_e+1}{n_e+1}\right)^{1/3}\left[(n_e+1)+(t_{21})_{(2n_e+1)}(n_e)\right]-(n'_e+1)}{[\; n'_e]}$$

(v) Constant weight and flexural rigidity

$$(t_{21})_{(2n'_e+1)} = \frac{\left(\frac{n'_e+1}{n_e+1}\right)^{1/3}\left[(n_e+1)+(\rho_{21})_{(2n_e+1)}(t_{21})_{(2n_e+1)}(n_e)\right]-(n'_e+1)}{\left[(\rho_{21})_{(2n'_e+1)}\;(n'_e)\right]}$$

Figures (5.3-5.4) show the effect of core thickness parameter (t_{21}) on first and second modal frequency parameters η_1 and η_2 of the sandwich beam with three, five and seven layers. Modal frequency parameter is defined as the ratio of resonant frequency of the corresponding mode for the sandwich beam to ω_o. For all the three types of beam shear parameter $(g)_N$ has been taken as 5.0. It is observed from the graphs that for a beam of particular number of layers, both the frequency parameters increase linearly with increase in core thickness parameter. Also with increase in number of layers when core thickness parameter is same for all types of beam, both the frequency parameters increase. The increase in resonant frequencies with number of layers is more for higher values of core thickness parameter.

Figures (5.5-5.6) show the effect of core thickness parameter on η_1 and η_2 for constant size case. Both the frequency parameters increase with increase in core thickness parameter. For constant size case with increase in number of layers both the frequency parameters decrease with increase in number of layers when the core thickness parameter is kept unchanged.

Figures (5.7-5.8) show the variation of η_1 and η_2 for constant weight case. The behaviours are same as those for constant size case.

Figures (5.9-5.10) show the variation of η_1 and η_2 for constant flexural rigidity case. The first mode frequency parameter shows a linear variation with core thickness parameter. Irrespective of the value of core thickness parameter with increase in number of layers there is an increase in fundamental frequency parameter η_1. Second mode frequency parameter decreases with increase in number of layers for lower values of core thickness parameter. For higher values of core thickness parameter the trend is reverse.

Figures (5.11-5.12) show the effect of core thickness parameter on η_1 and η_2 for constant size and flexural rigidity case. Both the frequency parameters increase with increase in core thickness parameter. For lower value of core thickness parameter with increase in number of layers both the frequency parameters increase. For higher values of core thickness parameter the effect of increase in number of layers becomes less dominant on resonant frequencies and frequency parameters converge to the same value irrespective of number of layers.

Figures (5.13-5.14) show the same curves for constant weight and flexural rigidity case. The trend of the curves is same as those for constant size and flexural rigidity case, but the effect is more pronounced compared to constant size and flexural rigidity case.

Figures (5.15-5.16) show the instability zones for three, five and seven layered beams with ρ_c equal to 0.18 and t_{21} equal to 1/3 and 2/3 respectively. For beams with the same number of layers, instability zones are also shown in figs. (5.17 and 5.18) for ρ_c equal to 0.3 and core thickness parameter t_{21} equal to 1/3 and 2/3 respectively. Comparison of fig.(5.15) with fig.(5.16) and fig.(5.17) with fig.(5.18) shows that with increase in t_{21} with ρ_c and N fixed, the instability regions shift to higher frequencies of excitation along the frequency axis and they also move vertically up along the dynamic load factor axis. More over their areas decrease and some of the instability regions also vanish with increase in t_{21}. This shows improved stability with increase in core thickness parameter.

From figs. (5.15-5.18), it can be observed that with increase in number of layers with t_{21} and ρ_c fixed, the instability zones shift to higher frequencies of excitation and they start at higher values of dynamic load factor. There is reduction in areas of the instability zones and some instability zones vanish. This indicates improved stability with increase in number of layers, keeping the core thickness parameter fixed.

Figures (5.15 and 5.17) show the instability zones for three, five and seven layer beams with core thickness parameter 1/3 and core loss factor 0.18 and 0.3 respectively. Instability zones for beams with similar number of layers are also shown in figs. (5.16 and 5.18) for core thickness parameter 2/3 and same values of core loss factor. It is seen that for beams with same $t_{21,}$ with increase in core loss factor the instability zones shift to higher values of dynamic load component and there is reduction in their areas also. Some instability zones also disappear with increase in core loss factor. This shows improvement in stability with increase in core loss factor. Howeverthere is no marked shift in the positions of the instability regions along the frequency axis with increase in core loss factor.

Figure (5.19) shows the instability zones for the constant size case with $(g)_3 = 1.0$ and core thickness parameter $(t_{21})_3 = 1.0$ for the reference three layer beam. It is observed that with increase in number of layers the instability zones shift to lower frequencies of excitation. This is due to decrease in resonant frequencies of the beam with increase in number of layers for constant size case. But with increase in number of layers the instability regions of sum type vanishes, also other principal instability regions start at higher values of dynamic load component. So there may be deterioration or improvement in stability depending on the applied excitation frequency and dynamic load component.

In fig. (5.20) the instability regions for constant weight case are shown for same values of $(g)_3$ and $(t_{21})_3$. Similar behaviour as those for constant size case is observed.

Figure (5.21) shows the instability zones for the constant flexural rigidity case. It is seen that with increase in number of layers the first instability zone shifts to higher frequency of excitation, where as the second instability zone shifts to lower frequency of excitation. This is due to the fact that the fundamental resonant frequency for constant flexural rigidity case increases with increase in number of layers for any value of core thickness parameter between 0.01 and 5.0. But with increase in number of layers there is decrease in second modal frequency parameter for lower values of $t_{21,}$ for higher values of t_{21} the trend is reverse (fig-5.10). With increase in number of layers, there is reduction in areas of both the first and second simple instability zones, also the instability region of combination resonance type vanishes and instability commences with higher dynamic load component, indicating improved stability.

Figure (5.22) shows the instability zones for constant size and flexural rigidity case for parameters $(g)_3 = 0.2$ and core thickness parameter $(t_{21})_3 = 4.0$. It is seen that with increase in number of layers the instability zones shift to higher frequency of excitation, there is reduction in areas of the instability zones and instability starts with higher value of dynamic load component, this indicates improvement in stability with increase in number of layers.

Figure (5.23) shows the instability zones for constant weight and flexural rigidity case for parameters $(g)_3 = 0.2$ and core thickness parameter $(t_{21})_3 = 4.0$. Similar trends as those for constant size and flexural rigidity case are observed, but the effect is more pronounced in this case compared to constant size and flexural rigidity case. This is because of large change in resonant frequencies with increase in number of layers for constant weight and flexural rigidity case compared to constant size and flexural rigidity case, figs. (5.11-5.14).

5.5 Closure

The first and second resonant frequencies increase with increase in core thickness parameter and number of layers. For constant size and constant weight cases with increase in core thickness parameter the resonant frequencies increase and frequencies decrease with increase in number of layers for a particular core thickness parameter. For the case of constant flexural rigidity the fundamental resonant frequency increases with increase in number of layers or core thickness parameter. The second resonant frequency may increase or decrease with increase in number of layers depending on the core thickness parameter. For constant size and flexural rigidity case increase in number of layers or core thickness parameter increases the resonant frequencies. For higher values of core thickness parameter increase in number of layers has marginal effect on the resonant frequencies. For constant weight and flexural rigidity case, increase in core thickness parameter or number of layers increase the resonant frequencies. The effect of these two factors on resonant frequencies for this case is more pronounced than that of constant size and flexural rigidity case. For higher values of core thickness parameter the effect of increase in number of layers also becomes less effective as in the case of constant size and flexural rigidity case.

Increase in core thickness parameter, number of layers and core loss factor has stabilizing effect. For constant size and constant weight case, increase in number of layers deteriorates the stability with instability zones relocating them at lower frequencies of excitation, improves the stability with instability zones shifting to higher values on the dynamic load axis and disappearance of some instability regions. Constant flexural rigidity criterion improves stability with increase in number of layers. Among constant size, constant weight and constant flexural rigidity, constant flexural rigidity criterion is the most effective in improving the stability. Both constant size and flexural rigidity and constant weight and flexural rigidity criteria improve the stability with increase in number of layers. Constant weight and flexural rigidity case is more effective in improving the stability than constant size and flexural rigidity case.

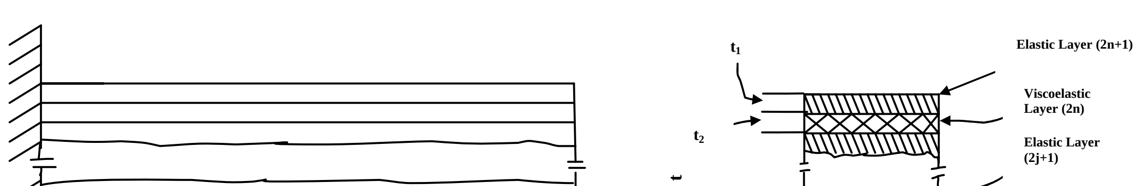

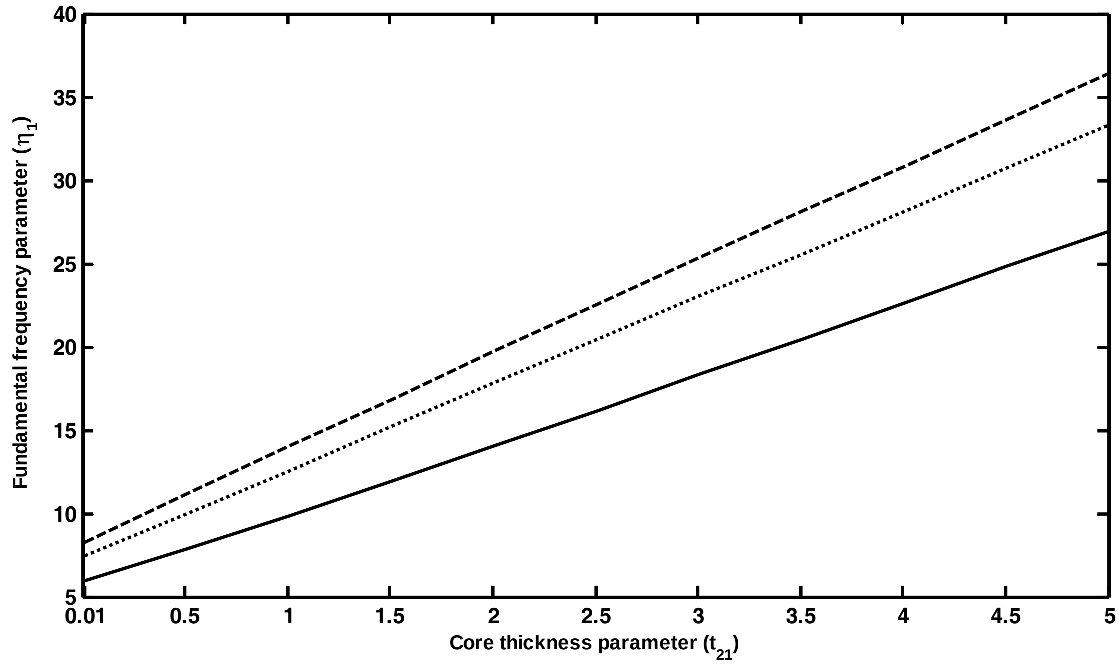

Fig.- 5. 3,Effect of core thickness parameter on fundamental frequency parameter, $(g)_N$= 5.0,η_c= 0.18;N=3;- ,N=5; ... ,N=7;- -,.

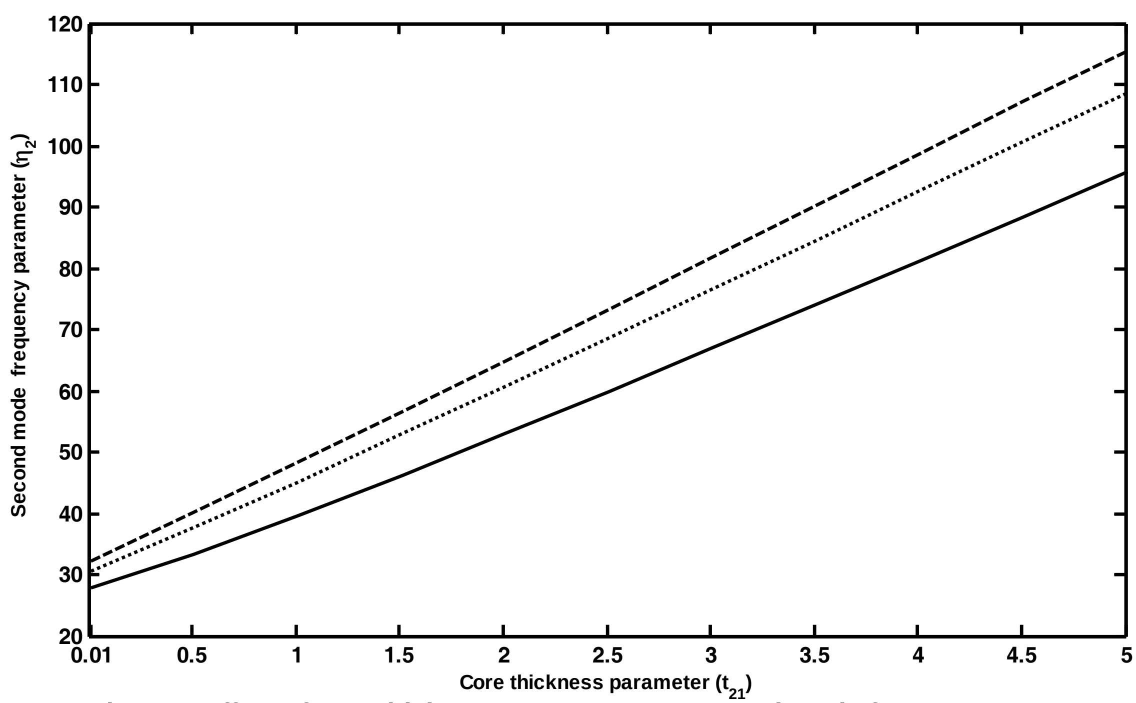

Fig.- 5.4 ,Effect of core thickness parameter on second mode frequency parameter $(g)_N$= 5.0, η_c= 0.18,key as fig.- 5.3.

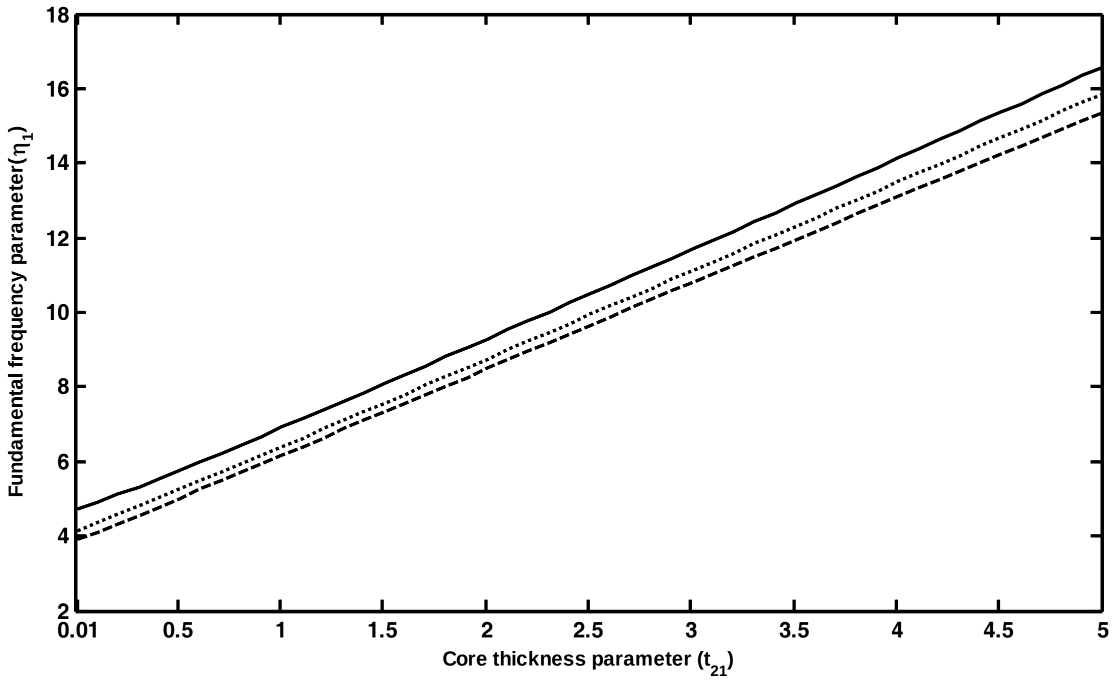

Fig.- 5.5 ,Effect of core thickness parameter on fundamental frequency parameter, constant size case,$(g)_3$=1.0,η_c= 0.18;N=3;- ,N=5; ... ,N=7;- -,.

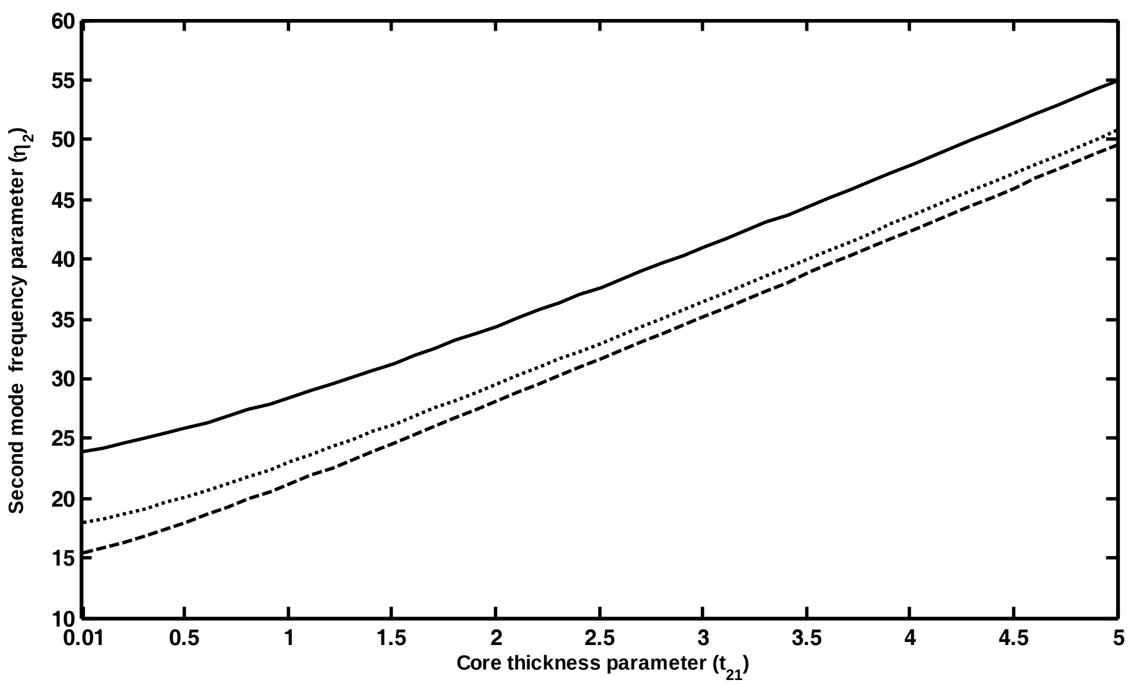

Fig.- 5.6 ,Effect of core thickness parameter on second mode frequency parameter, constant size case,$(g)_3$=1.0,η_c=0.18,key as fig.- 5.5.

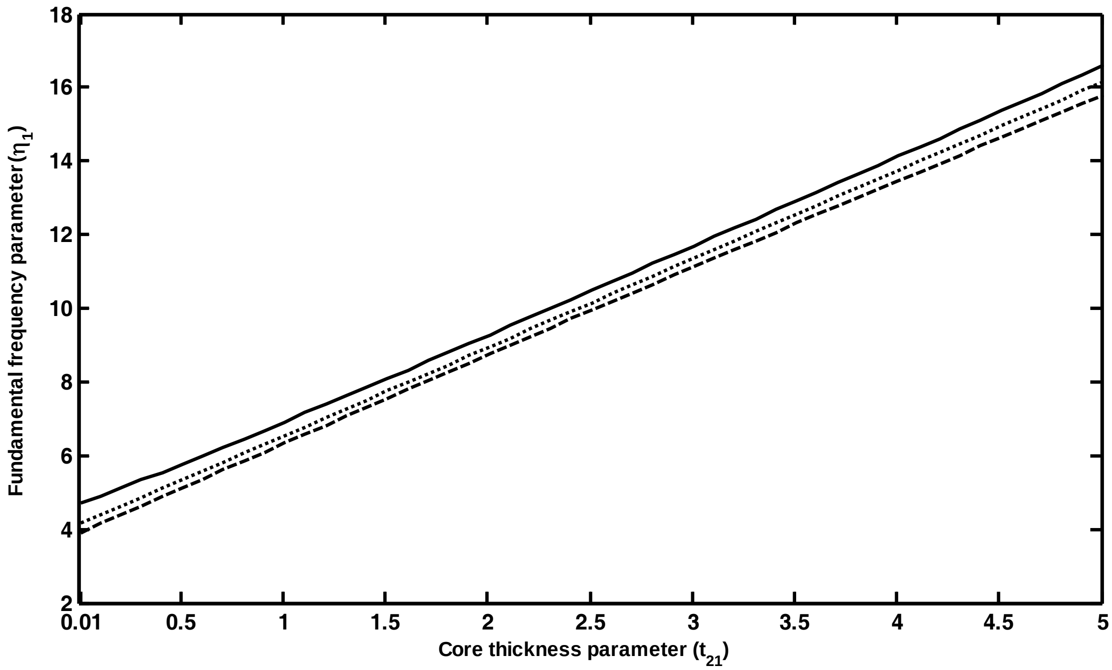

Fig.- 5.7,Effect of core thickness parameter on fundamental frequency parameter, constant weight case,$(g)_3$=1.0,η_c= 0.18,key as fig.- 5.5.

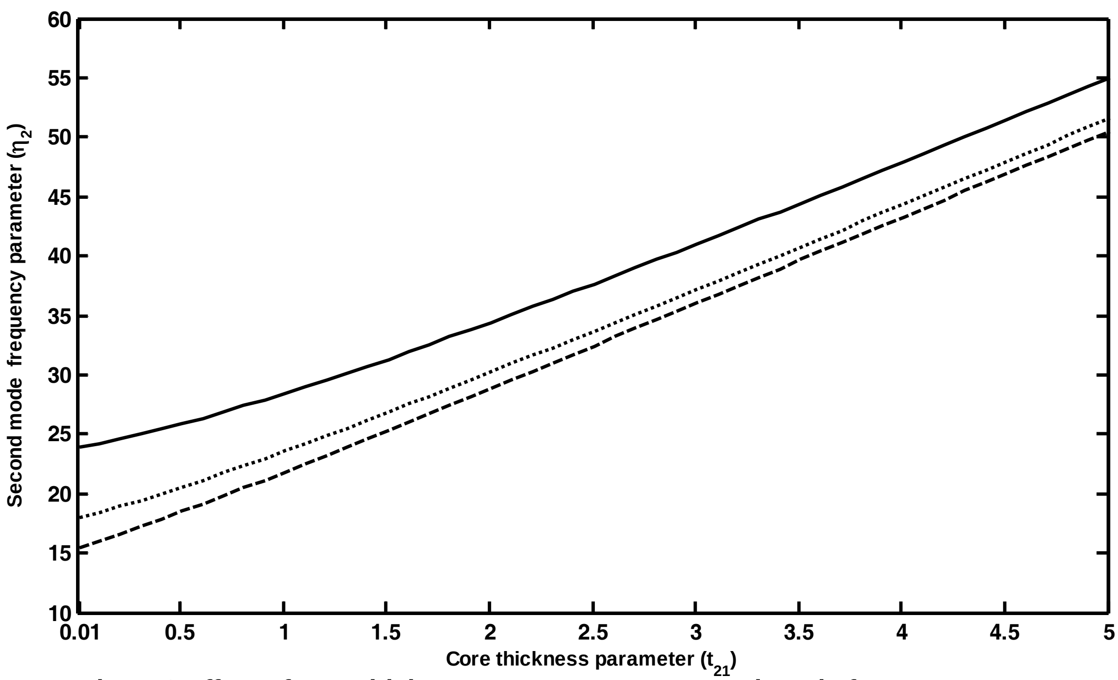

Fig.- 5.8,Effect of core thickness parameter on second mode frequency parameter, constant weight case,$(g)_3$=1.0,η_c= 0.18,key as fig.- 5.5.

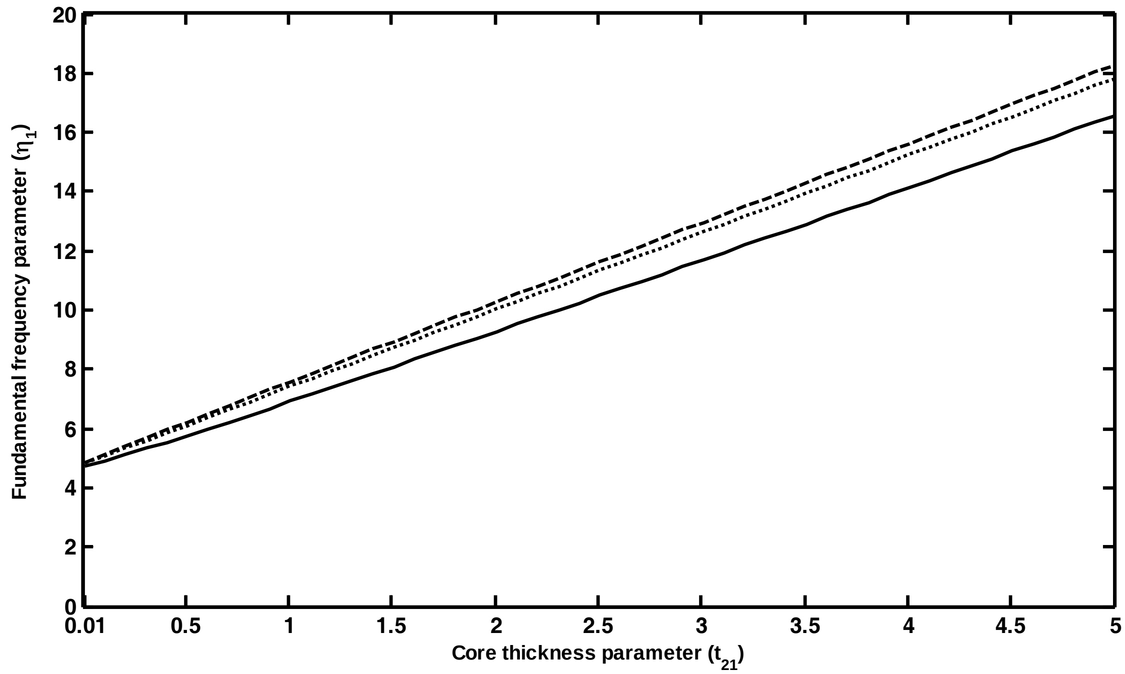

Fig.- 5.9,Effect of core thickness parameter on fundamental frequency parameter, constant flexural rigidity case,$(g)_3$=1.0,η_c= 0.18,key as fig.- 5.5.

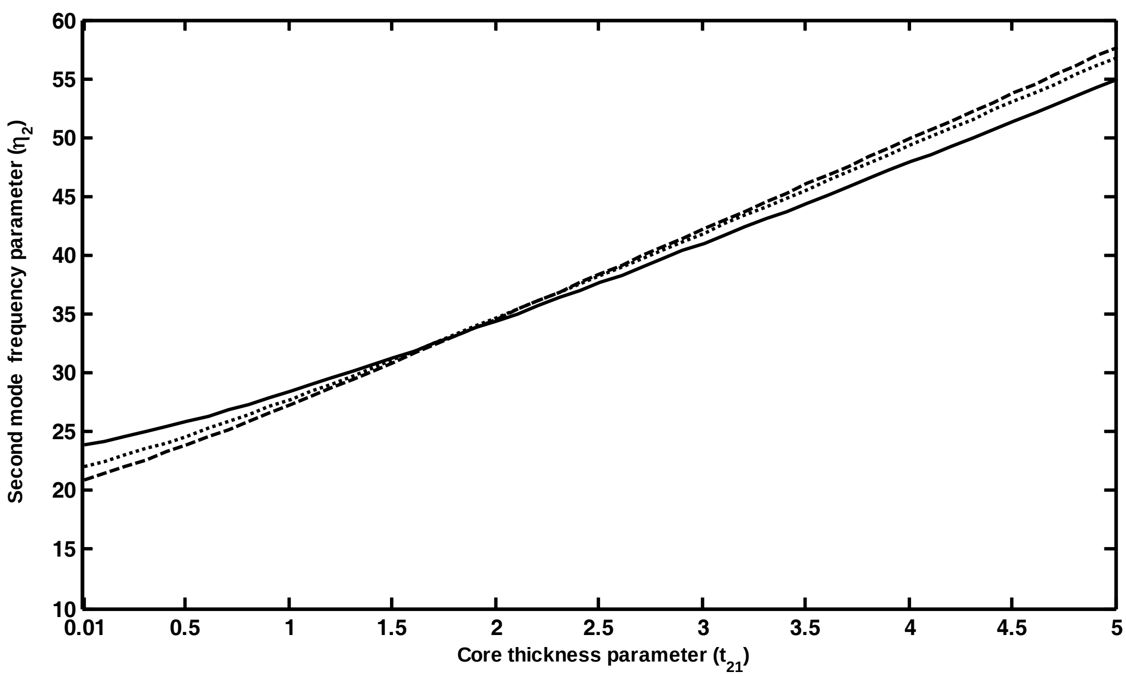

Fig.- 5.10,Effect of core thickness parameter on second mode frequency parameter, constant flexural rigidity case,$(g)_3$ =1.0,η_c= 0.18,key as fig.- 5.5.

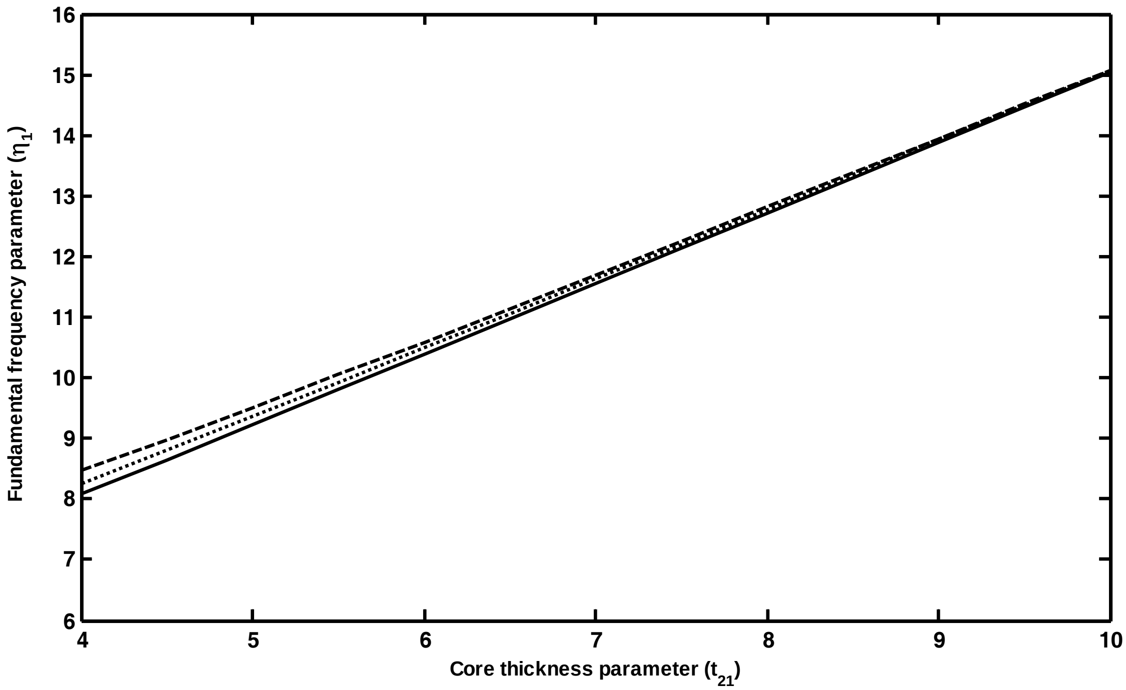

Fig.- 5.11,Effect of core thickness parameter on fundamental frequency parameter, constant size and flexural rigidity case, $(g)_3$ = 0.2,η_c= 0.3,key as fig.- 5.5.

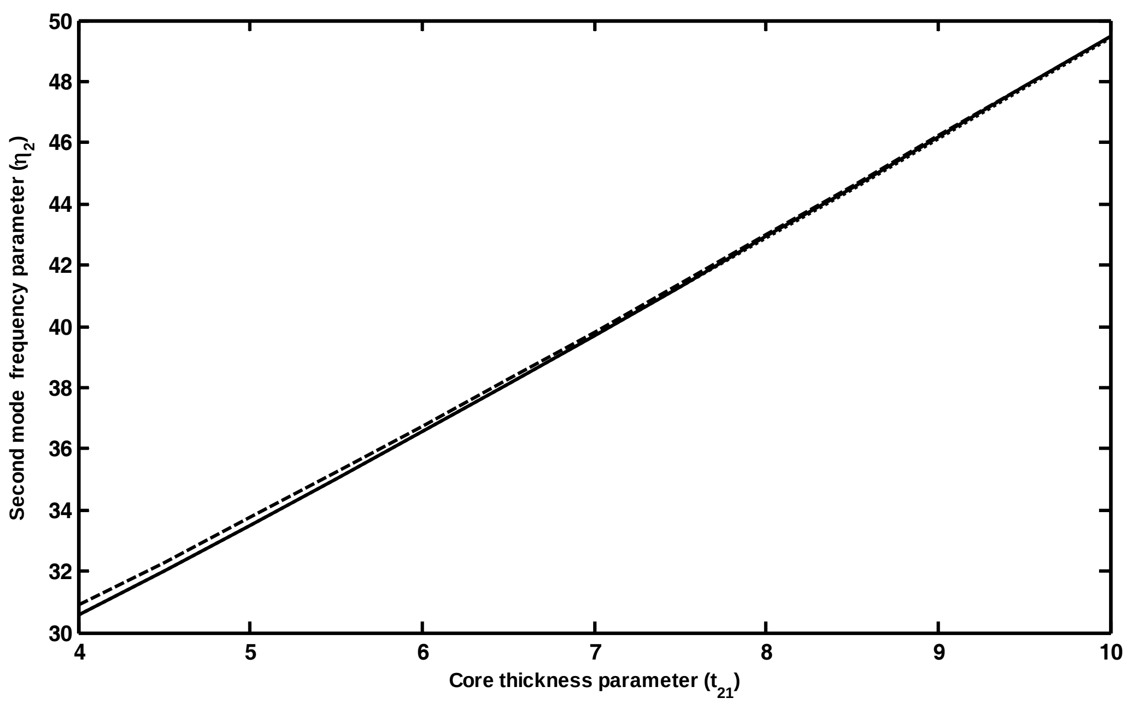

Fig.- 5.12 ,Effect of core thickness parameter on second mode frequency parameter, constant size and flexural rigidity,$(g)_3$= 0.2,η_c= 0.18,key as fig.- 5.5.

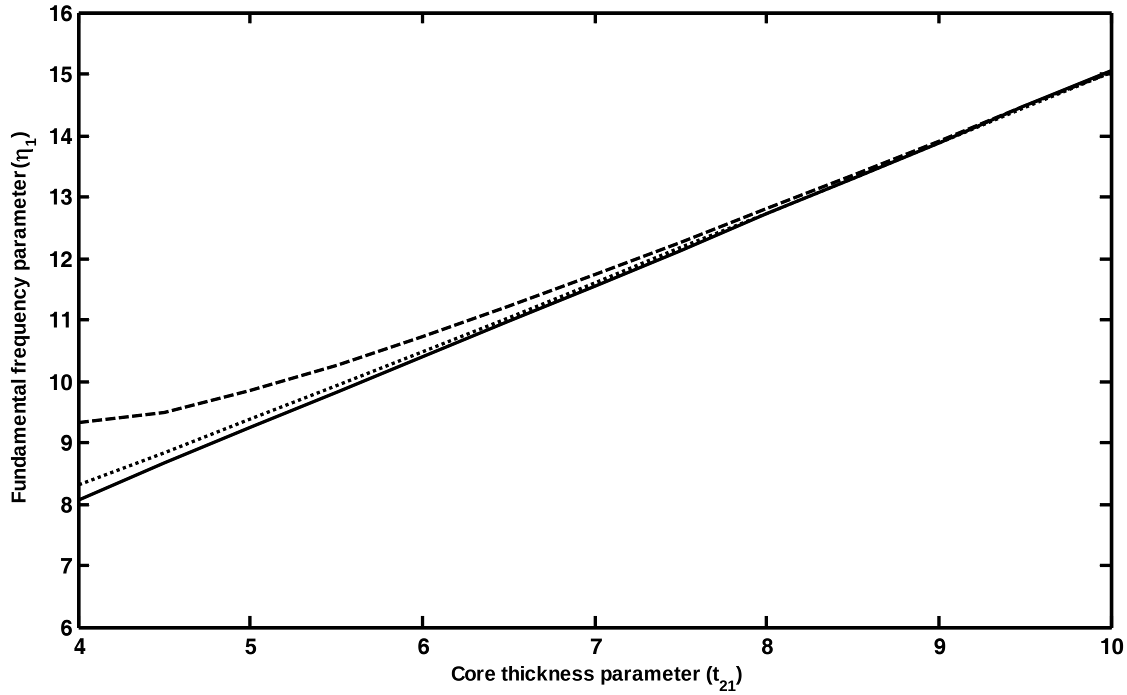

Fig.- 5.13,Effect of core thickness parameter on fundamental frequency parameter, constant weight and flexural rigidity case, $(g)_3$= 0.2,η_c= 0.3,key as fig.-5.5.

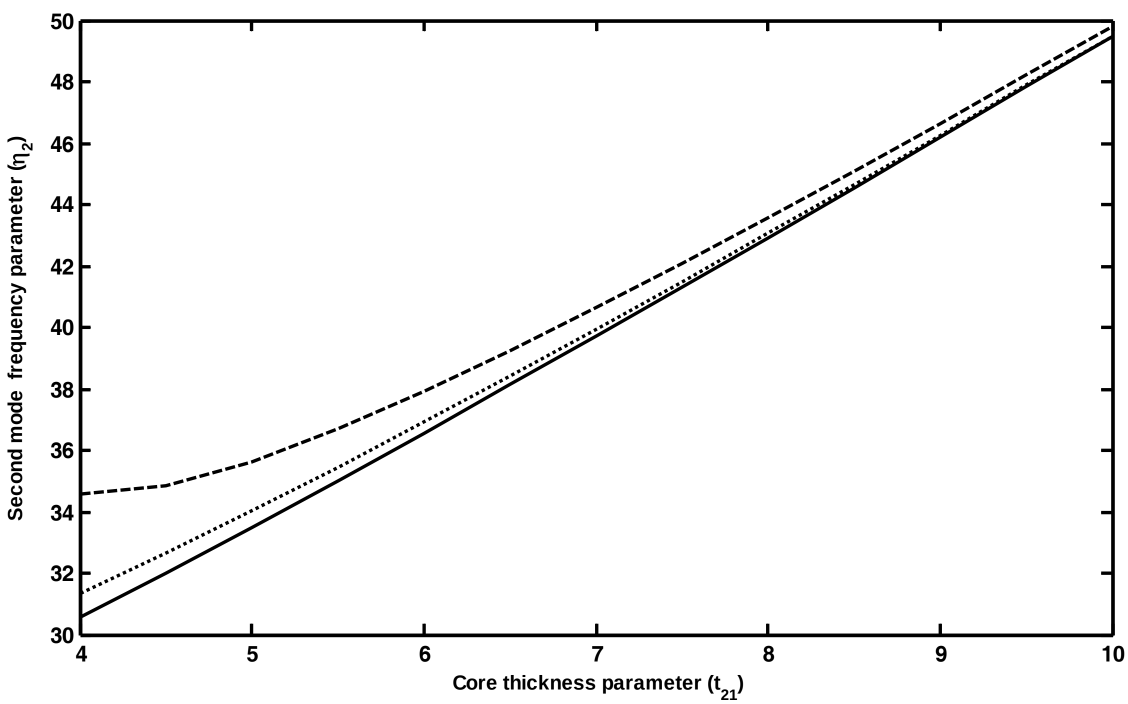

Fig.- 5.14,Effect of core thickness parameter on second mode frequency parameter, constant weight and flexural rigidity case,$(g)_3$= 0.2,η_c= 0.18,key as fig.5.5.

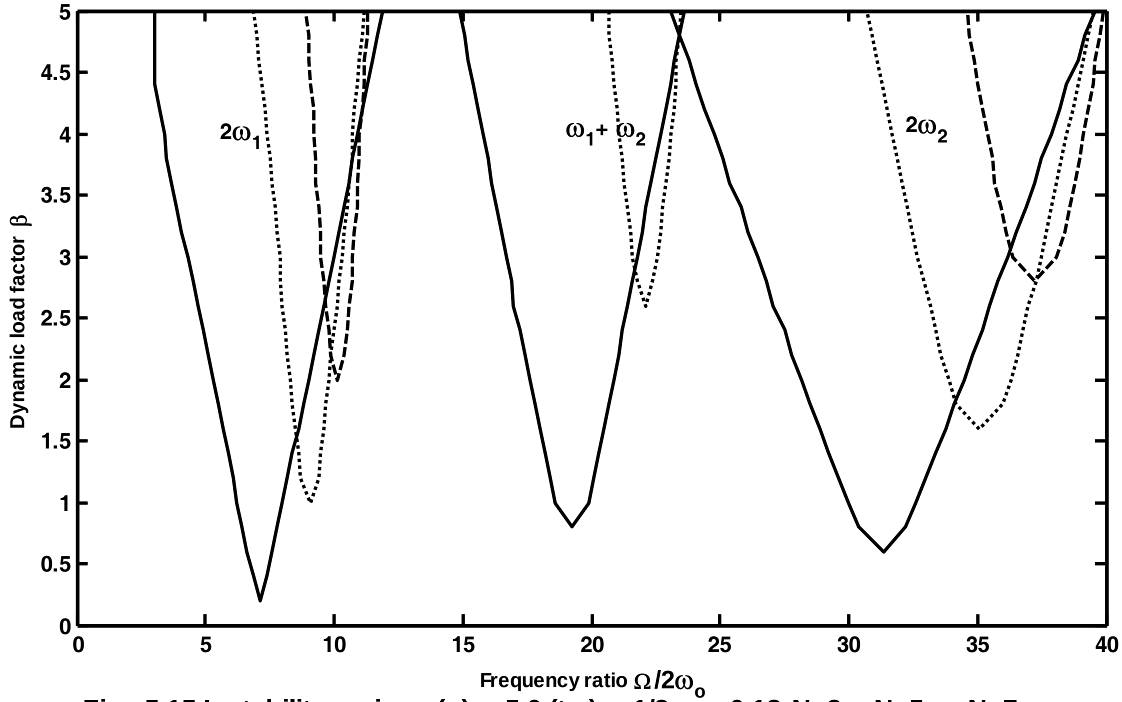

Fig.- 5.15,Instability regions,$(g)_N$= 5.0,$(t_{21})_N$ =1/3,η_c= 0.18;N=3;- ,N=5; ...,N=7;- -,.

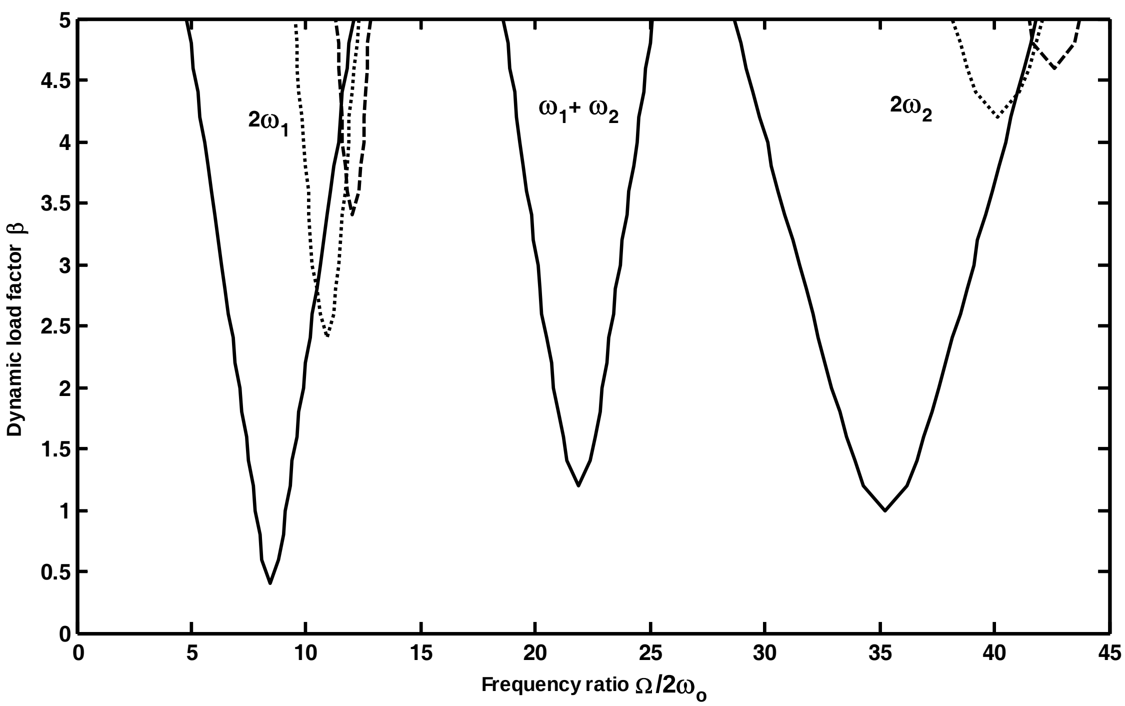

Fig.- 5.16,Instability regions,$(g)_N$ = 5.0,$(t_{21})_N$=2/3, η_c= 0.18,key as fig.- 5.15.

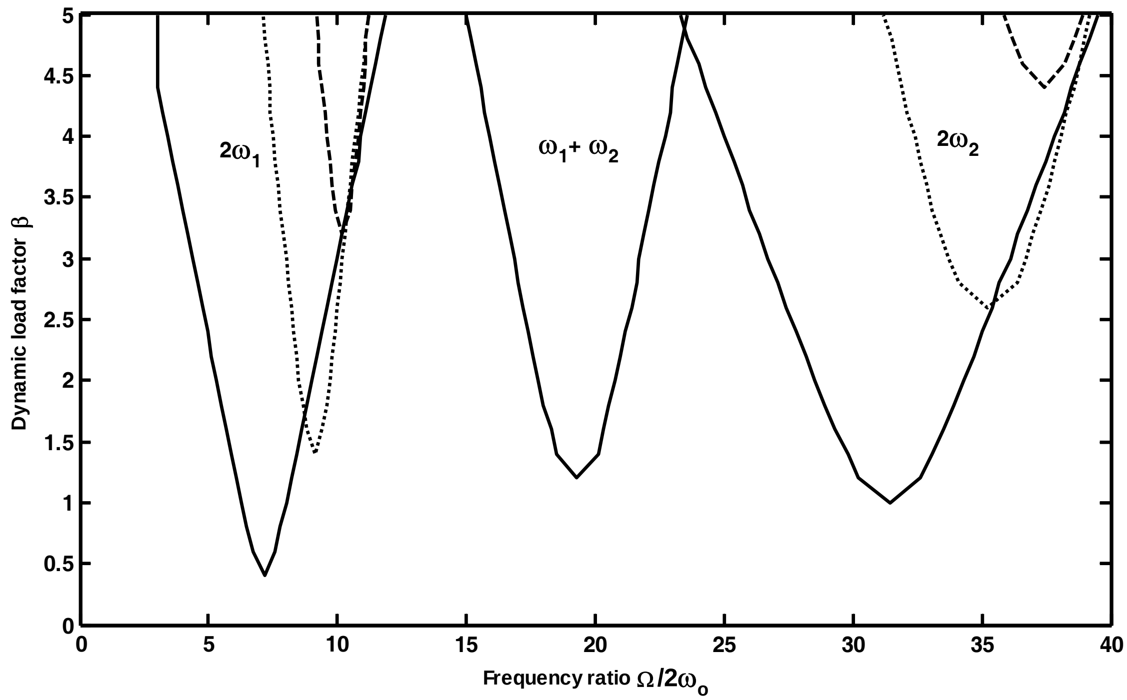

Fig.- 5.17,Instability regions,$(g)_N$= 5.0,$(t_{21})_N$ =1/3, η_c= 0.3,key as fig.- 5.15.

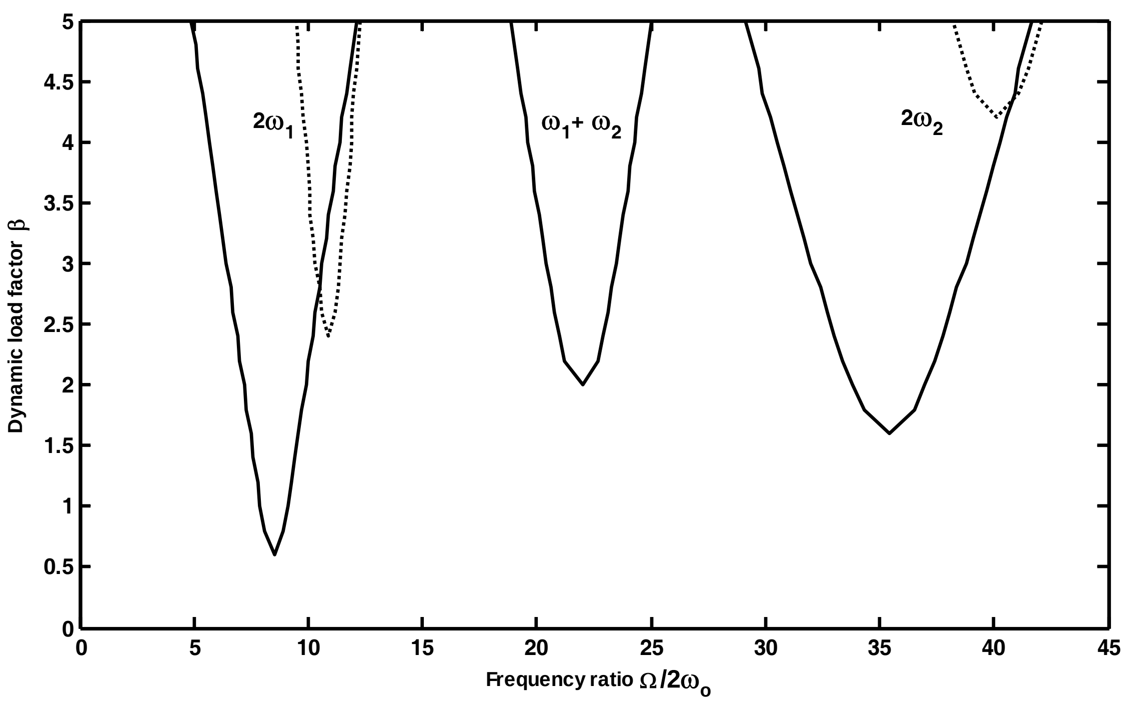

Fig.- 5.18,Instability regions,$(g)_N$= 5.0,$(t_{21})_N$ =2/3, η_c= 0.3,key as fig.- 5.15.

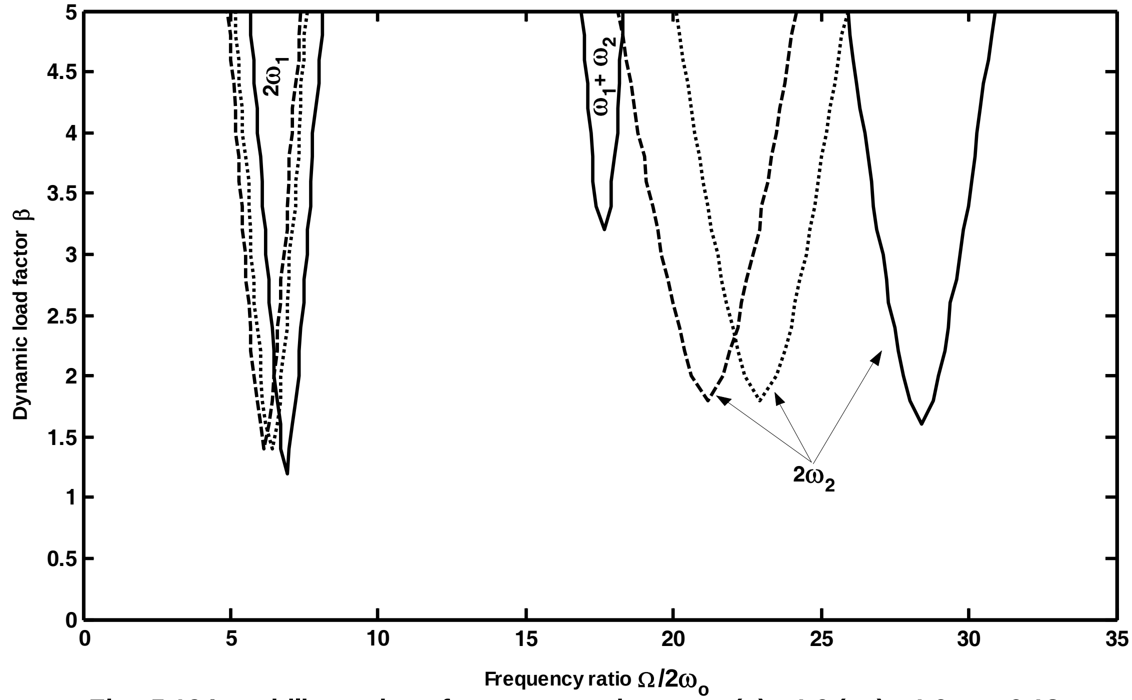

Fig.- 5.19,Instability regions for constant size case ,$(g)_3$=1.0,$(t_{21})_3$=1.0,η_c= 0.18; N=3;- ,N=5; ... ,N=7;- -,.

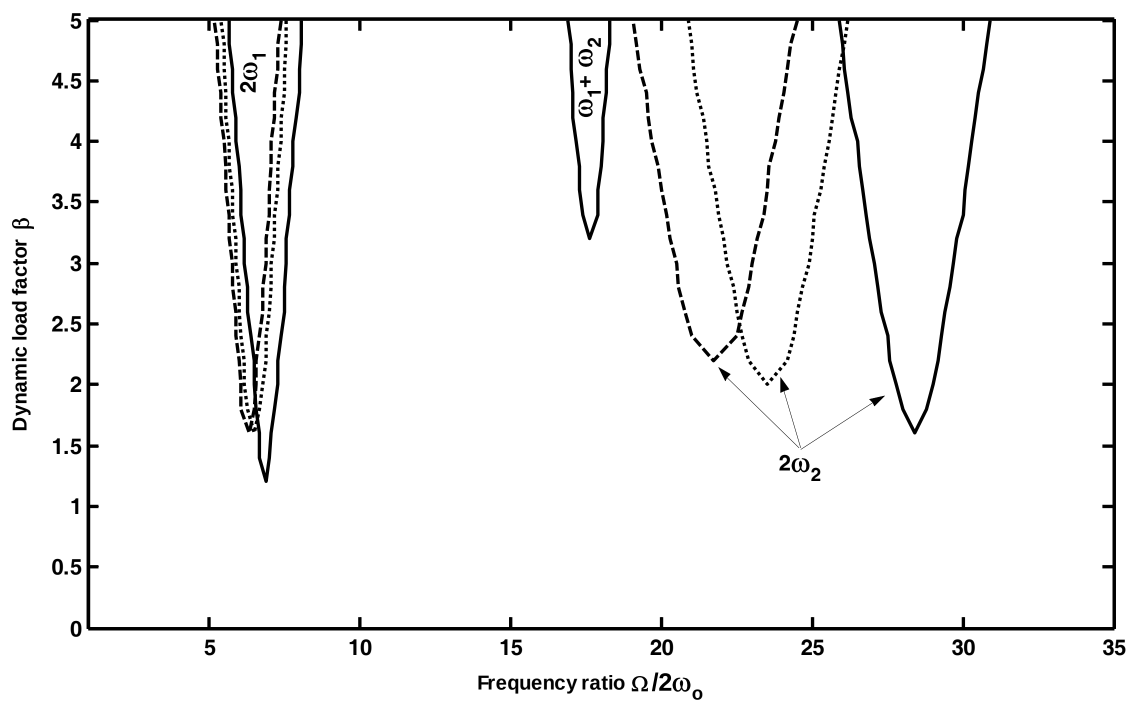

Fig.- 5.20,Instability regions for constant weight case,$(g)_3$=1.0,$(t_{21})_3$ = 1.0,η_c= 0.18, key as fig.- 5.19.

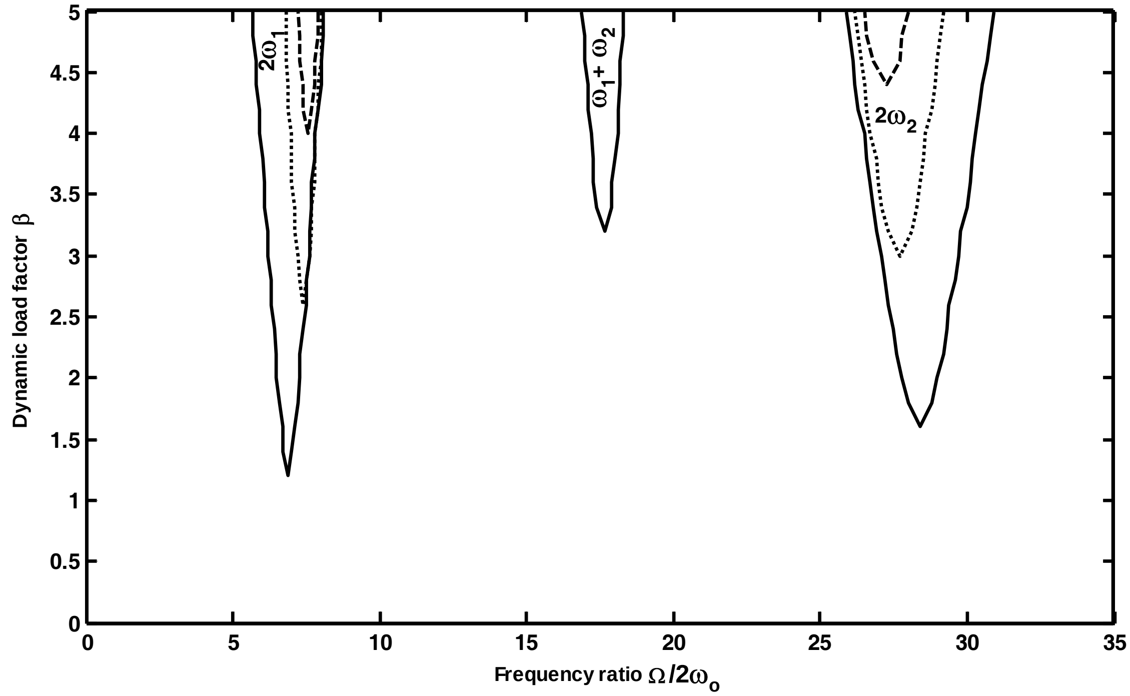

Fig.- 5.21,Instability regions for constant flexural rigidity case,$(g)_3$=1.0,$(t_{21})_3$=1.0, η_c= 0.18,key as fig.- 5.19.

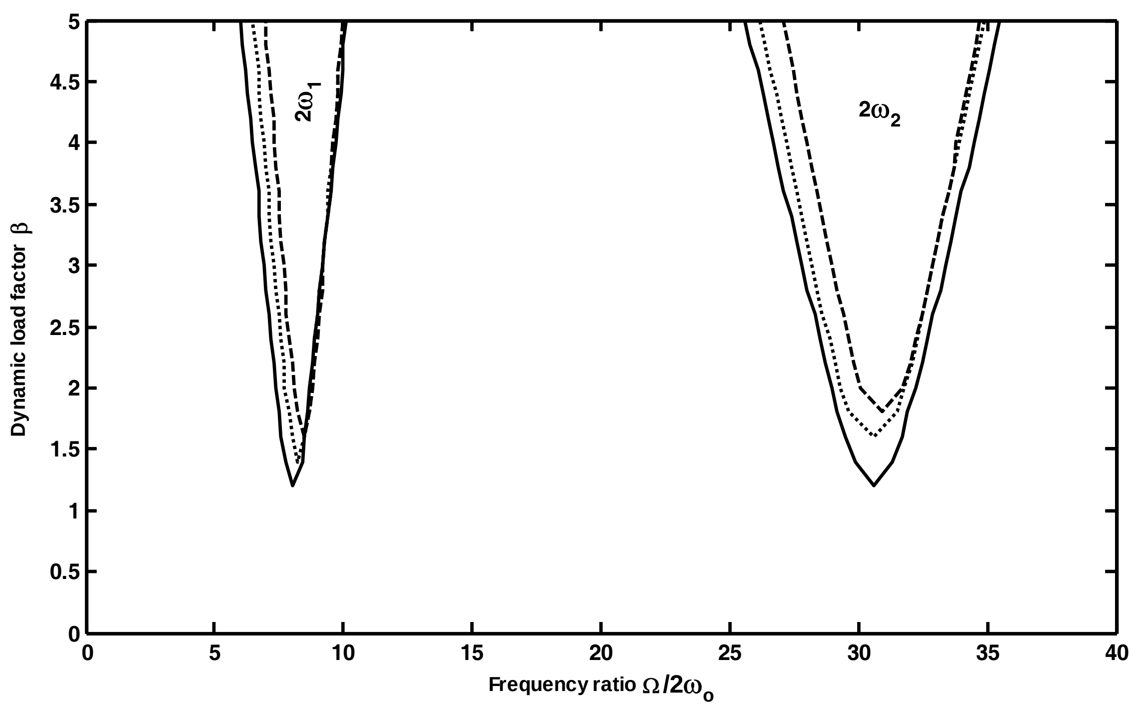

Fig.- 5.22 ,Instability regions for constant size and flexural rigidity case,$(g)_3$ =0.2, $(t_{21})_3$ = 4.0,η_c=0.18,key as fig.- 5.19.

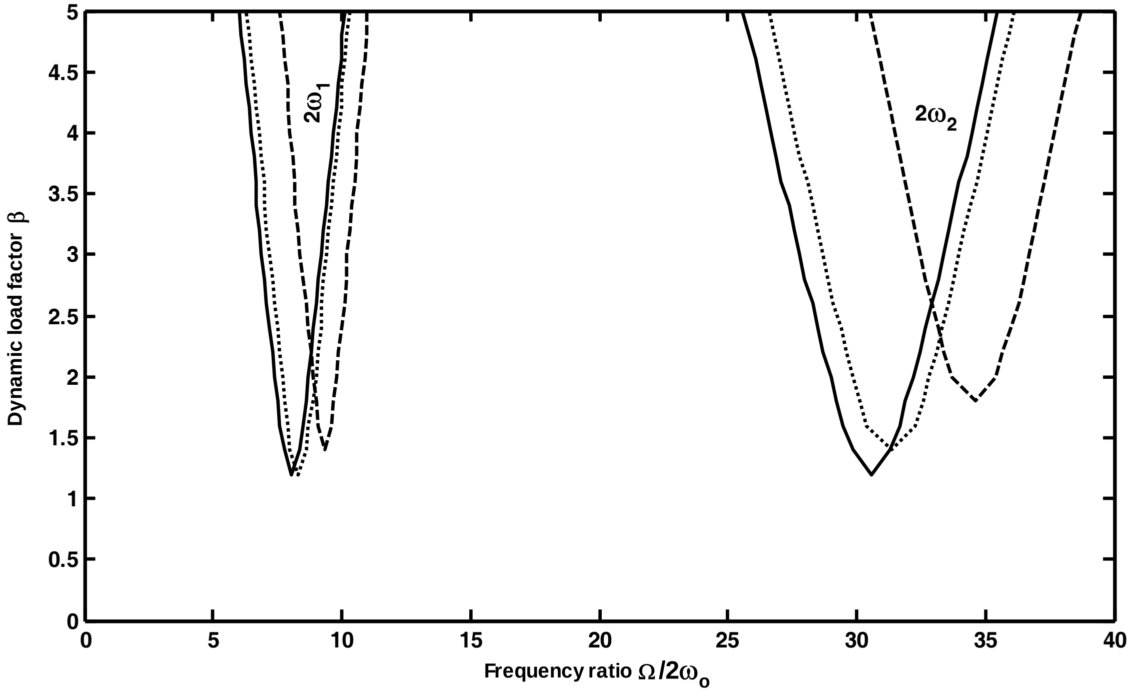

Fig.- 5.23,Instability regions for constant weight and flexural rigidity case,$(g)_3$ =0.2, $(t_{21})_3$ = 4.0,η_c= 0.18,key as fig.- 5.19.

Chapter 6

DYNAMIC STABILITY OF A SIMPLY SUPPORTED TAPERED BEAM WITH THERMAL GRADIENT

6.1 Introduction

The modulus of elasticity of the material is greatly affected by the temperature. In high-speed atmospheric flights, nuclear engineering applications, drilling operations and steam and gas turbines, the mechanical and structural parts are subjected to high temperature. For most of the engineering materials the Young's modulus varies linearly with temperature [44,114]. Such machine and structural components may be subjected to time varying forces, which may lead to their parametric instability. Thermal effect on the dynamic stability is an important aspect of investigation. Many structural and machine components may be modeled as tapered beams.

Brown et al. [18] studied the dynamic stability of uniform bars using finite element method. Dhotarad and Ganeshan [34] carried out vibration analysis of a rectangular plate subjected to a uniform thermal gradient. Datta and Chakrabarty [29] investigated the stability of a tapered beam by finite element method. Tomar and Jain [124] studied the effect of thermal gradient on the frequencies of rotating tapered beams. Mohanty and Kavi [82] in their other work studied the effect of thermal gradient on the dynamic stability of a Timoshenko beam.

The present work deals with the principal resonance of a parametrically excited simply supported tapered Euler beam subjected to thermal gradient along its length. Finite element method is employed to carry out the analysis. The principal regions of instability are determined by Floquet's theory.

6.2 Formulation of the problem

The simply supported beam of length L, tapered both in breadth and depth wise is shown in fig.6.1. A typical finite element is shown in fig.6.2. The element consists of two nodes i and j with v_i, θ_i, v_j and θ_j as the nodal displacements. v is the lateral displacement and θ represents the cross-sectional rotation. The lateral displacement v consists of only the bending displacement. The beam is subjected to a pulsating axial force $P(t) = P_s + P_t \cos\Omega t$, where Ω is the excitation frequency of the dynamic load component, P_s is the static and P_t is the amplitude of the time dependent component of the load acting along its undeformed axis.

6.2.1 Element matrices

The potential energy $\left(U^{(e)}\right)$ of an element of length 'l' subjected to an axial force '$P(t)$' is written as

$$U^{(e)} = \frac{1}{2}\int_0^l E(x)\,I(x)\left(\frac{d^2v}{dx^2}\right)^2 dx - \frac{1}{2}\int_0^l P(t)\left(\frac{dv}{dx}\right)^2 dx \tag{6.1}$$

The kinetic energy ($T^{(e)}$) for an element is given by

$$T^{(e)} = \frac{1}{2}\int_0^l \rho\, A(x)\left\{\dot{v}^2\right\}dx \tag{6.2}$$

A cubic displacement distribution for *v* is assumed over the element as

$$v = a_1 + a_2\, x + a_3\, x^2 + a_4 x^3 \tag{6.3}$$

where a_1, a_2, a_3, a_4 are called the generalised coordinates. Shape functions can be derived by using the expression of the static deflection of an Euler beam. The lateral displacement *v* within the element can be expressed in terms of the nodal displacement vector $\left\{\Delta^{(e)}\right\}$ as,

$$v = [N_1\ N_2\ N_3\ N_4]\begin{Bmatrix} v_i \\ \theta_i \\ v_j \\ \theta_j \end{Bmatrix}$$

$$= [N]\ \left\{\Delta^{(e)}\right\}$$

(6.4)

where $[N]$is the element shape function matrix,

$N_1 = [1\text{-}3\zeta^2 + 2\zeta^3]$

$N_2 = [\zeta\text{-}2\zeta^2 + \zeta^3]\ \mathrm{l}$

$N_3 = [3\zeta^2 \text{-}2\zeta^3]$

$N_4 = [\text{-}\zeta^2 + \zeta^3]\ \mathrm{l}$

$\zeta = \mathrm{x/l}$

With the help of eq. (6.4) the potential energy ($U^{(e)}$) and the kinetic energy($T^{(e)}$) can be written in terms of nodal displacement vector as, respectively,

$$U^{(e)} = \frac{1}{2}\left\{\Delta^{(e)}\right\}^T \left[K^{(e)}\right]\left\{\Delta^{(e)}\right\} - \frac{1}{2}\left\{\Delta^{(e)}\right\}^T P(t)\left[K_g^{(e)}\right]\left\{\Delta^{(e)}\right\} \tag{6.5}$$

$$T^{(e)} = \frac{1}{2}\left\{\dot{\Delta}^{(e)}\right\}^T \left[M^{(e)}\right]\left\{\dot{\Delta}^{(e)}\right\} \tag{6.6}$$

Element mass matrix, element elastic stiffness matrix and element stability matrix are given by the expressions

$$\left[M^{(e)}\right] = \int_o^l [N]^T \rho\ A(x)\,[N]\,dx \tag{6.7}$$

$$\left[K^{(e)}\right] = \int_0^l [N]''^T E(x)\,I(x)\,[N]''\,dx$$

(6.8)

$$\left[K_g^{(e)}\right] = \int_0^l [N]'^T [N]'\,dx \tag{6.9}$$

where $[N]'' = \frac{\partial^2}{\partial x^2}[N]$ *and* $[N]' = \frac{\partial}{\partial x}[N]$

6.2.2 Governing equations of motion

The element equation of motion for the beam is derived by using Hamilton's principle.

$$\delta\int_{t_1}^{t_2}\left(T^{(e)} - U^{(e)}\right)dt = 0 \tag{6.10}$$

Substituting eqs. (6.5), (6.6) in to eq. (6.10) the equation of motion for the beam element is obtained as follows:

$$\left[M^{(e)}\right]\left\{\ddot{\Delta}^{(e)}\right\} + \left[K^{(e)}\right]\left\{\Delta^{(e)}\right\} - P(t)\left[K_g^{(e)}\right]\left\{\Delta^{(e)}\right\} = 0 \tag{6.11}$$

Assembling mass, elastic stiffness and geometric stiffness matrices of individual element, the equation of motion for the global system is written as

$$[M]\{\ddot{\Delta}\}+[K]\{\Delta\}-P(t)[K_g]\{\Delta\}=0 \tag{6.12}$$

where $\{\Delta\}$ = Global displacement vector.

P_s the static and P_t the amplitude of time dependent component of the load can be represented as the fraction of the fundamental static buckling load P^* of the beam without thermal gradient. Hence substituting, $P(t) = \alpha P^* + \beta P^* \cos \Omega t$, with α and β as static and dynamic load factors respectively.

The eq. (6.12) becomes

$$[M]\{\ddot{\Delta}\}+\left([K]-\alpha P^*[K_g]_s-\beta P^* \cos\Omega t[K_g]_t\right)\{\Delta\}=0 \tag{6.13}$$

If the static and time dependent component of loads are applied in the same manner, then $[K_g]_s = [K_g]_t = [K_g]$.

Equation (6.13) represents a system of second order differential equations with periodic coefficients of the Mathieu-Hill type. The instability regions are established using the Floquet's theory and the same computational method as described in the chapter (3).

The Young's modulus E is assumed to vary linearly along the length of beam due to thermal gradient and is given by [34].

$$E(x) = E_1 [1-\beta_t T_o (1-x/L)]$$
$$= E_1 [1-\delta(1-x/L)] \tag{6.14}$$

E_1 is the Young's modulus of the material at the reference temperature T_o, which is at the reference point, x = L(tip), β_t is the slope of variation of E with T and $\delta=\beta_t T_o$ is the thermal gradient factor.

The width ,height and area moment of inertia of the cross-section at any position x measured from the root side, is given as

$$\left.\begin{aligned} b(x) &= b_1 - \delta_b x \\ h(x) &= h_1 - \delta_h x \\ A(x) &= \{b(x)\}\{h(x)\} \\ I(x) &= \{b(x)\}\{h(x)\}^3/12 \end{aligned}\right\} \tag{6.15}$$

δ_b and δ_h are the taper per unit length in width and height respectively. b_1 and h_1 are the width and height at the root,x=0.

The overall matrices, [K], [K_g] and [M] are obtained by assembling the corresponding element matrices. The displacement vector consists of only active nodal displacements.

6.3 Results and discussion

The following properties of the beam are taken for numerical computations: Length of the beam = 1m; cross – sectional dimension at the tip = 20 x 20 mm; cross – sectional dimension at the root = 120 x 120 mm; material mass density of the aluminum beam = 2800 kg /m^3; E_1 = 70 x 10^3 MPa.

A ten-element discretisation of the beam gives satisfactory convergence of natural frequencies and buckling loads for the first five modes. Also the instability regions obtained without thermal gradient match well with those of [29]. Comparison is given in Table 6.1.

Table-6.1 Comparison of boundary frequencies of the first instability region obtained from present analysis with reference [29]. Static load factor α=0.5. ω_1 is the fundamental frequency of the beam without thermal gradient

Dynamic load factor (β)	Lower limit of boundary frequency ratio (Ω_1/ω_1)		Upper limit of boundary frequency ratio (Ω_2/ω_1)	
	Reference [29]	Present	Reference [29]	Present
0	1.4551	1.4724	1.4551	1.4724
0.2	1.3006	1.3299	1.5983	1.5984
0.4	1.1850	1.1640	1.6850	1.7118
0.6	0.9538	0.9619	1.8208	1.8154
0.8	0.7154	0.6909	1.8844	1.9110
1.0	0.0000	0.0132	1.9940	2.0000

Figures (6.3) and (6.4) show the variation of natural frequency and buckling load respectively of the first three modes with thermal gradient factor δ. The values of both the frequency and buckling load decrease with increase in the value of δ. This decrease is negligible for fundamental natural frequency and buckling load. The rate of decrease is more for higher modes.

In order to study the stability of the beam, instability regions have been obtained for different values of thermal gradient factor δ and static load factor α. These are shown in figs. (6.5-6.9). First three regions of primary resonance have been shown in the figures. In these figures ω_1 is the fundamental frequency of the beam without thermal gradient.

Figure (6.5) shows the instability regions for α=0.4 and δ = 0, 0.3 and 0.6. It is seen that with thermal gradient present, the lower boundary of the first instability region curls towards the dynamic load factor axis, thereby making the first instability region wider. For higher values of thermal gradient factor the lower boundary truncates on the β-axis at values of β less than one. For example, for α = 0.4 and δ= 0.6 the lower boundary of the first instability region truncates on the β-axis at β = 0.8. Truncation of lower boundary on the β-axis at values of β less than one indicates instability for amplitude of time dependent component of the load less than the fundamental static buckling load. There is also increase in areas of the other two instabilities regions. Moreover increase in thermal gradient factor (δ) shifts the instability regions towards the dynamic load factor axis, that is the instability occurs at lower frequency of excitation. This shift is less for the first instability region but for other two regions it is relatively large.

Figure (6.6) shows the instability regions for α=0.5 and δ = 0, 0.3 and 0.6 respectively. Increase of thermal gradient factor has the same effect on the instability regions as discussed above.

Figure (6.7) shows the instability regions for α=0.8 and δ = 0, 0.3 and 0.6 respectively. The instability regions show the same behaviour with increase in δ as discussed earlier. For α=0.8 and δ = 0.6 the lower boundary of the first instability region vanishes.

Figure (6.8) shows the instability regions for δ = 0.3 and α=0.4, 0.5 and 0.8. It is seen that with increase in static load factor, the instability region shifts towards dynamic factor axis. Also there is increase in area of the instability region with increase in α. The increase in area of the first instability region is quite large compared to second and third one.

Figure (6.9) shows the instability regions for δ = 0.6 and α =0.4, 0.5 and 0.8. The effect of α on the instability regions is same as discussed earlier.

To study the relative effect of α and δ on the instability regions three sets of values of α and δ, i)α=0.5 and δ= 0.0 ii) α=0.5 and δ= 0.3 iii) α=0.6118 and δ= 0.0 have been considered. The additional load factor 0.1183, in addition to 0.5, in case (iii) corresponds to the difference in fundamental buckling load for the beam without thermal gradient and with thermal gradient (α=0.3). This is shown in fig. (6.10). It is seen that with α=0.5 and δ= 0.0, when in one case the load factor is increased to 0.6183 with δ=0.0 and in other case with α=0.5 there is a thermal gradient, δ= 0.3, all the three instability regions shifts towards lower frequency of excitation. Because of thermal gradient the shift of regions towards lower frequency is more than compared to an equivalent increase in static load factor. The relative effect on the first primary resonance zone is not that much pronounced. But the thermal gradient factor shifts the second and third instability regions considerably more towards the dynamic factor axis as compared to the static load factor. This means that the thermal gradient factor has relatively more destabilising effect than static load factor.

6.4 Closure

Effect of thermal gradient and static load factor on the dynamic stability of a simply supported tapered beam is analysed by finite element method in conjunction with Floquet's theory. Present investigation reveals that an increase in thermal gradient factor decreases the natural frequency and the static buckling load. The effect is more pronounced on second and third modes than on first mode. Increase in static load component or thermal gradient factor has a destabilising effect. Thermal gradient factor has a greater destablising effect than static load factor, for an equivalent change in static load component.

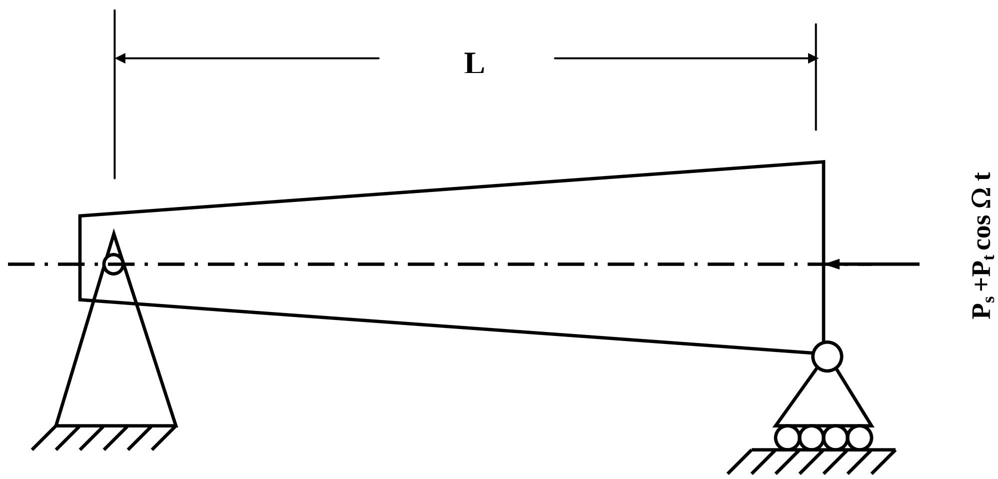

Fig. – 6.1, Simply supported tapered beam with thermal gradient

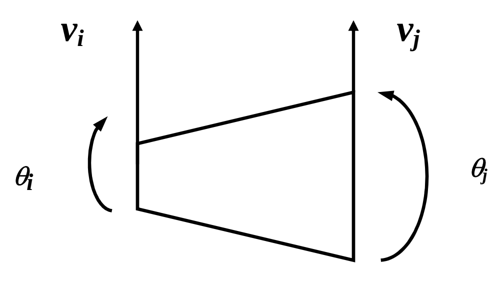

Fig. - 6.2, Tapered beam element

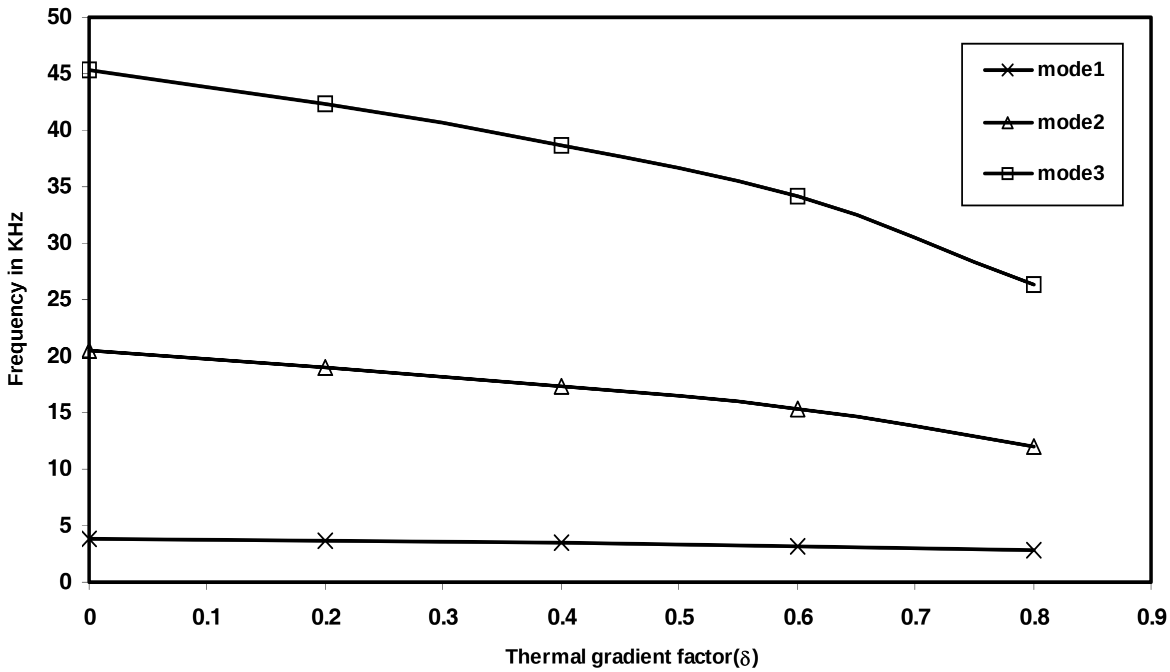

Fig. - 6.3, Effect of thermal gradient factor on fundamental frequency

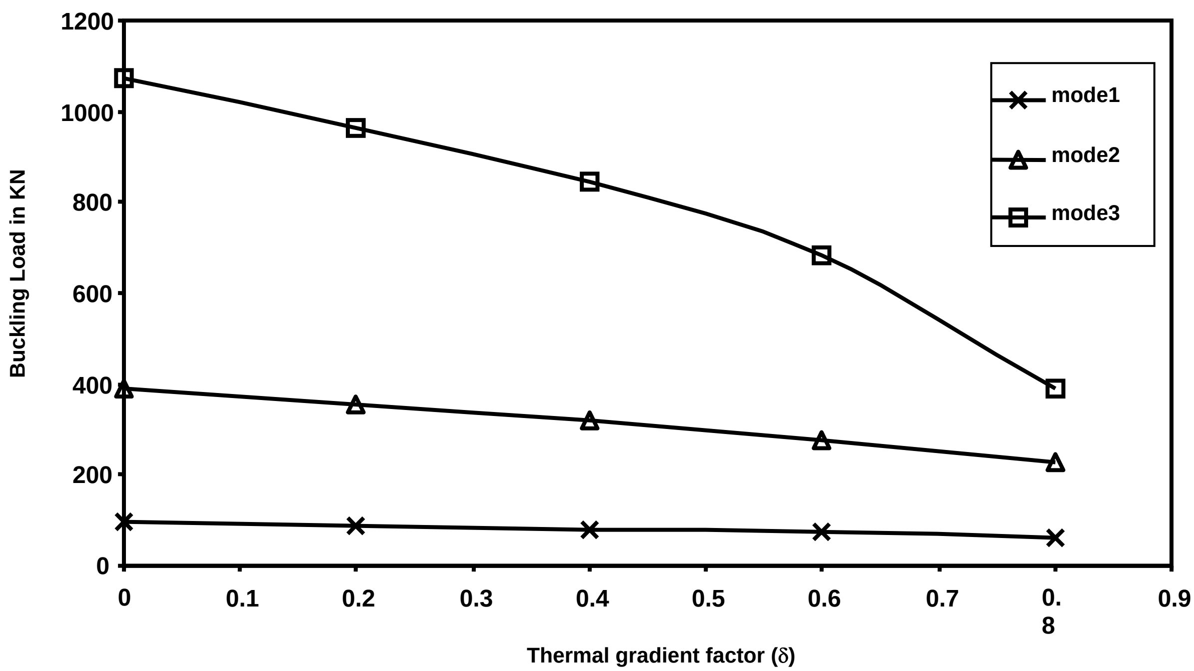

Fig.- 6.4, Effect of thermal gradient factor on critical buckling load

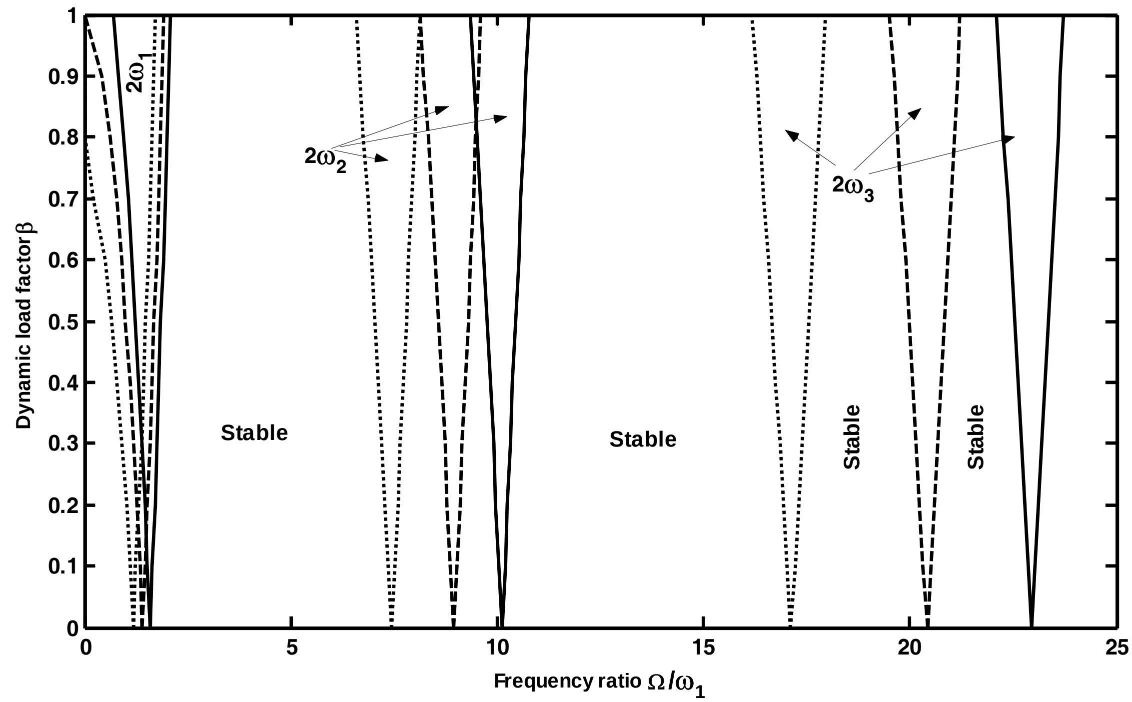

Fig.- 6.5,Instability regions for,α=0.4,δ =0.0;- ,δ=0.3;- -,δ=0.6;... ,.

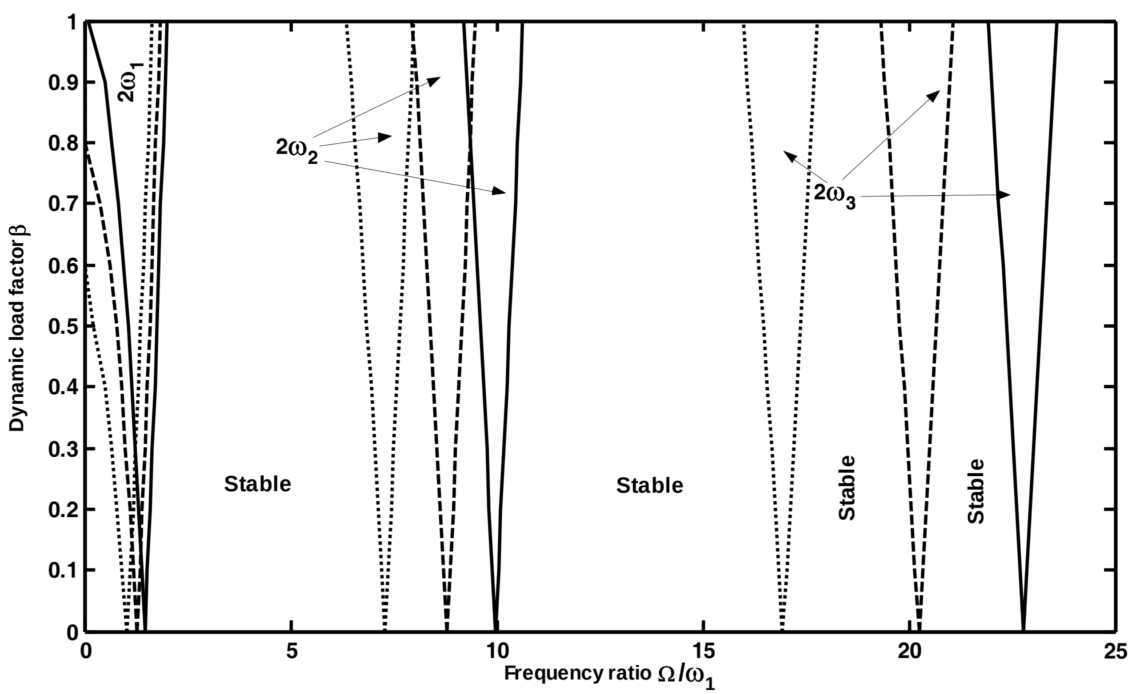

Fig.- 6.6,Instability regions for, α=0.5,key as fig.6.5.

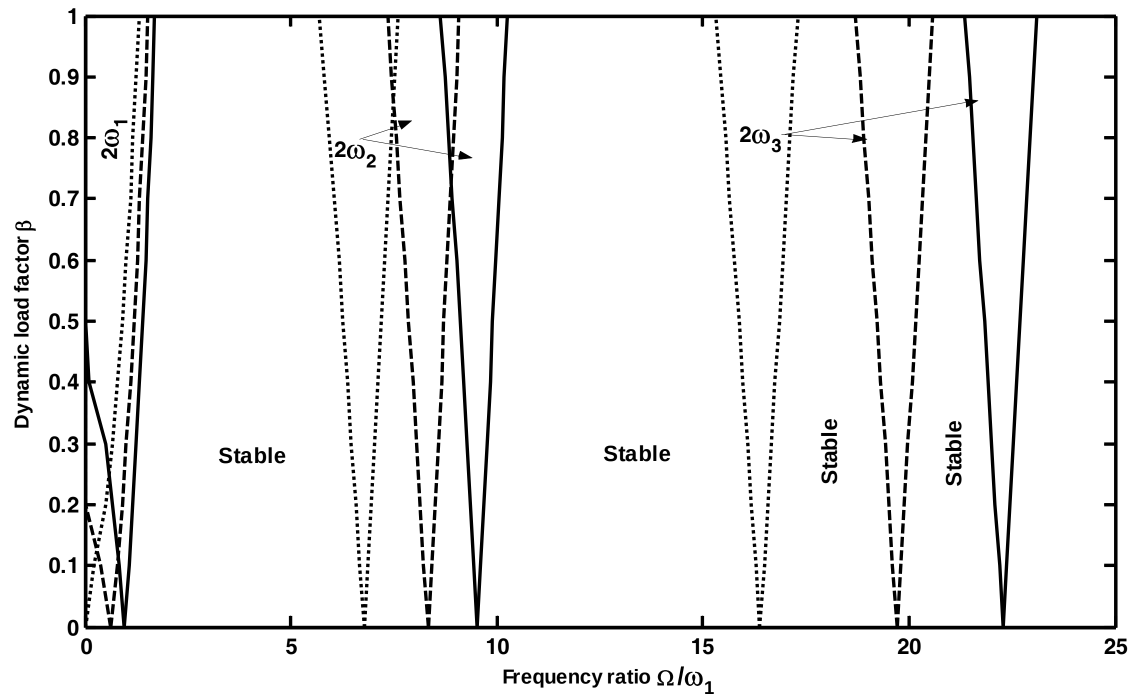

Fig.- 6.7,Instability regions for, α=0.8,key as fig.6.5.

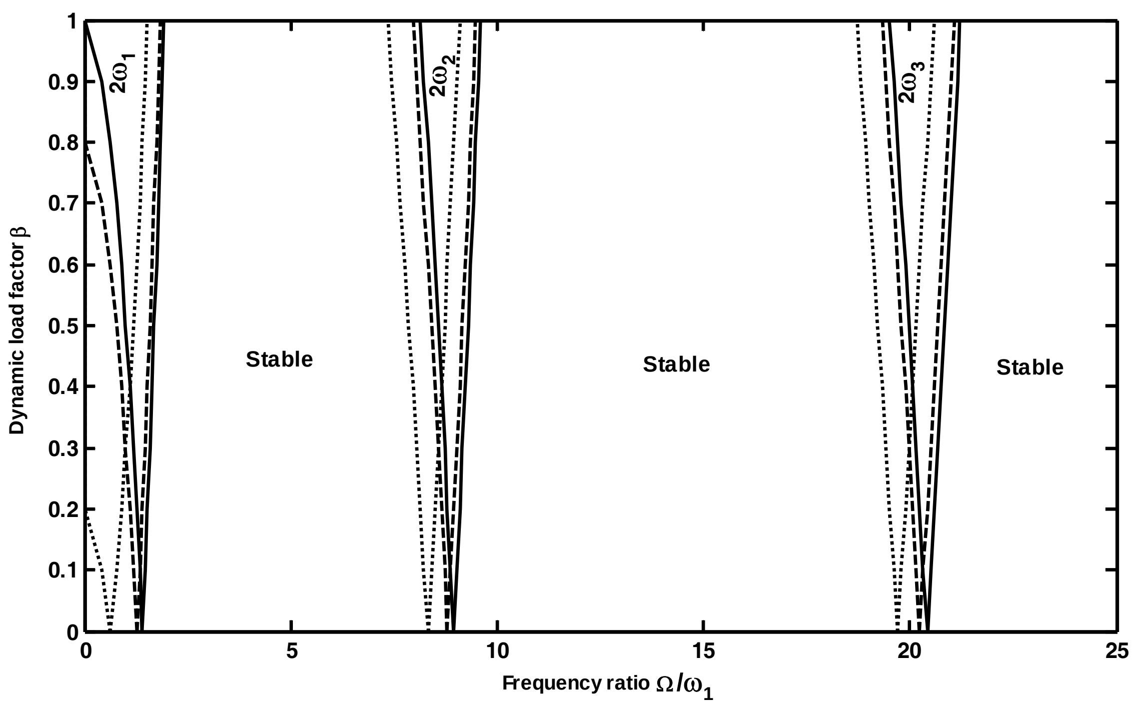

Fig.- 6.8,Instability regions for, δ=0.3 ,α =0.4;- , α=0.5;- -, α=0.8;... ,.

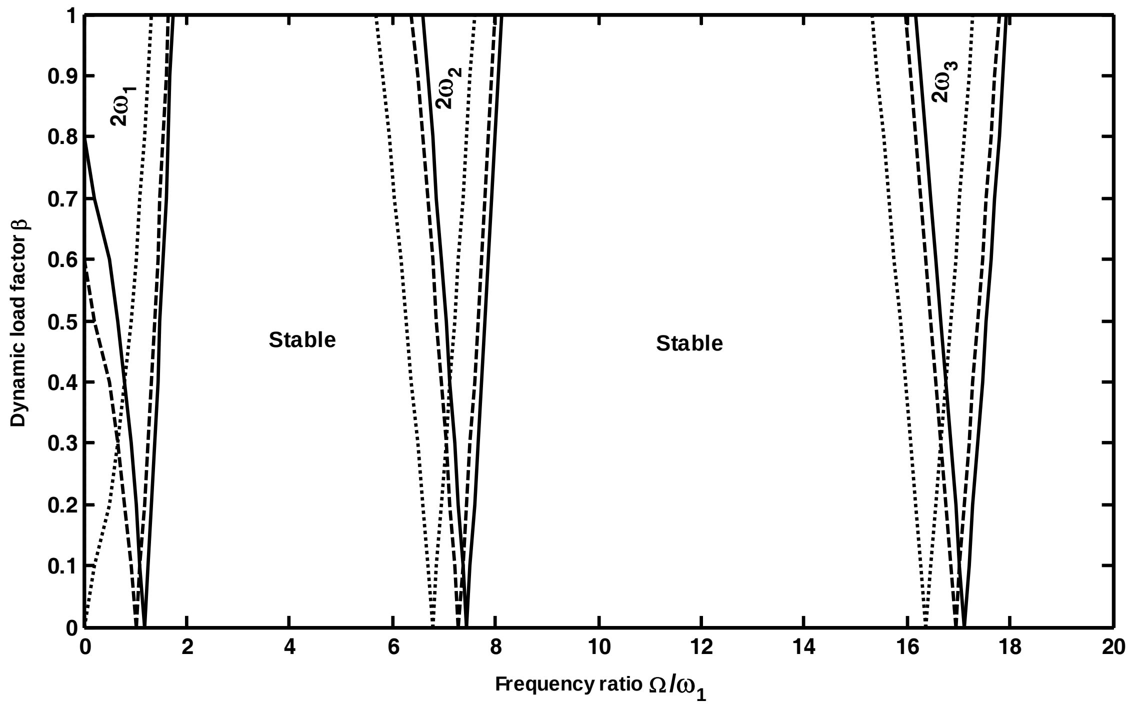

Fig.- 6.9,Instability regions for, δ=0.6,key as fig.- 6.8.

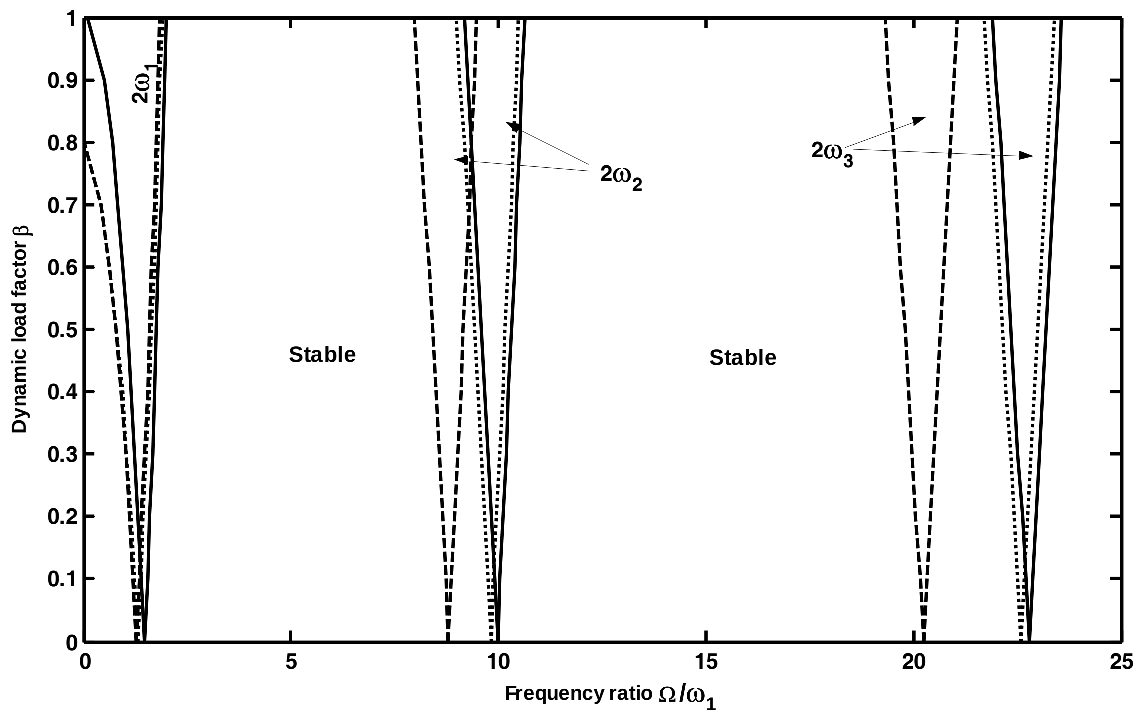

Fig.- 6.10,Instability regions for, α=0.5,δ=0.0;-,α=0.5,δ=0.3;--,α=0.6138,δ=0.0;... ,.

Chapter 7

EXPERIMENTAL WORK

7.1 Introduction

The aim of the experimental work is to establish experimentally the stability diagrams for a few typical cases related to beams with localised damage and for sandwich beams, described in chapters (3-5). For uniform Timoshenko beam and pretwisted cantilever beam with localised damage, the instability regions have been experimentally determined for the positions of the damage for which the first instability region occurs at minimum frequency of excitation. For uniform beam with localised damage these positions of the damage for fixed-free, pinned-pinned, fixed-fixed and fixed-pinned boundary conditions, correspond to position parameters $\psi = 0.1$, $\psi = 0.5$, $\psi = 0.5$ and $\psi = 0.7$ respectively. For uniform twisted cantilever beam the instability regions have been experimentally determined for $\psi=0.1$. For sandwich beams, the stability diagrams have been experimentally established for 3, 5 and 7 layered beams. The theoretical and experimental stability diagrams have been compared to assess the accuracy of the theoretical results.

7.2 Description of the experimental set up

The schematic diagram of the equipments used for the experiment and photographic view of the experimental set up are shown in the fig.7.1 and Plate-1 respectively. The set up consists of a framework fabricated from steel channel sections by welding. The frame is fixed in vertical position to the foundation by means of foundation bolts and it has the provision to accommodate beams of different lengths. The periodic axial load $P_t \cos \Omega t$ is applied to the specimen by a 500N capacity electrodynamic shaker (Saraswati Dynamics, India, Model no. SEV-005). The static load can be applied to the specimen by means of a screw jack fixed to the frame at the upper end. The applied load on the specimen is measured by a piezoelectric load cell (Brüel & Kjaer, model no. 2310-100), which is fixed between the shaker and the specimen. The vibration response of the test specimen is measured by means of vibration pick-ups (B&K type, model no. MM-0002). The signals from the pickups and load cell are observed on a computer through a six-channel data acquisition system (B&K, 3560-C), which works on Pulse software platform (B&K 7770, Version 9.0).

In order to achieve pin end condition for the beam end, an attachment is provided. The attachment has a pin mounted on two ball bearings as shown in Plate-2. The beam end is adhered to the pin. For pin end condition at both the ends of the beam, two such attachments, one fixed to the load cell and other attached to the screw jack are provided. For fixed end condition the beam end is rigidly clamped to the steel angle bars by means of screws (Plate- 2).

7.3 Preparation of specimens

i) Beams with localised damage

The specimens were prepared from aluminum strips of 1.612mm thickness and 25.4mm wide. Rectangular cutouts of suitable dimension were made on the strip at required places to produce artificial damage of specified extent of damage and size. For example to produce a damage with extent of damage ξ = 0.5, size parameter τ = 0.2 and position parameter ψ = 0.5, a slot of width equal to the half the width of the strip, length equal to 0.2 times the length of the specimen was cut symmetrically about the longitudinal axis at the middle of the beam. The cutouts were filled with suitable filler material (M-seal) of weight equal the weight of the material removed to produce the slot. The filler material was uniformly distributed over the slot area so that mass per unit length of the beam was same as that of the original beam. To fabricate twisted beam with damage, the aluminum strips were twisted, clamping one end and twisting the other end to the required angle. Care was taken that the angle of twist varies linearly from clamped end to the free end. The slot of required size was cut at the required position and filled with filler material. The details of the physical and geometric data of the specimens are given in Tables 7.1-7.4. The photographs of the specimens are also shown in Plate-3.

ii) Sandwich beams

Sandwich beams were fabricated from strips cut from mild steel sheets of suitable thickness. The viscoelastic core of the sandwich beam is P.V.C. In preparing the sandwich beams the face layers were made free from dirt, grease etc. by cleaning their surfaces with acetone and carbon tetrachloride. The adhesive used for bonding the layers is commercially available dendrite. After application of thin layer of adhesive on the surfaces, the layers were bonded and the sandwich beams were kept under load for about six hours. Slipping of the layers was avoided by providing positioning guides at all the edges of the specimen during the setting time. The Young's modulus of the specimen materials was determined by measuring the static deflection of a test specimen under known load. Mass density of the specimen materials was measured by measuring the weight and volume of a piece of specimen material. The details of the physical and geometric data of the specimens are given in Tables 7.5-7.6 and the photographs of the specimen are shown in Plate-3.

7.4 Testing procedure

An oscillator cum power amplifier unit drives the electrodynamic vibration shaker used for providing the dynamic loading. The beam response was recorded by the non-contacting vibration pickups. For straight beams with pinned-pinned, fixed-fixed and fixed-pinned end conditions two pickups, one at each end of the beam were used, where as for fixed-free end condition only one pick up was placed near to the fixed end to sense the vibration response of the beam. For twisted cantilever to sense the response of the beam in two fixed perpendicular directions, two pickups mutually perpendicular to each other were placed near the fixed end. The air gap between the pick-ups and the vibrating surface were so adjusted that the measurements were in the linear range. The amplitude of the signal gives no absolute displacement since it is not calibrated.

Initially the beam was excited at certain frequency and the amplitude of excitation was increased till the response was observed. Then the amplitude of excitation was kept constant and frequency of excitation was changed in steps of 0.1 Hz. The excitation frequency was controlled with the help of Pulse software. The generator module of the

Pulse software can produce an output signal of specified frequency; this signal is fed to the shaker through its control unit. The experimental boundaries of instability regions were marked by the parameters (P_t,Ω), which were measured just before a sudden increase of the amplitude of the lateral vibration. The order of increase in amplitude of lateral vibration has been taken to be around 4.0, to record the boundary frequency of instability. For accurate measurement of the excitation frequency an accelerometer was fixed to the moving platform of the exciter, its response was observed on computer in the frequency domain. The dynamic load component of the applied load was measured from the response curve of the load cell. For ordinary beams the excitation frequency was divided by the reference frequency ω_1 to get the nondimensional excitation frequency (Ω/ω_1). For sandwich beams the excitation frequency was divided by $2\omega_0$ to get the non-dimensional excitation frequency ($\Omega/2\omega_0$). Similarly the dynamic load amplitude was divided by the reference load P^* to get the dynamic load factor β. . The details of observations are given in Tables 7.7-7.16.

7.5 Results and discussion

The boundary frequencies obtained from experiments are shown in Tables 7.7-7.16 and also in figs.7.2-7.11. In Tables 7.7-7.16, the second column shows the experimentally measured amplitude of the applied dynamic load (P_t). The columns 3rd, 5th and 7th of these tables show the experimentally measured lower limits (excitation frequencies) of the instability regions, whereas frequencies shown in the columns 4th, 6th and 8th of the same tables are the experimentally determined upper limits of the instability regions. In the 9th column, the calculated dynamic load factor (β), which is obtained by dividing the dynamic load amplitude (P_t) by P^* has been recorded. In the columns 10 to 15 the calculated boundary frequency ratios corresponding to the lower and upper limits of the instability regions are shown. For example in the row, corresponding to sl.no.-1 in the Table 7.7, the experimentally measured amplitude of the dynamic load component is 1.4N. The experimentally obtained excitation frequencies corresponding to the lower boundary of the first, second and third instability regions are 17.0, 133.7 and 383.8 Hz respectively. The experimentally obtained excitation frequencies corresponding to the upper boundary of the first, second and third instability regions are 18.8, 135 and 386.0 Hz respectively. The calculated corresponding dynamic load factor is 0.118. The calculated frequency ratios corresponding to the lower limits of the first, second and third instability regions are 1.45, 11.4 and 32.72 respectively, whereas corresponding upper limits are 1.6, 11.51 and 32.91 respectively.

i) Timoshenko beam with localised damage.

Figures (7.2-7.5) show the theoretical instability regions along with the experimentally obtained boundary frequencies of the instability regions for uniform Timoshenko beam with localised damage and with fixed-free, pinned-pinned, fixed-fixed and fixed-pinned boundary conditions respectively. Figures 7.2 (a)-7.2(c) show the instability regions for fixed-free case. It is seen that the experimental boundary frequencies are close to the theoretical boundaries. The maximum differences between the theoretical and experimental values of the excitation frequency ratio for the first three instability regions are 0.11, 0.15 and 0.2 respectively. In terms of the absolute value of the excitation frequency, these values correspond to a difference of 1.3Hz, 1.8Hz and 2.3Hz respectively, which show reasonable agreement between the theoretical and experimental results. Figures 7.3(a)-7.3(c) show the instability regions for pinned-pinned case. The maximum differences between the theoretical and experimental values of the excitation frequency ratio for the three instability regions are 0.27, 0.36 and 0.84 respectively, In terms of the absolute value of the excitation frequencies, these values correspond to a difference of 4.3Hz, 5.7 Hz and 13.4 Hz respectively, which show considerable deviation between the theoretical and experimental results. From figs. 7.4(a)-7.4(c), it is seen that the experimental boundary frequencies are very close to the theoretical boundaries for fixed-fixed case. The maximum differences between the theoretical and experimental values of the excitation frequency ratio for the first three instability regions are 0.05, 0.09 and 0.1 respectively. In terms of the absolute value of the excitation frequency these values correspond to a difference of 0.9Hz, 1.6 Hz and 1.8 Hz respectively, which show close agreement between the theoretical and experimental results. Figures 7.5(a)-7.5(c) show the instability regions for fixed-pinned case. The maximum differences between the theoretical and experimental values of the excitation frequency ratio for the first three instability regions are 0.12, 0.14 and 0.18 respectively. In terms of the absolute value of the excitation frequency these values correspond to a difference of 3.0Hz, 3.5 Hz and 4.5 Hz respectively. It is seen that for fixed-free and fixed-fixed cases there is reasonable agreement between the theoretical and experimental results. For pinned-pinned and fixed-pinned case there is deviation in the theoretical and experimental results, particularly in case of pinned-pinned end condition the difference is quite considerable. Svensson [121] has observed that damping in hinges shifts the instability regions to lower frequencies. In this case also the experimentally observed points are at lower values compared to the theoretical ones. So this difference may be due to the damping present in the hinged ends, which has not been taken in to account in the theoretical analysis.

ii) Twisted cantilever beam with localised damage.

Figures 7.6(a)-7.6(c) show the theoretical and the experimental instability regions for the twisted beam with an angle of pretwist 30^0. It is seen that there is close agreement between these two results. The maximum deviation in frequency ratio occurs in case of the second instability zone and this is equal to 0.1. This deviation in frequency ratio is equivalent to a difference of 1.3 Hz in the theoretical and experimental values of the excitation frequency. Figures7.7 (a)-7.7(c) show the instability regions for twisted beam with an angle of pretwist 60^0. In this case there is also close agreement between theoretical and experimental results, maximum deviation in excitation frequency being 1.72 Hz, which occurs in case of third instability region. Instability regions for twisted beam with an angle of pretwist 90^0 are shown in figs.7.8 (a)-7.8(c). In this case there is also close agreement between theoretical and experimental results, maximum deviation in excitation frequency being 1.1 Hz, which occurs in case of second instability region.

iii) Multilayer cantilever sandwich beams.

The theoretical and experimentally obtained first two resonant frequencies for the three, five and seven layer beams having the physical and geometrical parameters as given in Table-7.5 are presented in Table-7.6. These values show reasonable agreement. Figure (7.9) shows the theoretical and experimental instability diagrams for a three layer cantilever sandwich beam. It is seen that first simple instability region and the instability region of combination type from theoretical analysis are fairly close to the experimental ones. There is marked deviation between the theoretical and experimental second simple instability region. This may be due to the deviation in the theoretical and actual values of the second resonant frequency, Table-7.6. Figure (7.10) shows the theoretical and experimental instability regions for a five layer cantilever sandwich beam. In this case for the geometrical and physical parameters of the beam, the instability regions of combination resonance of sum type or difference type and second simple resonance do not occur within the value of dynamic load factor β=5.0. The figure shows reasonable agreement between the experimental and theoretical results. Figure (7.11) shows the theoretical and experimental instability diagrams for a seven layer cantilever sandwich beam. In this case also first simple instability region and the instability region of combination type from theoretical analysis are fairly close to the experimental ones. There is marked deviation between the theoretical and experimental second simple instability region, which may be due to the deviation in the theoretical and actual value of the second resonant frequency, Table -7.6.

7.6 Closure

The theoretical and experimental instability diagrams have been compared to assess the accuracy of the theoretical results. It has been found that for Timoshenko beam with localised damage, the theoretical and experimental results are in close agreement for fixed-free and fixed-fixed boundary conditions. But there is deviation in case of pinned-pinned and fixed-pinned end conditions. This deviation may be due to the presence of damping in the hinges. For pretwisted cantilever beams there is close agreement between the theoretical and experimental instability regions. For sandwich beams there is reasonable agreement between the theoretical and experimental results.

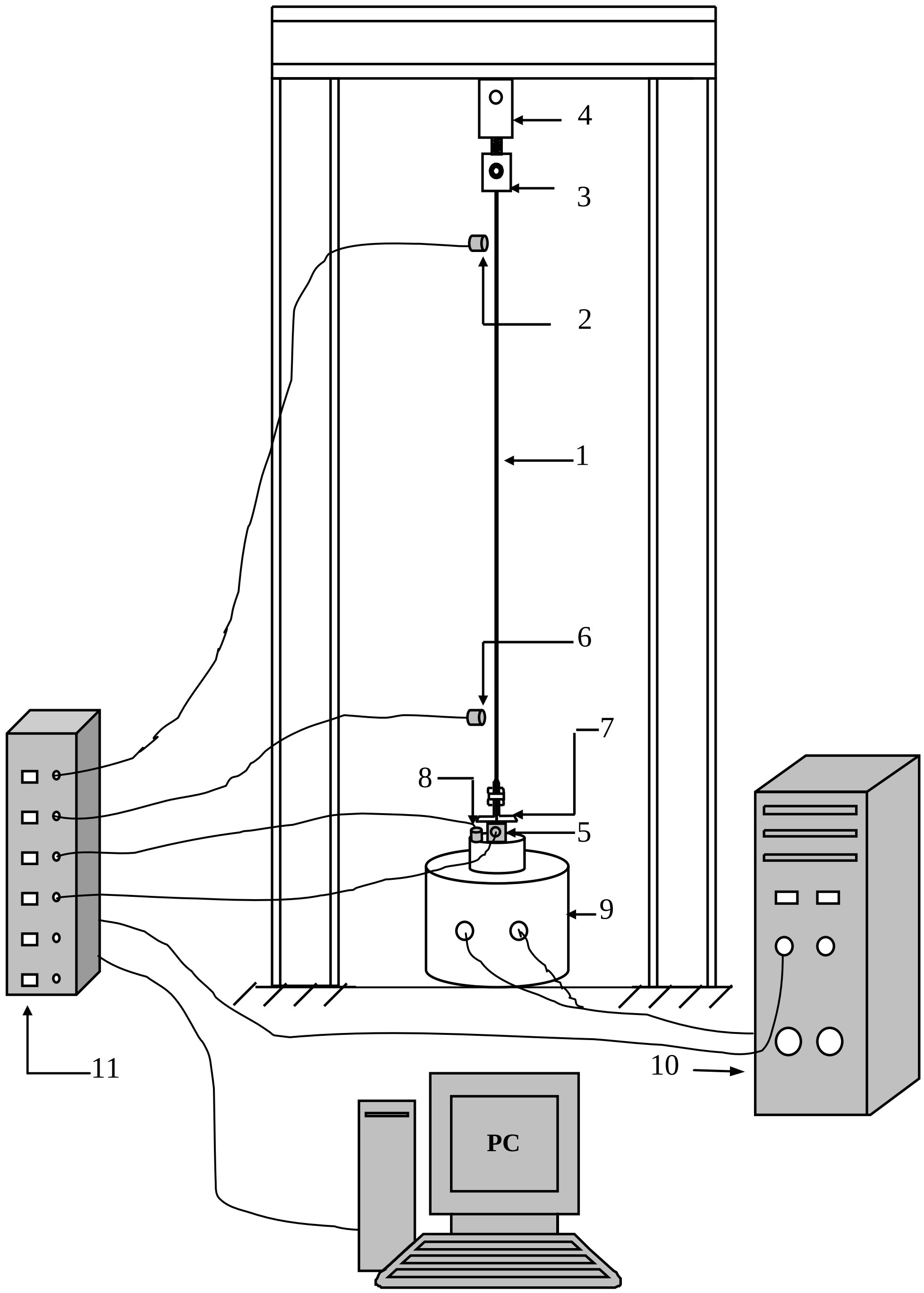

Fig. 7.1, Schematic diagram of the test set up, 1-Specimen, 2-Upper pickup, 3-Upper support (Pinned end), 4-Screw jack, 5-Load cell, 6-Lower pickup, 7-Lower support (Clamped end),8-Accelerometer, 9-Vibration generator, 10-Oscillator and amplifier,11-Data acquisition system.

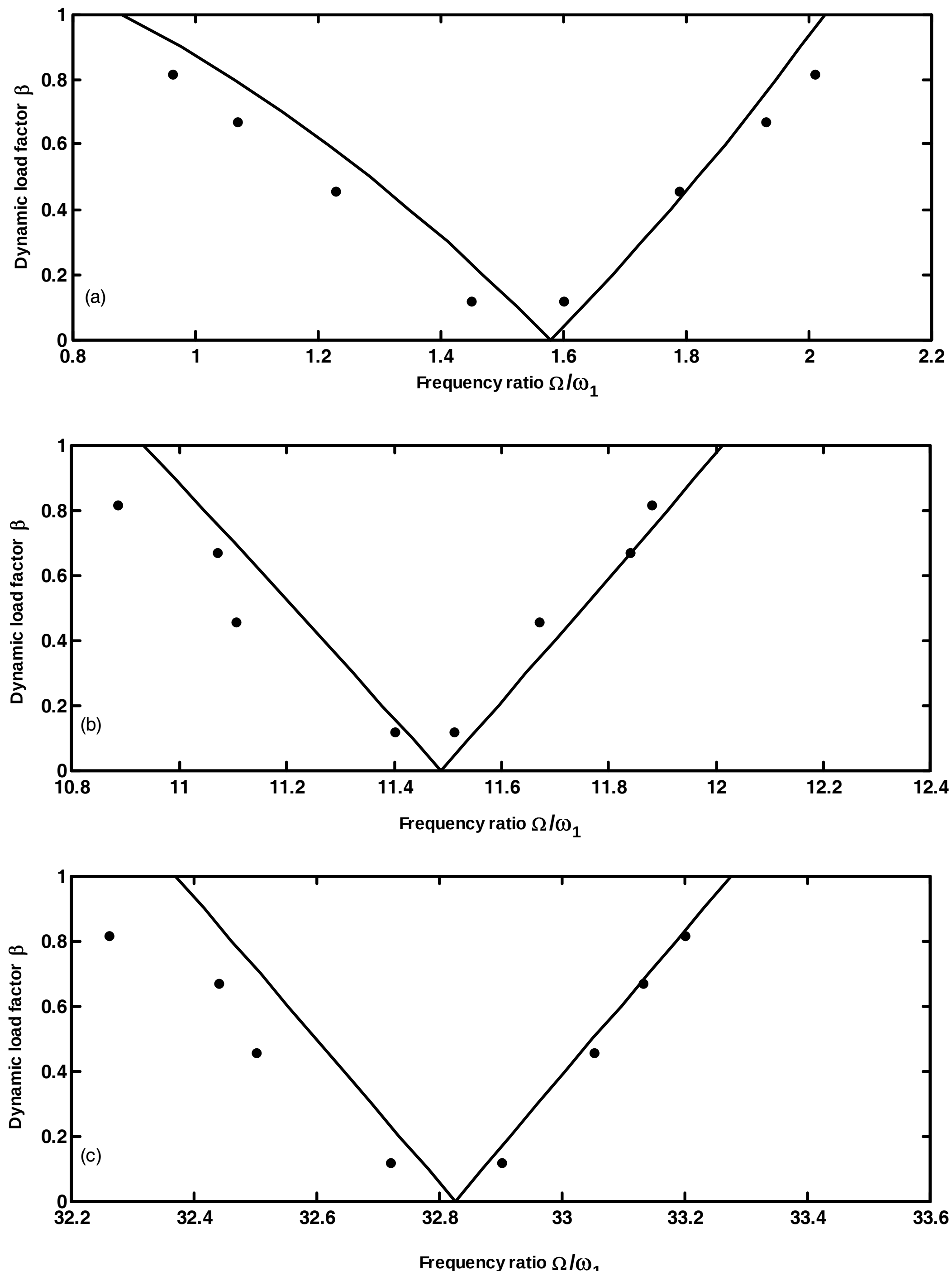

Fig.7.2,Instability regions,for fixed-free case,ξ=0.5,ψ=0.1,τ=0.2, Theoretical cal boundary from FEM;-, Experimental data;•.

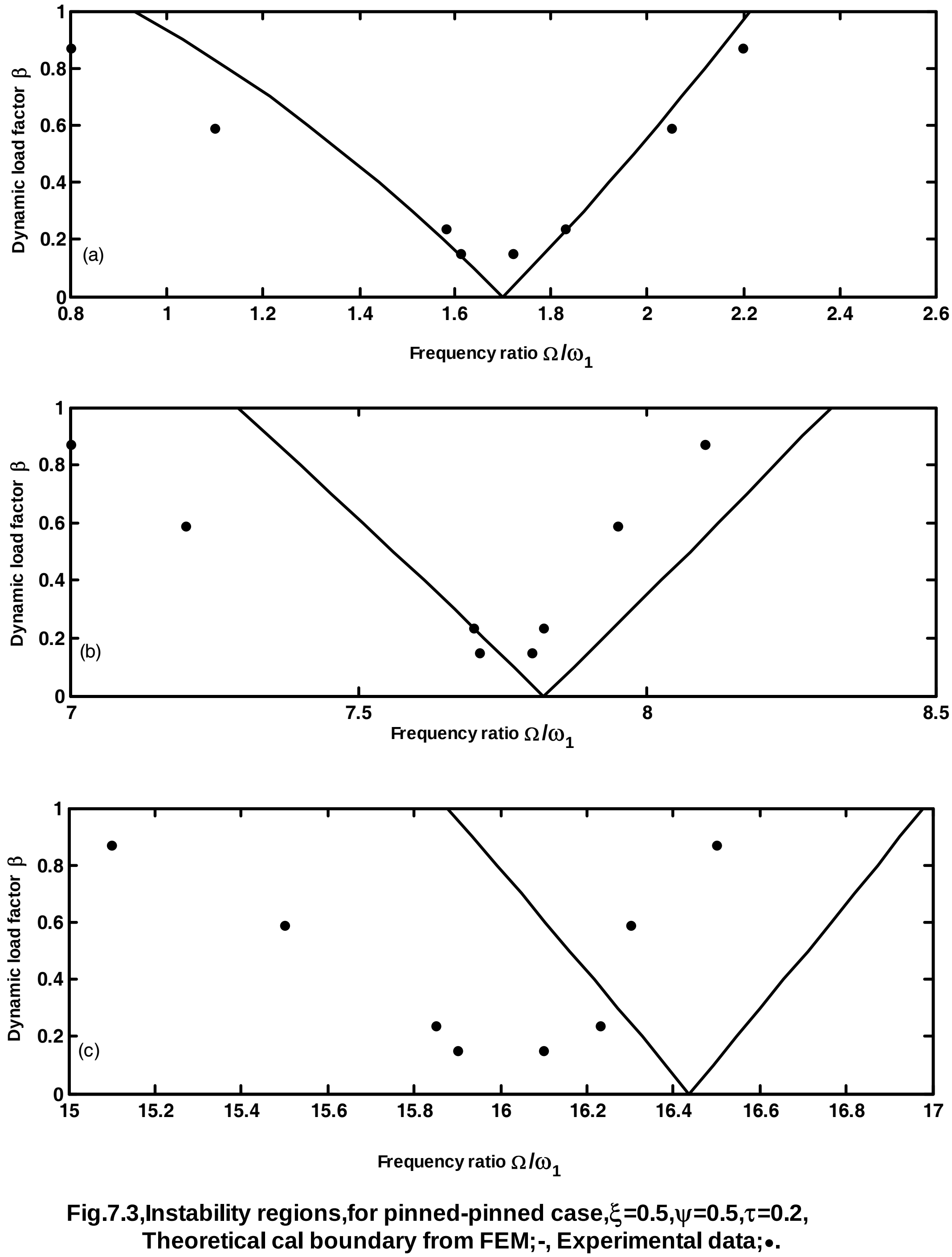

Fig.7.3,Instability regions,for pinned-pinned case,ξ=0.5,ψ=0.5,τ=0.2, Theoretical cal boundary from FEM;-, Experimental data;•.

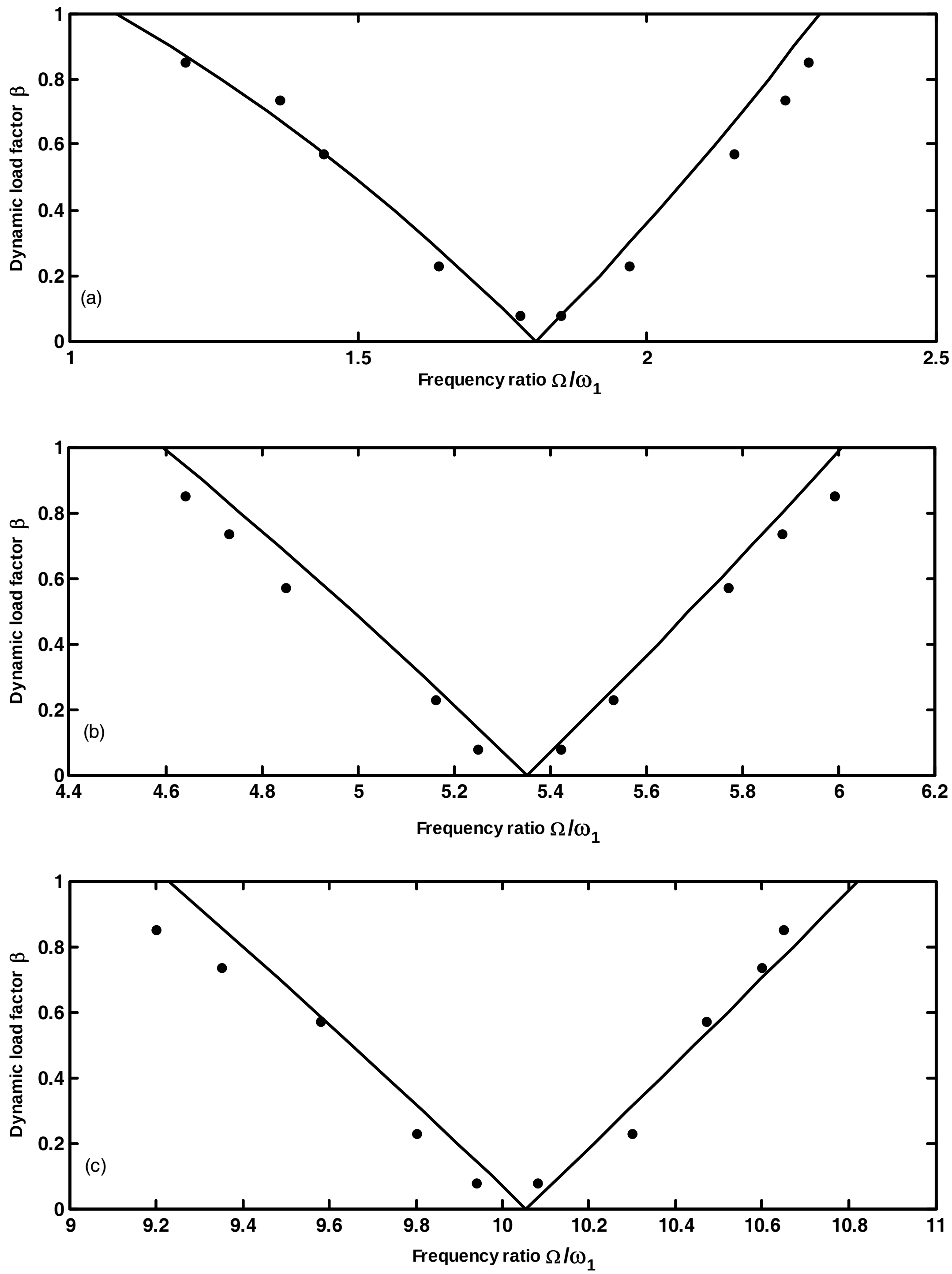

Fig.7.4,Instability regions,for fixed-fixed case,ξ=0.5,ψ=0.5,τ=0.2, Theoretical cal boundary from FEM;-, Experimental data;•.

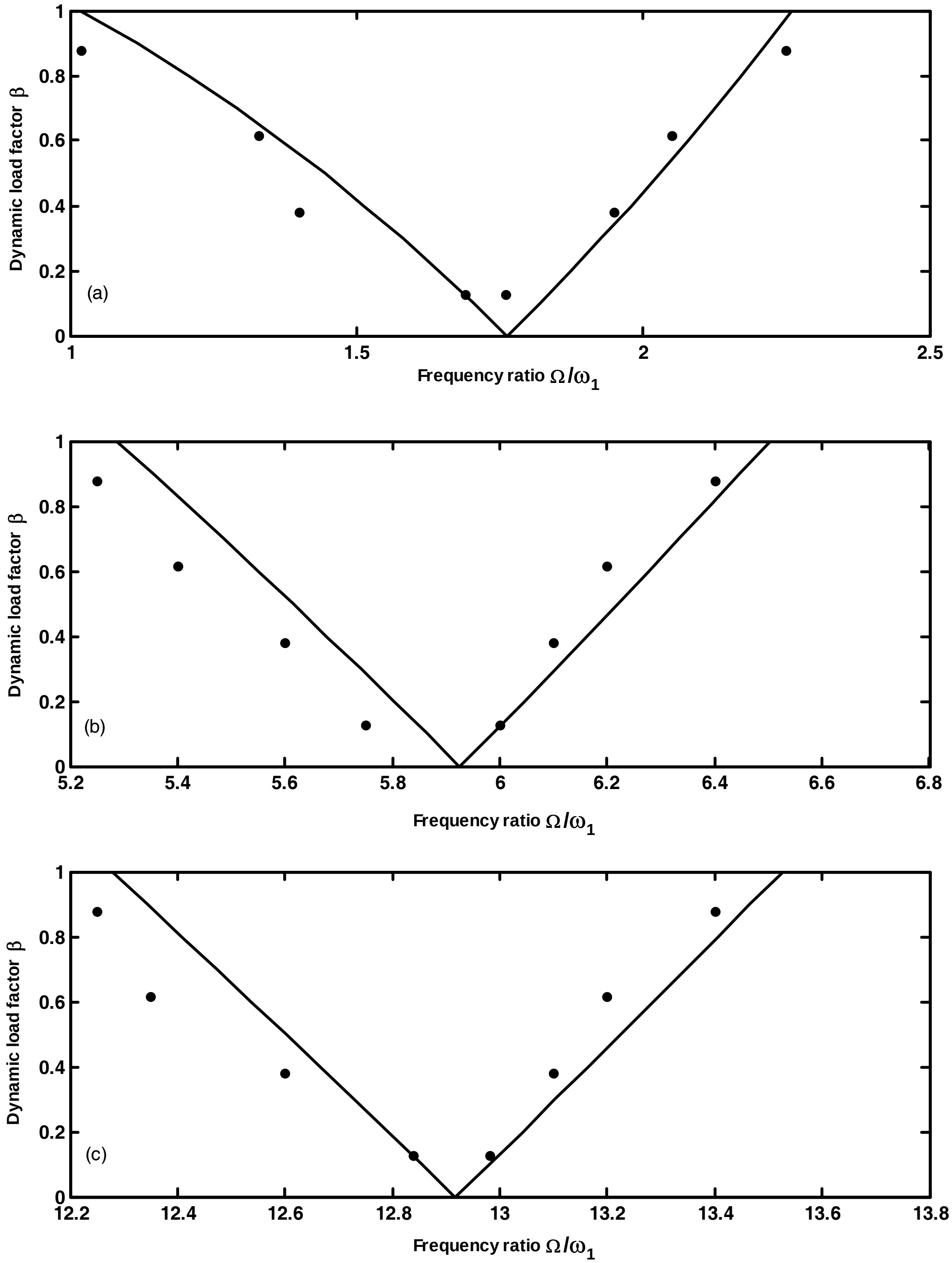

Fig.7.5,Instability regions,for fixed-pinned case,ξ=0.5,ψ=0.7,τ=0.2, Theoretical cal boundary from FEM;-, Experimental data;•.

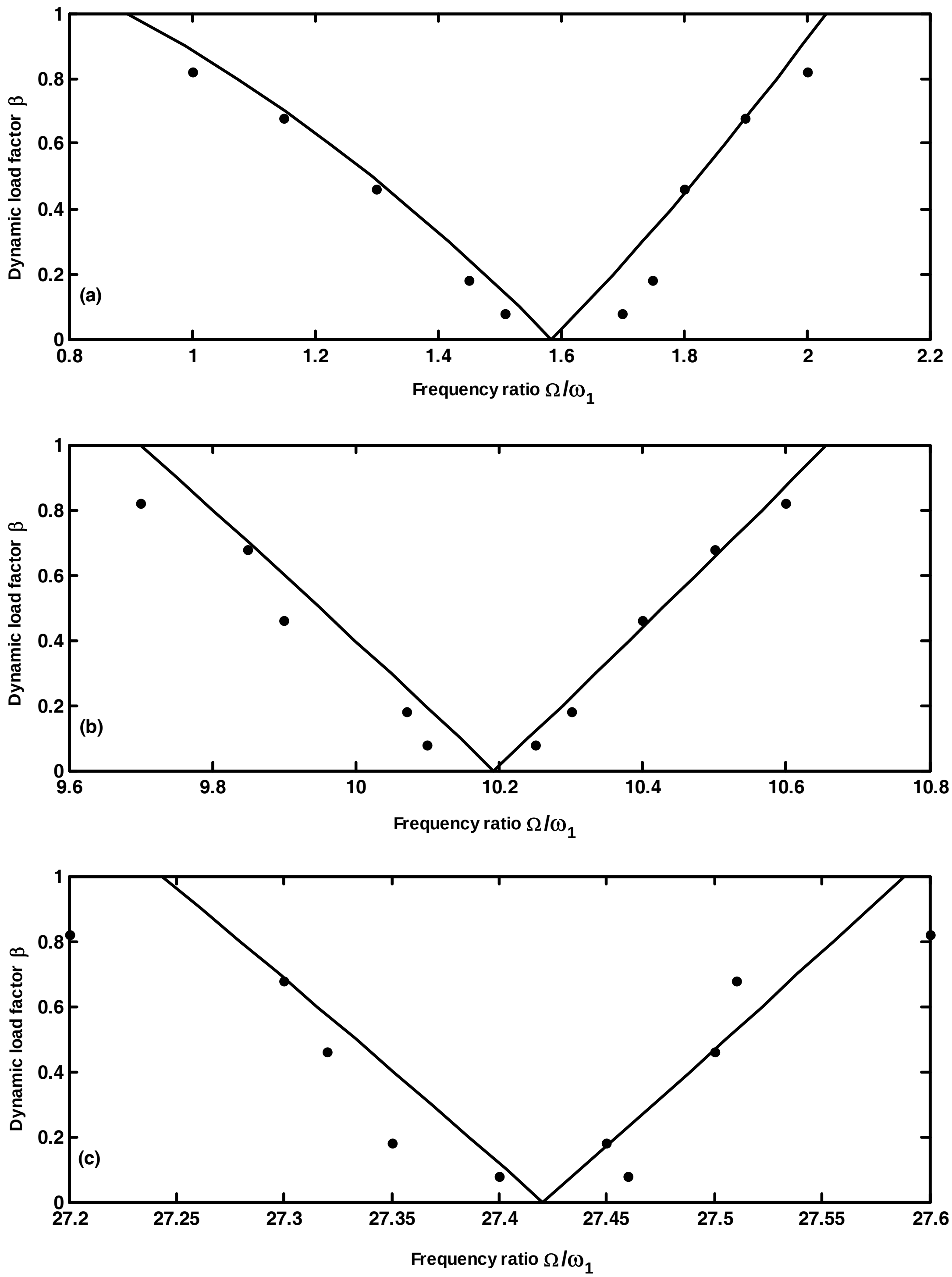

Fig.- 7.6 ,Instability regions,θ_1=30^0,ξ=0.5,ψ=0.1,ϕ=0.2,

Theoretical Boundary from FEM;- , Experimental data;•.

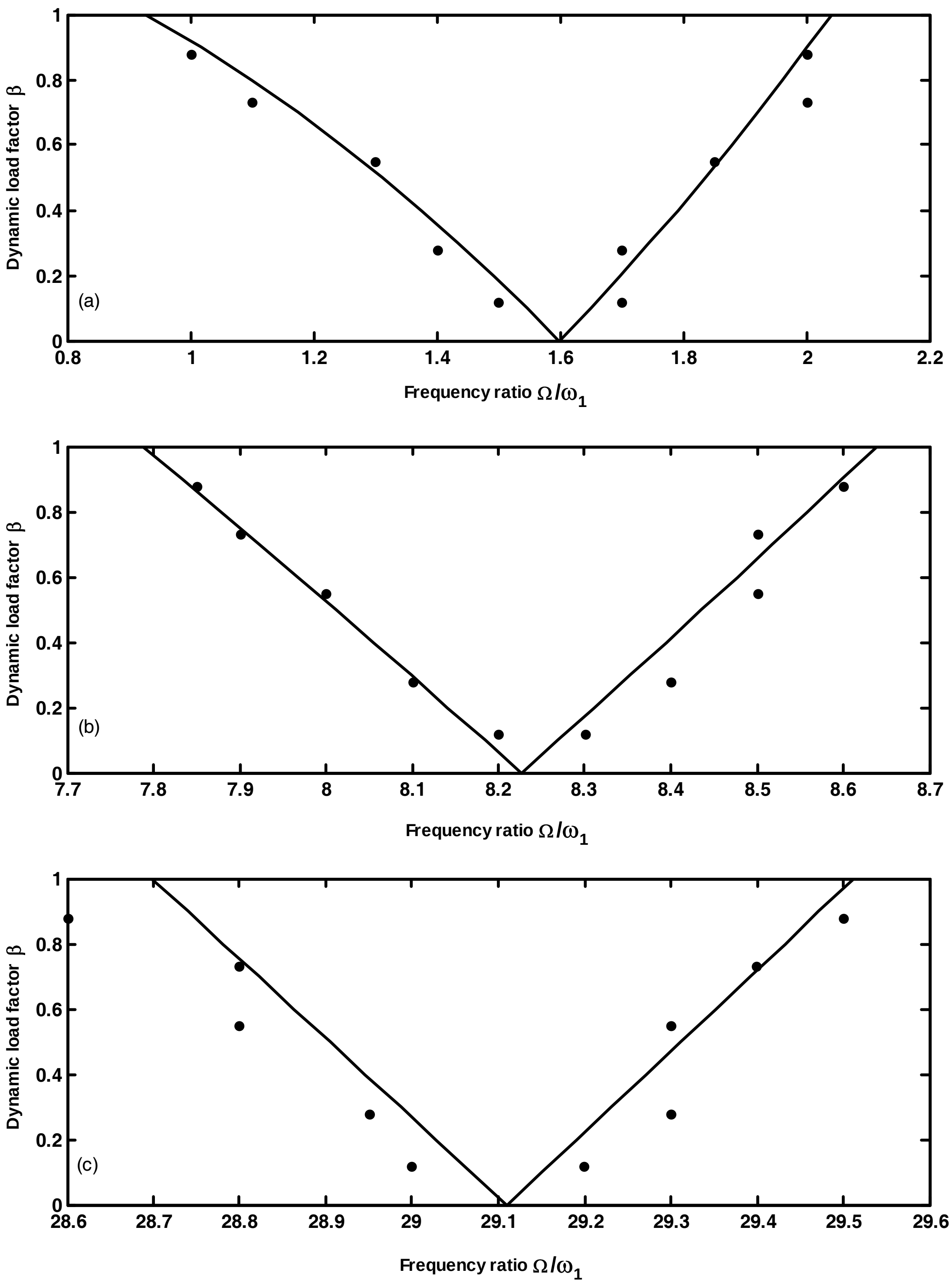

Fig.- 7.7 ,Instability regions,θ_1=60^0,ξ=0.5,ψ=0.1,ϕ=0.2,

Theoretical Boundary from FEM;- , Experimental data;•.

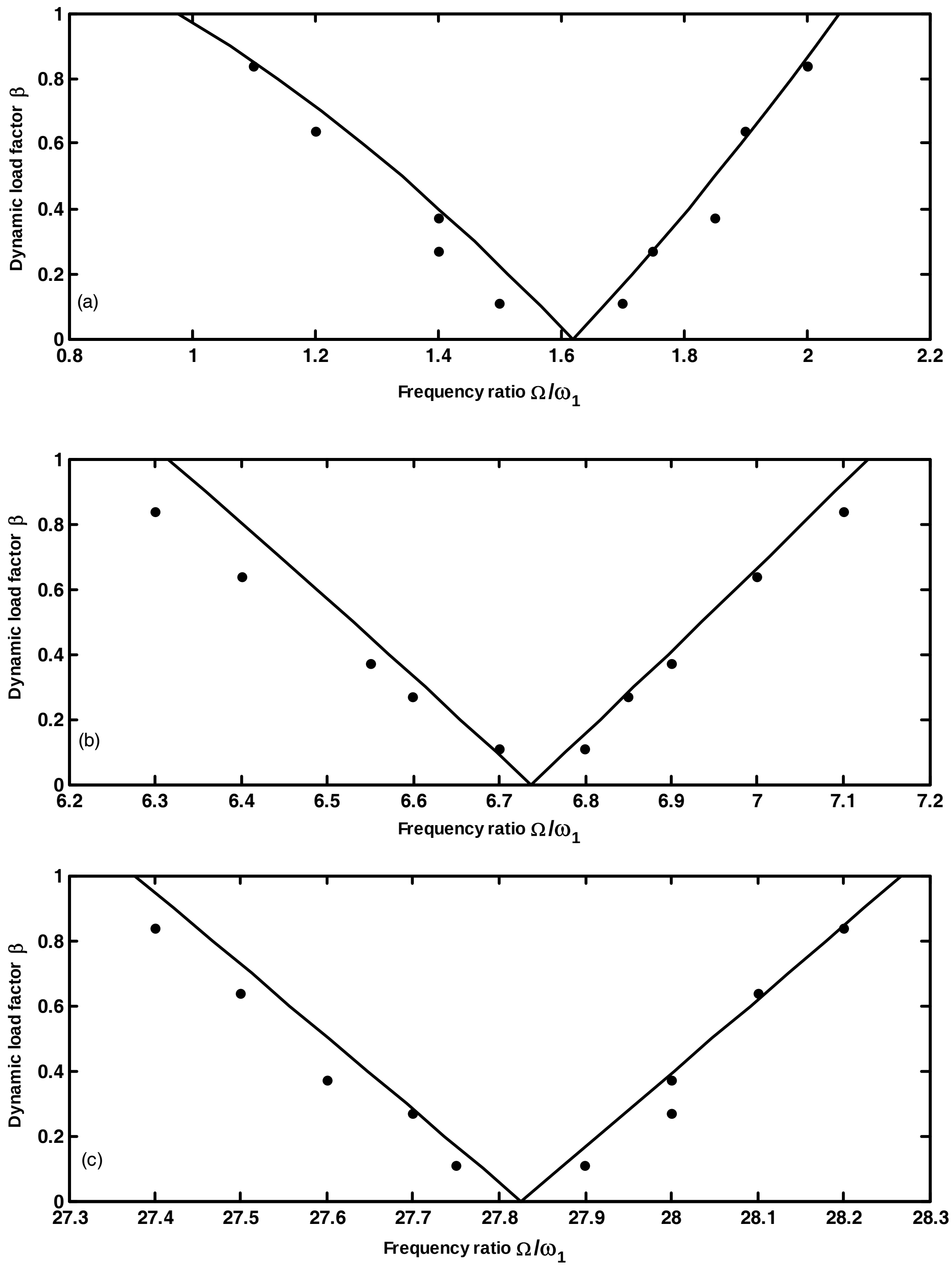

Fig.-7.8 ,Instability regions,$\theta_1=90^0$,$\xi=0.5$,$\psi=0.1$,$\phi=0.2$,
Theoretical Boundary from FEM;- , Experimental data;•.

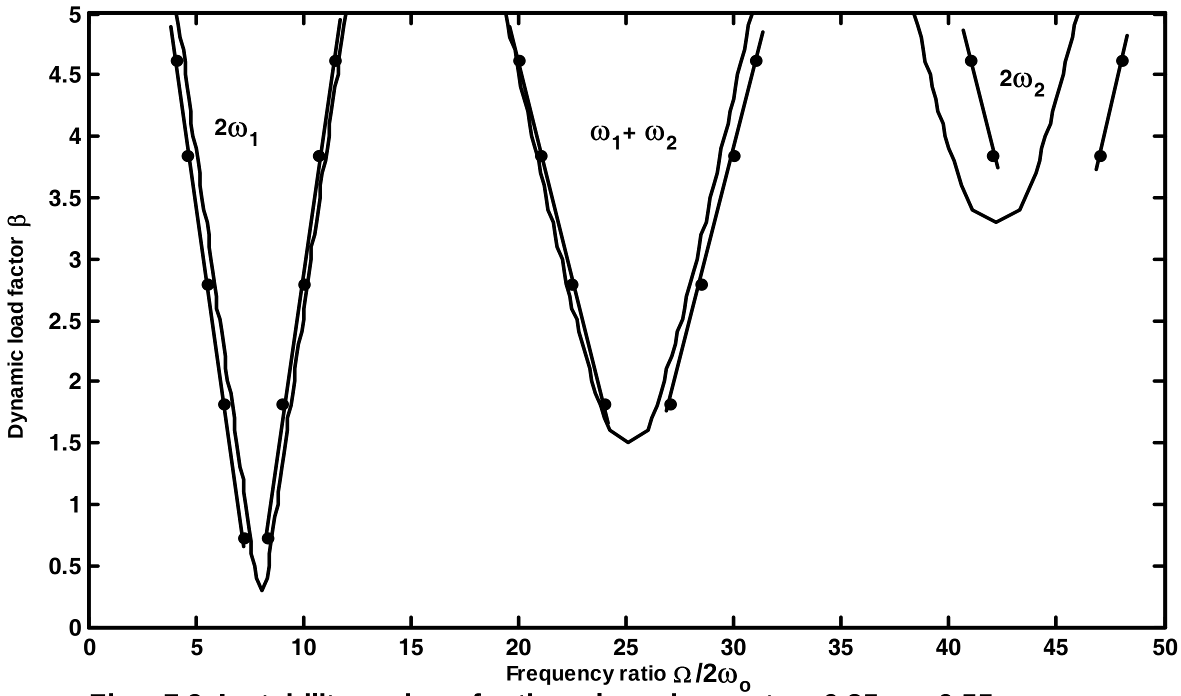

Fig. - 7.9 ,Instability regions for three layer beam:,t_{21} =0.25,η_c=0.55, Theoretical Boundary from FEM;-, Experimental data;•.

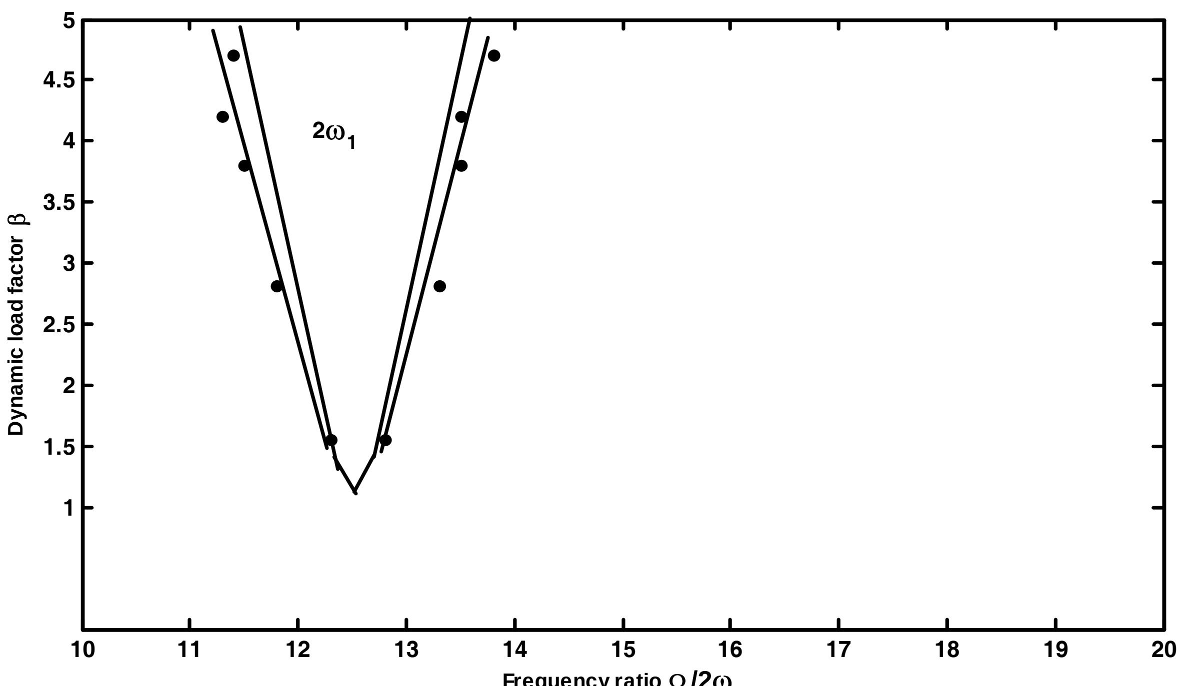

Fig. - 7.10,Instability regions for five layer beam:,t_{21} =0.25,η_c=0.55, Theoretical Boundary from FEM;-, Experimental data;•.

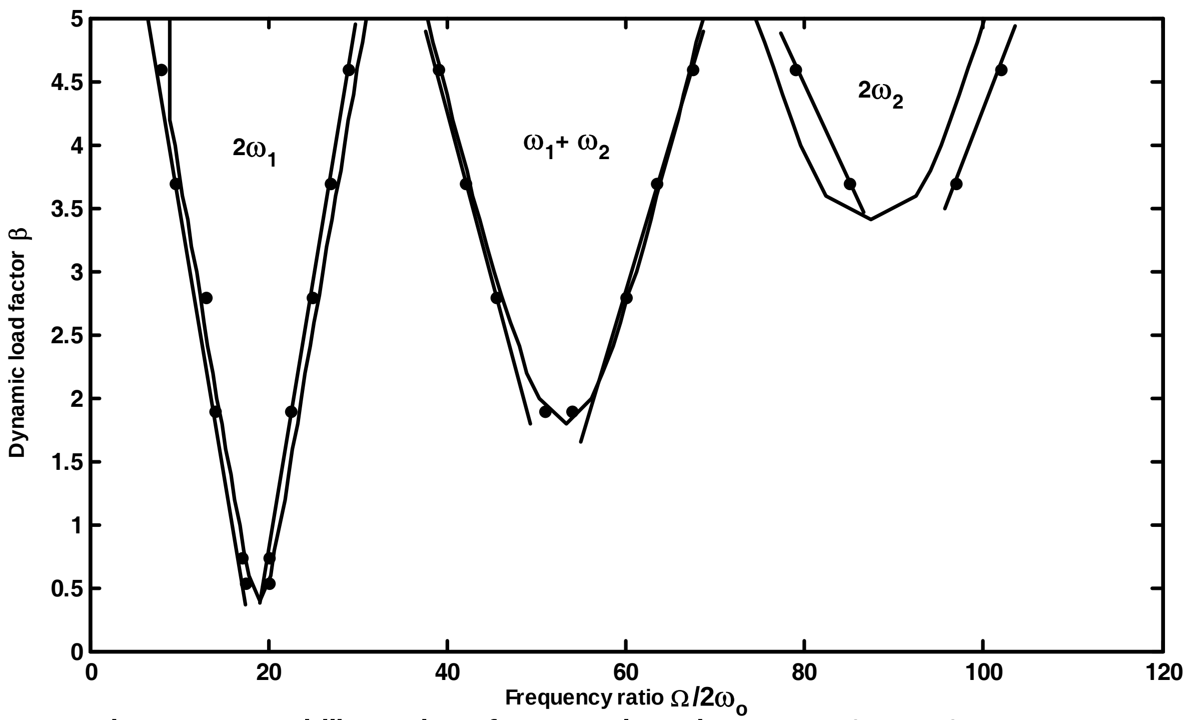

Fig. - 7.11 ,Instability regions for seven layer beam:,t_{21} =0.5,η_c=0.55, Theoretical Boundary from FEM;-, Experimental data;•.

PHYSICAL AND GEOMETRICAL PARAMETERS OF THE TEST SPECIMENS.

Table-7.1, Beams with localised damage and various boundary conditions.

Material of the specimens: Aluminium

Young's Modulus of the Aluminium material, $E_{Al} = 55.583 \times 10^{9}\ N/m^{2}$ and

Mass density of Aluminium, $\rho_{Al} = 2613\, Kg/m^{3}$.

CASE	Length of the beam in mm	Width of the beam in mm	Thickness of the beam in mm
Fixed-free	320	25.4	1.612
Pinned-pinned	460	-do-	-do-
Fixed-fixed	650	-do-	-do-
Fixed-pinned	460	-do-	-do-

Table-7.2, Theoretical values of fundamental natural frequency and critical buckling load of uniform undamaged beams with various boundary conditions.

CASE	Fundamental frequency in Hz.	Critical buckling load in N.
Fixed-free	11.73	11.87
Pinned-pinned	15.93	22.99
Fixed-fixed	18.09	46.05
Fixed-pinned	24.89	45.97

Table-7.3, Pretwisted cantilever beams with localised damage.
Physical and geometrical parameters of the test specimens.

Material of the specimens: Aluminium

Young's Modulus of the Aluminium material, $E_{Al} = 55.583 \times 10^{9}\ N/m^{2}$ and

Mass density of Aluminium, $\rho_{Al} = 2613\, Kg/m^{3}$.

Length of the beams in mm	Width of the beams in mm	Thickness of the beam in mm
300	25.4	1.612

Table-7.4, Theoretical values of natural frequency and critical buckling load of straight undamaged cantilever beam.

Fundamental frequency in Hz.	Critical buckling load in N.
13.34	13.511

Table- 7.5, Physical and geometrical data of sandwich beam specimens.

Three layer beam

L	t_1	t_2	G_v^*	η_c	E_1
0.3	0.001	0.00025	9.33×10^6	0.55	2.08×10^{11}

Five layer beam

L	t_1	t_2	G_v^*	η_c	E_1
0.5	0.001	0.00025	9.33×10^6	0.55	2.08×10^{11}

Seven layer beam

L	t_1	t_2	G_v^*	η_c	E_1
0.3	0.0005	0.00025	9.33×10^6	0.55	2.08×10^{11}

L =Length of the beam in m.

$t_{1=}$ Thickness of the elastic layer in m.

$t_{2=}$Thickness of the viscoelastic layer in m .

G_v^* =Shear modulus of viscoelastic core layer in N/m^2.

η_c =Core loss factor .

$E_{1=}$ Young's modulus of the elastic layer in N/m^2.

Elastic layer is made up of mild steel sheet and Viscoelastic core material is of PVC.

Table 7.6, Theoretical and experimental resonant frequencies of Multilayer beams.

Resonant frequency of three-layer beam in Hz

Mode	Theoretical	Experimental	% Error
First	25.64	24.2	-5.6
Second	134.43	145	+7.9

Resonant frequency of Five-layer beam in Hz

Mode	Theoretical	Experimental	% Error
First	13.32	12	-9.9
Second	71.21	80.6	+13.2

Resonant frequency of Seven-layer beam in Hz

Mode	Theoretical	Experimental	% Error
First	39.06	37.0	-5.2
Second	179.59	190.0	+5.7

Experimental boundary frequencies of instability regions

Uniform beam with localised damage and different boundary conditions.

Table-7.7, Experimental boundary frequencies of instability regions for uniform beam with localised damage, Fixed-free end conditions, P^*=11.87 N, ω_1=11.73 Hz.

Sl No	Dynamic load Amplitude (P_t) in N	Excitation Frequency (Ω)						Dynamic Load Factor $\beta = P_t / P^*$	Excitation frequency ratio Ω/ω_1					
		1st Zone		2nd Zone		3rd Zone			1st Zone		2nd Zone		3rd Zone	
		Lower limit (Ω_{11})	Upper limit (Ω_{12})	Lower limit (Ω_{21})	Upper limit (Ω_{22})	Lower limit (Ω_{31})	Upper limit (Ω_{32})		Lower limit (Ω_{11}/ω_1)	Upper limit (Ω_{12}/ω_1)	Lower limit (Ω_{21}/ω_1)	Upper limit (Ω_{22}/ω_1)	Lower limit (Ω_{31}/ω_1)	Upper limit (Ω_{32}/ω_1)
1	1.4	17.0	18.8	133.7	135.0	383.8	386.0	0.118	1.45	1.6	11.4	11.51	32.72	32.91
2	5.38	14.3	21.0	130.3	136.9	381.2	387.7	0.453	1.22	1.79	11.11	11.67	32.5	33.05
3	7.89	12.4	22.6	129.8	138.9	380.5	388.6	0.665	1.06	1.93	11.07	11.84	32.44	33.13
4	9.61	11.2	23.6	127.7	139.4	378.4	389.4	0.81	0.95	2.01	10.89	11.88	32.26	33.2

Table-7.8, Experimental boundary frequencies of instability regions for uniform beam with localised damage, Pinned-pinned end conditions, P^*= 22.99 N, ω_1= 15.93 Hz.

Sl No	Dynamic load Amplitude (P_t) in N	Excitation Frequency (Ω)						Dynamic Load Factor $\beta = P_t / P^*$	Excitation frequency ratio Ω/ω_1					
		1st Zone		2nd Zone		3rd Zone			1st Zone		2nd Zone		3rd Zone	
		Lower limit (Ω_{11})	Upper limit (Ω_{12})	Lower limit (Ω_{21})	Upper limit (Ω_{22})	Lower limit (Ω_{31})	Upper limit (Ω_{32})		Lower limit (Ω_{11}/ω_1)	Upper limit (Ω_{12}/ω_1)	Lower limit (Ω_{21}/ω_1)	Upper limit (Ω_{22}/ω_1)	Lower limit (Ω_{31}/ω_1)	Upper limit (Ω_{32}/ω_1)
1	3.47	25.6	27.4	122.8	124.2	253.0	256.6	0.151	1.61	1.72	7.71	7.80	15.90	16.10
2	5.4	25.00	29.2	122.6	124.6	252.5	258.6	0.235	1.58	1.83	7.70	7.82	15.85	16.23
3	13.5	17.6	32.8	114.6	126.6	247.0	260.0	0.587	1.10	2.05	7.20	7.95	15.50	16.3
4	20	12.8	40.4	111.6	129.0	240.6	263.0	0.87	0.8	2.54	7.00	8.10	15.10	16.5

Table-7.9, Experimental boundary frequencies of instability regions for uniform beam with localised damage, Fixed-fixed end conditions, P^{*}= 46.05 N, ω_1= 18.09 Hz.

Sl No	Dynamic load Amplitude (P_t) in N	Excitation Frequency (Ω)						Dynamic Load Factor $\beta = P_t / P^*$	Excitation frequency ratio Ω/ω_1					
		1st Zone		2nd Zone		3rd Zone			1st Zone		2nd Zone		3rd Zone	
		Lower limit (Ω_{11})	Upper limit (Ω_{12})	Lower limit (Ω_{21})	Upper limit (Ω_{22})	Lower limit (Ω_{31})	Upper limit (Ω_{32})		Lower limit (Ω_{11}/ω_1)	Upper limit (Ω_{12}/ω_1)	Lower limit (Ω_{21}/ω_1)	Upper limit (Ω_{22}/ω_1)	Lower limit (Ω_{31}/ω_1)	Upper limit (Ω_{32}/ω_1)
1	3.6	32.2	33.6	95	98.0	179.8	182.4	0.078	1.78	1.86	5.25	5.42	9.94	10.08
2	10.45	29.8	35.6	93.4	100.0	177.2	186.2	0.227	1.65	1.97	5.16	5.53	9.8	10.29
3	26.39	26.0	39.0	87.8	104.4	173.4	189.4	0.573	1.44	2.15	4.85	5.77	9.58	10.47
4	33.9	24.8	40.6	85.6	106.4	169.2	191.8	0.737	1.37	2.24	4.73	5.88	9.35	10.6
5	39.2	21.8	41.2	84.0	108.4	166.4	192.6	0.851	1.21	2.28	4.64	5.99	9.2	10.65

Table-7.10, Experimental boundary frequencies of instability regions for uniform beam with localised damage, Fixed-pinned end conditions. P^{*}= 45.97 N, ω_1= 24.89Hz.

Sl No	Dynamic load Amplitude (P_t) in N	Excitation Frequency (Ω)						Dynamic Load Factor $\beta = P_t / P^*$	Excitation frequency ratio Ω/ω_1					
		1st Zone		2nd Zone		3rd Zone			1st Zone		2nd Zone		3rd Zone	
		Lower limit (Ω_{11})	Upper limit (Ω_{12})	Lower limit (Ω_{21})	Upper limit (Ω_{22})	Lower limit (Ω_{31})	Upper limit (Ω_{32})		Lower limit (Ω_{11}/ω_1)	Upper limit (Ω_{12}/ω_1)	Lower limit (Ω_{21}/ω_1)	Upper limit (Ω_{22}/ω_1)	Lower limit (Ω_{31}/ω_1)	Upper limit (Ω_{32}/ω_1)
1	5.75	42.1	45.7	143.1	149.6	319.6	323.0	0.125	1.69	1.84	5.75	6.0	12.84	12.98
2	17.5	34.9	48.8	139.4	153.0	313.6	326.1	0.38	1.4	1.96	5.6	6.15	12.6	13.1
3	28.36	32.4	52.3	134.4	157.0	307.4	328.5	0.617	1.33	2.1	5.4	6.31	12.35	13.2
4	40.5	25.4	55.0	130.7	160.5	304.9	305.0	0.88	1.02	2.21	5.25	6.45	12.25	13.4

Cantilever twisted beam with localised damage.

Table-7.11, Experimental boundary frequencies of instability regions for twisted beam with localised damage $L=0.3m, \theta_1 = 30^0, \psi=0.1, \tau=0.2, P^*= 13.511$ N, $\omega_1= 13.34$Hz.

Sl No	Dynamic load Amplitude (P_t) in N	Excitation Frequency (Ω)						Dynamic Load Factor $\beta= P_t / P^*$	Excitation frequency ratio Ω/ω_1					
		1st Zone		2nd Zone		3rd Zone			1st Zone		2nd Zone		3rd Zone	
		Lower limit (Ω_{11})	Upper limit (Ω_{12})	Lower limit (Ω_{21})	Upper limit (Ω_{22})	Lower limit (Ω_{31})	Upper limit (Ω_{32})		Lower limit (Ω_{11}/ω_1)	Upper limit (Ω_{12}/ω_1)	Lower limit (Ω_{21} / ω_1)	Upper limit (Ω_{22} / ω_1)	Lower limit (Ω_{31}/ω_1)	Upper limit (Ω_{32} /ω_1)
1	1.08	20.2	22.8	134.8	136.8	365.6	366.4	0.08	1.51	1.7	10.1	10.25	27.4	27.46
2	2.43	19.4	23.4	134.4	137.4	364.8	366.2	0.18	1.45	1.75	10.07	10.3	27.35	27.45
3	6.22	17.4	24.0	132.0	138.8	364.4	368.0	0.46	1.3	1.8	9.9	10.4	27.32	27.5
4	9.19	15.4	25.4	131.4	140.0	364.2	367.0	0.68	1.15	1.9	9.85	10.5	27.3	27.51
5	11.08	13.4	26.8	129.4	141.4	362.8	368.2	0.82	1.0	2.0	9.7	10.6	27.2	27.6

Table-7.12, Experimental boundary frequencies of instability regions for twisted beam with localised damage $L= 0.3m, \theta_1 = 60^0, \psi=0.1, \tau=0.2, P^*= 13.511$ N, $\omega_1= 13.34$Hz.

Sl No	Dynamic load Amplitude (P_t) in N	Excitation Frequency (Ω)						Dynamic Load Factor $\beta= P_t / P^*$	Excitation frequency ratio Ω/ω_1					
		1st Zone		2nd Zone		3rd Zone			1st Zone		2nd Zone		3rd Zone	
		Lower limit (Ω_{11})	Upper limit (Ω_{12})	Lower limit (Ω_{21})	Upper limit (Ω_{22})	Lower limit (Ω_{31})	Upper limit (Ω_{32})		Lower limit (Ω_{11}/ω_1)	Upper limit (Ω_{12}/ω_1)	Lower limit (Ω_{21} / ω_1)	Upper limit (Ω_{22} / ω_1)	Lower limit (Ω_{31}/ω_1)	Upper limit (Ω_{32} /ω_1)
1	1.62	20.0	22.7	109.4	110.7	386.9	389.5	0.12	1.5	1.7	8.2	8.3	29.0	29.2
2	3.78	26.2	22.7	108.1	112.0	386.2	390.9	0.28	1.4	1.7	8.1	8.4	28.95	29.3
3	7.43	17.4	24.7	106.7	113.4	384.2	390.9	0.55	1.3	1.85	8.0	8.5	28.8	29.3
4	9.86	14.6	26.0	105.4	113.4	384.2	390.2	0.73	1.1	2.0	7.9	8.5	28.8	29.4
5	11.89	13.4	26.7	104.7	115.0	381.5	390.5	0.88	1.0	2.0	7.85	8.6	28.6	29.5

Table-7.13, Experimental boundary frequencies of instability regions for twisted beam with localised damage L=0.3m,θ_1 = 90^0, ψ=0.1, τ=0.2, P* = 13.511 N, ω_1= 13.34Hz.

Sl No	Dynamic load Amplitude (P_t)	Excitation Frequency (Ω)						Dynamic Load Factor β= P_t / P*	Excitation frequency ratio Ω/ω_1					
		1st Zone		2nd Zone		3rd Zone			1st Zone		2nd Zone		3rd Zone	
		Lower limit (Ω_{11})	Upper limit (Ω_{12})	Lower limit (Ω_{21})	Upper limit (Ω_{22})	Lower limit (Ω_{31})	Upper limit (Ω_{32})		Lower limit (Ω_{11}/ω_1)	Upper limit (Ω_{12}/ω_1)	Lower limit (Ω_{21}/ω_1)	Upper limit (Ω_{22}/ω_1)	Lower limit (Ω_{31}/ω_1)	Upper limit (Ω_{32}/ω_1)
1	1.49	20.0	22.7	89.4	90.7	370.2	372.2	0.11	1.5	1.7	6.7	6.8	27.75	27.9
2	3.65	18.7	23.3	88.0	91.4	369.5	373.5	0.27	1.4	1.75	6.6	6.85	27.7	28.0
3	5.0	18.7	24.7	87.4	92.0	368.2	373.5	0.37	1.4	1.85	6.55	6.9	27.6	28.0
4	8.65	16.0	25.4	85.4	93.4	366.9	374.8	0.64	1.2	1.9	6.4	7.0	27.5	28.1
5	11.35	14.7	26.7	84.0	94.7	365.5	376.2	0.84	1.1	2.0	6.3	7.1	27.4	28.2

Multilayered sandwich beams

Table-7.14, Experimental boundary frequencies of instability regions for 3-layered sandwich beam, L= 0.3m, t_1=0.001m, t_{21} = 0.25, P^*=7.7 N, ω_o=2.96 Hz.

Sl No	Dynamic load Amplitude (P_t)	Excitation Frequency (Ω)						Dynamic Load Factor $\beta = P_t / P^*$	Excitation frequency ratio $\Omega/2\omega_o$					
		$2\omega_1$		$\omega_1+\omega_2$		$2\omega_2$			$2\omega_1$		$\omega_1+\omega_2$		$2\omega_2$	
		Lower limit (Ω_{11})	Upper limit (Ω_{12})	Lower limit (Ω_{21})	Upper limit (Ω_{22})	Lower limit (Ω_{31})	Upper limit (Ω_{32})		Lower limit ($\Omega_{11}/2\omega_o$)	Upper limit ($\Omega_{12}/2\omega_o$)	Lower limit ($\Omega_{21}/2\omega_o$)	Upper limit ($\Omega_{22}/2\omega_o$)	Lower limit ($\Omega_{31}/2\omega_o$)	Upper limit ($\Omega_{32}/2\omega_o$)
1	5.62	42.6	49.1					0.73	7.2	8.29	-	-	-	-
2	14.0	37.3	53.3	142.1	159.8			1.82	6.3	9.0	24	26.94	-	-
3	21.56	32.6	59.0	133.2	168.7			2.8	5.51	9.97	22.5	28.5	-	-
4	29.65	27.2	63.4	124.3	177.6	248.6	278.2	3.85	4.59	10.71	21	30	42.0	46.0
5	35.57	24.3	68.1	118.4	183.5	242.7	284.2	4.62	4.1	11.5	20	31	47.0	48.0

Table-7.15, Experimental boundary frequencies of instability regions for 5-layered sandwich beam, L= 0.5m, t_1=0.001m, t_{21} = 0.25, P^*=4.16 N, ω_o=1.07Hz.

Sl No	Dynamic load Amplitude (P_t)	Excitation Frequency (Ω)						Dynamic Load Factor $\beta = P_t / P^*$	Excitation frequency ratio $\Omega/2\omega_o$					
		$2\omega_1$		$\omega_1+\omega_2$		$2\omega_2$			$2\omega_1$		$\omega_1+\omega_2$		$2\omega_2$	
		Lower limit (Ω_{11})	Upper limit (Ω_{12})	Lower limit (Ω_{21})	Upper limit (Ω_{22})	Lower limit (Ω_{31})	Upper limit (Ω_{32})		Lower limit ($\Omega_{11}/2\omega_o$)	Upper limit ($\Omega_{12}/2\omega_o$)	Lower limit ($\Omega_{21}/2\omega_o$)	Upper limit ($\Omega_{22}/2\omega_o$)	Lower limit ($\Omega_{31}/2\omega_o$)	Upper limit ($\Omega_{32}/2\omega_o$)
1	6.45	26.3	27.3	-	-	-	-	1.55	12.3	12.76	-	-	-	-
2	11.69	25.3	28.5	-	-	-	-	2.81	11.8	13.32	-	-	-	-
3	15.85	24.6	28.9	-	-	-	-	3.81	11.5	13.5	-	-	-	-
4	17.47	24.2	28.9	-	-	-	-	4.2	11.3	13.5	-	-	-	-
5	19.55	24.4	29.5	-	-	-	-	4.7	11.4	13.79	-	-	-	-

Table-7.16, Experimental boundary frequencies of instability regions for 7-layered sandwich beam, L= 0.3m, t_1=0.0005m, t_{21} = 0.5, P^*=1.9259 N, ω_o=2.05Hz.

Sl No	Dynamic load Amplitude (P_t)	Excitation Frequency (Ω)						Dynamic Load Factor $\beta = P_t / P^*$	Excitation frequency ratio $\Omega/2\omega_o$					
		$2\omega_1$		$\omega_1+\omega_2$		$2\omega_2$			$2\omega_1$		$\omega_1+\omega_2$		$2\omega_2$	
		Lower limit (Ω_{11})	Upper limit (Ω_{12})	Lower limit (Ω_{21})	Upper limit (Ω_{22})	Lower limit (Ω_{31})	Upper limit (Ω_{32})		Lower limit ($\Omega_{11}/2\omega_o$)	Upper limit ($\Omega_{12}/2\omega_o$)	Lower limit ($\Omega_{21}/2\omega_o$)	Upper limit ($\Omega_{22}/2\omega_o$)	Lower limit ($\Omega_{31}/2\omega_o$)	Upper limit ($\Omega_{32}/2\omega_o$)
1	1.04	71.7	82.0					0.54	17.5	20	-	-	-	-
2	1.41	70.0	82.0					0.73	17.0	20	-	-	-	-
3	3.66	57.4	92.3	209.1	221.4			1.9	14.0	22.5	51.0	54.0	-	-
4	5.4	53.7	102.5	186.6	246.0			2.8	13.1	25.0	45.5	60.0	-	-
5	7.13	39.0	110.7	172.2	260.4	348.5	397.7	3.7	9.5	27.0	42.0	63.5	85.0	97.0
6	8.86	32.8	160.0	160.0	276.8	324.0	418.0	4.6	8.0	29.0	39.02	67.5	79.0	101.95

Plate-1: Photograph of experimental setup

Plate-2, Photograph of attachments for,
(A)-Pinned end (B)- Clamped end.

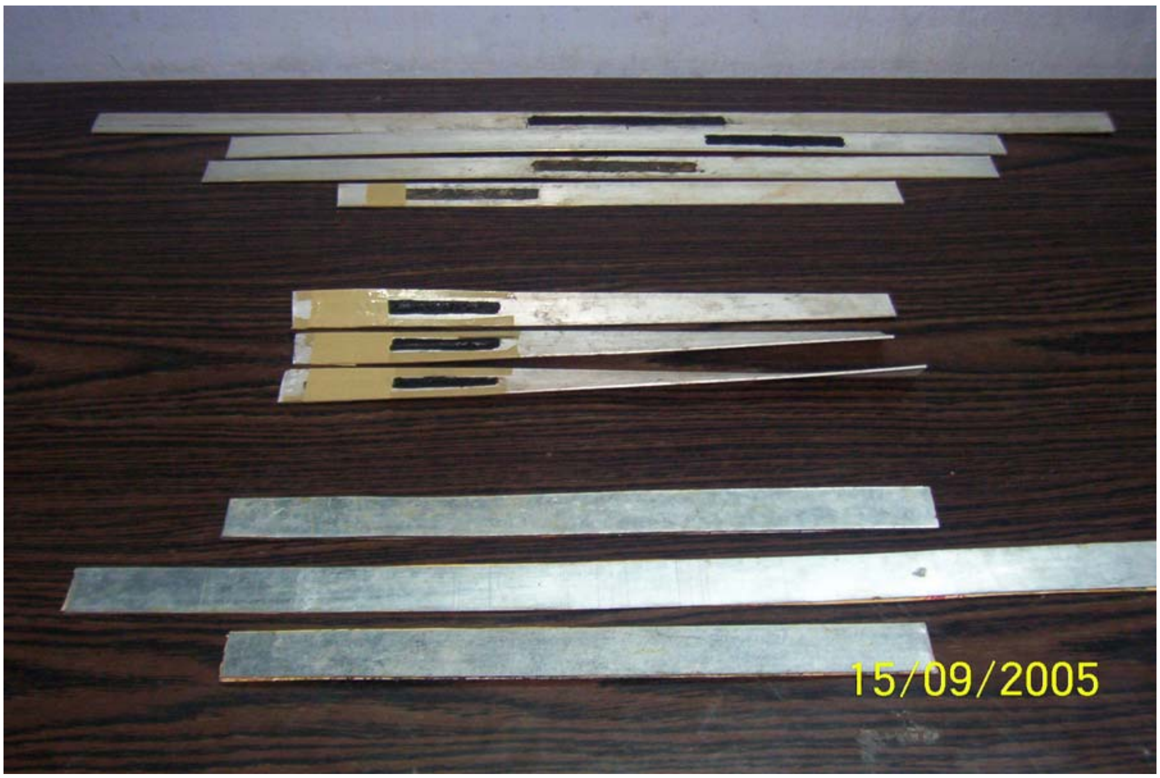
15/09/2005

Chapter **8**

CONCLUSION AND SCOPE FOR FURTHER RESEARCH

8.1 Conclusion

The present work deals with the theoretical and experimental investigation of dynamic stability of ordinary and sandwich beams under parametric excitation. The governing equations of motion for the system have been derived using finite element method. The primary instability regions for ordinary beams have been established by applying the Floquet's theory developed by Bolotin. For sandwich beam, stability criteria proposed by Saito and Otomi have been applied to determine the instability regions. The following important conclusions have been drawn from the various studies.

In chapter 3, the dynamic stability of a uniform Timoshenko beam with localised damage and different boundary conditions have been studied. The beam is subjected to an axial periodic load along its undeformed axis. Fixed-free, pinned-pinned, fixed-fixed and fixed-pinned boundary conditions have been considered in the analysis.

It is observed that presence of localised damage or in other words extent of damage enhances the instability of the beam for all the boundary conditions.

For fixed-free end condition the damage near the fixed end is more severe on the dynamic instability behavior than that of the damage located at other positions, so far as first instability region is concerned. The beam is most susceptible to instability so far as second instability region is concerned, when the damage is located at the middle. The third principal instability region relocates itself at minimum frequency of excitation when the damage position is in between the middle and free end.

For pinned-pinned end condition the first instability region occurs at minimum frequency of excitation when the damage is located at the middle. The beam is more stable when the damage is located towards any of the pinned end from middle. The second instability region occurs at minimum frequency of excitation when the damage is located in between the middle and any one of the pin ends and at highest frequency when the damage is located at the middle. The third instability zone occurs at minimum frequency of excitation when the damage is at the middle.

For the beam with fixed-fixed end condition the presence of damage at the middle makes the occurrence of first mode primary resonance most probable. The second instability region occurs at minimum frequency of excitation when the damage is in between the middle and either of the fixed ends of the beam. Third instability region occurs at minimum frequency of excitation when the damage is at the middle.

For fixed-pinned end condition the first instability region occurs at minimum frequency of excitation when the damage position is in between the middle and the pinned end. The second principal instability region occurs at minimum frequency of excitation when the damage is located in between the fixed end and the middle. Whereas the third principal instability region occurs at minimum frequency of excitation when the damage is located nearer to the pinned end.

Increase in static load component has a destabilising effect for all the four boundary conditions.

Chapter 4 deals with the dynamic stability of a pretwisted cantilever beam with localised damage and subjected to end parametric excitation. Angle of pretwist has significant effect on second and third instability zones. Increase in pretwist angle has a stabilising effect on the third instability zone and destabilising effect on the second instability zone. Change in pretwist angle does not have significant effect on the first instability region. Localised damage has a greater destabilising effect when it is located near the fixed end than when it is towards the free end, irrespective of the magnitude of pretwist angle. Increase in extent of damage increases the instability in terms of the shifting of instability zones to lower frequencies of excitation and increase in the areas of the instability zones. Increase in static load component enhances the instability of the beam. The effect is more pronounced on first instability region.

In chapter 5 dynamic stability of a multilayered symmetric cantilever sandwich beam subjected to parametric excitation has been studied. It is observed that increase in core thickness parameter, core loss factor and number of layers has stabilising effect. For constant size and constant weight cases, increase in number of layers deteriorates the stability with instability zones relocating them at lower frequencies of excitation, improves the stability with stability zones shifting to higher values on the dynamic load axis and disappearance of some instability regions. Constant flexural rigidity criterion improves stability with increase in number of layers. Among constant size, constant weight and constant flexural rigidity criteria, constant flexural rigidity is the most effective in improving the stability. Both constant size and flexural rigidity and constant weight and flexural rigidity criteria improve the stability with increase in number of layers. Constant weight and flexural rigidity case is more effective in improving the stability than constant size and flexural rigidity case.

Chapter 6 addresses the problem of dynamic stability of a simply supported tapered beam with uniform thermal gradient. It is observed that increase in thermal gradient decreases the natural frequency and the static buckling load. The effect is more pronounced on second and third modes than on first mode. Increase in static load component or thermal gradient has a destabilising effect. Thermal gradient has a greater destabilising effect than static load factor, for an equivalent change in static load component.

In chapter 7 experimental results are reported. Experimental results corroborate the theoretical findings except for the case of uniform Timoshenko beam with localised damage and with pinned-pinned and fixed-pinned end conditions. The discrepancies in these two cases may be due to the damping in the hinged ends.

A summary of the important conclusions may be stated as follows:

A) For a uniform Timoshenko beam with localised damage,

i) presence of damage always increases the instability of the beam,

ii) the critical position of the damage for maximum destabilising effect on the beam is different depending on the boundary conditions and the principal regions of instability of interest,

iii) increase in static load component has a destabilising effect for all boundary conditions considered and

iv) dynamic behaviour of the beam depends upon the boundary conditions as well as the location of the damage. Such mechanical components should be carefully designed with respect to the applied frequency of excitation, dynamic and static load components of the excitation force.

B) For pretwisted cantilever beam with localised damage,

i) angle of pretwist has significant effect on second and third instability zones. Increase in pretwist angle has a stabilising effect on the third instability zone and destabilising effect on the second instability zone. Change in pretwist angle does not have significant effect on the first instability region,

ii) extent of damage has always a destabilising effect on all the instability regions,

iii) localised damage has a greater destabilising effect when it is located near the fixed end than when it is towards the free end, irrespective of pretwist angle and

iv) increase in static load component has a destabilising effect on all the instability regions irrespective of pretwist angle.

C) For multilayered cantilever sandwich beam,

i) increase in core thickness parameter, core loss factor and number of layers has stabilising effect,

ii) for constant size and constant weight cases, increase in number of layers may deteriorate or improve the stability,

iii) constant flexural rigidity criterion improves stability with increase in number of layers,

iv) among constant size, constant weight and constant flexural rigidity criteria, constant flexural rigidity is the most effective one in improving the stability and

v) both constant size and flexural rigidity and constant weight and flexural rigidity criteria improve the stability. Constant weight and flexural rigidity case is more effective in improving the stability than constant size and flexural rigidity case.

D) For simply supported tapered beam with thermal gradient

i) increase in static load component or thermal gradient worsens the stability of the beam.

8.2 Scope for further research

Some of the possible areas for further research on dynamic stability of beams are described below.

i) Effort was made to experimentally establish the stability diagram for the simply supported tapered beam with thermal gradient. It was realised that substantial redesign of the experimental setup is required to achieve uniform thermal gradient along the length of the beam. This could be the subject of considerable further work.

ii) In actual practice the beams may be subjected to loads like combination of forced and parametric excitation, parametric excitations consisting of more than one frequency i.e. multifrequency excitation and random excitation etc. The dynamic behaviour of beams under these types of excitations may be explored.

iii) Study of dynamic stability of beams considering material and geometric non-linearities may also be an aspect of investigation.

REFERENCES

1. Abbas, B.A. H. and Thomas, J., Dynamic stability of Timoshenko beams resting on an elastic foundation. Journal of sound and vibration, 60, 33 – 44, 1978.

2. Abbas, B.A.H., Dynamic stability of a rotating Timoshenko beam with a flexible root. Journal of sound and vibration, 108, 25 – 32, 1986.

3. Agbasiere, J.A. and Grootenhuis, P., Flexural vibration of symmetric multilayered beams with viscoelastic damping. Journal of Mechanical Engineering Science, 10,269-274, 1968.

4. Anlinker M and Troesch B.A., Lateral vibrations of pretwisted rods with various boundary conditions. Zeitschrift für .Angewandte. Mathematik und Physik. 14, 218-236, 1963.

5. Ariarathnam, S.T., Parametric resonance, proceedings of the tenth U.S. National Congress of applied Mechanics.1986.

6. Asnani, N.T. and Nakra, B.C., Vibration analysis of multilayered beams with alternate elastic and viscoelastic layers. Journal of Institution of Engineers India, Mechanical Engineering Division, 50,187-193, 1970.

7. Asnani, N.T. and Nakra, B.C., Vibration analysis of sandwich beams with viscoelastic core. Jr. Aeronautical Society of India, 24,288-294,1972,

8. Asnani, N.T. and Nakra, B.C., Forced Vibration damping characteristics of multilayered beams with constrained viscoelastic layers. J. Eng. (Indus), Trans. ASME, Series B. 98, 895 –901, 1976.

9. Banerjee, J.R., Free vibration analysis of a twisted beam using the dynamic stiffness method. International Journal of Solids and Structures, 38, 6703-6722, 2001.

10. Banerjee, J.R., Free vibration of sandwich beams using the dynamic stiffness method. Computers and Structures, 81, 1915-1922, 2003.

11. Bauchau, O.A. and Hong, C.H., Nonlinear response and stability analysis of beams using finite elements in time. AIAA J., 26, 1135–1141, 1988.

12. Bauld, N. R. Jr., Dynamic stability of sandwich columns under pulsating axial loads. AIAA J., 5, 1514 – 1516, 1967.

13. Beliaev, N.M., Stability of prismatic rods subjected to variable longitudinal forces. Collection of papers: Eng. Construct, Struct. Mech., Put’, Leningrad, 149 – 167, 1924.

14. Berkovits, A. and Gold, A., Buckling of an elastic column containing a fatigue crack. Experimental Mechanics, 8,368-371, 1972.

15. Bhimaraddi, A., Sandwich beam theory and the analysis of constrained layer damping. Journal of sound and vibration, 179, 591-602, 1995.

16. Briseghella, G., Majorana, C.E., Pellegrino, C., Dynamic stability of elastic structures: a finite element approach. Computer and structures, 69, 11-25, 1998.

17. Bolotin, V.V., The dynamic stability of elastic Systems. Holden – Day, Inc., san Frasncisco, 1964.

18. Brown, J.E., Hutt, J.M. and Salama, A.E., Finite element solution to dynamic stability of bars. AIAA J., 6, 1423-1425, 1968.

19. Carneige, W., Vibrations of pre-twisted cantilever blading. Proc. Inst. Mech. Engrs. London. 173,343-347, 1959.

20. W.Carneige and L. Thomas, The coupled bending- bending vibration of pre-twisted tapered cantilever blading. J.Engg Ind., Trans of ASME, 75,255 1972.

21. Celep, Z., Dynamic stability of pretwisted columns under periodic axial loads. Journal of sound and vibration, 103, 35–48, 1985.

22. Chatterjee, A. and Baumgarten, J.R., An analysis of viscoelastic damping characteristics of a simply supported sandwich beam. Journal of Engineering for Industry, Trans of ASME, 93, 1239-1244, 1971.

23. Chen, L.W. and Ku, M.K., Dynamic stability of a cantilever shaft-disk system. Journal of Vibration and Acoustics, Trans of ASME, 114,326-329, 1992.

24. Chen, M.L. and Liao, Y.S., Vibrations of pretwisted spinning beams under axial compressive loads with elastic constraints. Journal of sound and Vibration, 147, 497-513, 1991.

25. Chen, Q. and Chan, Y.W., Integral finite element method for dynamical analysis of elastic-viscoelastic composite structures. Computers and structures, 74, 51-64, 2000.

26. Chonan, S. Vibration and stability of sandwich beams with elastic bonding. Journal of sound and vibration, 85, 525 – 537, 1982.

27. Chonan, S., Vibration and stability of a two- layered beam with imperfect bonding. J. of Acoustical Society of America, 72, 208 – 213, 1982.

28. Das, A.K. and Dey S.S., Random vibration of beams with localized region of damage. Computers and structures, 51, 33-38, 1994.

29. Datta, P. K. and Chakraborty, S., Parametric instability of tapered beams by finite element method. J. Mech. Eng. Sci., 24, 205 – 208, 1982.

30. Datta P.K. and Lal, M.K., Static stability of a tapered beam with localized damage subjected to an intermediate concentrated load. Computers and Structures, 43,971-974, 1992.

31. Datta, P. K. and Nagraj, C.S., Dynamic instability behaviour of tapered bars with flaws supported on an elastic foundation. Journal of sound and vibration, 131, 229 – 237, 1989.

32. Dawson, B., Coupled bending vibrations of pretwisted cantilever blading treated by Rayleigh-Ritz method. J.Mech. Engng. Sci, 10,381-386, 1968.

33. Dewa, H., Okada, Y. and Nagai, B. Damping characteristics of flexural vibration for partially covered beams with constrained viscoelastic layers. JSME International Journal, series iii, 34,210-217, 1991.

34. Dhotarad, M.S., and Ganeshan, N., Vibration analysis of a rectangular plate subjected to a thermal gradient. Journal of sound and vibration. 60,481-497, 1978.

35. DiTaranto, R.A., Theory of vibratory bending for elastic and viscoelastic layered finite length beams. Journal of Applied Mechanics, Trans of ASME, 87,881-886, 1965.

36. DiTaranto, R.A. and Blasingame, W., Composite loss factors of selected laminated beams. Journal of the Acoustical Society of America, 40,187-194, 1966.

37. Dokumaci, E., Dynamic stability of pre-twisted blades under lateral parametric excitation. ASME Paper No. 79 – DET – 91, 1979.

38. Dufour, R. and Berlioz, A., Parametric instability of a beam due to axial excitations and to boundary conditions. Journal of Vibration and Acoustics, Trans of the ASME, 120, 461-467, 1998.

39. Evan – Iwanowski, R. M. On the parametric response of structures. Applied Mechanics review, 18, 699 – 702, 1965.

40. Faraday, M., On a peculiar class of acoustical figures and on certain forms assumed by a group of particles upon vibrating elastic surfaces. Phil. Trans., Roy. Soc., London, 299 – 318, 1831.

41. Fasana, A., and Marchesiello, S., Rayleigh-Ritz analysis of sandwich beams. Journal of sound and vibration, 241,643-652, 2001.

42. Frisch-Fay, R., Buckling of pre-twisted bars. Int. J. Mech. Sci., 15, 171-181, 1973.

43. Frosting, Y. and Baruch, M., Bending of sandwich beams with transversely flexible core. AIAA Journal, 28,523-527, 1990.

44. Garrick, I.E., Survey of aeroelasticity. Journal of Aerospace Engineering, 22,140-147, 1963.

45. Gorrepati, M. and Rao, M.D., Analysis of modal parameters of adhesively bonded double-strap joints by the modal strain energy method. Journal of Vibration and Acoustics, Trans of ASME, 118, 28-35, 1996.

46. Gupta R.S. and Rao S.S., Finite element eigenvalue analysis of tapered and twisted Timoshenko beams. Journal of sound and vibration, 56, 187-200, 1978.

47. Gürgöze, M., On the dynamic stability of a pre-twisted beam subject to a pulsating axial load. Journal of sound and vibration, 102, 415 – 422, 1985.

48. Ha, K.H., Exact analysis of bending and overall buckling of sandwich beam systems. Computers and structures, 45, 31-40, 1992.

49. Habip, L.M., A survey of modern developments in the analysis of sandwich structures. Applied Mechanics Reviews, 18, 93-98, 1965.

50. He, S. and Rao, M.D., Prediction of loss factors of curved sandwich beams. Journal of Sound and Vibration, 159, 101-113, 1992.

51. He,S. and Rao, M.D., Vibration and damping analysis of multi span sandwich beams with arbitrary boundary conditions. Trans. of the ASME, Journal of vibration and acoustics, 114, 330-337, 1992.

52. Hsu, C. S., On the parametric excitation of a dynamic system having multiple degrees of freedom. J. Appl. Mech., Trans. ASME, 30, 367 – 372, 1963.

53. Hsu, C. S., Further results on parametric excitation of a dynamic system. J. Appl. Mech., Trans. ASME, 32, 373 – 377, 1965.

54. Ibrahim, R. A. and Barr, A. D. S., Parametric vibration, Part I: Mechanics of linear problems. Shock Vib. Dig., 10(1), 15 – 29, 1978.

55. Ibrahim, R. A. and Barr, A. D. S., Parametric vibration, part II: Mechanics of nonlinear problems. Shock Vib. Dig., 10(20), 9 – 24, 1978.

56. Ibrahim, R. A., Parametric vibration, Part III: Current problems (1). Shock vib. Dig., 10 (3), 41 –57, 1978.

57. Ibrahim, R. A., Parametric vibration, Part IV: Current problems (2). Shock Vib Dig., 10 (4), 19 – 47, 1978.

58. Ibrahim, R. A., and Roberts, J. W., parametric vibration, Part V: Stochastic problems. Shock Vib. Dig., 10 (5), 17 – 38, 1978.

59. Ibrahim, R. A., Parametric vibration, Part Vi: Stochastic problems (2). Shock Vib. Dig., 13 (9), 23 – 35, 1981.

60. Ibrahim, R. A., Parametric Random Vibration, Research Studies Press Ltd., England, 1985.

61. Imaino, W. and Harrison,J.C., A comment on constrained layer damping structures with low viscoelastic modulus. Journal of sound and vibration, 149, 354-361, 1991.

62. Ishida, Y., Ikeda, T., Yamamoto, T. and Esaka, T., Parametrically excited oscillations of a rotating Shaft under a periodic axial force. JSME Int. J., Series III, 31, 698 – 704, 1988.

63. Iwatsubo, T., Saigo, M. and Sugiyama, Y., Parametric instability of clamped – clamped and clamped – simply supported columns under periodic axial load. Journal of sound and vibration, 30, 65 – 77, 1973.

64. Iwatsubo, T., Sugiyama, Y. and ogino, S., Simple and combination resonances of columns under periodic axial loads. Journal of sound and vibration, 33, 211 – 221, 1974.

65. Johnson, C.D., Kienholz, D.A.,Rogers, L.C., Finite element prediction of damping in beams with constrained viscoelastic layers, Shock and vibration bulletin, 51(1),71-81,1981.

66. Johnson, C.D., Kienholz, D.A., Finite element prediction of damping in structures with constrained viscoelastic layers, AIAA Journal, 20(9), 1284-1290, 1982.

67. Jones. I.W., Salerno.N.L. and Savacchiop. A., An analytical and experimental evaluation of the damping capacity of sandwich beams with viscoelastic cores. Journal of Engineering for Industry, Trans. of ASME, 89, 438-445, 1967.

68. Kapur, A.D., Nakra, B.C. and Chawla, D.R., Shock response of viscoelastically damped beams. Journal of sound and vibration, 55,351-362, 1977.

69. Kar, R.C. and Hauger, W., Stability of a sandwich beam subjected to a non-conservative force. Computer and structures, 46,955-958, 1993.

70. Kavi, N., and Asnani, N.T., Forced vibrations of stringer stiffened damped sandwich panel. The shock and vibration bulletin, 56,167-178, 1986.

71. Kerwin, E.M.Jr., Damping of flexural waves by a constrained viscoelastic layer. Journal of the Acoustical Society of America, 31, 952 -962, 1959.

72. Lall. A.K., Asnani, N.T. and Nakra, B.C., Damping analysis of partially covered sandwich beams. Journal of sound and vibration, 123,247-255, 1988.

73. Lau, S.L. Cheung, Y. K. and Wu, S. Y., A variable parameter incrementation method for dynamic instability if linear and nonlinear elastic systems. J. Appl. Mech., Trans. ASME, 49, 849 – 853, 1982.

74. Liebowitz, H. and Claus, W.D., Failure of notched columns with fixed ends. Int. Journal of solids and structures, 5,941-950, 1969.

75. Lin, C.Y., and Chen, L.W., Dynamic stability of a rotating beam with a constrained-damping layer. Journal of sound and vibration, 267,209-225, 2002.

76. Mace, M., Damping of beam vibrations by means of a thin constrained viscoelastic layer: Evaluation of a new theory. Journal of sound and vibration, 172,577-591, 1994.

77. Markus, S., Damping mechanism of beams partially covered by constrained viscoelastic layer, ACTA Technica CSAV 2.179-194, 1974.

78. Mead, D. J. and Markus, S., The forced vibration of three – layer, damped sandwich beams with arbitrary boundary conditions. Journal of sound and vibration, 10, 163 – 175, 1969.

79. Melde, F., über erregung stehender wellen eines fadenformigen korpers. ANN. PHys. Chem., 109, 193 – 215, 1859.

80. Mettler, E., Allgemeine theorie der stabilitat erzwungener schwingungen elastischer koper. Ing. Arch, 17, 418-449, 1949.

81. Mohanty, S.C. and Kavi, N., Static stability of a tapered simply supported beam with localised damage subjected to an intermediate concentrated load considering shear deformation. Jr. of Mechanical Engg., Space Society of Mechanical Engineers, India, 7, 22-26, 2004.

82. Mohanty, S.C. and Kavi, N., Dynamic stability of simply supported tapered Timoshenko beam with thermal gradient by finite element method. Jr. of Mechanical Engg., Space Society of Mechanical Engineers, India, 64, 63-71, 2002.

83. Nakra, B.C. and Grootenhuis, P., Structural damping using a four layer sandwich. Journal of Engineering for industry, Trans. of ASME, 74, 81-86, 1972.

84. Nakra, B.C., Vibration control with viscoelastic materials. The Shock and Vibration Digest, 8, 3-12, 1976.

85. Nakra, B.C., Vibration control with viscoelastic materials-II. The Shock and Vibration Digest, 13, 17-20, 1981.

86. Nakra, B.C., Vibration control with viscoelastic materials-III. The Shock and Vibration Digest, 16, 17-22, 1984.

87. Nakra, B.C., Vibration control in machines and structures using Viscoelastic damping. Journal of sound and vibration. 211, 449-465, 1998.

88. Nayfeh, A. H. and Mook, D.T., Nonlinear Oscillations. John Willey & Sons, Inc., New York, 1979.

89. Nayfeh, S.A., Damping of flexural vibration in the plane of lamination of elastic-viscoelastic sandwich beams. Journal of Sound and Vibration, 276,689-711, 2004.

90. Parekh, V.N. and Carlson, R.L., Effects of localized region of damage on the parametric excitation of a bar, Int. J. Mech. Sci., 19, 547-533, 1977.

91. Qian, C.and Demao, Z., Vibration analysis theory and application to elastic-viscoelastic composite structures. Computers and structures, 37,585-592, 1990.

92. Rao, D. K., Transverse vibrations of pre-twisted sandwich beams. Journal of sound and vibration, 44 159 – 168, 1976.

93. Rao, D.K. and Stühler, W., Frequency and loss factors of tapped symmetric sandwich beams. J. Appl. Mech., Trans. ASME, 99, 511 – 513, 1977.

94. Rao D. K., Vibration of short sandwich beams. Journal of sound and vibration, 52, 253 – 263, 1977.

95. Rao, D. K., Forced vibration of a damped sandwich beam subjected to moving forces. Journal of sound and vibration, 54, 215 – 227, 1977.

96. Rao, D.K., Frequency and loss factors of sandwich beams under various boundary conditions. J. Mech. Eng. Sci., 20, 271 – 282, 1978.

97. Rao, J.S., Coupled vibrations of turbomachine blades. Shock Vibration Bulletin. 47,107-127, 1977.

98. Rao, Y.V.K.S., Vibration of dual core sandwich beams, Journal of Sound and Vibration, 32,175-187, 1974.

99. Ray, K. and Kar, R.C., Parametric instability of a sandwich beam under various boundary conditions. Computers and structures, 55,857-870, 1995.

100. Ray, K. and Kar, R.C., The parametric instability of partially covered sandwich beams. Journal of Sound and Vibration, 197,137-152, 1996.

101. Ray, K. and Kar, R.C., Parametric instability of a dual cored sandwich beam. Computers and structures, 61,665671, 1996.

102. Ray, K. and Kar, R.C., Parametric instability of a symmetric sandwich beam with higher order effects. Computers and structures, 60,817-824, 1996.

103. Rubayi, N.A. and Charoenree, S., Natural frequencies of vibration of cantilever sandwich beams. Computers and structures. 6, 345 – 353, 1976.

104. Saito, H. and Otomi, K., Parametric response of viscoelastically supported beams. Journal of Sound and Vibration, 63, 169 – 178 1979.

105. Saito H. and Koizumi, N., Parametric vibrations of a horizontal beam with a concentrated mass at one end. Int. J. Mech. Sci., 24, 755 – 761 1982.

106. Sakiyama, T., Matsuda, H. and Morita, C., Free vibration analysis of continuous sandwich beams with elastic or viscoelastic cores by applying the discrete Green function. Journal of Sound and Vibration, 198,439-445, 1996.

107. Salet, T.A.M. and Hamelink, S.A., Numerical analysis of sandwich beams. Computers and structures, 41, 1231-1239, 1991.

108. Sharma, S.R. and Rao, D.K., Static deflection and stresses in sandwich beams under various boundary conditions. Journal of Mechanical Engineering Science, IMechE.24, 11-18, 1982.

109. Schmidt, G., Parametererregte Schwingungen. VEB Deutscher verlag der Wissenschaften, Berlin, 1975.

110. Shastry, B.P. and Rao, G. V., Dynamic stability of a cantilever column with an intermediate concentrated periodic load. Journal of Sound and Vibration, 113, 194 – 197, 1987.

111. Shastry, B.P. and Rao, G.V., Stability boundaries of a cantilever column subjected to an intermediate periodic concentrated axial load. Journal of Sound and Vibration, 116, 195 – 198, 1987.

112. Shastry, B.P. and Rao, G. V., Stability boundaries of short cantilever columns subjected to an intermediate periodic concentrated axial load. Journal of Sound and Vibration, 118, 181 – 185, 1987.

113. Simitses, G. J., Instability of dynamically – loaded structures. Appl. Mech, Rev., 40, 1403 – 1408, 1987.

114. Spinner, S., Temperature dependence of elastic constants of some cerment specimens. Journal of the National Bureau of Standards, Civil Engineering and Instrumentation, 65 C, 89-96, 1961.

115. Stevens, K.K., On the parametric excitation of a viscoelastic column. AIAA journal, 4, 2111-2115, 1966.

116. Stevens, K.K. and Evan-Iwanowski, R.M., Parametric resonance of viscoelastic columns. International journal of solids and structures, 5,755-761, 1969.

117. Subrahmanyam, K.B., Kulkarni, S.K.and Rao, J.S., Coupled bending-bending vibration of pre-twisted cantilever blading allowing for shear deformation and rotary inertia by the Reissner method. Int. J. Mech. Sci 23,517-530. 1981.

118. Sugiyama, Y., Katayama, K. and Kiriyama, K., Experimental verification of dynamic stability of vertical cantilevered columns subjected to a sub-tangential force. Journal of sound and vibration, 236,193-207, 2000.

119. Sun, C.T., Sankar, B.V. and Rao, V.S., Damping and vibration control of unidirectional composite laminates using add-on viscoelastic materials. Journal of Sound and Vibration, 139,277-290, 1990.

120. Sunakawa, M. and Higuchi, K., Nonlinear behaviour of thin columns under a parametrically excited load. AIAA J., 22, 1791 – 1796 1984.

121. Svensson, I., Dynamic instability regions in a damped system. Journal of Sound and Vibration, 244,779-793, 2001.

122. Takahashi, K., An approach to investigate the instability of the multiple-degree-of-freedom parametric dynamic systems. Journal of Sound and Vibration, 78, 519 – 529, 1981.

123. Tan, T.H., Lee, H.P. and Leng, G.S.B., Parametric instability of spinning pretwisted beams subjected to sinusoidal compressive axial loads. Computers and structures, 66, 745-764, 1998.

124. Tomar, J.S. and Jain, R., Effect of thermal gradient on frequencies of wedge shaped rotating beams. AIAA Jr. 22, 848-850, 1984.

125. Trompette, P., Boillot, D., and Ravanel, M.A., The effect of boundary conditions on the vibration of a viscoelsticlly damped cantilever beam. Journal of Sound and Vibration, 60,345-350, 1978.

126. Troesch B.A., Anlinker M. and Ziegler H, Lateral vibrations of twisted rods Zeitschrift für .Angewandte. Mathematik und Physik. 12,163-173,1954.

127. Ungar. E.E., Loss factors of viscoelastically damped beam structures. Journal of the Acoustical Society of America, 34, 1082-1086, 1962.

128. Vaswani, J., Asnani, N.T. and Nakra, B.C., Vibration and damping analysis of curved multilayered beams. Transactions of the CSME, 9, 59-63, 1985.

129. Yang, S.M. and Tsao, S.M., Dynamic stability of a pretwisted blade under nonconstant rotating speed, computer and structures, 62,643-651, 1997.

130. Yokoyama, T., Parametric instability of Timoshenko beams resting on an elastic foundation. Computer and structures. 28, 207 – 216, 1988.

131. Zajaczkowski, J. and Lipinski, J. Vibrations of parametrically excited systems. Journal of Sound and Vibration, 63, 1 – 7, 1979.

132. Zajaczkowski, J., An approximate method of analysis of parametric vibration. Journal of Sound and Vibration, 79, 581 – 588, 1981.

133. Zavodney, L.D., A theoretical and experimental investigation of parametrically excited non-linear mechanical systems. Ph. D. Dissertation, Dept. of Eng. Sci. and mech., Virginia polytechnic Institute and State university, 1987.

134. Zavodney, L.D. and Nayfeh, A.H., The non-linear response of a slender beam carrying a lumped mass to a principal parametric excitation: theory and experiment. Int. J. Non-linear mech., 24, 105 – 125, 1989.

135. MATLAB reference guide, version 6.5, July 2002.

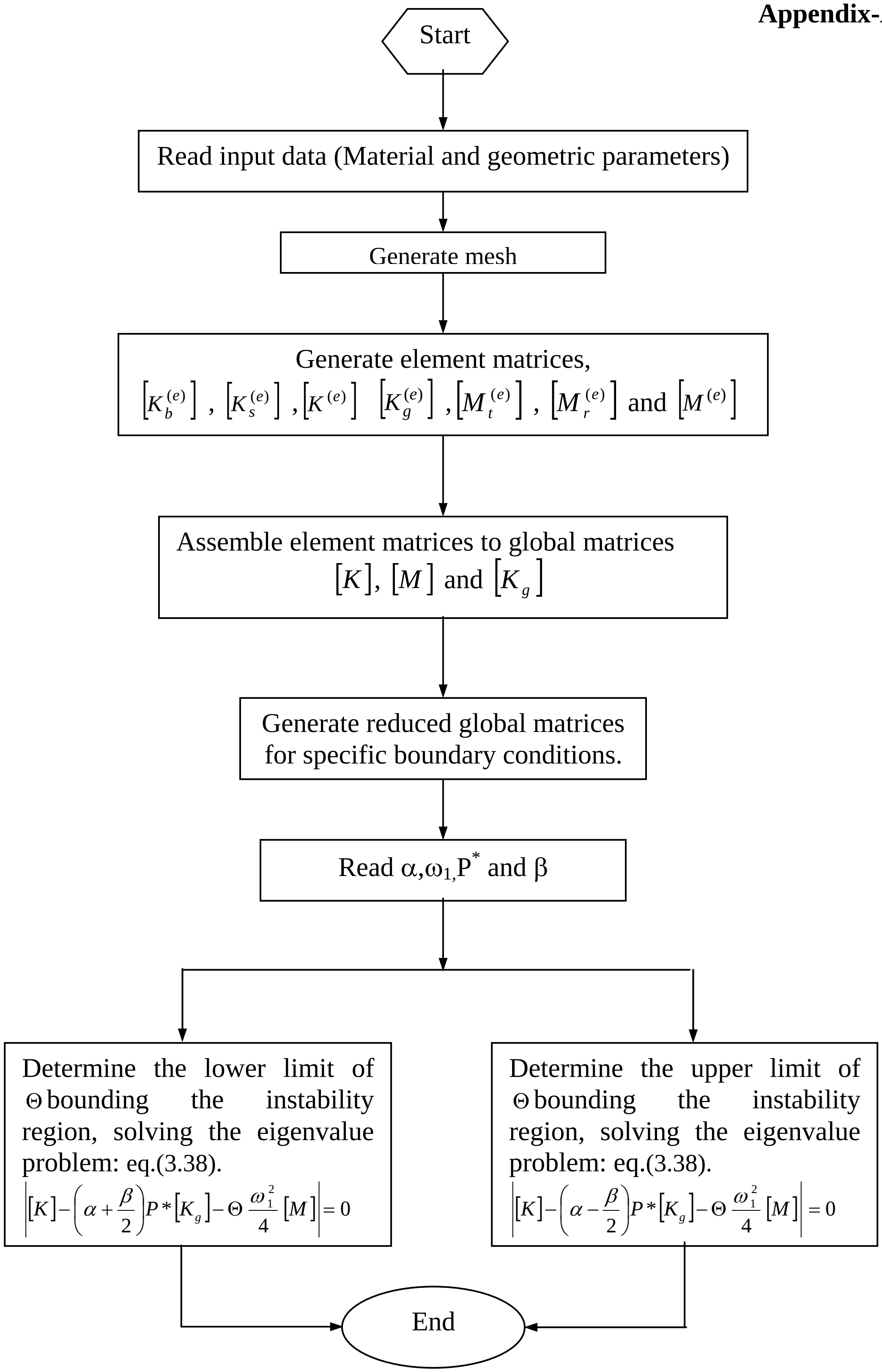

Flow chart for calculating the lower and upper boundary limits of instability regions based on Floquet's theory.

Appendix-B

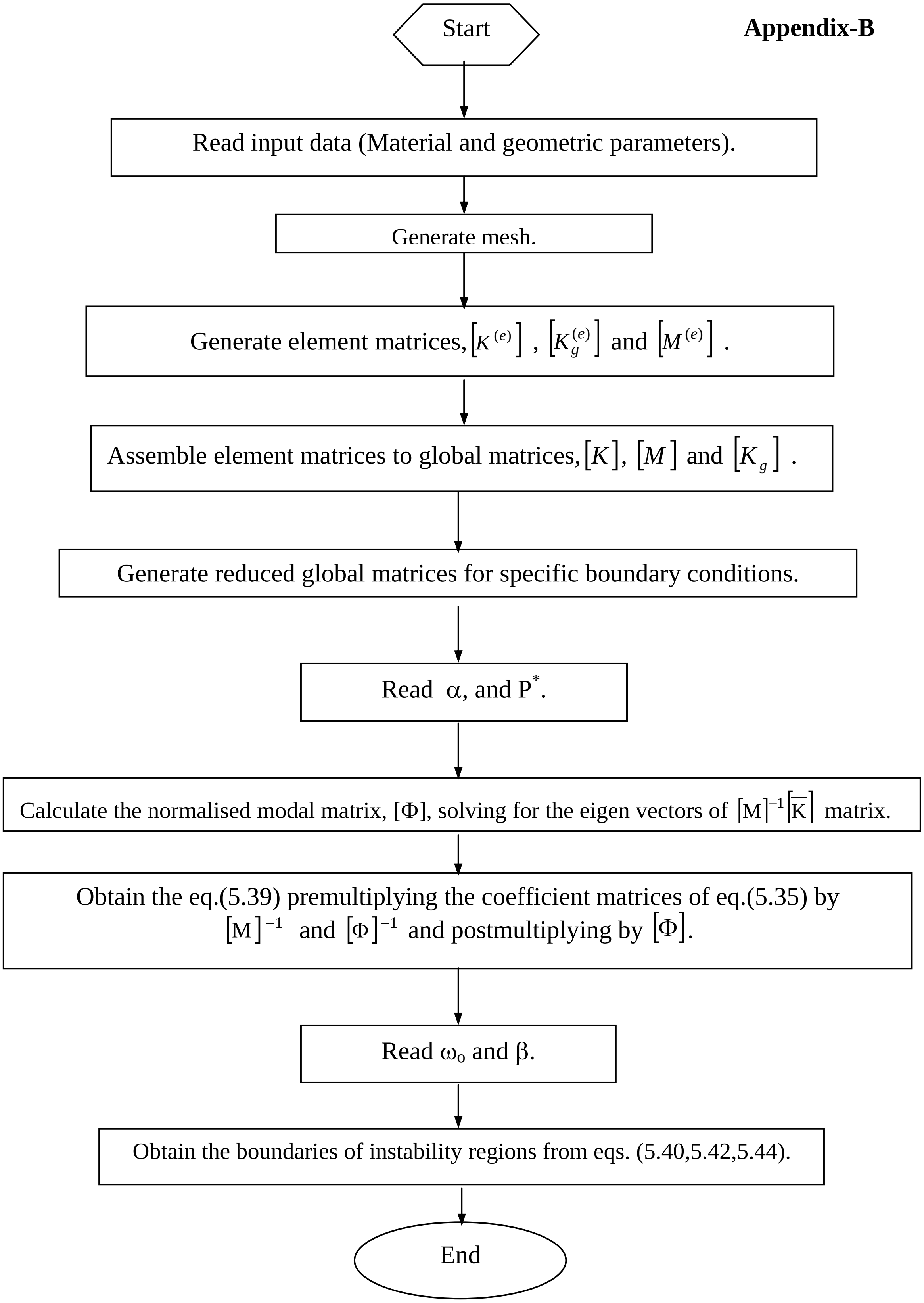

Flow chart for calculating the lower and upper boundary limits of instability regions based on Hsu's criteria.

Bio-Data

Name: Mr. Sukesh Chandra Mohanty.

Date of birth: 04-07-1965.

Permanent address: At: Pathuria Sahi, Po: Puri, Dist: Puri, Orissa, India, Pin-752001.

Educational qualifications:

Degree	University	Year of passing	Class/Division
B.Sc. (Engineering) (Mechanical)	Sambalpur University	1987	First div.
M.Tech.(Machine design specialisation)	Beneras Hindu University	1990	-do-

Teaching experience: Faculty in Mechanical Engineering Department, N.I.T, Rourkela since 16-09-1991.(Lecturer-16.09.91 to27.09.97, Senior lecturer-28.09.97 to14.02.2004, Lecturer (Selection grade) - 15.02-04 to 27-09-05, Asst. Professor-28-09-05 till date)

Merit certificate received: Received the certificate of merit from the Institution of Engineers, India for 2003-2004 for the published paper titled “Tooth Load Sharing and Contact Stress Analysis of High Contact Ratio Spur Gears in Mesh.”